TO MY MOTHER

AND THE MEMORY

OF MY FATHER

THE MECHANICS OF ULTRASONIC TUBE BENDING

by

IBRAHIM NAIROUZ IBRAHIM

Submitted in fulfilment of the requirements

for the degree of

DOCTOR OF PHILOSOPHY

Faculty of Engineering

Department of Production Technology and Production Management

The University of Aston in Birmingham

September 1983

Supervisor: Professor D H Sansome

DECLARATION

No part of the work reported in this thesis has been submitted in support of an application for another degree or qualification of this or any other university or institution.

I N IBRAHIM

THE UNIVERSITY OF ASTON IN BIRMINGHAM
Department of Production Technology and Production Management

THE MECHANICS OF ULTRASONIC TUBE BENDING

Submitted in fulfilment of the requirements
for the degree of Doctor of Philosophy

Author: IBRAHIM NAIROUZ IBRAHIM Year: 1983

Summary

The technology of precision bending of tubes has recently increased in importance and is widely demanded for many industrial applications. However, whilst attention has been concentrated on automation and increasing the production rate of the bending machines, it seems that with one exception very little work has been done in order to understand and therefore fundamentally improve the bending process.

A new development for the process of draw-bending of tubes, in which the supporting mandrel is axially vibrated at an ultrasonic frequency, has been perfected. A research programme was undertaken to study the mechanics of tube bending under both vibratory and non-vibratory conditions. For this purpose, a conventional tube-bending machine was modified and equipped with an oscillatory system.

Thin-walled mild steel tubes of different diameter to thickness ratios were bent to mean bend radii having various values from 1.5 to 2.0 times the tube diameter. It was found that the application of ultrasonic vibration reduces the process forces and that the force reduction increases with increasing the vibration amplitude. A reduction in the bending torque of up to 30 per cent was recorded and a reduction in the maximum tube-wall thinning of about 15 per cent was observed. The friction vector reversal mechanism as well as a reduction in friction account for the changes of the forces and the strains. Monitoring the mandrel friction during bending showed, in some cases, that the axial vibration reverses the mandrel mean force from tension to compression and, thus, the mandrel is assisting the tube motion instead of resisting it.

A theory has been proposed to describe the mechanics of deformation during draw-bending of tubes, which embodies the conditions of both "with" and "without" mandrel axial vibration. A theoretical analysis, based on the equilibrium of forces approach, has been developed in which the basic process parameters were taken into consideration. The stresses, the strains and the bending torque were calculated utilising this new solution, and a specially written computer programme was used to perform the computations.

It was shown that the theory is in good agreement with the measured values of the strains under vibratory and non-vibratory conditions. Also, the predicted bending torque showed a similar trend to that recorded experimentally.

Key words: mechanics of bending, draw-bending of tubes, ultrasonic vibrations, oscillatory metal deformation

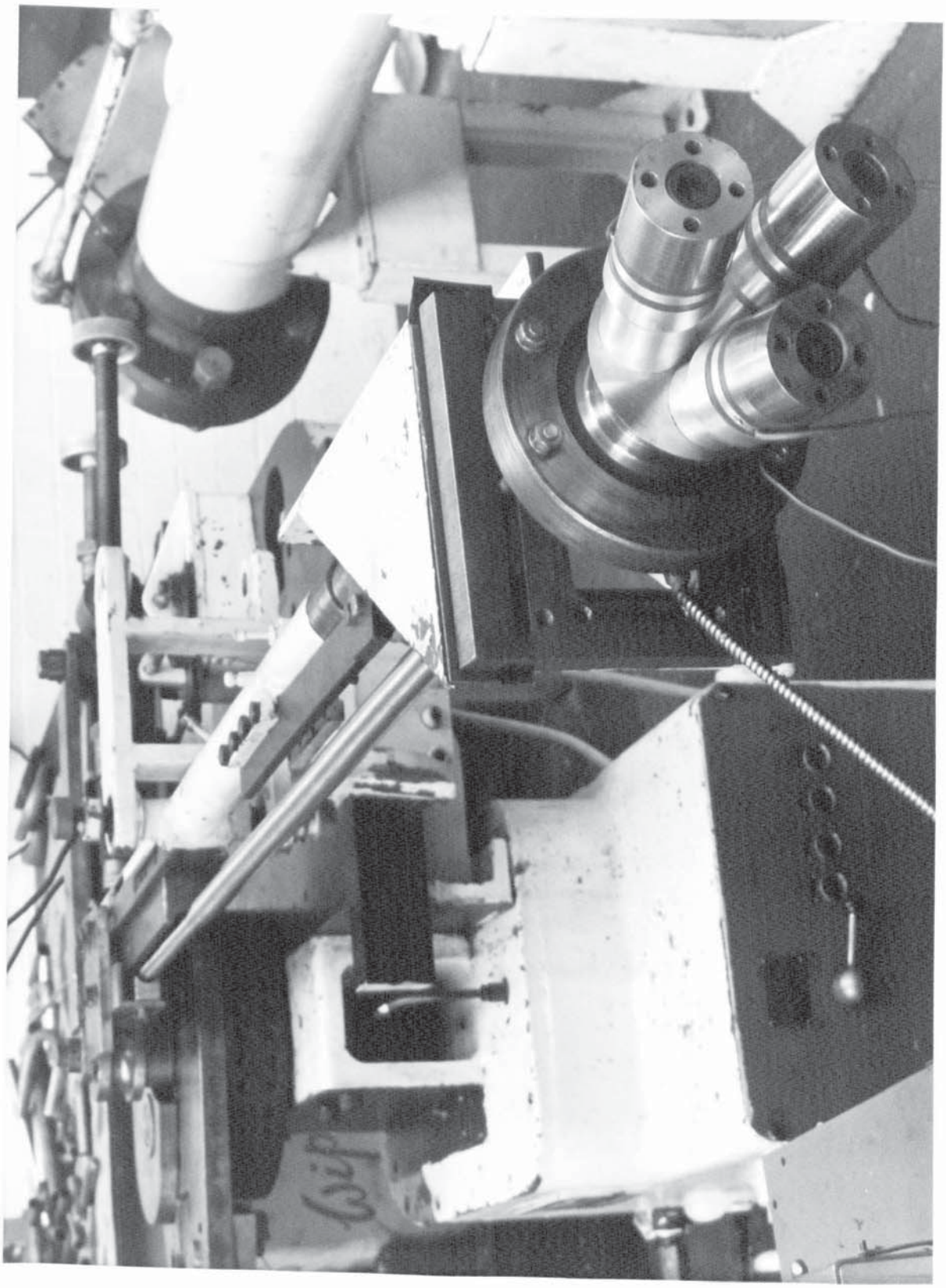

Frontispiece: The tube-bending machine equipped with the oscillatory system

CONTENTS

LIST OF FIGURES

LIST OF PHOTOGRAPHS

LIST OF TABLES

NOMENCLATURE

A	=	displacement amplitude of vibration
A_{aI} and A_{aII}	=	average displacement amplitudes in zones I and II
A_m	=	maximum displacement amplitude of vibration
d_i	=	tube inside diameter
d_o	=	tube outside diameter
F_o	=	initial friction force
$\bar{F}_o$	=	initial friction force with mandrel vibration
F_s	=	slider force
f	=	frequency of vibration
h	=	strain-hardening coefficient
N	=	speed of bending machine (rev min^{-1})
n	=	strain-hardening exponent
p_F	=	former pressure
p_M	=	mandrel-tip pressure
p_m	=	mandrel-shank pressure
p_s	=	slider pressure
Q	=	bending torque
Q_f	=	torque required to overcome friction in zone IIf

R = radius of bend at any angle ϕ

R_o = mean radius of bend

r_m = mean radius of tube

T = time of an oscillation period

t = tube wall-thickness at any angle ϕ

t_o = initial wall-thickness of tube

V_{TM} = mean velocity of tube

V_{TR} = tangential velocity of any point on tube contact surface

v_v = vibratory velocity

v'_v = component of the vibratory velocity in the direction of tube motion

v'_{va} = average vibratory velocity in zone II in the direction of tube motion

W_f = frictional work per unit volume

Y = yield stress of tube material

δA_1 = incremental area of tube section

$\delta\varepsilon_\theta$ = incremental longitudinal strain

$\delta\varepsilon_\phi$ = incremental hoop strain

$\delta\varepsilon_t$ = incremental thickness strain

$\delta\bar{\varepsilon}$ = incremental equivalent strain

ε_θ = natural longitudinal strain

ε_ϕ = natural hoop strain

ε_t = natural thickness strain

$\bar{\varepsilon}$ = equivalent strain

θ = current angle of bend

θ_1 = angle contained between the entry and exit planes

λ = wave-length of vibration

μ = coefficient of friction

μ' = coefficient of friction under oscillatory conditions

σ_θ = longitudinal stress

$\bar{\sigma}_\theta$ = longitudinal stress under oscillatory conditions

σ_ϕ = hoop stress

σ_r = radial stress

$\bar{\sigma}$ = equivalent stress

ϕ = angular position of a small element of tube

ϕ_N = angular position of the neutral plane

ω = angular velocity of a vibration wave

0, 1 = refer to the entry and exit planes respectively

s, m, M and F = refer to slider, mandrel-shank, mandrel-tip and former respectively

NB Other symbols used in this text are defined as they appear

CHAPTER ONE

INTRODUCTION

Although tubes can be joined at the corners by fittings, welding or brazing, bending has proved to be better in service and as a production process much faster, cheaper and more practical particularly when high production rates are required and/or when great accuracy is needed. Consequently, tube-bending technology has, in recent years, become very advanced and bending machines have been developed in order to satisfy a sophisticated and increasingly demanding market.

There are several methods of bending tubes but the rotary draw-bending process is most commonly used. An important advantage of draw-bending is that thin-walled tubes can be bent to tight radii with minimum distortion and high precision. Such bends are in great demand for many technological applications such as in chemical engineering and in the aircraft and nuclear power industries. Figure 1.1 shows the draw bending operation in which the tube is initially clamped between a gripper and a former which then rotates, bending and drawing the tube while its straight part is supported by a slider which follows the tube forward. Although those basic tools ie. the former, the gripper and the slider are essential, a mandrel and a wiper die may be used when it is necessary to produce high quality bends for especially thin tubes and small bend radii.

In an ideal bend, there is no flattening or buckling and no thinning or thickening of the tube wall on the outer and inner peripheries respectively; however this ideal objective is not realised

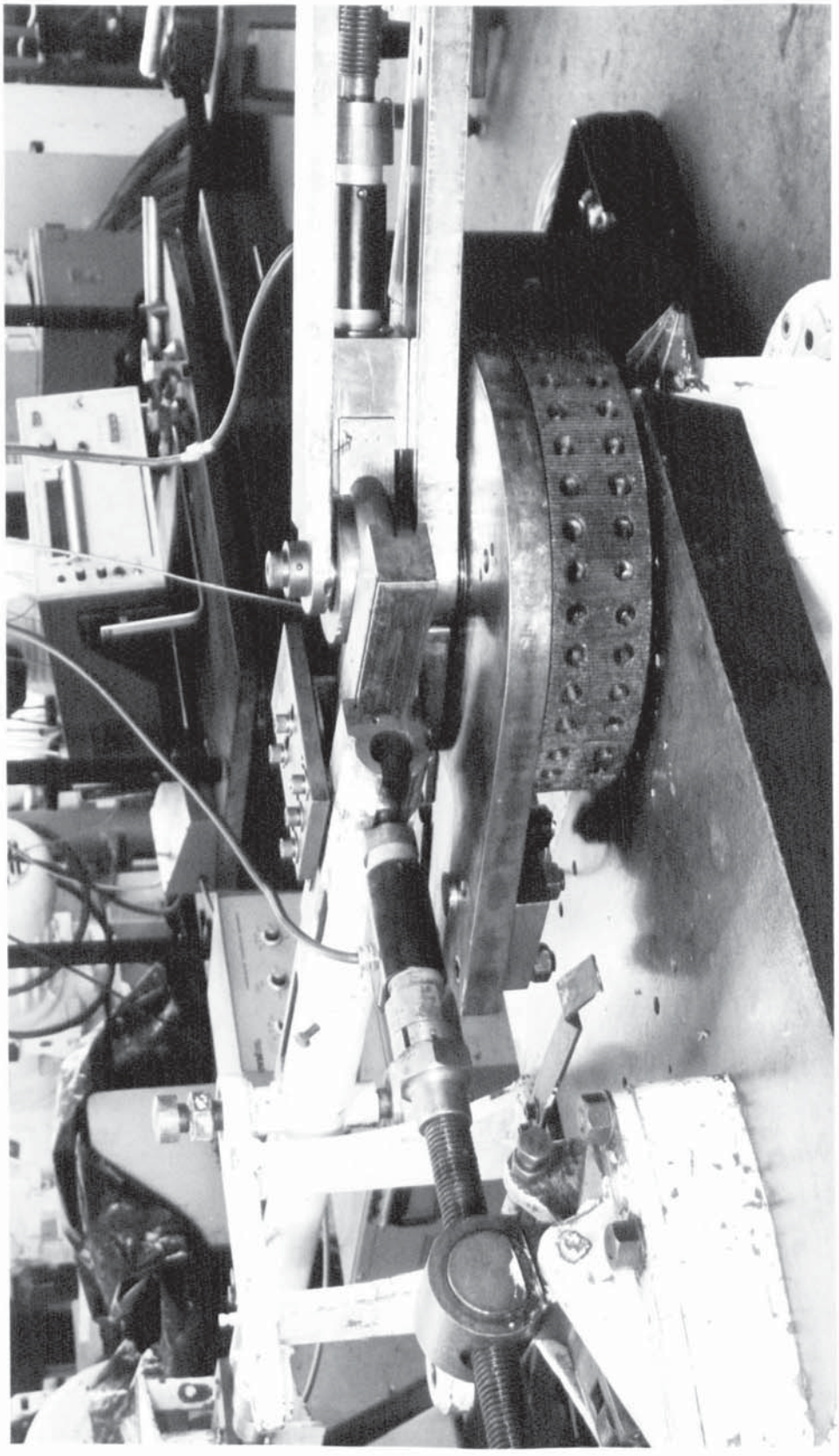

Figure 1.1: The tube-bending operation and the tooling arrangement

in practice. Considering the basic concept of bending, as illustrated in figure 1.2, it is quite obvious from the geometrical configuration that the outside of the bend is stretched under tension resulting in a consequential thinning of the tube outside wall. Also, the bend inside shortens under compression and this causes the inside wall to thicken. The boundary line between the tensile and compressive parts of the tube section is known as the 'neutral axis'. It can be shown from figure 1.2 that the position of the neutral axis has moved closer to the centre of bend as a result of the thinning and thickening effects. In addition, because of the unsymmetrical deformation on the outside and inside of the bend, the tube tends to flatten or collapse; however the amount of flattening is small if the tube is thick and the bend radius is relatively large.

When bending thin or ultrathin tubes to small bend radii, an excessive amount of tube flattening occurs and also the tube material tends to buckle on the inner periphery. Therefore, it is then necessary to support the tube internally by using a mandrel which helps to prevent flattening and wrinkling of the tube during bending. However, the friction between the tube bore and fixed mandrel will cause an increase in the applied tension and consequently the neutral axis will move closer to the centre of bend. The result of this is a greater amount of thinning and less thickening of tube wall on the outer and inner peripheries respectively. Further, additional work would have to be done in order to overcome the friction resistance and this explains the increase in the bending torque and the process forces when a fixed mandrel is used. Since high strength-to-weight ratios are most desirable for many industrial applications of tube bends, it is essential that the strength-to-weight ratio of a bent tube should be the

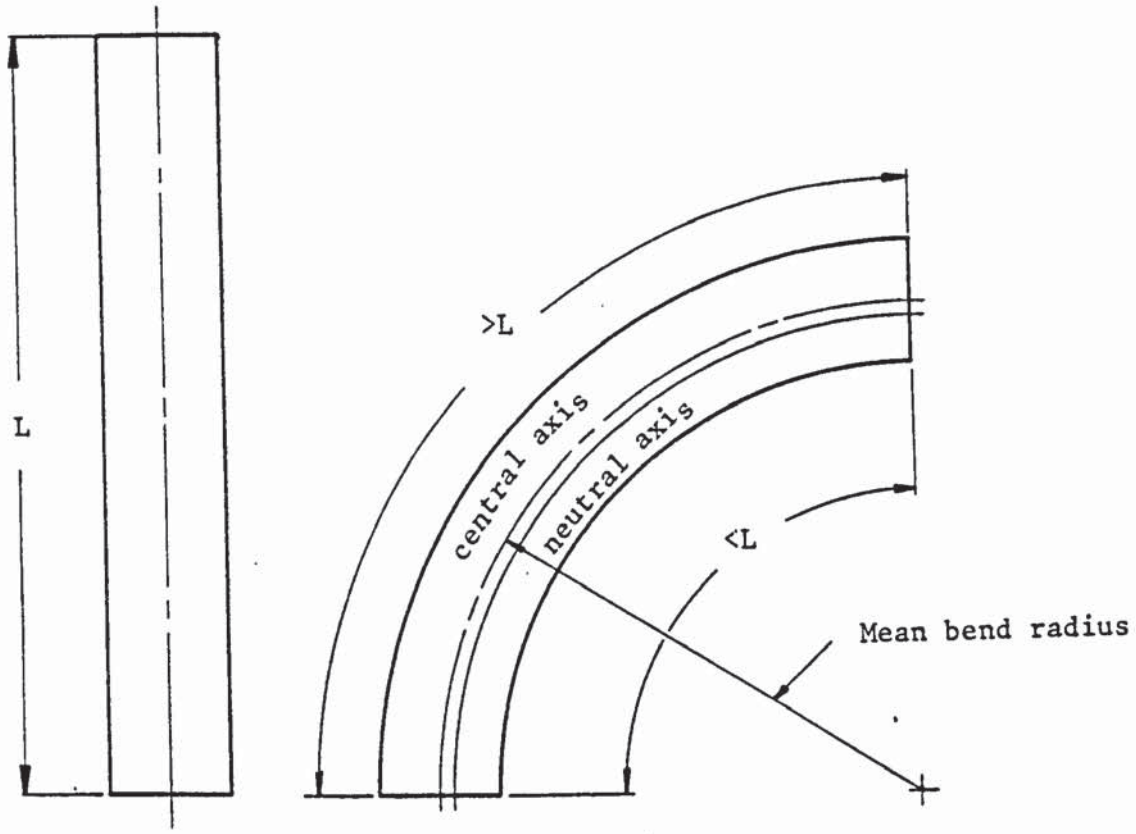

Figure 1.2a Comparison of length element of a tube before and after bending

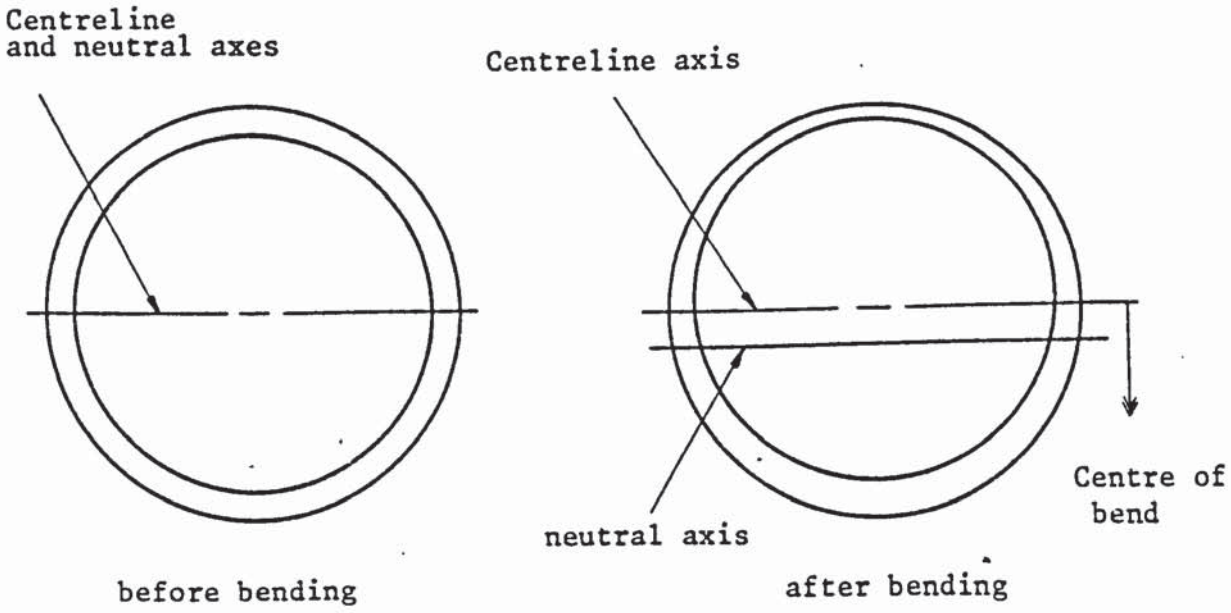

Figure 1.2b Thinning and thickening of the tube wall at the outside and the inside of bend respectively

same as that of the original tube; this is not normally achievable due to the thinning of the tube outside wall. Therefore, the use of a mandrel can have a detrimental effect on the strength-to-weight ratio on the bend outside particularly in the case of thin tubes and tight bend radii. This is a major disadvantage of draw-bending of tubes using a fixed mandrel. Practically, to keep the outside tube wall within the desired limits and also to achieve a satisfactory strength-to-weight ratio, thicker-walled tubes have to be employed. Consequently, the material cost is higher and also the unit weight of the straight tube between bends increases; this can be a significant disadvantage for industries such as the aircraft industry. Additionally, the increase of bending torque and forces due to mandrel friction can result in other industrial disadvantages such as restricting the bending-machine capacity and its ability to produce very tight bends without causing the tube to fail.

Different techniques have already been developed in order to reduce the friction effect when draw bending tubes with a supporting mandrel. For example, a high quality lubricant may be used to provide effective lubrication of the tube bore and consequently to reduce the coefficient of friction. Also, a mandrel which is especially coated can have less interfacial friction and tool wear. However, the cost and the practical restrictions of certain good lubricants and of special treatments or coatings of mandrels are factors which sometimes detract from the use of such techniques. For instance, lubricants containing chlorine often guarantee friction reduction but their use may cause corrosion with consequential damage of the surfaces. This makes tube so bent to be unacceptable for use in some applications, eg. in the aerospace assemblies. Further, no one lubricant works equally well for

all tube materials which means that the application of an effective lubricant might not be economical. On the other hand, despite the fact that especially coated mandrels can have longer tool-life, such tooling may prove not to be the most economical due to the need to apply this special treatment to a large number of mandrels of different sizes in order to accommodate a wide range of tube outside diameters and wall thicknesses. Another technique, which is now used in practice, to counteract friction at the tube-mandrel interface is the application of a superimposed axial compressive force (booster force) to the slider and/or the tube. This additional compression can result in a reduction in the amount of the outside tube-wall thinning. However, booster force applied directly to thin tubes is not practical since it may cause tube damage or collapse.

A successful technique which has proved to be effective in reducing the interfacial friction in several metal deformation processes is the use of ultrasonic vibrations. It has been known for some time that when a cyclic motion, or stress, is applied to the tools or the workpiece during metal deformation, the resulting effects can cause the process forces to be reduced, the achievable deformation to be increased or the product quality to be improved. Extensive research into the ultrasonic metal-working processes has been carried out in order to investigate the beneficial effects of applying vibrations and also to clarify the fundamental mechanisms which contribute to such effects. Accordingly, it has been widely justified that the application of vibrations can have two major effects: (a) a "volume effect" which implies a reduction in the deformation forces as a result of changes induced in the bulk of the deforming metal, (b) a "surface effect" ie. a reduction in contact friction at the tool-workpiece interface. The

relative importance of these two effects varies according to the characteristics of the particular metal deformation process and the mode of oscillations being applied to the mechanical system. In addition, one of the most important factors which can affect the friction reduction mechanism is the speed of processing. It has been shown that slow speed forming processes which include a substantial amount of frictional work are most advantageously affected by the application of ultrasonic vibrations. For example, an appropriate axial vibration of the plug or radial vibration of the die in the fixed-plug or floating-plug in tube-drawing processes respectively, substantially reduces the draw load as a result of a considerable reduction in friction. The process of draw-bending of tube over a mandrel is one of the slower forming processes and in addition there is a large frictional component within the total deformation work. Thus, for those two reasons this process can benefit significantly from the application of ultrasonic vibrations.

Preliminary tests were performed by Colloff[1] in order to investigate the effects of applying vibratory energy to the mandrel supporting the tube bore during bending. It was shown that at a given mean bend radius, for a given diameter to thickness ratio the non-oscillatory tube-wall thinning at the outer surface of the bend was greater than when the mandrel was axially vibrated at an ultrasonic frequency. Also, a reduction in the bending torque of up to 10 per cent was recorded.

The current research programme is concerned with the mechanics of tube bending and with the application of ultrasonic vibrations to the process. Therefore, it has two main objectives: first, to investigate experimentally the conventional process of draw bending of tubes and to

show some of the achievable improvements in the process when the mandrel is axially oscillated. The use of a powerful and efficient generator and a properly designed and accurately tuned ultrasonic system can result in considerable reductions in the process forces and in the amount of wall-thinning on the bend outside. Secondly, since very little work has been published on the relevant theoretical aspects of tube bending, a theory has been written to describe the mechanics of metal deformation taking place during the process. The theoretical analysis which is based on the "equilibrium of forces approach" takes into account the principal parameters involved in the bending process and embodies the conditions of both "with" and "without" applied ultrasonic oscillations. Consequently, using this new theoretical solution the bending torque and the stresses and the strains can be calculated with the aid of a newly written computer programme.

CHAPTER TWO

REVIEW OF THE LITERATURE

2.1 The technology of rotary draw-bending of tube

2.1.1. Introduction

Bending tubes is one of the oldest established operations in metalworking but it has only recently been studied in depth like other metal forming processes. Also, it is now realised that bending can reduce or eliminate considerable machining, welding or other more costly operations. Consequently, bending technology has increased in importance in response to the wide demand of tubes for many industrial applications. As a result, new bending methods have been developed and bending machines have become very advanced and sophisticated in order to meet the increasing demand for higher production rates and to achieve greater accuracy, precision and nullify springback.

In general, tubes can be bent in many ways, eg. compression, press, roll and stretch. However, the draw bending process is perhaps the most versatile and precise system of bending. It can produce high quality bends to the tightest radii for thin-walled tubes. Basically, the tube is clamped against a bending die called a 'former' which then rotates, bending and pulling the tube while its straight part is being supported by a pressure die termed the 'slider', as illustrated in figure 2.1. This tooling arrangement is sufficient when bending thick tubes to large bend radii, but as the wall thickness becomes thinner

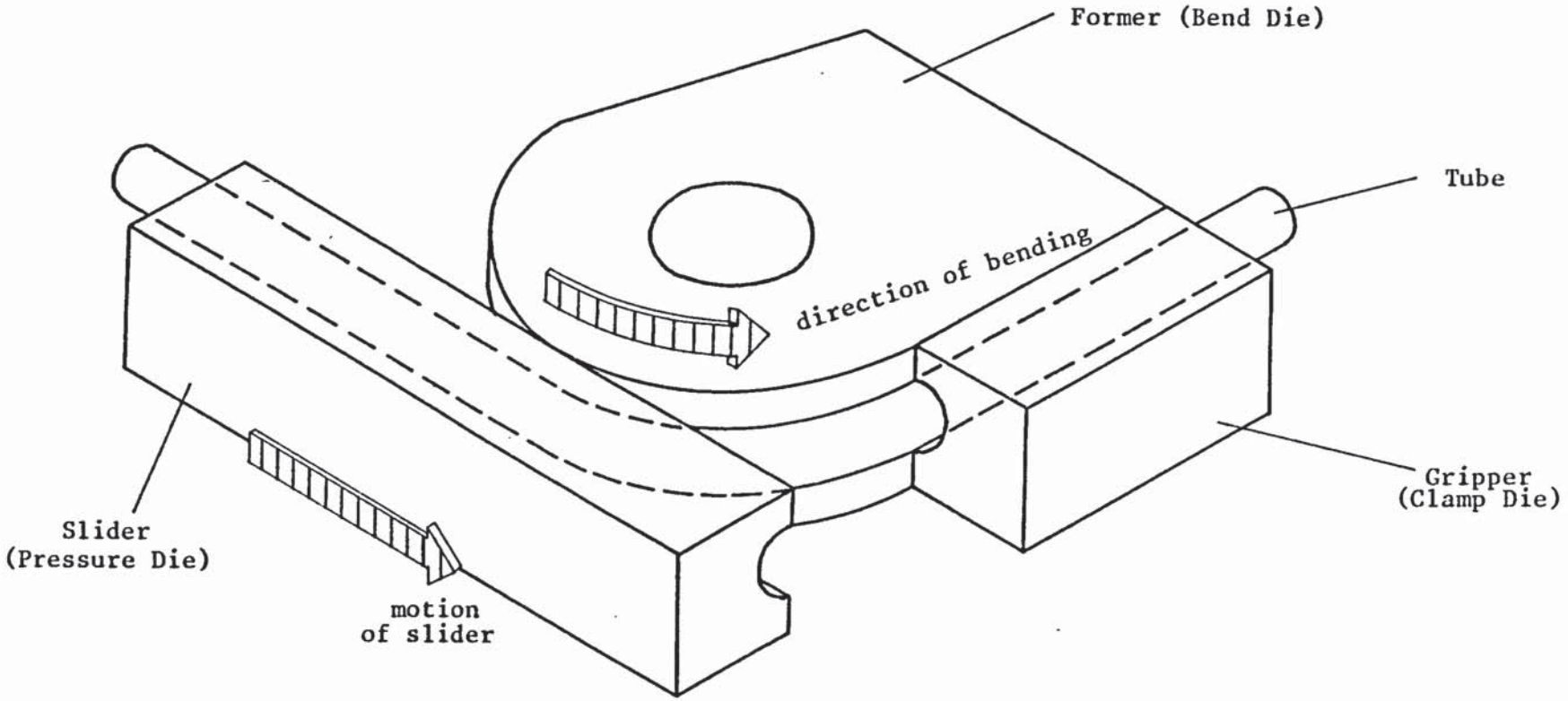

Figure 2.1: A diagrammatic representation of the rotary draw-bending of tubes

and/or the radius of the bend is decreased, a mandrel and a wiper die may be required. A complete set of bending tools is shown in figure 2.2. Principally, the aim of tube bending is to produce good quality bends with minimum flattening of tube section and free from wrinkles. Also, it is desirable to minimise the amount of thinning of tube-wall on the bend outside.

2.1.2 Tooling design and requirements

As shown in figure 2.2, there are five basic tools associated with rotary draw-bending of tube: (1) former (bend die), (2) gripper (clamp die), (3) slider (pressure die), (4) mandrel, (5) wiper die. The first three are always required but the last two are support tools employed when bending thin tubes to tight radii. The design and manufacture of the tools are influenced by several factors: desired production rate, tube material and dimensions, mean radius of bend, type of bender used, distance between bends and the required quality of the bend, which depends on the specific application. All tooling should be in a good condition and their positions, when fitted to the bending machine, must be correct in order to achieve bends of good quality. The necessary requirements for the design and the manufacture of bending tools mentioned in this section are discussed in detail in several references[2-15].

(1) Former

The former is the primary tool around which the workpiece is formed to produce a specific mean bend radius. . It must have a tube groove equal in depth to, at least, half of the tube outside diameter in order

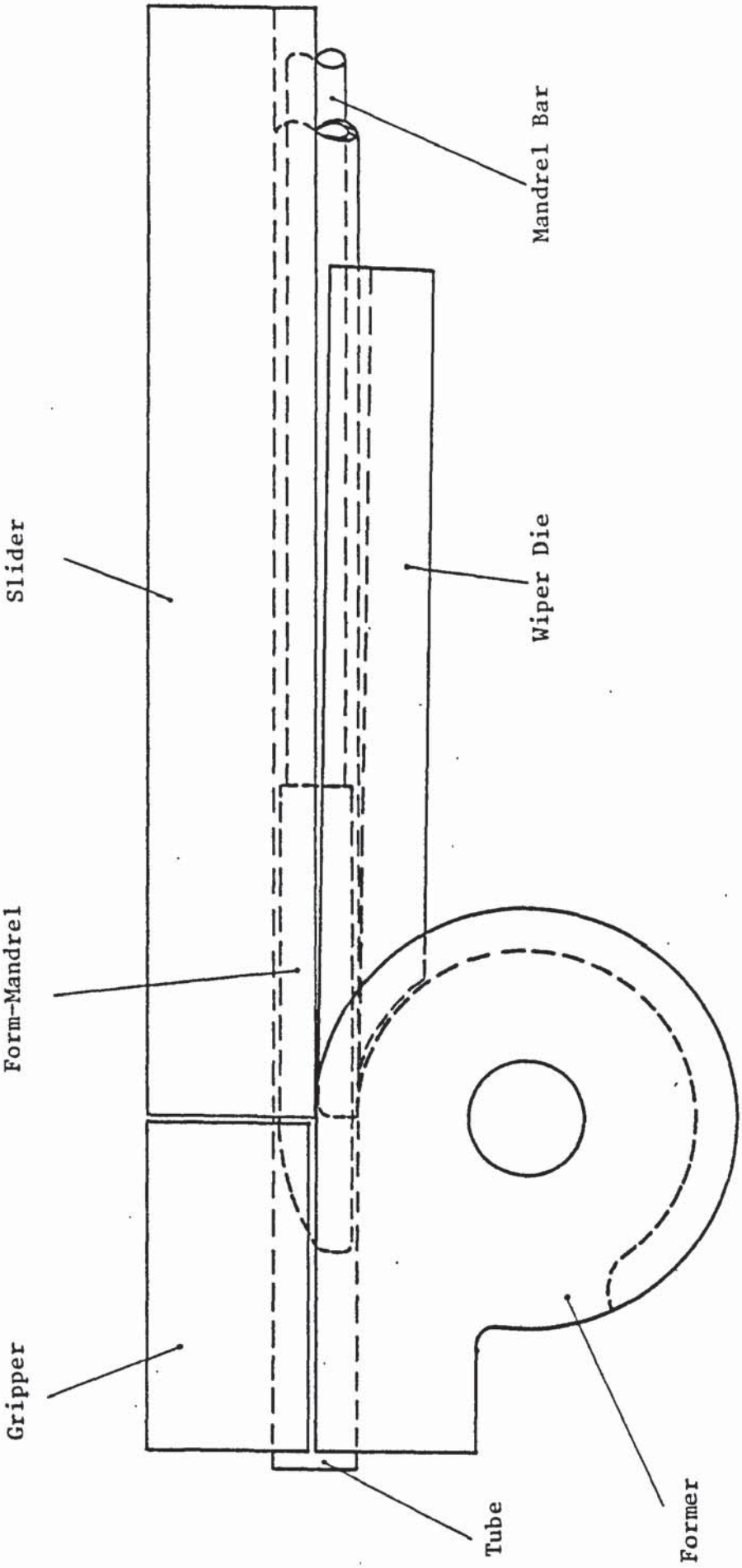

Figure 2.2 : The arrangement of tooling in draw-bending of tubes

to prevent marking of the tube outside surface. Normally, minimum groove dimensions should be the nominal tube outside diameter plus a maximum tolerance not more than .001 in. Also, the groove radial angle should be equal to the desired bend angle plus an amount of overbend for springback compensation. Provision for attachment to the bending machine is required and the former must be exactly centred on the machine such that an arc of constant radius will be circumscribed as the former rotates. Adequate length of the former straight part where the tube is clamped is necessary and its groove diameter should not be undersized more than 10 per cent of tube wall-thickness relative to the tube outside diameter. The clamping areas should have a moderately rough surface or it may be cleated, flared or beaded. The former material must be harder than the tube material to avoid possible deformation of the tube groove when wrinkles occur. Mild steel formers, hardened to 40-45 R_c, are commonly used. However, the former may be manufactured from standard heat-treated tool steels or low-temperature case hardened steels of not less than 40 R_c in order to resist wear and deformation. Nevertheless, the quality of former material depends on the specific requirements such as the bend radius and the production rate. Different designs of formers are shown in figure 2.3.

(2) Gripper

The gripper operates in such close conjunction with the former that it may be considered as part of the same tool. It is the matching half to the former grip-length section and must grip the greatest possible area of material with the least chance of slipping to avoid damaging the tube. Enough pressure from the gripper on the tube is required,

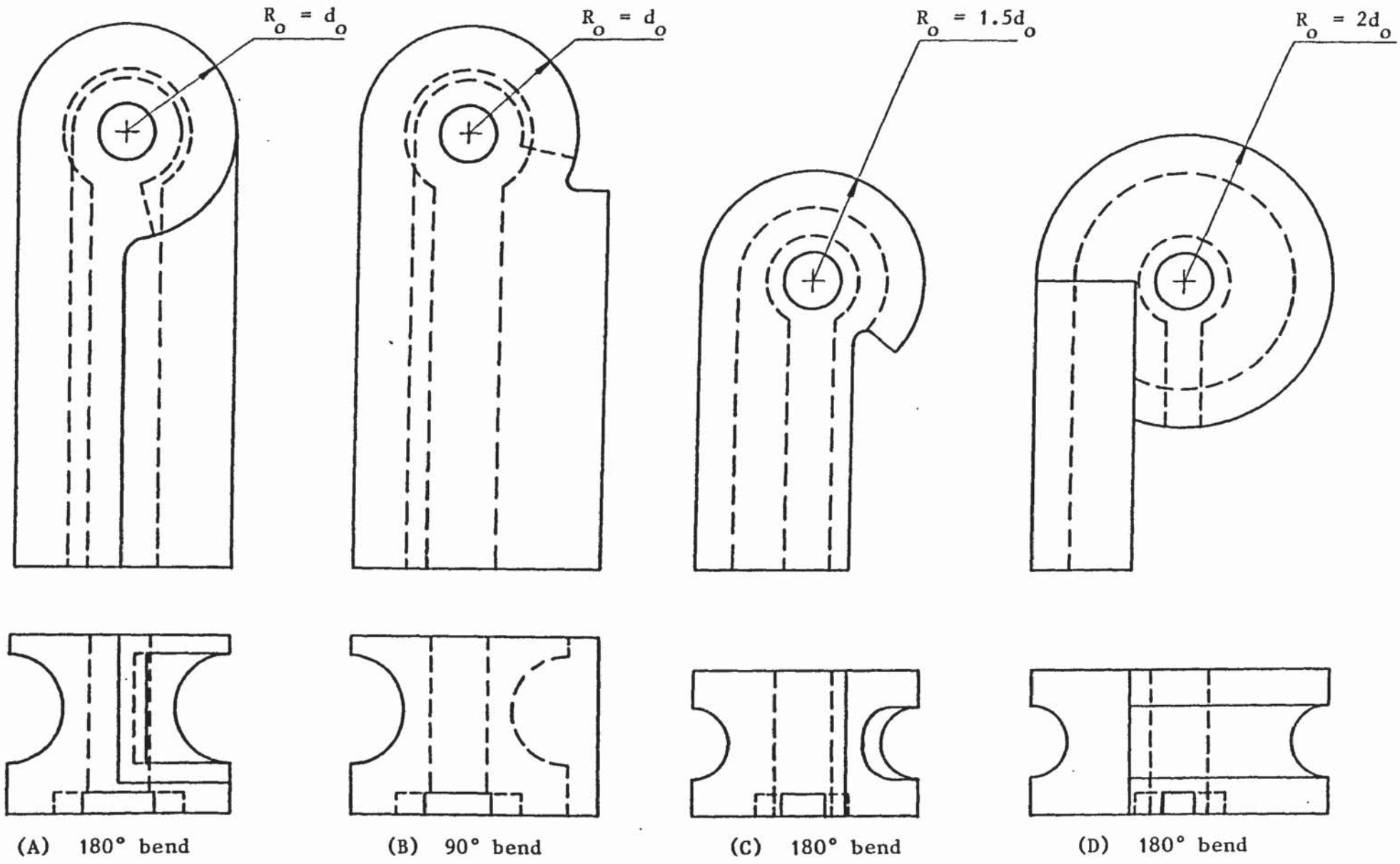

Figure 2.3 : Different designs of formers (bend dies) (14)

however, excessive pressure can result in tube distortion or collapse particularly when thin tubes are employed. In that case, a cleated clamp plug may be necessary to protect the tube. The gripper groove has a depth slightly less than the tube outside diameter in order to leave enough gap for gripping and its surface is often roughened by grit blasting, metallic or carbide sprays, cleats and/or serrations to increase the gripping friction. Normally, the gripper material is similar to that of the former, and its length is the same as the former straight-part. However, the gripper is usually set back slightly behind the tangent line in order to allow the slider a slight advance and consequently this may help by reducing the amount of springback of tube material. The gripper and the former are sometimes provided with an interlocking mechanism which helps to ensure correct alignment and to speed-up the setting of the tools especially for numerically controlled machines and for tight bends of thin-walled tubes. This mechanism would also help to eliminate marking and distortion of the tube.

(3) Slider

The main function of the slider is to contain the tube in the former groove during bending. It has two critical dimensions: the tube groove dimension which must match the former groove, and the groove linear parallelism which is important in keeping enough pressure at the tangent as the slider advances forward during the bending cycle. The slider should have an adequate length depending on the bend mean radius and the angle of bend. The material of the slider is similar to the former material but it does not require hardness standards as high as those of the former; a standard of 30 R_c may be adequate. Before bending starts, the slider should be adjusted for a light pressure

against the tube but too low a pressure can result in wrinkling the tube surface on the bend inside.

(4) Wiper die

The wiper die is a supporting tool which establishes a straight 'flow line' behind the tangent on the inside of the bend. It is required when bending thin-walled tubes to tight radii or when the resistance of the tube material to compression is high. The function of a wiper die is to fill the gap behind the former and confine the metal into a smooth, wrinkle-free compression on the inside of the bend, as illustrated in figure 2.4. The wiper die is grooved dimensionally similar to the former and the slider specifications. In addition, a radius tip is required to reach the former supporting groove at the tangent where the compressive force begins. The wiper die groove is preferably ground and plated to minimise contact friction with the tube. The tip is subjected to considerable pressure during bending, so it must have sufficient ductility to prevent breakage. However, the die should not be softer than 30 R_c. Mild steel may be used as wiper die material but tool steel can have better wear resistance. Wiper dies can be precisely cut from pre-formed blanks of alloy steel for non-ferrous or mild steel tubes, or from an aluminium bronze alloy for stainless steel or for other high tool pressure applications. The two basic styles of wiper dies are shown in figure 2.5.

(5) Mandrel

The mandrel is employed when it is necessary to provide an internal support for the tube during bending. Its primary function is to prevent collapse or excessive flattening of the material being bent by

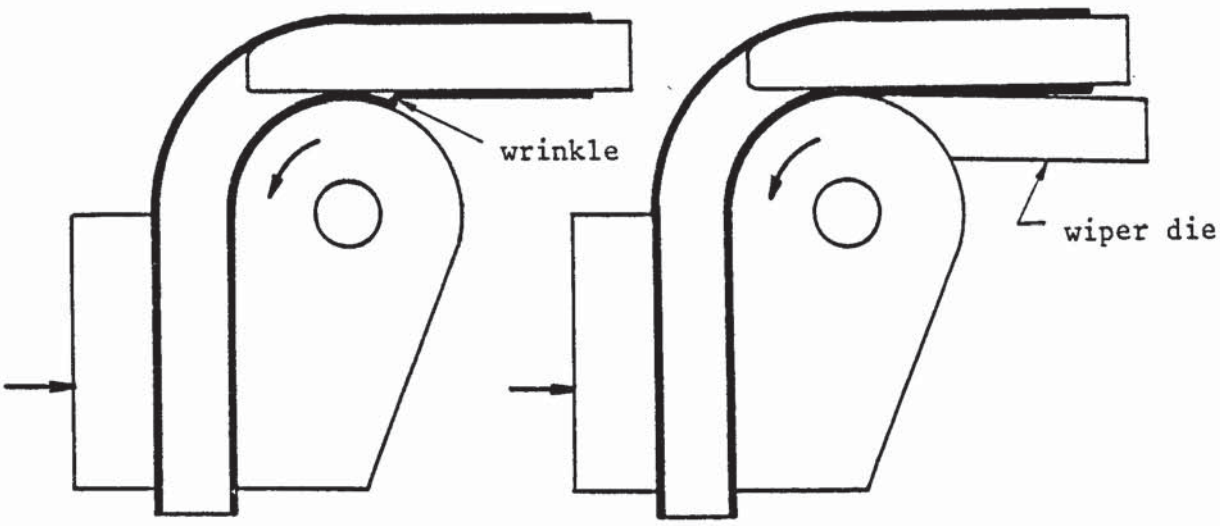

(a) a bend with wrinkles (b) a good quality bend

Figure 2.4: A wiper die helps prevent wrinkling the inside of bend[12]

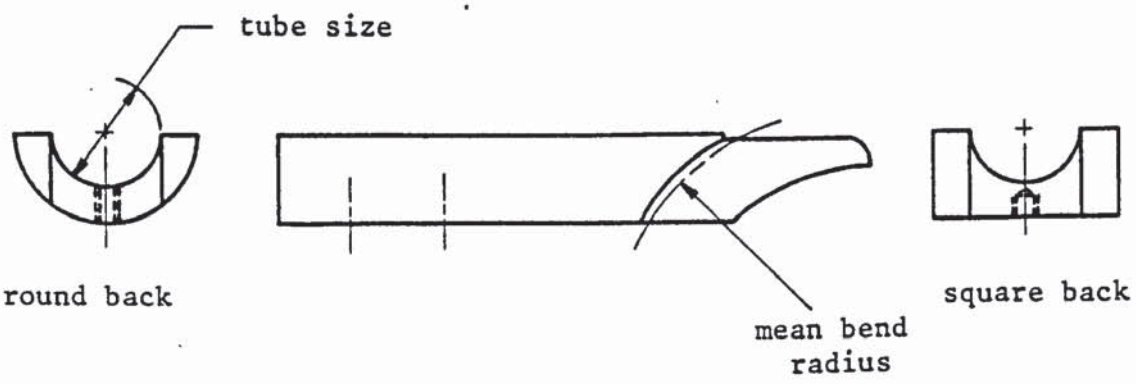

Figure 2.5: Two basic styles of wiper dies [15]

supporting the outside wall of tube. But it helps also in preventing tube wrinkling on the bend inside since it supports internally the inside tube wall at the tangent line. As shown in figure 2.6, there are three basic types of mandrel available for draw-bending of tubes: plug, form and flexible-ball. However, the choice of mandrel type depends mainly on the tube outside diameter to wall thickness ratio (normally widely known as the "D/t ratio"), and the mean bend radius to the tube outside diameter ratio. In general, a plug-mandrel can be used for bending thick-walled tube to large bend radii but for thinner tubes and smaller bend radii, the form-mandrel may be necessary. The flexible-ball mandrel is expensive and is usually reserved for bending very thin-walled tubes to tight radii. Recommended charts and tables are available in technical publications[12,15].

Since the mandrel is fixed in position during bending, the tube is then pulled over the mandrel causing relative motion, friction and wear. Therefore, to minimise the mandrel friction and wear a variety of non-galling materials and finishes are used. Mandrels are lathe-turned, machine-finished, and ground-finished or plated, depending on bend quality and tool economy. Tool steels of about 70 R_c hardness with a good finish are commonly used as mandrel-materials. Chromium plating is also a common practice. However, for such materials like stainless steel and titanium, aluminium-bronze alloys are used with good success. The size of the mandrel should be nearly that of the tube inside diameter, so that maximum support of the tube wall is gained. However, a sufficient clearance, of not more than 10-15 per cent of the wall-thickness, must be maintained so that the material can slide on and off the mandrel. Wrinkles may form as a result of employing an undersized mandrel as shown in figure 2.7. Finally, the position of the mandrel

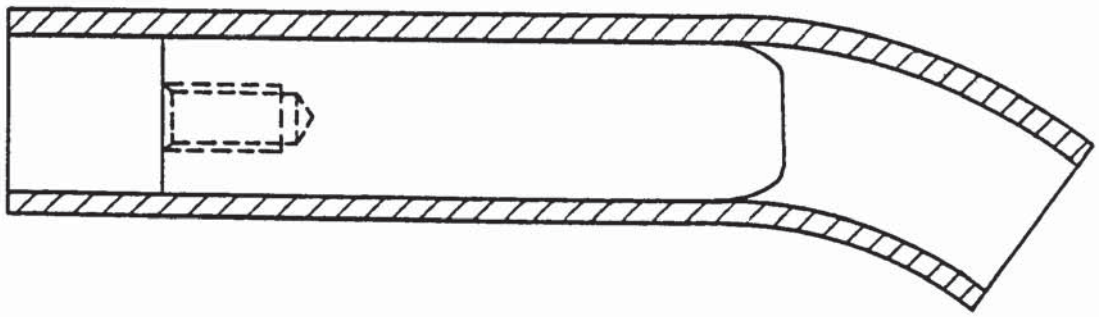

PLUG

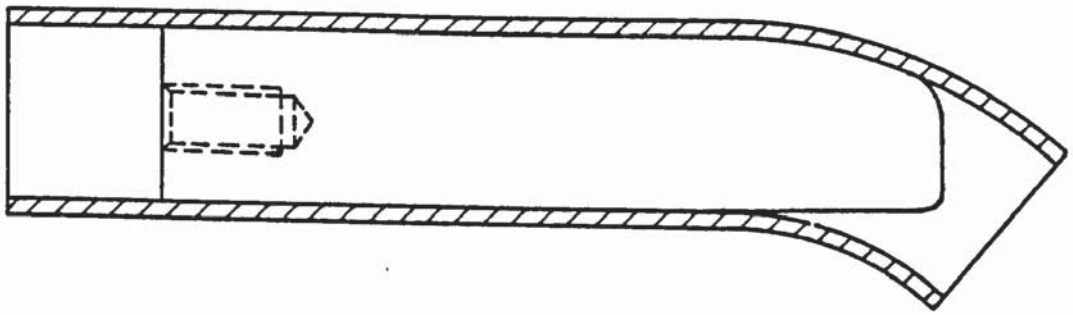

FORM

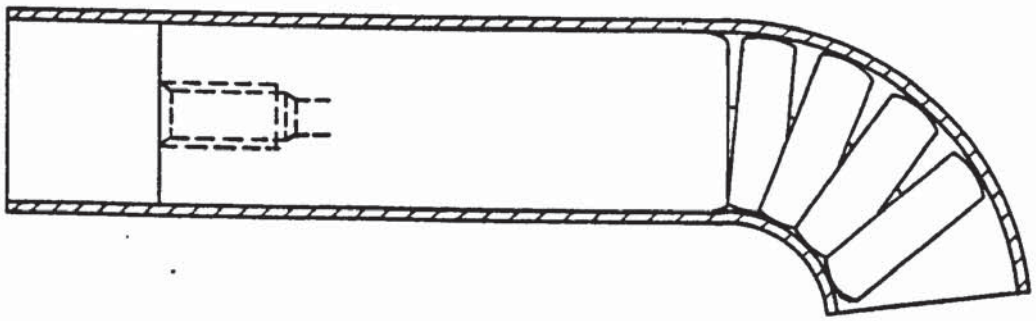

FLEXIBLE BALL

Figure 2.6: Basic types of mandrel

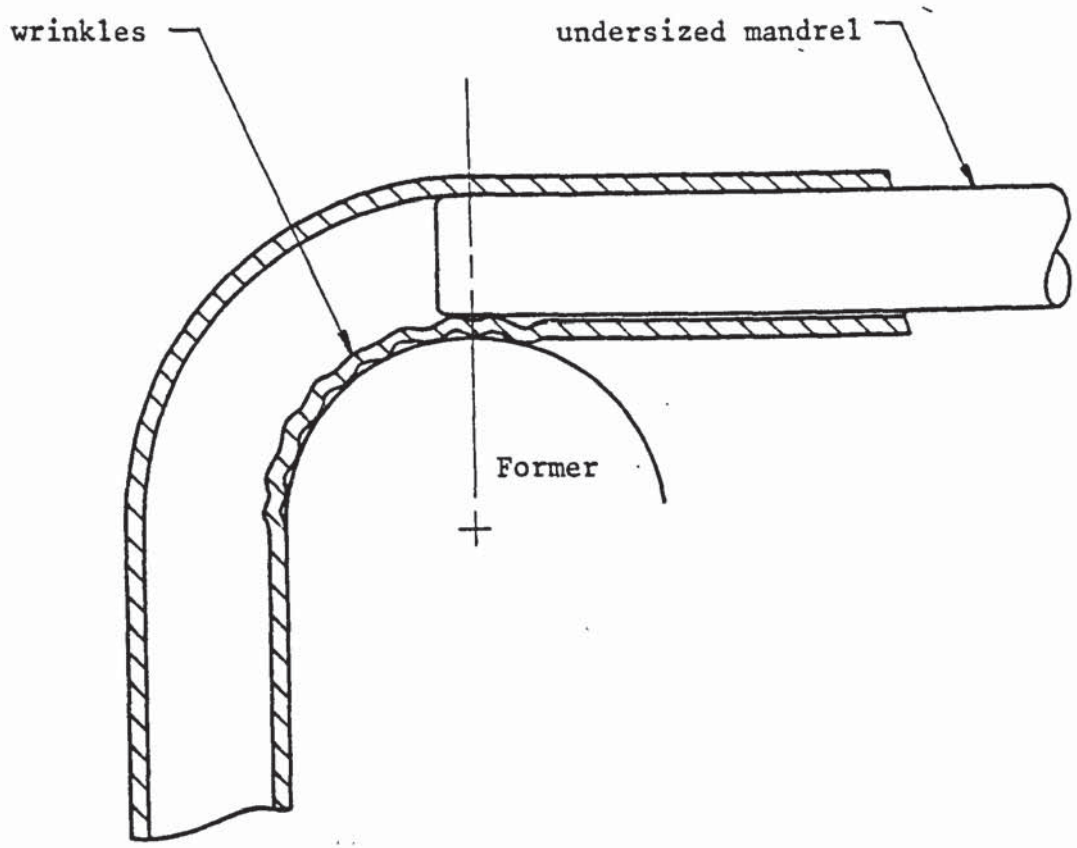

Figure 2.7: Employing an undersized mandrel results in the formation of wrinkles

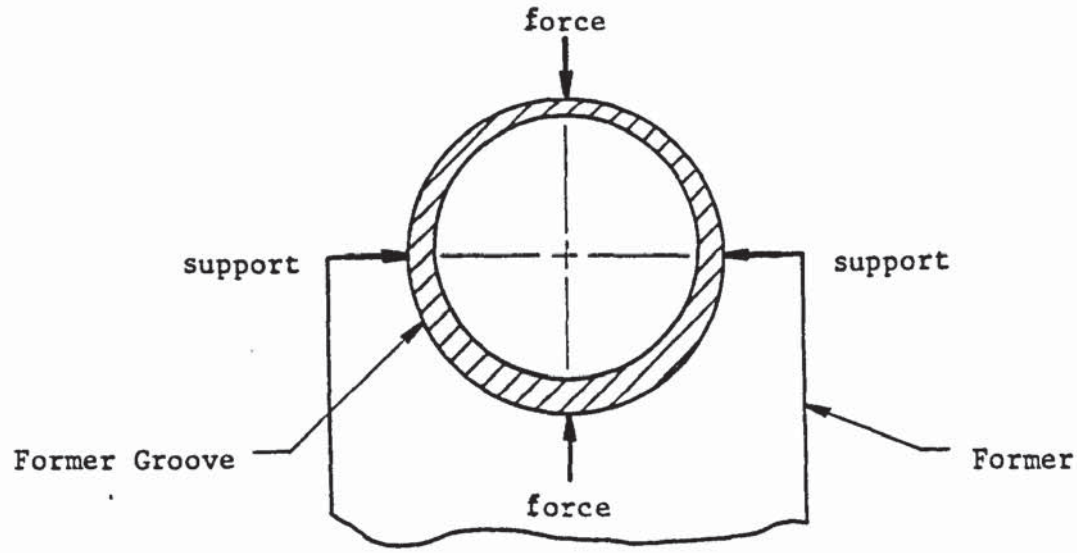

Figure 2.8: A former supports the tube section during bending and helps to prevent its flattening

with respect to the other bending tools is very important. From experience, the mandrel-tip must always be advanced forward a little, to give the best support to the tube during bending.

2.1.3 Some important considerations in the bending process

Producing a good quality bend does not only depend on the proper design and manufacture of bending tools but also on their correct adjustment and fitting before bending. Some technical publications[4,10] have discussed the basic requirements of tooling set-up in order to help avoid serious defects which may result during bending and to avoid poor quality bends.

Considering the effects of bending without a mandrel, when the tube outside diameter to wall thickness ratio is relatively small and the mean bend radius is, for example, less than four times the tube diameter; the forces across the tube section in the bending area, ie. in the vicinity of the tangent line, tend to make the tube oval. Although in this case excessive flattening of the tube should not occur but the outside and the inside of the bend have a tendency to pull towards the centreline of tube resulting in its flattening. The support given to the sides of the tube by the grooved former helps to prevent the tube from flattening, figure 2.8. Also, the springback effect which will cause the tube to unbend to a certain extent, depending on the radius of bend, is excessive when a mandrel is not used. However, the amount of tube springback can be affected by the location and the initial pressure of the slider. The correct setting of the slider, as illustrated in figure 2.9, helps also to prevent the tube from being kinked or buckled, figure 2.10, as the material, not being able to compress, pushes in

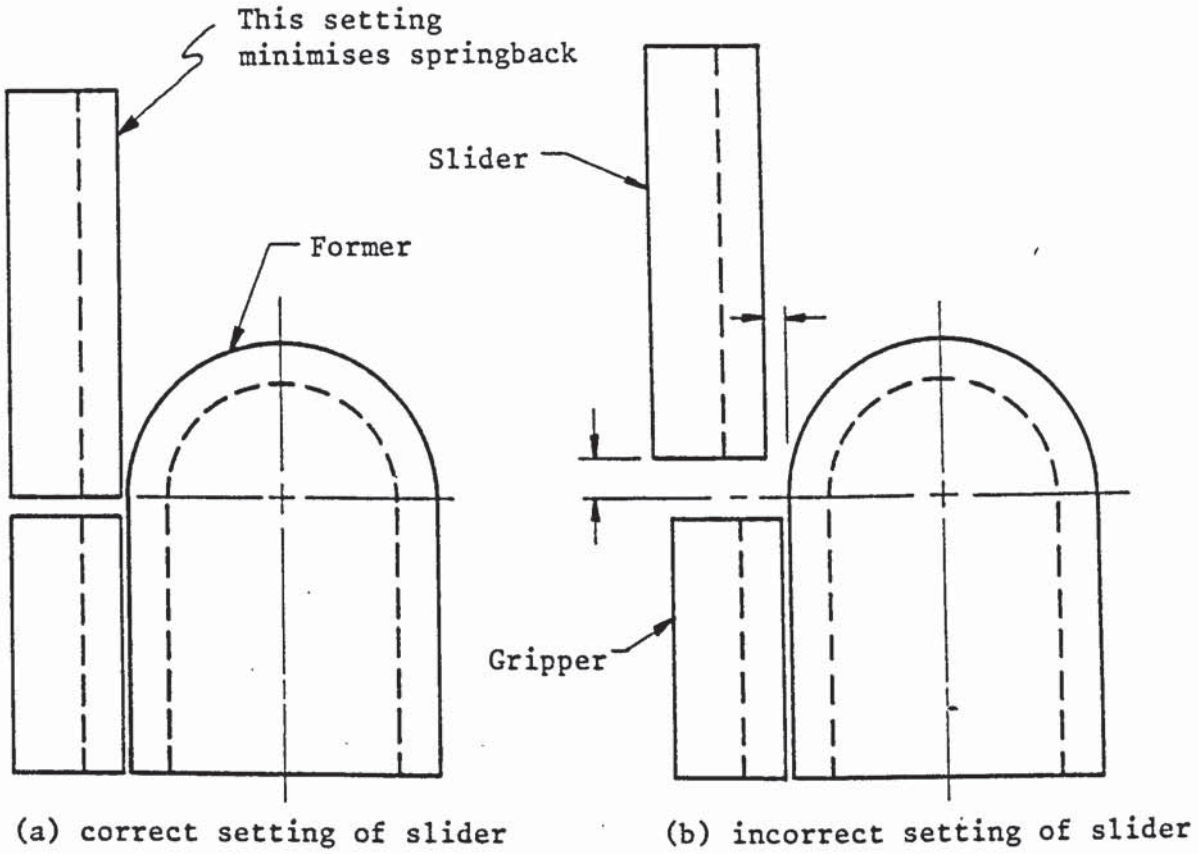

Figure 2.9: Correct setting of slider helps minimise springback and prevent wrinkles (10)

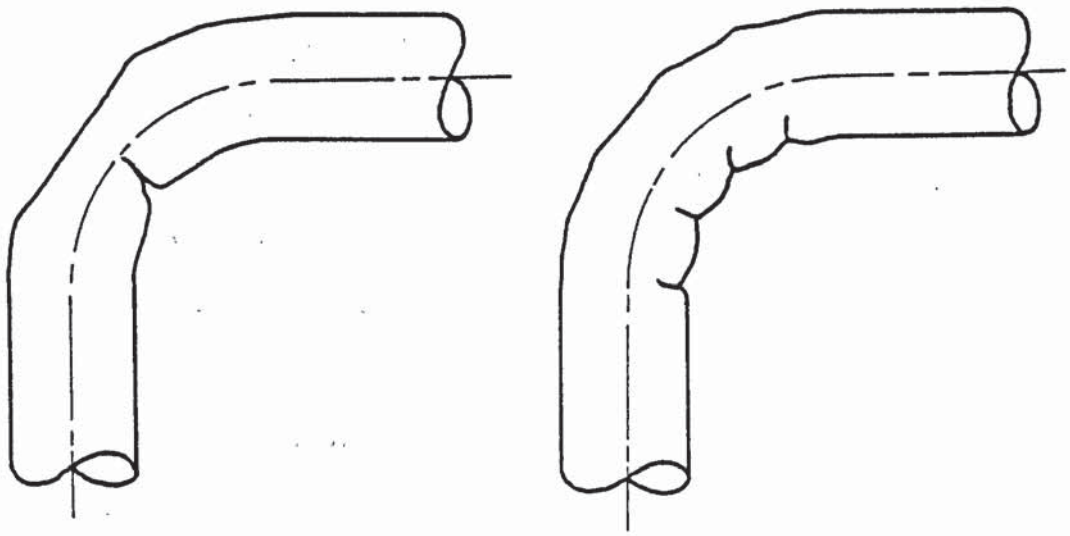

Figure 2.10: Kinked or buckled bends (10)

towards the tube centreline.

As the tube-wall thickness decreases and the bend radius becomes small, and because the tube material is stretched on the outside of bend and compressed on the inside, excessive flattening is almost certain to occur at the outside surface of the bend as this stretching takes place. Accordingly, it should, in this case, be necessary to support the tube internally during bending with the use of a mandrel in order to prevent the tube from flattening and buckling. As shown in figure 2.12, the material stretching is done on the forward tip of the mandrel and consequently the pressure exerted on the mandrel-tip supports the inside of the bend; holding it firmly into the former groove and minimising the tendency of tube-wall to wrinkle. Thus, because the tube material stretches mainly just after the tangent line, it is essential to set the mandrel adequately forward. However, the location of the mandrel with respect to the tangent line is very delicate and important. Obviously, if the mandrel is too far back, and apart from a greater amount of flattening, the developed pressure is not high enough to prevent wrinkles, figure 2.11. As the mandrel is positioned further forward, as shown in figure 2.12, the 'correct' pressure is developed and the tube-wall thickens only under compression without wrinkles. Conversely, when the mandrel is too far forward, as illustrated in figure 2.13, bumps may appear on the outside of the bend at the terminal tangent and a step is created on the bend inside at the starting tangent. This setting may also result in tube slippage from the clamping area or, possibly, in tube breakage. There is, however, no specification for correct mandrel setting, which depends very much on trial and error. As a general guide the amount the mandrel is advanced should be increased as the bend radius becomes larger, see figure 2.14.

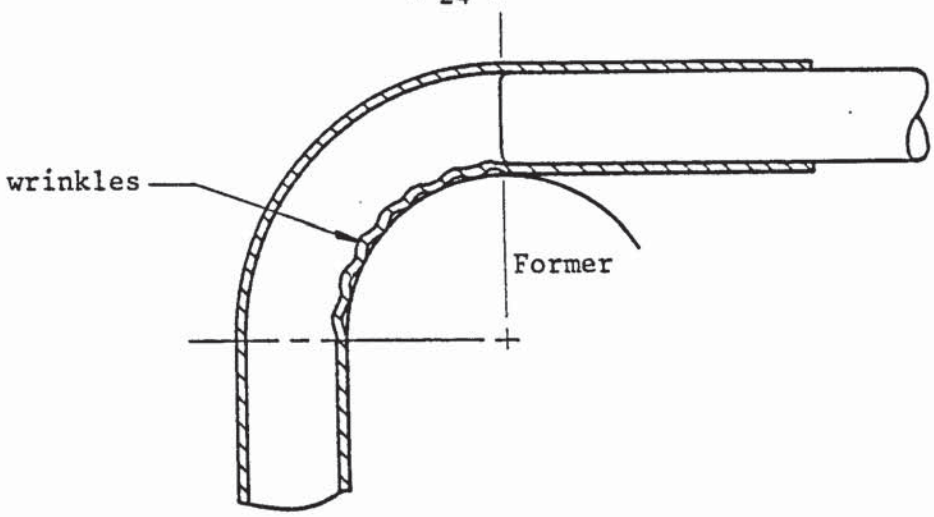

Figure 2.11: Mandrel too far back

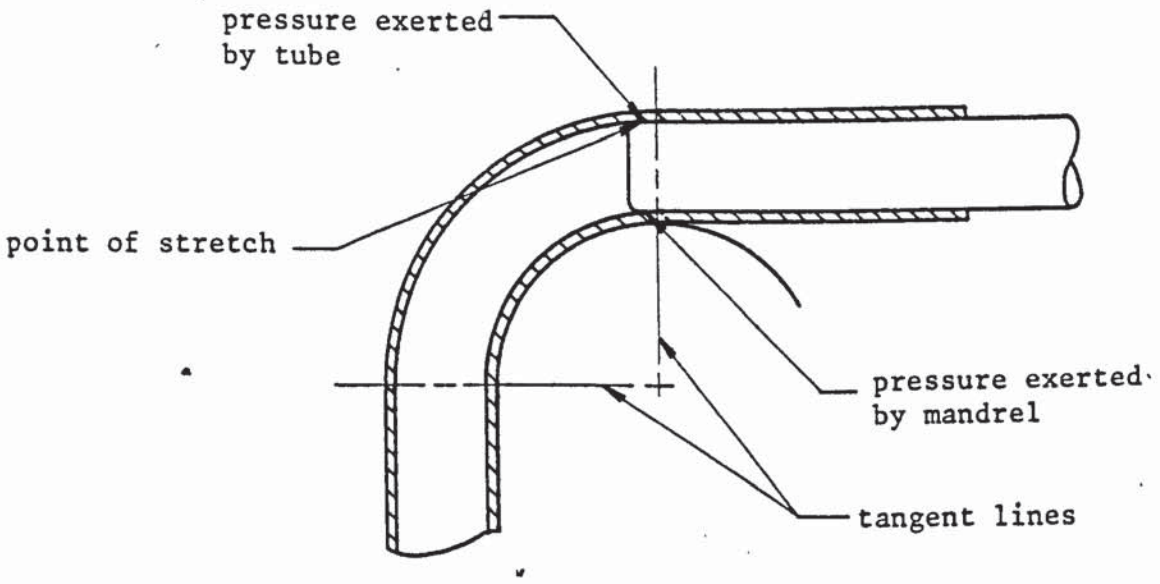

Figure 2.12: Mandrel in correct position

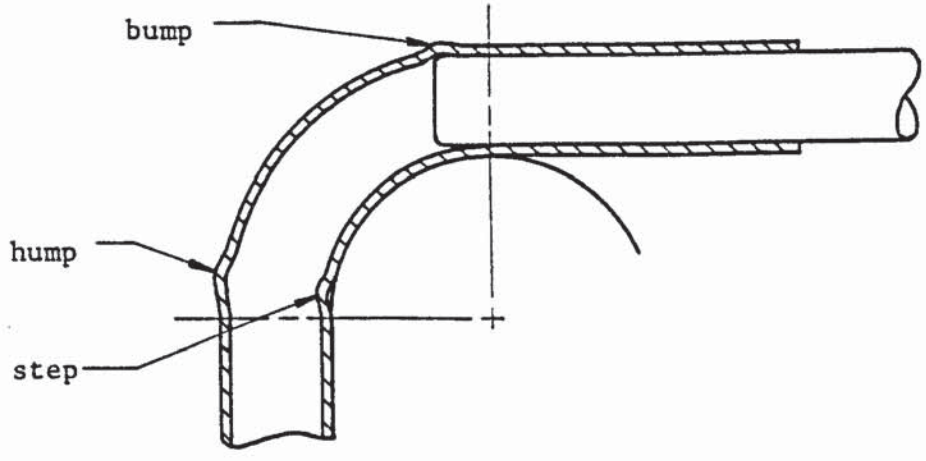

Figure 2.13: Mandrel too far forward

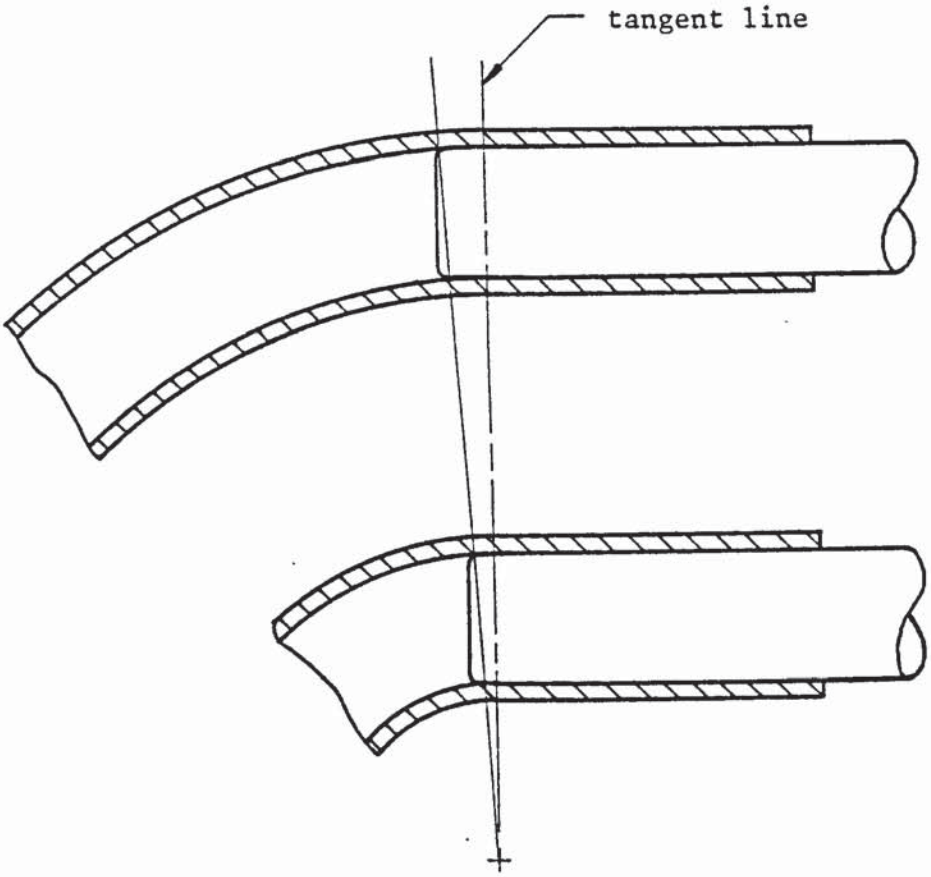

Figure 2.14: Mandrel advance beyond the tangent line increases as the bend radius becomes larger

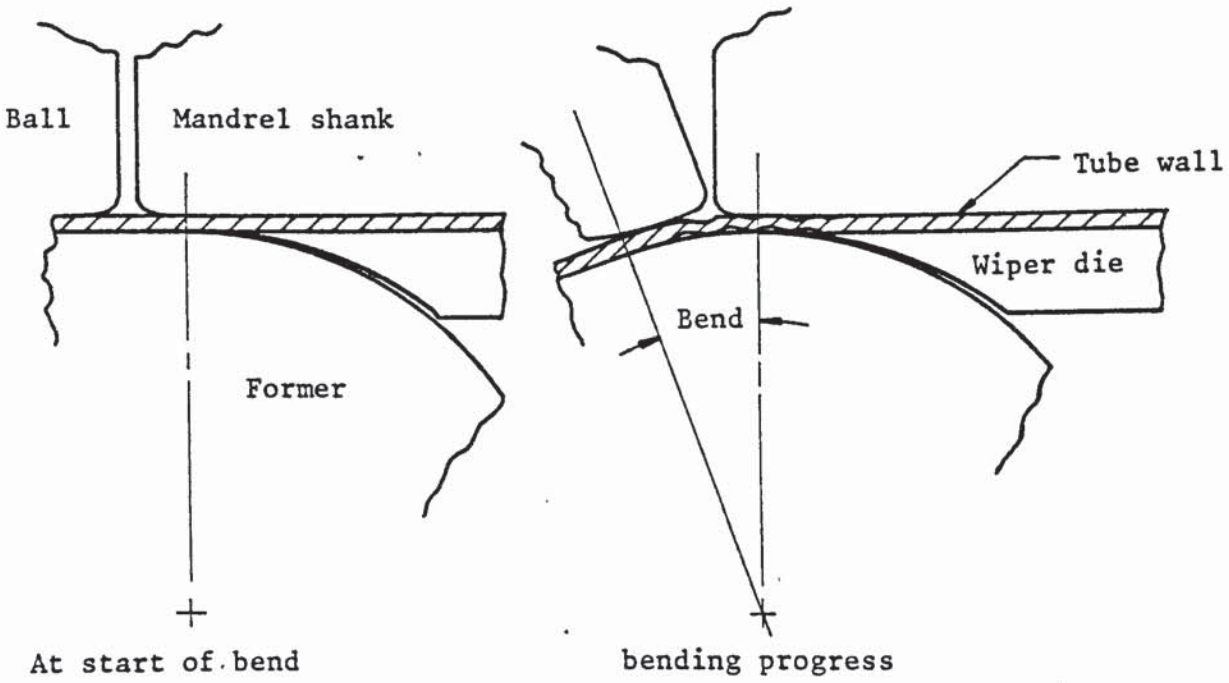

Figure 2.15: Improper setting of wiper die causes wrinkles on the bend inside

It can be concluded that with the use of mandrel, either plug, form or flexible-ball, the considerations mentioned before should be borne in mind as an incorrect positioning of the mandrel can result in poor quality bends. Also, those considerations as described for the plug-mandrel do apply for the form and flexible-ball mandrels.

When bending thin tubes to small bend radii, it may be essential to employ a wiper die which helps to avoid wrinkles forming on the inside of the bend. Fitting the wiper die correctly is most important to achieve acceptable results. The trailing edge of the wiper die must be supported by the former groove otherwise it will spring away from the mandrel and cause the tube inside-wall to wrinkle as illustrated in figure 2.15. It is also necessary to bring back the flat end of the wiper die out of contact with the tube surface in order to minimise drag. This rake should be adjusted properly and the wiper die has to be advanced as close as the tangent line for good quality bends to be produced.

2.2 Literature review of the mechanics of tube bending

2.2.1 Previous theories

The practice of tube bending is considered to be much more advanced than any published theoretical understanding of the mechanics of deformation taking place during the process. Few theoretical results have been published on draw-bending of tubes and thus it is an area of metal deformation which is largely unexplored. However, reviewing the previous theories of tube bending with more attention being paid to the latest theoretical approaches can provide a basis for the development of

any new models.

2.2.1.1 Distribution of strains in a bent tube

In their early theory to predict the strain distribution in a tube bend, Weil et al[16] assumed no meridional strain (around the periphery of the tube section) developing during deformation. The circumferential strain, ie. along the tube length, at any angular position (ϕ) was defined as:

$$\varepsilon_\theta = \ln(1 + \frac{r}{R}\sin\phi)$$

where r is the tube radius, and R is the bend centreline radius. Considering the condition of volume constancy during plastic flow, the radial strain was:

$$\varepsilon_r = -\varepsilon_\theta$$

However, the experimental results by Inoue and Mellor[17] showed that the meridional strain is quite significant in tube bending and indeed should not be ignored. Hence, the assumption of zero meridional strain is not necessarily valid since it would overestimate the radial strain and also the amount of outside-wall thinning. Weil et al[16] also assumed that the tube centreline axis remains unchanged during bending and consequently the change in the position of the neutral axis was neglected in the strain calculations. However, it is clear, due to the thinning and the thickening of the tube wall, that the neutral axis must lie well

below the centreline axis, ie. closer to the centre of bend. Furthermore, no friction effects were taken into account in the theoretical analysis although in all industrial bending processes friction has a significant effect on metal deformation.

More recently, Inoue and Mellor[17] proposed a theory to predict the strain distribution in tube bends. It was assumed that bending occurs under simple tension, and that the circular cross-section did not change and all friction forces were neglected. The circumferential strain at any bend radius R was defined as:

$$\varepsilon_\theta = \ln \frac{R}{R_N} \qquad 2.1$$

where R_N is the radius to the neutral plane of the tube bend. The relationship between the three principal strains is:

$$\varepsilon_\theta = -2\varepsilon_r = -2\varepsilon_\alpha$$

where ε_r and ε_α are the thickness and meridional strains respectively.

The position of the neutral plane (R_N) was determined from a compatability condition which assumes that the sum of the meridional strains over the tube section is zero, ie:

$$\int_{-\frac{\pi}{2}}^{\frac{\pi}{2}} \varepsilon_\alpha \, . \, d\alpha = 0 \qquad 2.2$$

It was shown that the theory has a reasonable correlation with the

measured strains when bending tubes to a mean bend radius of approximately three times the tube outside diameter. However, it was clear that the measured thickness strains have greater numerical values than the measured meridional strains. In a further study[18], it was shown that the theory proposed by Inoue and Mellor[17] proved to be inadequate for the prediction of the strain distribution when bending tube to tight radii, eg. for mean bend radius to tube outside diameter equal to 1.5. The difference between the measured and predicted values is understandable since the bending process is far from being a uniaxial stress operation and the friction between the tube bore and the mandrel can be high and hence it has a significant effect on the mechanics of deformation during bending.

Inoue[19] adopted another theoretical approach to predict the distribution of strains, which included the effect of the meridional stress. The circumferential and meridional stresses were assumed to be in the principal directions. Also the thickness stress, being small compared with the material yield stress, was neglected. The distribution of the thickness strain was assumed to be:

$$\varepsilon_t = c(\sin\alpha - \sin\alpha_n)$$

where c is a constant satisfying the compatability condition, ie. equation 2.2, and α_n is the angular position of the neutral plane which was determined from the equilibrium equation. The circumferential strain was obtained according to equation 2.1 while the meridional strain was calculated from the condition of constant

volume, ie:

$$\varepsilon_\alpha = -(\varepsilon_\theta + \varepsilon_t)$$

It was shown that this solution gives a reasonable prediction of the distribution of strains under certain friction conditions.

A recent theory was developed by Kasim[20] to predict the strain distribution in a bent tube. In the theoretical solution, the apparent circumferential strain was predicted as:

$$E_c = \ln\left(\frac{CLR + r\cos\alpha'}{RU}\right)$$

where CLR = the centreline bend radius

RU = the radius of the unstretched fibre

r = the mean radius of tube

and α' = the angular position of any fibre in the meridional direction after bending

as shown in figure 2.16.

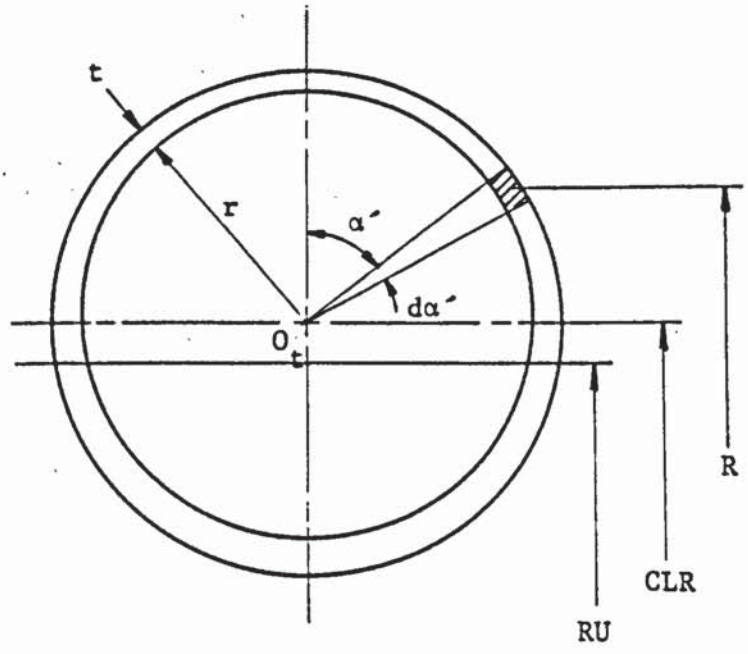

Figure 2.16: A small element of tube [20]

Assuming no change in tube radius r after bending, the apparent meridional strain was calculated such that:

$$E_m = \ln \frac{d\alpha'}{d\alpha}$$

The condition of compatability between the tensile and compressive parts of tube section was assumed to be:

$$\sum_{k=1}^{m} d\alpha = \sum_{k=1}^{m} d\alpha' = \pi \qquad 2.3$$

where $d\alpha$ and $d\alpha'$ are the angles of a small element before and after bending respectively, and m is the number of elements in the tube cross-section.

One of the predicted solutions was based on the uniaxial stress conditions, the material was assumed to be non-workhardening and thus the state of stress, at any point on a tube section, was given by:

$$\sigma_c = Y, \ \sigma_m = 0 \text{ and } \sigma_t = 0$$

where σ_c, σ_m and σ_t are the principal circumferential, meridional and thickness stresses respectively, and Y is the yield stress of tube material.

Also, the three principal strains were related such that:

$$E_c = -2E_m = -2E_t$$

Using the compatability equation 2.3, the radius of the unstretched

fibre was predicted as:

$$RU = \frac{\int_0^{\pi} \sqrt{CLR + r\cos\alpha'}\, d\alpha'}{\pi}$$

It was concluded, however, that this theory is not adequate since the equilibrium of forces was not taken into consideration and the ratio between the strains was always considered constant. Consequently, the equilibrium equation would not necessarily be satisfied and also different materials were assumed to have the same strain pattern[20].

Kasim in the same thesis considered a more precise solution in which the states of stress and strain were related to the material properties such that:

$$\bar{\sigma} = H\bar{\epsilon}^{n}$$

where $\bar{\sigma} = [\sigma_c^2 - \sigma_c \cdot \sigma_m + \sigma_m^2]^{\frac{1}{2}}$

and $d\bar{\epsilon} = [1.333(dE_c^2 + dE_c \cdot dE_m + dE_m^2)]^{\frac{1}{2}}$

The thickness stress was considered to be small compared with the material yield stress and thus it was neglected. The incremental strains were related to the stresses through the flow rule. Thus, the incremental apparent strains were derived such that:

$$dE_m = [(2\sigma_m - \sigma_c) / (2\sigma_c - \sigma_m)] \cdot dE_c$$

$$dE_c = [(\sigma_c - .5\sigma_m) \cdot d\bar{\varepsilon}/\bar{\sigma}]$$

and $dE_t = -(dE_c + dE_m)$

Additionally, the equilibrium of forces in the circumferential, meridional and thickness directions were considered, which led to the following equations:

$$(1) \quad \Sigma\sigma_c \cdot dA = F$$

where F is the axial force at the end of tube

$$(2) \quad d\sigma_m = -\frac{r}{R} \cdot \sin\alpha' \cdot \sigma_c \cdot d\alpha'$$

which was used to predict the meridional stress around the tube periphery

$$(3) \quad p = [\frac{\sigma_c}{R} + \frac{\sigma_m}{r}] \cdot t$$

where p is the pressure exerted on the tube internal surface by the mandrel and on the tube external surface by the former (bend die). The friction force was represented by a tensile force, F, at the end of the tube. The effect of applying a superimposed compressive force (booster force) at the tube end was also considered. The theoretical solution based on the previous analysis was developed and the calculations were performed using a computer programme. A comparison between the theoretical strain distribution and a limited experimental range of data was made.

It was shown that the predicted apparent circumferential strains were in good correlation with the experimental values. However, the greatest deviation between the experiments and the theory for both the meridional and thickness strains were at the inside of the bend. The author attributed this difference to the lack of information about the behaviour of material in compression, particularly for high strain values.

2.2.1.2 Variation of tube-wall thickness after bending

One of the most important problems associated with draw bending of tubes is the variation of tube-wall thickness due to bending. Based on their theory, Weil et al[16] determined the wall-thickness variation in a tube bend as:

$$\frac{t}{t_o} = \frac{1}{1 + k \sin\phi}$$

where t_o = the initial tube-wall thickness

t = the final thickness at an angle ϕ

k = the ratio between the tube radius (r) and the centreline radius (R)

In the same paper, the following expression for the minimum wall thickness in a bent tube was reported by Gardner:

$$\frac{t}{t_o} = (1 + k)^{-\frac{1}{2}}$$

based on the assumption of equal meridional and thickness strains.

Möller[21] assumed uniform deformation along the tube bend axis. Thus the ratio between the minimum wall-thickness (s_a) at the outside of the bend and the wall-thickness (s) in the straight tube is equal to the ratio between the bent length of the outer fibre and that of the neutral fibre, ie:

$$s_a = s / (1 + \frac{d_a}{2R_m}) \qquad 2.4$$

Similarly, the maximum tube-wall thickness at the inside of the bend is:

$$s_i = s / (1 - \frac{d_a}{2R_m}) \qquad 2.5$$

where d_a = the tube outside diameter

R_m = the centreline bend radius

However, it can be seen from equations 2.4 and 2.5 that the neutral axis was assumed to coincide with the geometrical centreline axis and thus the wall-thinning and -thickening effect on the equilibrium of forces was neglected.

Other formulae were reported by Oehler[22] for the minimum and maximum wall thicknesses, S_z and S_d, at the outside and the inside of a tube bend respectively. Taking into account the effect of the bend angle (α) in comparison with 90 degree bend angle as a datum, the following expressions were given:

$$s_z = s_o - \frac{0.8d_i}{2r_m} \sqrt[4]{\frac{\alpha}{90}} \qquad 2.6$$

$$\text{and } s_d = s_o + \frac{0.9d_i}{2r_m}\sqrt[4]{\frac{\alpha}{90}} \qquad 2.7$$

where d_i = the tube inside diameter

r_m = the centreline bend radius

s_o = the initial tube-wall thickness

Equations 2.6 and 2.7 are empirical and are not based on any theoretical analysis.

Both Möller and Oehler ignored the effects of mandrel friction and tube material work-hardening characteristics on the variation of tube-wall thickness as a result of bending.

A numerical analysis which predicted the change in wall thickness of the tube during bending was developed by Sato and Takahashi[23]. The calculations were based on the assumption of uniaxial tension and the wall-thickness was considered small compared with the tube diameter. The authors examined the effects of the anisotropy of tube material, as represented by the r-value, and the superimposed compressive force on the changes of tube-wall thickness which showed good agreement with their experimental results using copper tubes.

2.2.1.3 Bending torque

The torque M_b required to bend a tube having an outside diameter d_a and an inside diameter d_i was given by Ohler[22] as:

$$M_b = 50\sigma_s \cdot \frac{(d_a^4 - d_i^4)}{d_a}$$

where σ_s is the yield stress of tube material. In the same paper, Ohler reported the following expression for the bending moment M_d [kp.m] required to bend a tube of outside diameter d_a [mm] to a centreline radius r_m [mm]:

$$M_d = 0.001 \mu \cdot W \cdot \sigma_B \cdot \sqrt[3]{\frac{d_a}{r_m}}$$

where W is a correction factor which is equal to:

$$0.1 \left(\frac{d_a^4 - d_i^4}{d_a}\right) \quad \text{for thick tubes, ie. } s > .06\, d_a$$

$$\text{or} \quad 0.8\,(d_a - s)^2 \quad \text{for thin tubes, ie. } s < .06\, d_a$$

where d_i = the tube inside diameter [mm]

s = the original tube-wall thickness [mm]

μ = 2 for normal plug

= 3 for flexible mandrel

= 5-8 for dry conditions

σ_B = the tensile strength of tube material [kp/mm^2]

An empirical approximate value for the bending machine torque TBM can be obtained from the following formula:

$$TBM = K[OD^3 - (OD - 2t)^3] \text{ [tonf.in]} \qquad 2.8$$

where OD and t are the outside diameter and initial wall thickness

of tube and K is a factor depending on the tube material properties and is equal to 5.5, 8 and 10.5 for copper, steel and stainless steel respectively.

Equation 2.8 was reported in "Tube Bending" booklet[4] which gives an additional factor having different values depending on the mandrel type.

2.2.2 Experimental results

Franz[24], using a form-mandrel, considered the bending of relatively thick-walled tubes to a mean bend radius which was approximately equal to the tube outside diameter. It was reported that the amount of wall thinning can be reduced by applying a direct booster force to the tube during bending.

Recker and Buchmüller[25] desribed the process of draw-bending of tube without the internal support of a mandrel. Steel tubes having 38 mm outside diameter and 4 mm wall thickness were bent to a mean bend radius of 60 mm. Th effect of applying a booster force to the slider and the tube during bending was examined. It was shown that the booster force reduces the maximum tube-wall thinning at the bend outside while increasing considerably the maximum thickening of the tube wall at the inside of the bend. Also, it was observed that the out-of-roundness of the tube section was less with applied booster force than under conventional conditions. Recently, similar results were obtained by "Tools for Bending, Inc."[26] using an 'incremental pressure die assist' system with 'empty' bending tools. It was also shown that the use of a mandrel oscillator could achieve better results. The application of mandrel oscillators was described by Stange[14].

Devices that retract and advance the mandrel while the tube is being bent can be used for bending thin-walled tubes; low frequencies in the range from 1 to 500 cycles per minute and strokes in the range from $^1/_8$ to 1 inch can be used. It was reported that oscillating the mandrel, multi-ball type, prevents the tube from being formed around the mandrel balls and also helps to minimise wall "thin-out" and preserve tube roundness.

In a statistical manner, Möller[21] examined the changes in tube-wall thickness and out-of-roundness of tube section after bending. The effects of tube outside diameter, initial wall thickness and centreline bend radius on the maximum amounts of thinning and thickening on the outside and the inside of tube bend respectively were considered. Further, the results of testing the tube bends under high hydraulic pressure (high surge rupture test) were reported.

Inoue and Mellor[18] investigated the radial-draw bending of thin-walled stainless steel tubes to centreline bend radii varying from 1.5 to 4 times the outside tube diameter. The effects of changing lubrication conditions on the strain distribution, the mandrel-bar tension and the bending torque were examined. It was shown that improving the effectiveness of lubrication between the mandrel and the tube bore reduced the amount of tube-wall thinning on the bend outside. Also, when a booster force was applied to the pressure die (slider), the authors found that effects similar to an improvement in lubrication were obtained.

More recently, Kasim and Mellor[27] studied the effect of material properties on the strain distribution in draw bending tubes. Experimental results for bending mild steel and stainless steel thin-walled tubes to a centreline bend radius equal to 1.5 times the outside

diameter were reported. It was found that the maximum circumferential strain on the outside of bend is higher for mild steel than for stainless steel. The authors attributed this result to the greater effect of frictional forces on the straining of mild steel tubes when compared with stainless steel. However, the mandrel tension for the two materials was almost the same and hence the authors suggested that lubrication was more effective with the stainless steel than with the mild steel.

In their experimental study of the influence of the anisotropy of copper tubes, Sato et al[28] described a process of tube fabrication to achieve certain anisotropy. The influence of the r-value, ie. the ratio between the circumferential and thickness strains on the strain distibution in a bent tube was reported. It was shown that both thinning and thickening of tube wall on the outer and inner peripheries respectively can be reduced if the tube material has high r-value. Thus, it was claimed that it may be possible to achieve copper bends with wall thickness evenly distributed by the use of tubes having considerably higher r-values.

2.3 Ultrasonic metal deformation

The objective of this section is to provide an adequate understanding of the subject of ultrasonic metal deformation. The early theories of the influence of applied vibratory energy on the properties of metals as well as on the contact friction will be reviewed briefly. Also, the fundamental mechanisms which explain the effects of applying ultrasonic oscillations to metal working processes are outlined. Finally, despite the fact that no extensive studies on the application

of ultrasonic vibrations to the process of draw-bending of tube have been made, it is worthwhile to review some of the published results concerning ultrasonic metal deformation processes. However, it is not intended to perform an exhaustive review of the literature but rather to concentrate on those publications which have contributed significantly to a better understanding of the mechanics of metal deformation under oscillatory conditions.

2.3.1 General introduction

2.3.1.1 Influence of vibrations on metal properties

The influence of applying ultrasonic energy on the plastic deformation of metals was first observed by Blaha and Langenecker[29], in 1955, who discovered the decrease in the static stress due to superimposed ultrasonic vibrations in tensile testing of zinc crystals. An ultrasonic generator operating at 800 kHz with a maximum output of 25 watt (2 w/cm^2) was used. It was shown, figure 2.17, that intermittent applications of vibration reduced the tensile stress by about 40% and that upon turning off the power, the stress returned to its original value. Figure 2.17 shows also that continuous application of ultrasonic vibration during the tensile test lowered considerably the stress-strain curve. Similar results[30] were obtained when testing cadmium and zinc crystals at frequencies in the range of 15 kHz to 1.5 MHz which confirmed that the amount of reduction in the tensile stress is proportional to the intensity of ultrasonic power and does not depend on the vibration frequency.

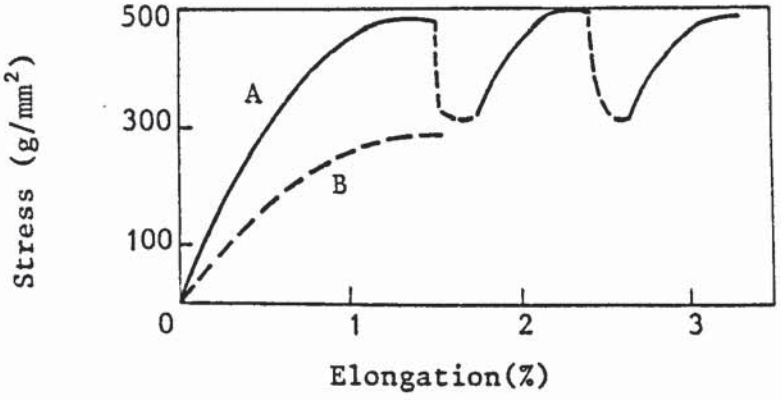

Figure 2.17: Effect of superimposed 800 kHz ultrasound on the tensile deformation of zinc crystals. Specimen coupled to ultrasonic generator by immersion in insonated liquid bath. A - Intermittent application of ultrasound; B - continuous application of ultrasound (after Blaha and Langenecker[29])

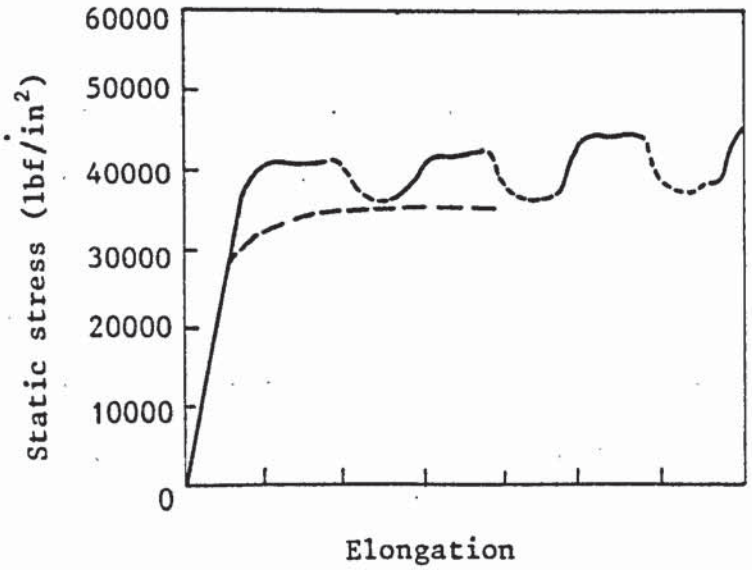

Figure 2.18: Effect of superimposed mechanical vibrations of 15 to 80 kHz on the tensile deformation of low-carbon steel wires. Upper curve - intermittent application of vibrations; lower curve - continuous application of vibrations (after Nevill and Brotzen[31])

In 1957, Nevill and Brotzen[31] investigated the effect of mechanical vibrations of frequencies between 15 and 80 kHz on the tensile plastic deformation of low-carbon steel wires. Under a small amount of tension, the wire specimen was vibrated and the frequency of oscillations was adjusted until longitudinal standing waves were obtained. It was reported that with ultrasonic vibrations, figure 2.18, the stress necessary to cause plastic deformation was reduced and that the amount of stress reductions proved to be proportional to the amplitude of vibrations as shown in figure 2.19. Also, the drop in the apparent yield stress was found to be independent of vibration frequency. The results obtained by the authors[31] were explained by the superposition of steady and alternating stresses.

In a later work, Pohlman and Lehfeldt[32] carried out a series of tensile tests on pure polycrystalline copper with applied ultrasonic vibrations at a frequency of 20 kHz. The ultrasonic power was provided with the use of a magneto-strictive transducer. The total length of the sample was $3\lambda/2$, λ is the vibration wavelength, so that resonance occurred at the operating frequency while the gripping planes were at vibrational displacement nodes. It was found that the observed reduction in the tensile stress is proportional to the oscillatory stress amplitude and this result was explained also by the superposition of the induced acoustic stress on the static stress.

More recently, Winsper and Sansome[33] studied the mechanism of reduced stress by conducting a series of tensile tests on duralumin and plain-carbon steel specimens with superimposed oscillatory energy. The tests were performed at a frequency of

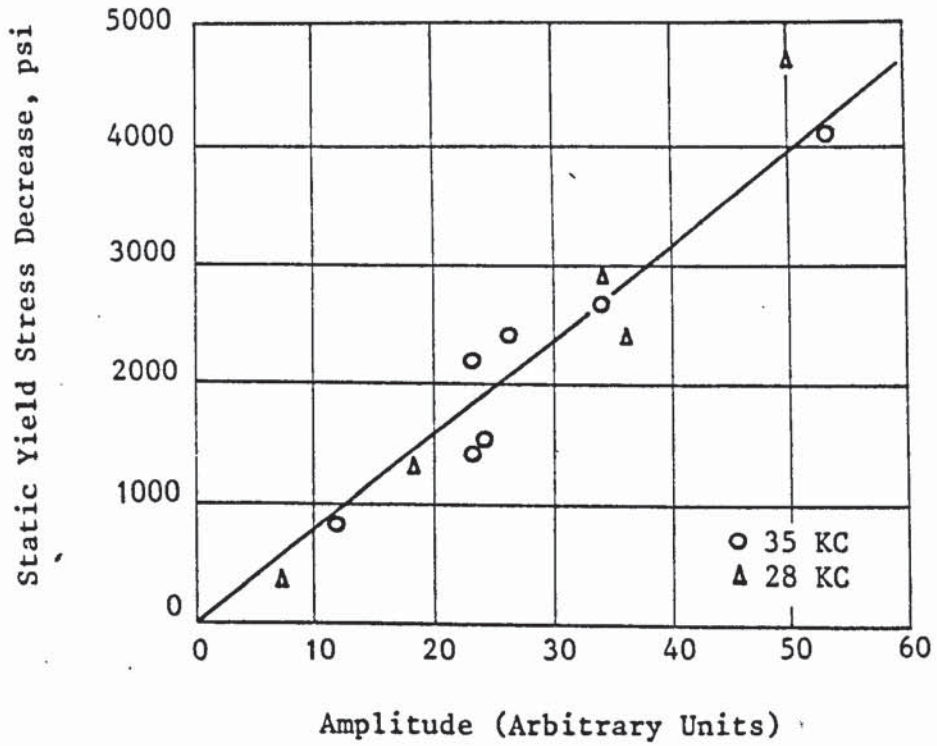

Figure 2.19: Effect of amplitude of vibration on static yield stress decrease at room temperature (after Nevill and Brotzen[31])

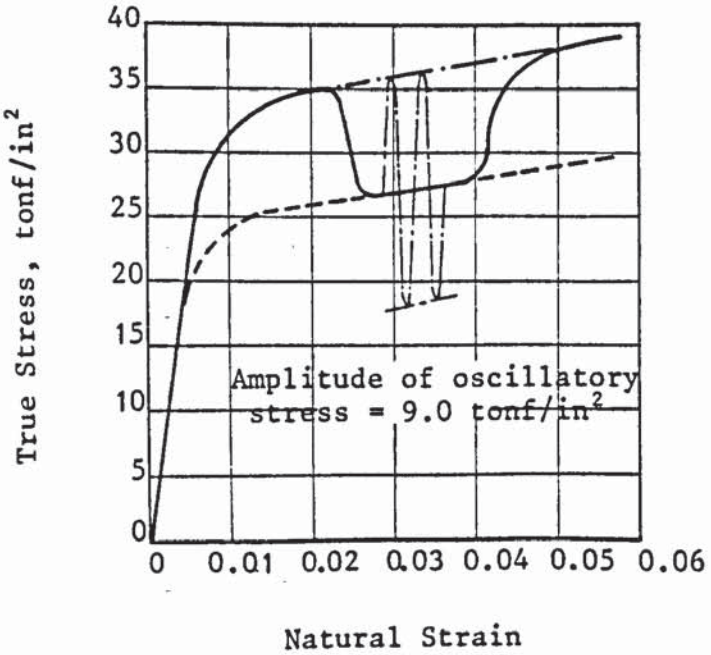

Figure 2.20: Stress/strain curve for Duralumin, showing the effect of applying oscillatory energy (after Winsper and Sansome[33])

100 kHz. It was found that the yield stress was reduced abruptly on applying oscillations and that the amount of reduction in the static stress was equal to the amplitude of superimposed oscillatory stress as shown in figure 2.20.

In subsequent work Langenecker and colleagues[34-36] examined the effects of much higher intensities of ultrasonic power. Interesting data were obtained, figure 2.21 and 2.22, for the stress-strain curves of zinc and aluminium single crystals during tensile deformation. Tests were carried out at different amplitudes of vibration at room temperature or without vibrations at different temperatures. It was shown that upon reaching a certain level of ultrasonic energy, which depends on the properties of the metal, plastic deformation would occur at room temperature without an external load. It is clear from a comparison of the curves of figure 2.22 that ultrasonic oscillations and heating have a similar effect on the static yield stress. However, to achieve the same reduction with the use of vibrations required significantly less energy than with heating. Langenecker et al[36] suggested that the effects observed were due to localised heating which takes place in regions around dislocations and other imperfections when ultrasonic energy is applied.

The phenomena of metal hardening with applied high amplitude ultrasonic vibrations was reported by Langenecker[37]. During tensile tests of zinc single crystals, ultrasonic vibrations at a frequency of 25 kHz and a stress amplitude of 360 lbf/in^2 were applied intermittently. Figure 2.23 shows the variation of shear stress with the glide strain. It can be seen that on initial application of vibrations the shear stress drops to point 'b' and

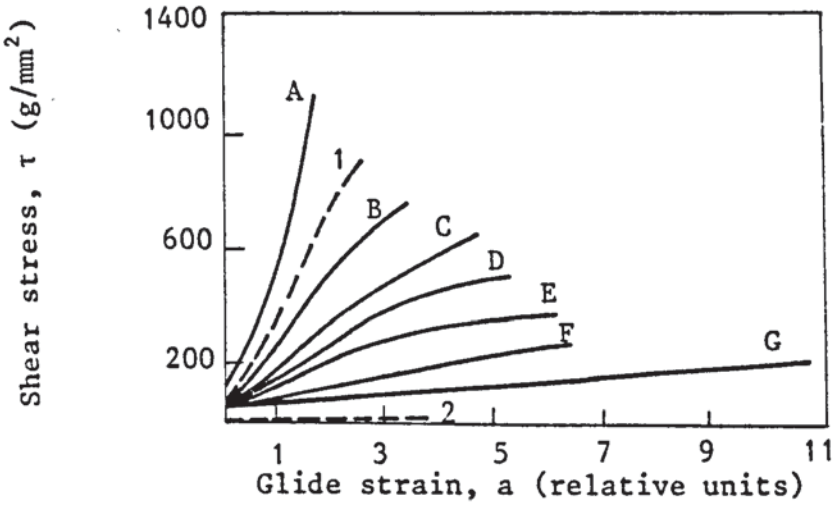

Figure 2.21: Stress-strain curves of zinc crystals obtained during continuous application at 25 kHz ultrasound at either amplitudes of (1) 2 W/cm^2 (8 x 10^6 dynes/cm^2) or (2) 30 W/cm^2 (4 x 10^7 dynes/cm^2) at room temperature (18°C) compared with stress-strain curves obtained without ultrasound at test temperatures ranging from 18 to 250°C. A - 18°; B - 100°; C - 132°; D - 150°; E - 170°; F - 200°; G - 250° (after Langenecker[34,35] and Langenecker et al[36])

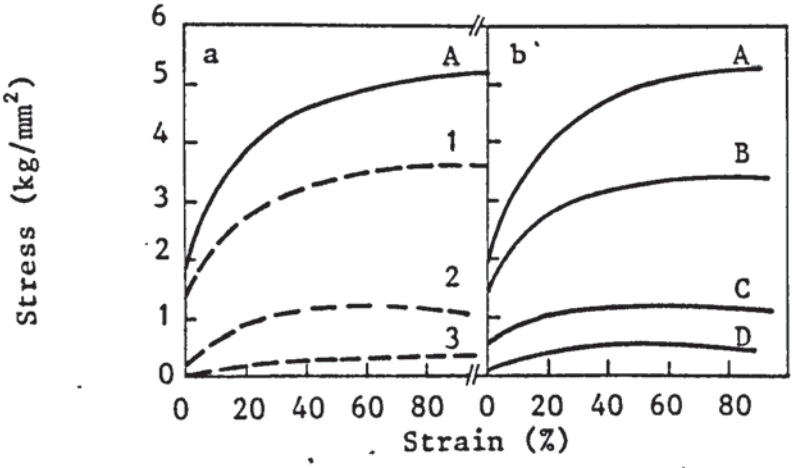

Figure 2.22: Stress-strain curves of aluminium crystals obtained (a) during continuous application of 20 kHz ultrasound at various power amplitudes at 18°C compared with those obtained (b) without ultrasound at test temperatures ranging from 18 to 600°C. a - 10^{15}; b - 10^{22}eV/cm^3. 1 - 15; 2 - 35; 3 - 50 W/cm^2. A - 18°; B - 200°; C - 400°; D - 600° (after Langenecker[35] and Langenecker et al[36])

then increases quite sharply during subsequent glide until point 'c'. When the ultrasonic power was switched off, the shear stress rose to a level 'd' which was considerably above the initial non-oscillatory 'a'. The shape of the curve in figure 2.23 proves that rapid hardening was occurring until it reached a saturation level. It was concluded, however, that there are two distinct values of acoustic stress amplitude, namely: threshold value and saturation value. The first defines the limit of amplitude below which the shear stress decreases (softening effect), while the saturation value implies that a constant shear stress will be maintained if the amplitude increases above that value. A pronounced hardening was observed between the threshold and saturation values (hardening effect).

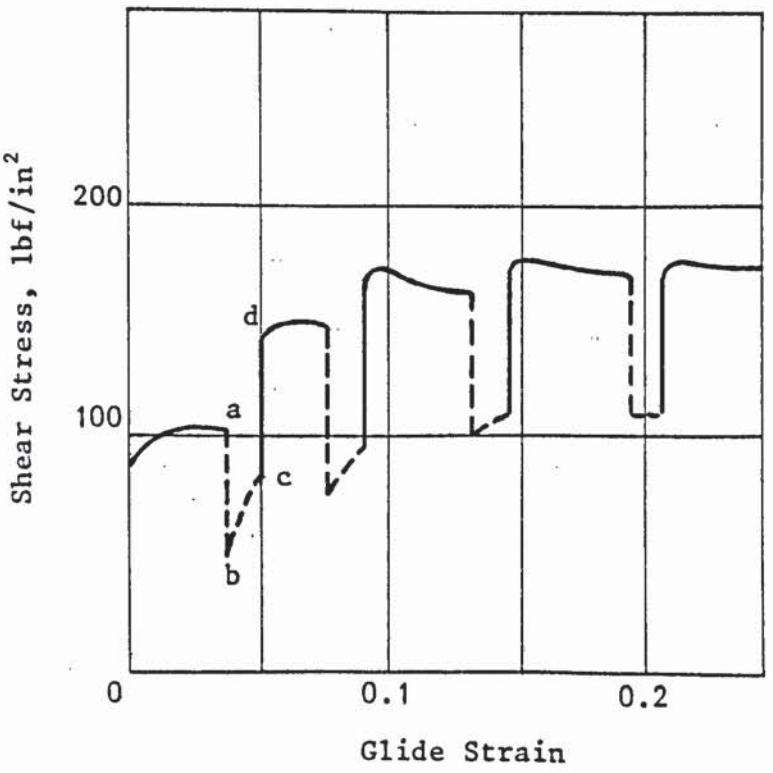

Figure 2.23: The hardening effect of zinc single crystals as a result of applying high-amplitude ultrasonic energy (after Langenecker[37])

2.3.1.2 Changes of contact friction with applied vibrations

The effect of vibrations on the coefficient of static friction between metallic surfaces was first explored in 1959 by Fridman and Levesque[38]. A vibrated inclined plane, at different frequencies in the range of 6.1 to 41 kHz, on which a steel block was permitted to slide, was used in the experiments. Typical results are shown in figure 2.24 which illustrate the effect of transducer power on the reduction in coefficient of static friction for three different vibration frequencies. It can be concluded that at low power levels there was a rapid rate of friction reduction which fell off slightly as the power was increased. The results indicated also that lower frequencies appear to have larger effect on the reduction in coefficient of friction.

In 1966, Pohlman and Lehfeldt[32] designed an experiment in order to examine the effect of applied ultrasonic vibrations on the contact friction between two metal surfaces using a rotating disc on which rests a vibrating ball. Vibrations were applied in four different ways as shown in figure 2.25. The weight R with which the ball presses on the friction surface was varied up to a maximum of 40 lbf and the friction force acting on the ball was measured. Figure 2.26 shows the friction reduction as represented by the ratio between oscillatory and non-oscillatory friction forces in per cent vs. the surface peripheral speed at constant vibration amplitude for various arrangements. The graph illustrates that arrangements a, b and c are very effective in reducing the friction force while arrangement 'd', where the oscillation direction is normal to both the friction direction and the contact surface,

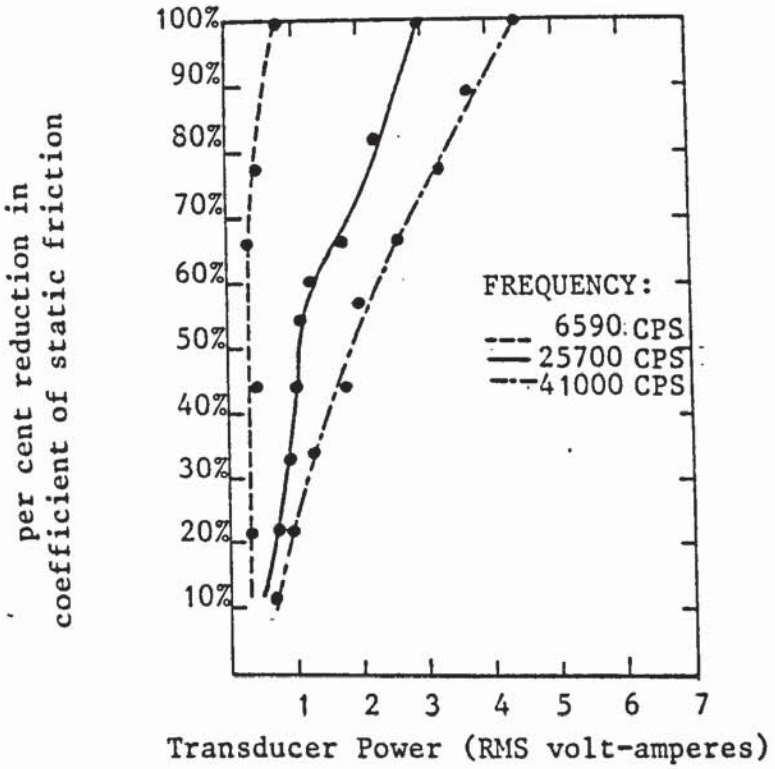

Figure 2.24: Coefficient of static friction vs transducer power for ground steel surfaces (after Fridman and Levesque[38])

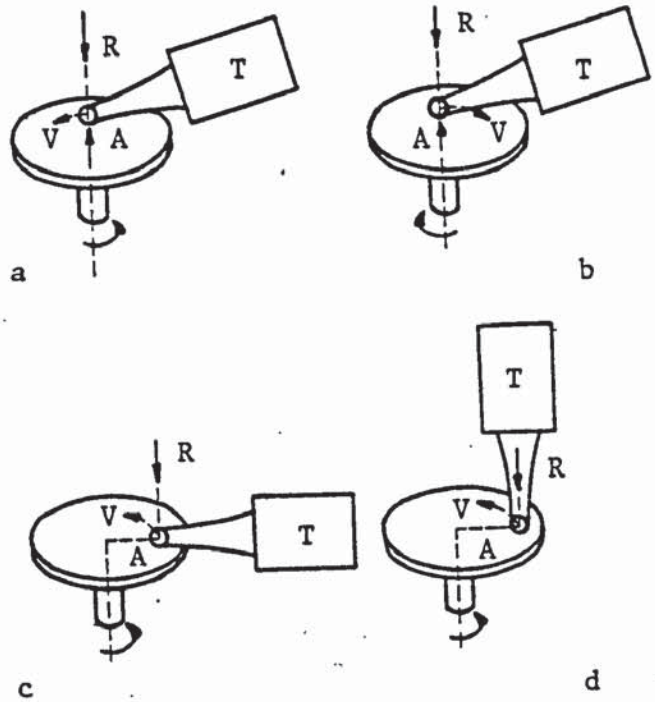

Figure 2.25: Experiments on friction reduction by ultrasound, using several different settings to find the most favourable oscillation direction (after Pohlman and Lehfeldt[32])

T: transducer, R: normal force, V: peripheral speed, A: vibration amplitude

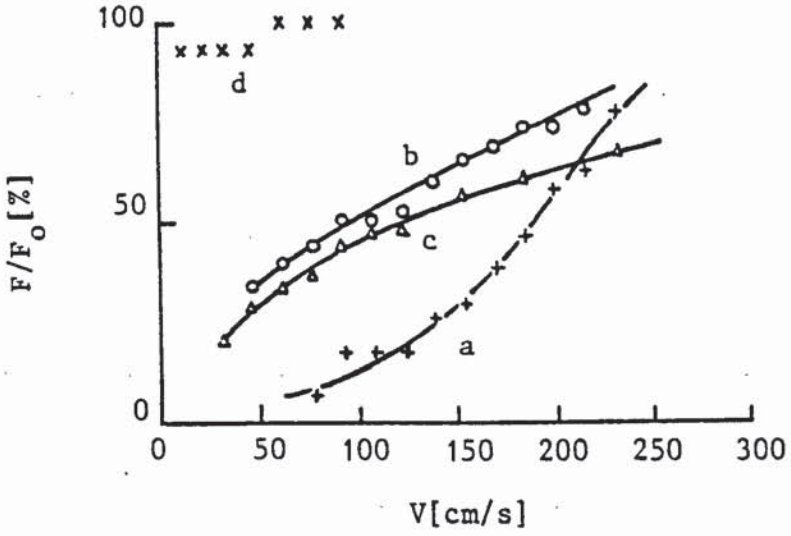

Figure 2.26: Friction reduction in relation to contact speed for several oscillation directions (after Pohlman and Lehfeldt[32])

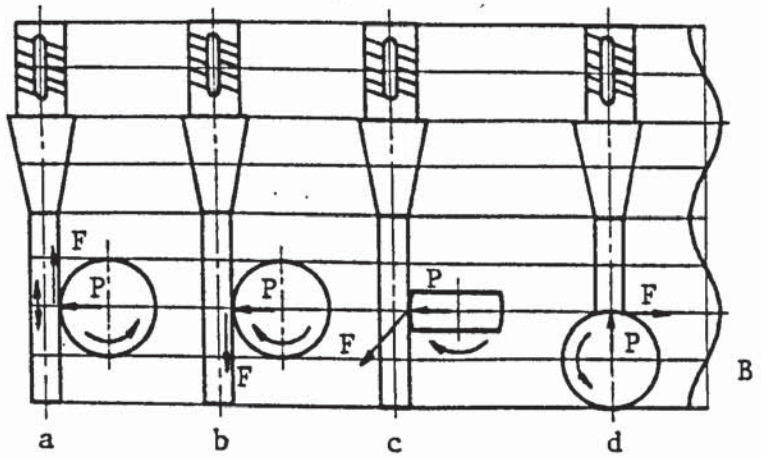

Figure 2.27: Ultrasonic input methods,[39]

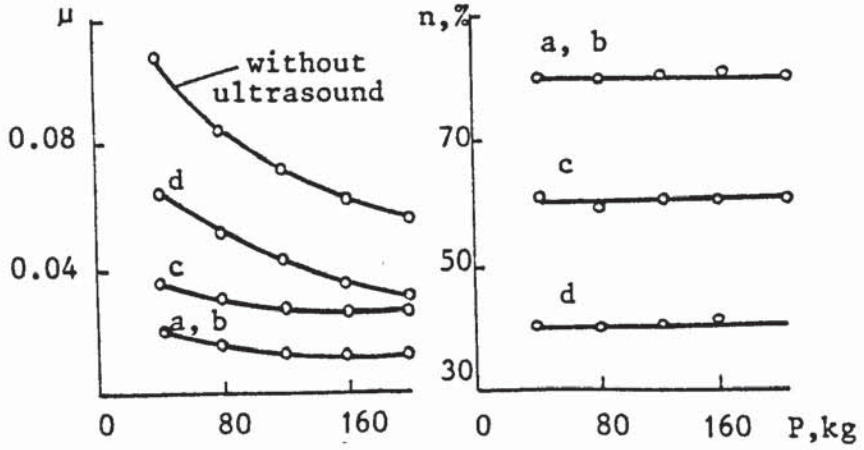

Figure 2.28: The influence of ultrasonic oscillations from different directions on the friction coefficient and the amount of its decrease as a function of the pressure. The curves are designated in accordance with Figure 2.27.

achieved practically no friction reduction. This was explained by the fact that during an oscillation period the ball is induced to strike heavily on the rotating disc surface but then bounces back elastically[39] and in this way the load would be increased during the downward stroke which would offset the reverse effect resulted during the upward stroke. Consequently, the mean normal load and hence the friction force is therefore virtually unchanged. Also, the friction reduction observed in cases a, b and c was attributed by the authors[32] to fatigue fracture of microwelds as a result of high alternating stress amplitude. However, no evidence supporting this mechanism was given.

Similar tests were conducted by Severdenko and colleagues[39] to study the influence of ultrasonic oscillations in various directions on contact friction using different apparatus which is represented diagrammatically in figure 2.27. In their experiments, the coefficient of friction is determined from the relation: $\mu = \frac{F}{P}$, and the effectiveness of ultrasonic vibrations in reducing the contact friction is quantitavely determined from the formula: $n = (\mu_w - \mu_u) / \mu_w$, where μ_u and μ_w are the coefficients of friction with and without applied vibrations. Figure 2.28 shows the variation of the coefficient of friction as well as the efficiency of ultrasonic vibrations with the applied load for steel-copper pair for various methods of vibration application. It was concluded that the friction reduction due to applied vibrations is most effective in methods a, b, ie. when the oscillations are parallel to the friction force and the contact surface. Conversely, the least effect was observed in the case of applied vibrations perpendicular to the friction force and the

contact surface, curve d. It was also reported[39] that the amount of reduction in friction forces as a result of applied ultrasonic vibrations in arrangements a, b and c decreased with the increase in the sliding rate (peripheral speed) at constant vibration amplitude. But in the case of applied vibration in case d, the friction reduction slightly increased with increasing the sliding rate.

Later work by Lenkiewicz[40] confirmed the dependence of the amount of reduction in friction force upon the sliding speed. A sample in the form of a flat strip vibrated at low frequency (20-120 Hz) was held tangentially against a rotating drum. The sliding speeds were varied between 0 and 60 in s^{-1}. It was found that higher amplitudes of vibration should be employed in order to achieve reduction in friction at high sliding speeds.

2.3.2 Fundamental principles

The early interesting observations and findings relating to the influence of vibrations on the flow stress of metals and on the interfacial friction have established a great interest in the application of vibrational energy to metal-working processes. Since the early sixties, considerable research work has been done in order to clarify the fundamental mechanisms which contribute to the beneficial effects of deforming metals with applied vibrations.

It is now generally agreed by many research workers that the observed effects of ultrasonic vibrations on the mechanics of metal deformation may be broadly divided into two categories, namely: 'volume effect' and 'surface effect'. The former being characterised by an

increase in the metal deformability while the surface effect implies a reduction in friction at the tool-workpiece interface. Over the past two decades, many results of studies and general reviews have been published, eg.[41-48], which contributed to a better understanding of those two major effects and their implications on the metal deformation processes. In general, it is now well established that five mechanisms may be used to explain the plastic deformation of metals under oscillatory conditions. These mechanisms can be listed as the: superposition mechanism, swaging effect, change in metallurgical properties, which constitute aspects of the 'volume effect', the friction vector effect and the change in the coefficient of friction, which are aspects of the 'surface effect'.

2.3.2.1 The volume effect

(a) Superposition mechanism

It can be defined as the addition of cyclic stresses generated by the ultrasonic oscillations to the static (non-oscillatory) stress such that their peaks, ideally, coincide with the stress-strain curve without applied oscillations. This mechanism, which results in a reduction in the mean stress required to cause plastic deformation of the material equal to the periodic stress amplitude, was first propounded by Nevill and Brotzen[31] and then confirmed in further studies[33,48].

The superposition mechanism was explicitly analysed by Sansome[41] who considered the state of stress in a cylindrical specimen subjected to uniaxial tension, in the absence of any frictional effects, with and without applied axial vibrations.

The results of this analysis showed the interesting conclusion that the mean and minimum stresses during plastic deformation under oscillatory conditions will follow loci parallel to the non-oscillatory stress-strain curve.

In industrial metal forming processes, eg. in wire drawing, where friction does exist it is inevitable that the peak cyclic stresses will be always above the non-oscillatory stress. This result was explained[49] by the presence of friction between the die and the wire which opposes drawing and it was concluded that the increase in the drawing stress is due to a combination of sticking friction and a change in die pressure as a result of a change in the steady state conditions. It is therefore unlikely that utilising the superposition mechanism alone would offer an advantage in oscillatory metalworking.

(b) Swaging effect

Although this mechanism is well known and widely exploited in conventional metal deformation processes, it has not been employed with the use of ultrasonic vibrations until recently. In general, the swaging effect mechanism can be defined as an increase in the lateral compressive stresses which produces a consequential reduction in the axial tensile stress. Thus, it may be considered now an important mechanism in ultrasonic metal deformation since by enabling the lateral compressive stress to be considerably increased, yield can be achieved by applying a smaller longitudinal tension than is required in the conventional process. This mechanism, therefore, offers a great potential for force reduction because most of the deformation work may be done laterally;

consequently, the conventional limiting factor, ie. the fracture stress in tension, becomes more remote.

A full explanation of the swaging effect was given by Sansome[41] who considered an element of metal in the deformation zone of a drawn bar. The element is assumed to be subjected to principal stresses σ_1, σ_2 and σ_3 acting in the directions shown in figure 2.29a. The state of stress can be represented on the π-plane, figure 2.29b, in which $0\sigma_1$, $0\sigma_2$ and $0\sigma_3$ are the principal tensile directions and the circle of centre 0 and radius Y is the von Mises yield surface. In the case of conventional bar drawing the co-ordinates of the principal stresses are σ_1, $-\sigma_2$ and $-\sigma_3$ which are represented on the yield surface by point 'A'. When the bar is swaged, due to applied ultrasonic vibrations, the lateral stresses will increase in magnitude to $-\sigma_{2s}$ and $-\sigma_{3s}$. Thus, it can be seen that the axial stress σ_{1s} is considerably decreased as a result of the swaging effect of applied vibrations.

(c) Metallurgical changes effect

As discussed in section 2.3.1.1, some investigators agree that the ultrasonic energy when applied to metals has an effect on their metallurgical properties which appears as a reduction in the yield stress. Furthermore, this reduction was very substantial when materials were subjected to high intensity ultrasonic oscillations. It has been postulated[49], however, that the vibratory energy is preferentially absorbed at dislocation sites within the lattice structure of material being deformed and thus the activated dislocations can more easily surmount the potential barriers resulting in a considerable reduction in the yield stress. This

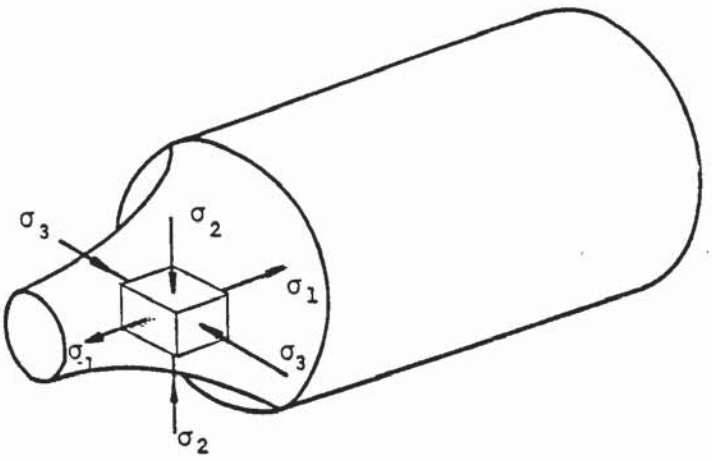

Figure 2.29a: Stresses acting on an element of metal in drawing of rod

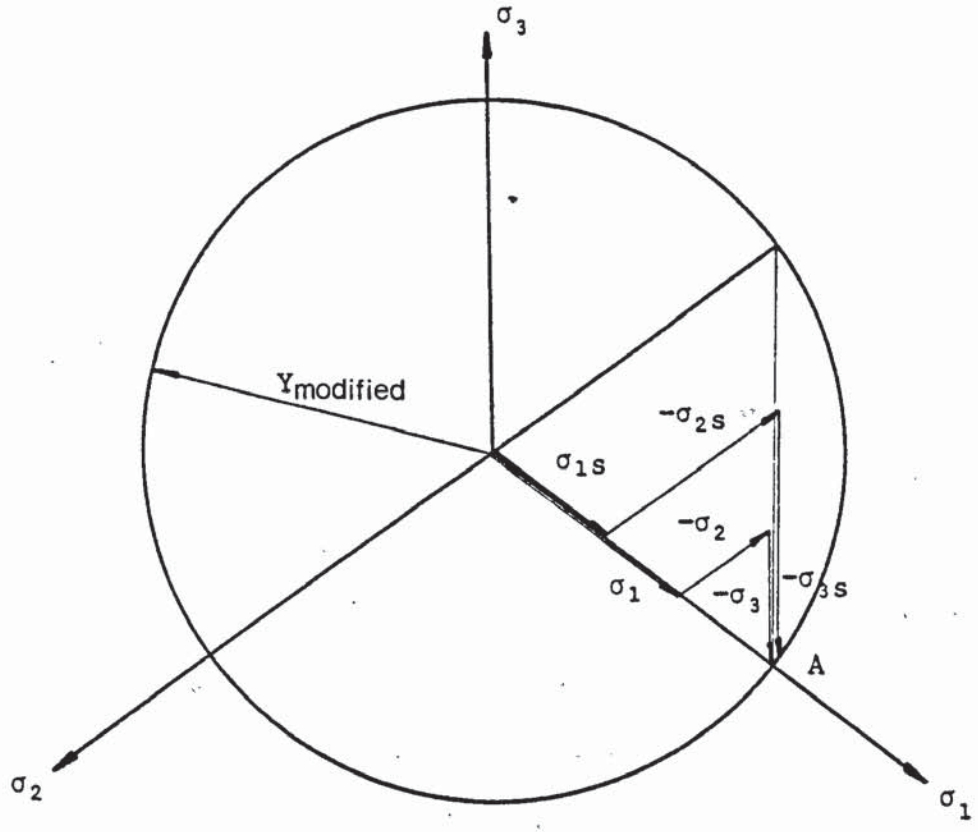

Figure 2.29b: von Mises yield surface, showing the swaging effect ($\sigma_{1s} < \sigma_1$) (after Sansome[41])

explanation may be arguable[41] since there often is a reduction in yield stress attributable to a rise in temperature during intense vibration and therefore further work is needed to establish if there is a reduction in the yield stress in the absence of a rise in temperature at the dislocation sites. Nevertheless, in applying ultrasonic vibrations to metal deformation processes, for any of these mechanisms to be effective, the ultrasonic energy must be sufficiently intense to result in a superficial rise in the local or the bulk temperature with a consequential influence on the metallurgical properties of the workpiece material. The use of this mechanism, however, can prove more expensive in practice than the direct application of heat from an external source.

2.3.2.2 The surface effect

(a) Friction vector effect

The mechanism of friction vector effect is now universally recognised as one of the main mechanisms which contribute to the load reduction in vibratory metal deformation processes. Simply, it occurs when the oscillatory velocity of tools exceeds the workpiece velocity. It is obvious that the friction vector results from the relative motion between the workpiece and the tools, and normally acts in a direction opposite to the workpiece motion. Thus, if the friction vector is reversed, when the tool is vibrated, such that it assists the motion of the workpiece, or its component in the working direction is reduced, then a consequent reduction in friction force can be achieved.

Generally, in metal deformation processes the work is done:

firstly to change the shape of metal in the required manner which may include an element of redundant work in internal friction, and secondly to overcome friction at the tool-workpiece interface. So, any method which may contribute to a reduction in the frictional work can result in a decrease in the total work, which is normally required, and indeed in a reduction in the process loads. For example, it is known that the draw force in mandrel-drawing of tube is less than its value for the identical fixed plug-drawing process. The reason for this is that when a fixed plug is employed, the friction force resists the tube motion and this is not the case in mandrel-drawing. Since the mandrel travels through the die with the speed of the drawn tube, then it assists the tube to flow through the die due to a reversed friction vector.

Another method which results in a reduction in the total deformation force attributable to the friction vector effect was explained by Sansome[41] for the process of rod drawing in which the die is rotated. It was considered that the total deformation force may be expressed as the vector sum of the force required to deform the material and the force necessary to overcome friction at the die-bar interface, as illustrated in figure 2.30a. If, then, the die is allowed to rotate and assuming there is no change in the coefficient of friction and the drawn bar does not 'wind up', the friction force vector opposes the direction of the resultant velocity vector[50]. It can be seen from figure 2.30b that the component of friction vector in the drawing direction is reduced and that a consequential reduction in the total deformation force is achieved. Also, it is clear that as the rotational velocity is

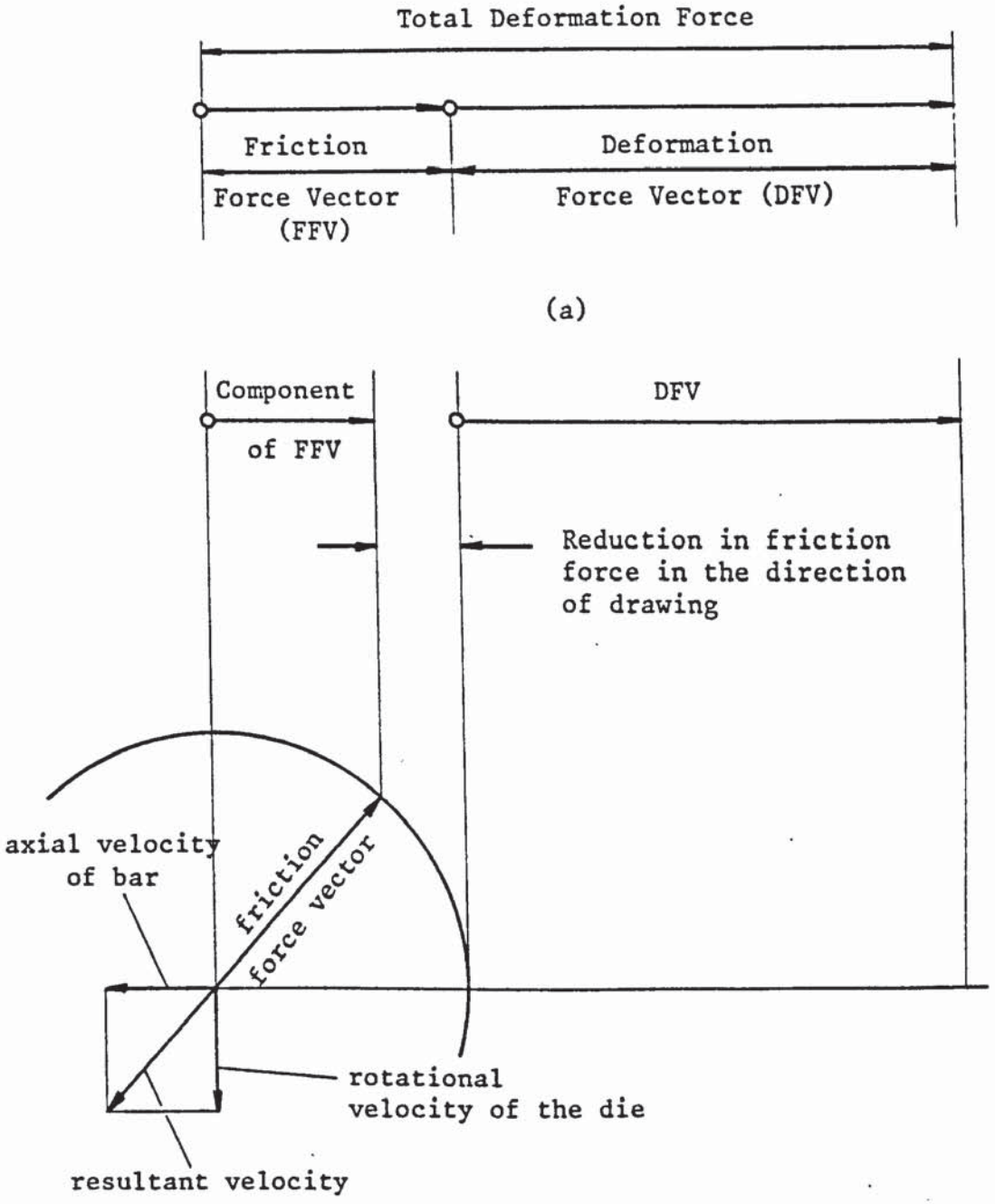

Figure 2.30: A diagrammatic representation of the friction vector effect when the die is rotated in drawing of bar (after Sansome[41])

increased, the amount of force reduction increases and this can be attributed only to the friction vector effect provided there is not a change in the coefficient of friction.

When drawing a tube over a fixed-plug which is axially vibrated, if the plug is pushed forward at a higher velocity than the draw-tube speed, then the friction vector will reverse and instead of friction opposing the tube motion it acts in the drawing direction and therefore assists deformation. Conversely, if on the backward movement of the plug, there are no other changes taking place, the friction vector remains the same as that occurring in non-vibratory drawing. Hence, a cyclic change in the direction of friction vector occurs and a cyclic reduction in the effective draw force, while assuming no reduction in the coefficient of friction, is achieved. It may be noted therefore that drawing a tube over an activated plug has a similar effect to that obtained when the die is rotated or when the tube is drawn over a moving mandrel.

(b) Change in coefficient of friction

It is evident that the application of vibrations in metal deformation processes can result in a friction reduction at the tool-workpiece interface. Considering no change in the friction force due to the friction vector reversal effect, which has been discussed in (a), the friction force may be expressed as the product of the coefficient of friction and the normal force. Some investigators[38, 39] showed a reduction in the frictional forces and in the coefficient of friction when vibrations were applied.

The reasons for the change in the coefficient of friction in

oscillatory metal-working are not fully understood and thus further research work is required to clarify such aspects. However, it has been postulated by some research workers that the changes in the coefficient of friction can arise as a result of the following:

(1) softening or melting of the asperities; with applied ultrasonic vibrations, the energy dissipated from the relative cyclic motion of the surfaces in contact, ie. those of the tool and the workpiece, is transmitted across the interface and causes a surface temperature rise. This results in a softening of the asperities and a consequential reduction in the yield stress in shear. However, the reduction in the yield shear stress appears to be largely dependent on the metallurgical properties of the workpiece material and the temperature rise. Further, since contact friction is a measure of the force necessary to shear the local asperity weldments, so it can be concluded that softening or melting of asperities may effectively reduce friction. It is also believed[41] that the frequency of vibrations is a factor affecting this mechanism which is unlikely to occur at sub-sonic frequencies.

(2) Separation of surfaces; if the vibration or motion of the surfaces are such that the surfaces in contact separate during a part of the vibration cycle, then a reduction in the average friction force may occur. However, this is not easily achieved since the displacement amplitude must be high enough to exceed the elastic recovery of the workpiece and the tool.

The mechanism of surface separation may be observed in some processes such as the upsetting process.

(3) pumping of lubricants; the thickness of lubricant film affects considerably the interfacial friction in metal deformation processes. The application of oscillations can result in a thicker film of lubricant between the contacting surfaces and hence a reduction in the coefficient of friction. Also, an increase in the lubricant film has been observed at low and high vibration frequencies. This mechanism, however, has not been investigated extensively and thus it is not clearly understood.

(4) Activation of lubricant; it has been suggested that the lubricant may be chemically more active with applied ultrasonic energy. This can be attributed, for example, to the temperature rise which accompanies the vibrations. Although this effect has not been adequately explored also, it is believed that a reaction between the metal surface and reactive lubricant molecules can cause organo-metallic compounds to be formed.

Finally, the extent to which these mechanisms may affect the coefficient of friction in a particular process has not been fully clear and still further work remains to be done to clearly establish the reasons for the observed changes in the coefficient of friction during oscillatory metal deformation processes. However, it is evident from past experience that mechanisms (1) and

(3) mostly contribute to a significant reduction in the coefficient of friction[42].

2.3.3 Application of ultrasonic vibrations to metal deformation processes

Since 1955 when oscillatory metal deformation research started, many attempts have been made to study vibrational effects in various processes, eg. extrusion, forging, upsetting, strip-, wire-, tube-, deep-drawing and rolling. The aim has always been to try to reduce the process forces and/or increase the achievable deformation. Many research results have been published, over the past twenty years, which not only showed the beneficial effects of applying vibrations to metal deformation processes but also considerably clarified the main mechanisms contributing to those effects. In this section, however, attention will be given to reviewing the literature associated with two oscillatory metal deformation processes, namely: tube drawing, and deep-drawing and draw-ironing. It has been shown that ultrasonic vibrations can be applied successfully to those processes and that, indeed, efforts have been made to exploit them in industry, making use of their practical and commercial advantages. Generally, emphasis will be placed on the mechanisms of oscillatory deformation rather than the design of equipment or the experimental technique.

2.3.3.1 Ultrasonic tube-drawing

Ultrasonic tube-drawing can now be considered an established process in which a substantial reduction in draw load can be

achieved. Its technical advantages may include: high reduction of area and consequently fewer draw passes than are possible in conventional drawing, improvement in surface finish, elimination of tool 'chatter' and employment of inexpensive lubricants. Several investigators have contributed to and confirmed such achievements.

(a) axial vibration of the die

Severdenko et al[51, 52] examined the influence of the direction of ultrasonic vibrations on the reduction in draw-force. Copper and brass tubes were drawn with longitudinal (axial) vibrations applied to the die or with the die oscillated in a transverse direction. It was shown that transverse oscillation has a less pronounced effect than longitudinal oscillation of the die. This conclusion was in agreement with the theoretical analysis made by the authors[51]. In a later work, Severdenko and co-workers[53] confirmed, for the tube-sinking, that longitudinal oscillations with the die placed at the displacement antinode were most effective in reducing the draw-force and that the effectiveness was greater when additional dies were placed at the entry and exit to complete the acoustic resonant system. However, the authors made no reference to the mechanisms contributing to the reduction in forces and also the cyclic stress component was not measured. Because the tube sinking is quite similar to wire- and bar-drawing, it was believed[42] that the results described by Severdenko et al[53] may be predicted using the superposition mechanism.

In their study of the tube-sinking process, Severdenko et al[54] compared several modes of die-excitation. When the die

was located at an axial displacement antinode, the draw-load was observed to vary with the length of tube. This periodic variation in the draw-load can be attributed to the superposition mechanism[42] which accounts also for the observed phenomena when a transverse mode of excitation was used. However, with the die placed at an axial stress antinode in the acoustic waveguide, a real reduction in the draw stress, in the absence of changes in the friction forces or material properties, was achieved. Eaves et al[42] believe that this result can be explained by the swaging effect as a result of the expansion and the contraction of the die-orifice, or the tube diameter.

Nosal' and Rymsha[55] investigated the effect of applying longitudinal vibrations at a frequency of approximately 20 kHz to the die during drawing tubes on a production draw bench and also under laboratory conditions on an experimental unit. It was found that the vibrations reduced the draw-force by 20-40%. The reduction in friction at the die-tube interface was believed to account for the reduction in the draw-force which depends on the ratio of the relative velocity of the oscillations to the velocity with which the tube moves through the die. A theoretical analysis, based on the friction reversal effect, was made and the predicted values showed agreement with their experimental results.

More recently, Zaporozhchenko and Stepanenko[56] considered the process of drawing tube over a floating mandrel with longitudinal vibration of the die. A theoretical analysis was made in which the friction reversal effect was adopted in order to predict the amount of reduction in the draw-stress. The change in the coefficient of friction was neglected. It was shown that when

drawing tubes over a floating mandrel, the reduction in draw-stress is higher than that achieved with the use of fixed-plug and that at small values of die angle, ie. at small reduction of area, the use of the floating mandrel is more effective. Experimental tests were conducted to confirm the calculated values of stress reduction under the vibratory conditions. Although the theoretical analysis predicted comparable magnitudes of stress reduction (about 34%) between the two cases, the predicted values were somewhat higher than the experimental data. The authors[56] attributed this disagreement to the damping of vibrations, ie. the reduction in amplitude of die vibration during drawing.

(b) axial vibration of the fixed-plug

It was reported[47] that ultrasonic oscillations can be applied axially to the plug-bar during tube drawing over a fixed plug (mandrel). However, for the oscillatory system to operate in resonance, the length of the plug-bar was chosen to be an even multiple of the half-wave lengths of the vibration wave in the plug-bar material. As a result, a standing wave with oscillation antinodes at the end was established in the plug-bar which was fastened at displacement nodes of oscillation. It was shown[57] that the draw-force was reduced by about 25-30% with the introduction of ultrasonic oscillation at a frequency of 20 kHz and at an amplitude of 3 μm. This reduction in draw-force was attributed to the friction reduction at the tube-plug interface. It was also stated that there was disagreement between the experimental results and the theoretical data, as predicted by the authors[57], and this was explained by the transmission of

ultrasonic oscillations to the die which partially reduced the friction force at the tube-die interface. However, neither the effects of stress superposition nor the change in the coefficient of friction were mentioned.

Winsper and Sansome[58] investigated the mechanics of fixed-plug tube drawing with axial oscillation applied to the plug. Thin-walled stainless steel tubes were drawn over an ultrasonically activated plug for several reductions of area. It was found that the mean draw force and the mean plug-bar force were reduced under oscillatory conditions and that the force reductions were directly proportional to the amplitude of oscillations. Improved surface finish, particularly on the bore surface, was observed. It was concluded that with applied vibrations greater reductions of area could be achieved than would be possible without vibration of the plug. The authors attributed the reduction in forces to the friction vector mechanism and partly to the force superposition effect.

Kolpashnikov et al[59] studied the effects of drawing aluminium tubes with an axial vibration of the plug at 20 kHz and supplied power of up to 1.5 kW. A reduction in the draw-force and a significant reduction in pick-up on the tools at low amplitudes and slow drawing speed were observed. It was reported that at high values of vibration amplitude the temperature rose significantly causing severe pick-up on both the tools and the tube. Further, the effect of the draw length of tube on the reduction of process forces was in agreement with the observations of Winsper and Sansome[58].

An increase in the achievable reduction of area, when applied

axial oscillation to the plug in tube-drawing was used and compared with the conventional process, was reported by Dragan and Segal[60]. The authors attributed this effect to a change in the material plastic properties. In a more recent paper[61], Dragan attributed the beneficial effects of drawing tubes over an ultrasonically activated plug to a surface effect, ie. the frictional reversal mechanism as well as to a volume effect characterised by a reduction in tensile stress, a decrease in hardness and an increase in ductility. A theoretical analysis of the friction vector reversal effect was made by the same authors[62] in order to predict the amount of friction reduction due to the axial vibration of plug during tube-drawing.

In another attempt to quantify the results of the friction effects, Sugahara et al[63] used an unconventional acoustic system to oscillate the plug in tube drawing. It was reported that the friction vector effect was responsible for the 90 per cent reduction in the plug-bar force which contributed only to approximately 15 per cent of the total draw-force. Plug 'chatter' was prevented, under oscillatory conditions, allowing low quality lubricants to be used and this effect was shown to be a speed dependent.

(c) radial vibration of the die

The ultrasonic vibrations applied radially to the die in tube drawing over a floating-plug was investigated by Dawson[64]. Ultrasonic power was supplied at 13 kHz and at an amplitude of up to 10 μm peak to peak. It was found that a reduction in the draw-force of up to 18 per cent may be achieved using radial vibrations

at a draw speed of 20 mm.s^{-1}. No cyclic axial stress was recorded and, thus, the reduction in draw-load was real. Also, it was observed that the chattering of the plug was almost eliminated with applied vibrations which can enable poorer lubricants to be employed successfully. No adverse effect on the tube surface finish was noted. The mechanism describing force reductions was explained by the author as the establishment of a neutral plane in the metal deformation zone. It is believed that the reversal of flow as a result of radial vibrations leads to a reversed friction force. Thus, the upstream back-tension is diminished and the total draw force is reduced. In addition, it was stated that under certain circumstances when the vibration amplitude is high enough and the draw speed is low and also the angle of friction is greater than the die angle, then the force reduction can be substantially high.

More recently, Kariyawasam et al[65] examined the radial vibration of die at an ultrsonic frequency of 20 kHz during drawing of tubes. The plug supporting the tube bore was axially vibrated in sympathy with the forced vibration of the die. It was shown that the draw-force was reduced with applied vibrations and that the amount of reduction increased with increasing vibration amplitude. The authors explained the reduction in process loads partly by the friction vector reversal effect which contributes to the friction reduction at the tube-plug interface, and partly by the swaging effect which results in increasing the radial and circumferential stresses and consequently decreasing the axial stress. Furthermore, it was stated that the coefficient of friction might be reduced due to applied vibrations. Also, it was

reported that with vibration, tube may be drawn to higher reductions in area than are possible by conventional methods.

2.3.3.2 Deep-drawing and draw-ironing with ultrasonic vibrations

In 1961, the application of ultrasonic energy to the deep-drawing process was first reported by McKaig[66]. With a vibrated die at an ultrasonic frequency, it was shown that the depth of draw can be 37 per cent greater than the non-vibratory value for a given loading. Neither the details of the ultrasonic system used were described nor the reasons for the vibration effects were given. It is believed[67], however, that besides a stress superposition effect there could have been frictional changes which would contribute to the achieved increase in the draw depth.

Langenecker et al[68] examined the ironing process with applied axial vibrations to the die during cup-drawing. In addition to a load reduction of 65 per cent a greater reduction of area per pass compared with the conventional method was claimed. The authors attributed those effects to a reduction in the yield stress of the material at high levels of ultrasonic power.

The results of superimposed vibrations, at frequencies between 20 Hz and 20 kHz, to the tools in deep-drawing and ironing of aluminium and steel were reported by Kristoffy[69]. The importance of dynamic force measurement was emphasised in the application of axial oscillations to the punch and radial oscillations to the die. Thus, it was concluded that the observed reduction in loads when the punch was axially vibrated is entirely

due to the stress superposition effect with no change in the peak force during the process. However, it was shown that when vibrating the die tangentially, with respect to the tooling axis, at 20 Hz and radially at 20 kHz, the same reduction in the punch force was obtained and thus it was considered a true effect. The author explained the reduction in the punch force in the case of low frequency vibration by a change in the direction of friction from axial to axial-tangential at the die-throat and consequently the friction force component in the axial direction is less than that without vibrations. The mechanism of friction reduction was demonstrated by Rothman and Sansome[50] who considered die rotation during the process of bar-drawing. When applying high frequency radial vibrations to the die, it was concluded that the force reduction may be due to changes in the state of stress when an additional radial compressive stress is applied. Also, it was said that despite the reduction in forming forces, the energy requirement of the process was unchanged.

As an analogue to the deep-drawing process, Young and Sansome[70] studied the effects of applying radial vibrations to the die in the wedge-drawing test. It was shown that reductions of up to 40 per cent in the punch load can be obtained. The authors attributed the load reduction mainly to the effective reduction in friction between the test-piece and the blank-holder and between the test-piece and the die profile radius, and partly to oscillatory force superposition. The results also showed a substantial reduction in blank-holder friction which may approach zero at high vibration amplitudes. In addition, an increase in the limiting draw-ratio was observed and attributed to the friction

reduction mechanism.

Similar results were obtained by Smith and Sansome[71] who examined the effect of vibrating the blank-holder in a radial mode using a modified form of the wedge test. The blank holders were subjected to in-phase ultrasonic vibrations in a plane perpendicular to the axis of the punch. It was shown that under vibratory conditions the punch load may be reduced by 25 per cent, and the limiting draw-ratio increased by about 12 per cent. The latter effect was attributed principally to the friction reversal effect while the reduction in punch load was believed to be due to both the friction vector and the stress-superposition mechanisms.

Biddell and Sansome[72] investigated the process of axisymmetric deep-drawing with applied radial ultrasonic vibrations to the die at a frequency of 13 kHz. The design of efficient radial resonators was described. It was shown that the radial vibration of the die increased the maximum depth of the drawn cup by up to 20 per cent when compared with the non-vibratory drawing. This result may be attributed to the swaging effect, ie. the reduction in the axial tensile stress due to the increase in the lateral compressive stresses when the die is radially vibrated. It was shown also that the punch load was considerably reduced particularly at low draw speeds and that the load reductions may be explained principally by the friction vector reversal effect on the upper die surface. The authors added that in the ironing part of the process at the die throat, the swaging effect contributed to a reduction in the punch load.

CHAPTER THREE

THEORETICAL ANALYSIS OF THE MECHANICS OF TUBE DRAW-BENDING

3.1 General approach to the mechanics of deformation

Whilst the concept of tube bending, as previously mentioned, is well known and may be considered simple; the mechanics of deformation in draw-bending of tubes is very complex and far from being fully understood. Therefore, one of the major objectives of this thesis is to devise a theory describing the mechanics of metal deformation which occurs during bending and to develop a theoretical solution which takes into account the principal parameters involved in the process.

As discussed in the previous chapter, the basic tools which support the tube during bending are the gripper, the former, the slider and the mandrel. Initially, the free end of the tube is firmly clamped between the straight part of the former and the gripper. The former then rotates with the gripper, bending and pulling the tube over the supporting mandrel. The straight part of the tube reacts against the slider which is forced to move with it. A diagrammatic representation of the tooling arrangement is shown in figure 3.1.

During bending, the tube passes through three distinct deformation zones, namely: I, II and III. In the first zone, the straight part of the tube is pulled over the mandrel-shank while still supported by the moving slider and thus it is subjected to internal and external pressures. The friction at the tube-mandrel and the tube-slider

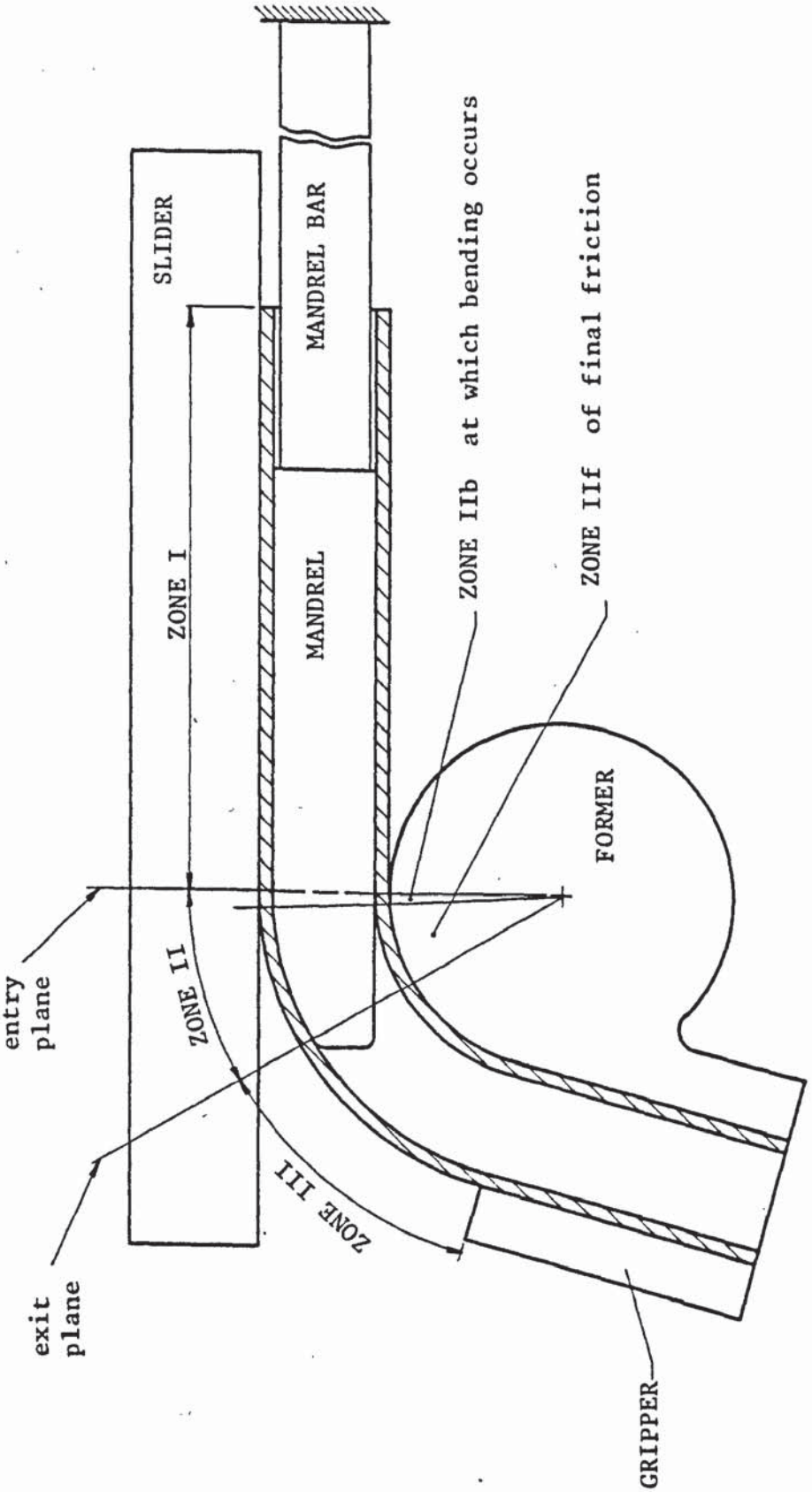

Figure 3.1: The tube and tooling arrangement as the tube passes through 3 zones of deformation

interfaces causes an induced stress in the longitudinal direction. This zone is called the "initial friction zone" or zone I and obviously the initial friction is primarily influenced by the external force applied by the slider. It is unlikely, however, that the tube is plastically deformed in most of zone I since the acting stresses are not high enough for the tube material to be stressed beyond its elastic limit. The second deformation zone starts as soon as the tube element passes the tangent line (or the entry plane). In this zone each tube element is bent to the specified mean bend radius and then pulled over the mandrel and around the former. Most of the plastic deformation occurs in zone IIb, which here is termed the "bending zone". But the tube material experiences additional plastic deformation due to friction in zone IIf or the "final friction zone". Although it is difficult to determine the boundary separation between the zones IIb and IIf, in general it can be said that zone II is bounded by the entry plane and an exit plane where the tube leaves the mandrel. Finally, the tube element in zone III is pulled around the former but is no longer supported internally by the mandrel. The friction between the tube external surface and the former may cause further deformation. However, such deformation can be considered insignificant when compared with the total plastic deformation.

Having established an understanding of the mechanics of deformation during the process of draw-bending of tubes, an attempt can be made to develop a theoretical solution. One of the possible solutions can be based on the "equilibrium of forces approach". This approach leads to a lower-bound solution which is useful for predicting the distribution of stresses and strains. Consequently, the basic process parameters such as: the bending torque, the variation of tube-wall thickness in a

bent tube, and the mandrel force can be calculated.

In the theoretical analysis, the following general assumptions are made:

1. the tube material is homogeneous and isotropic
2. the elastic strains, being small compared with the plastic strains, are neglected
3. the true stress-strain relationship under simple tension is assumed to follow the "Ludwig" impirical equation: $\bar{\sigma} = Y + H\bar{\varepsilon}^n$ which is also assumed to apply for simple compression
4. the shear stresses are neglected and the principal directions of stresses and strains are assumed to be in the longitudinal, hoop and radial directions
5. for thin-tubes, the variation of stresses through the wall thickness can be neglected
6. the circular cross-section of tube remains circular after deformation
7. the 'Coulomb' model of friction is assumed to apply

3.2 Equilibrium of forces and distribution of stresses

In this section, the equilibrium of forces approach is adopted to develop the basis of the theoretical solution for the mechanics of metal deformation in the process of draw-bending of tubes. The equilibrium equations in deformation zones I and II will be derived and then used to predict the distribution of stresses in the bent-tube sections. The radial pressures from the mandrel and the former on the tube-wall can also be calculated.

3.2.1 Equilibrium of forces acting on the tube in zone I

Figure 3.2 shows the tube and the tooling arrangement as well as the external forces applied on the tube in deformation zone I. Consider a tube element of length dx at a distance x from the entry plane. The forces acting on the element are illustrated in figure 3.3. The equilibrium equation for the forces in the x-direction is:

$$(F + dF) - F + \int_{A_{cs}} \mu_s \cdot p_s \cdot dA_{cs} \cdot dx$$

$$+ \int_{A_{cm}} \mu_m \cdot p_m \cdot dA_{cm} \cdot dx = 0 \qquad 3.1$$

where dA_{cs} and dA_{cm} are the incremental areas of contact between the tube-half external surface and the slider, and between the tube-half internal surface and the mandrel per unit length respectively, such that:

$$dA_{cs} = \frac{d_o}{2} \cdot d\phi \quad \text{and} \quad dA_{cm} = \frac{d_i}{2} \cdot d\phi \qquad 3.2$$

The slider pressure p_s and the mandrel pressure p_m are assumed to be uniform along the tube length as well as around its periphery. In addition, the coefficients of friction μ_s (slider) and μ_m (mandrel) are considered constant. Hence equation 3.1 can be written as:

$$dF + \mu_s \cdot p_s \int_{A_{cs}} dA_{cs} \cdot dx + \mu_m \cdot p_m \int_{A_{cm}} dA_{cm} \cdot dx = 0 \qquad 3.3$$

Substituting from equation 3.2 in equation 3.3 and integrating between

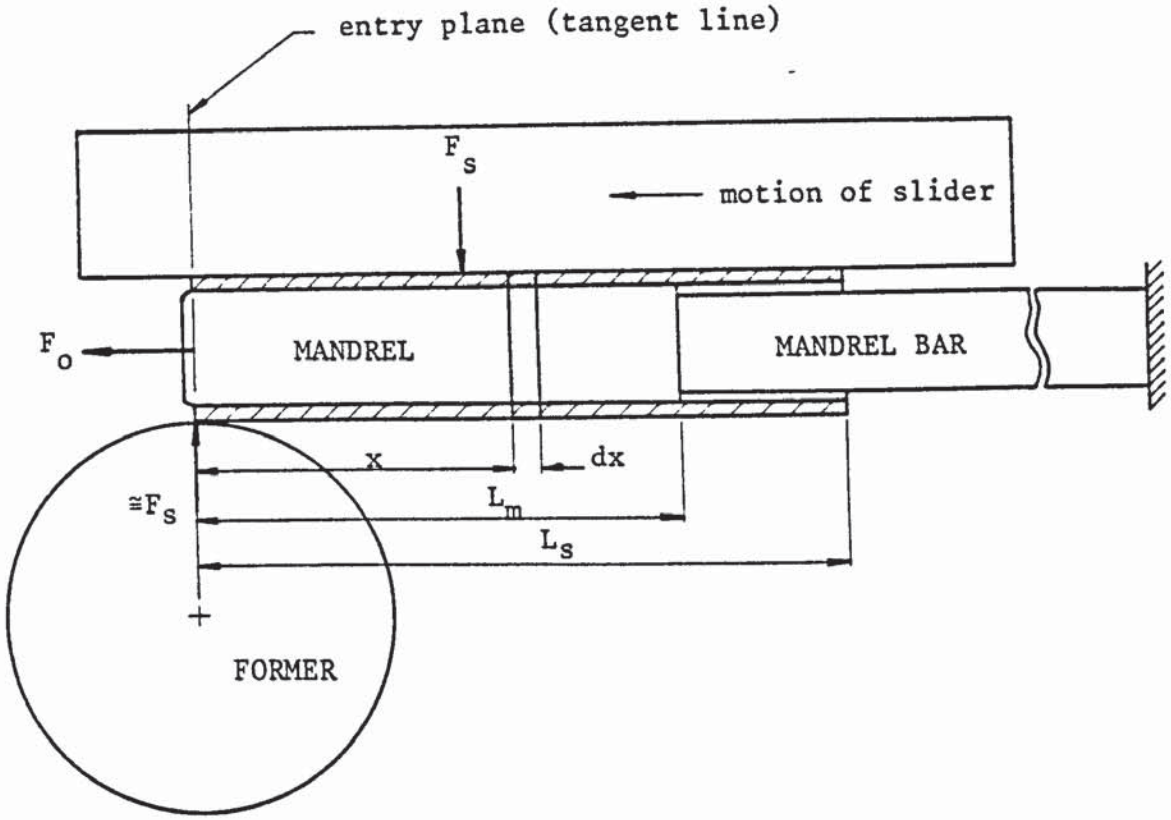

Figure 3.2: The tube and the tooling arrangement as the tube passes through Zone I

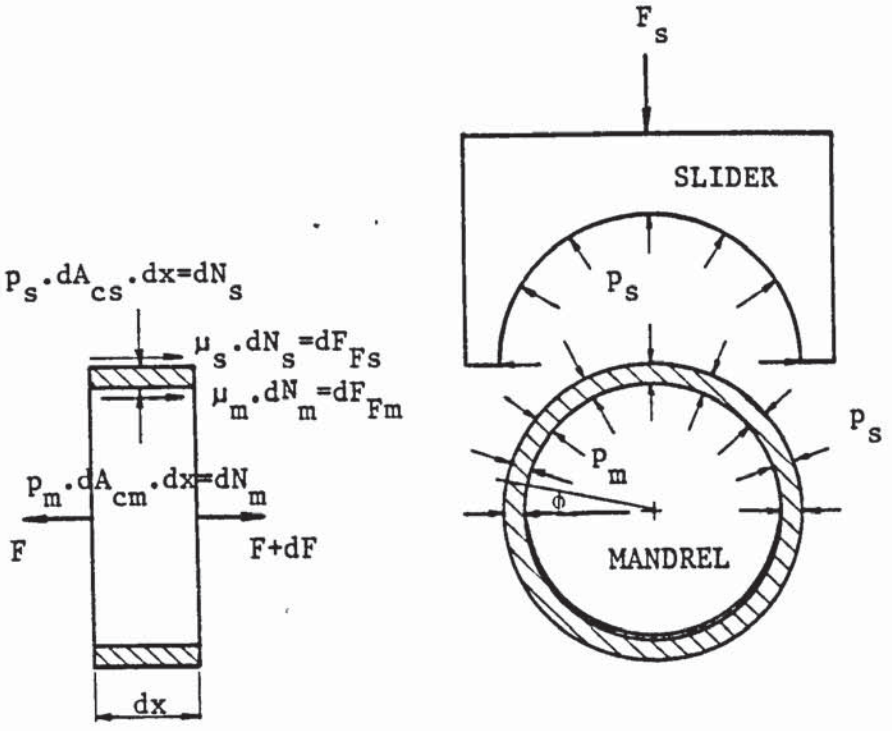

Figure 3.3: The pressures and forces acting on a tube element in deformation Zone I

the limits of ϕ and x; the equilibrium equation reduces to:

$$- F_o + \frac{\pi}{2}\mu_s \cdot d_o\, L_s \cdot p_s + \frac{\pi}{2}\mu_m \cdot d_i\, L_m \cdot p_m = 0 \qquad 3.4$$

The equilibrium equation of the forces in the y-direction is:

$$F_s = 2 \int_{\phi=0}^{\pi/2} dN_s \cdot \sin\phi$$

$$= 2 \int_{\phi=0}^{\pi/2} dN_m \cdot \sin\phi \qquad 3.5$$

where $dN_s = p_s \cdot dA_{cs} \cdot dx$ and $dN_m = p_m \cdot dA_{cm} \cdot dx$

Substituting from equation 3.2 in equation 3.5 and integrating between the limits of ϕ and x, equation 3.5 reduces to:

$$F_s = d_o \cdot L_s \cdot p_s$$
$$= d_i \cdot L_m \cdot p_m \qquad 3.6$$

Combining equations 3.4 and 3.6, and rearranging; then:

$$F_o = \frac{\pi}{2}\,(\mu_s + \mu_m) \cdot F_s \qquad 3.7$$

Equation 3.7 predicts the initial friction force (F_o) acting on the tube section at the entry plane where bending occurs. The external slider force F_s is measured experimentally during bending.

3.2.2 Equilibrium of forces acting on the tube in zone IIb

A tube element bounded by the entry plane and a plane at an angle $\delta\theta$, Figure 3.4, is considered. As a result of bending, the neutral plane N-N moves inward, ie. closer to the centre of bending and its angular position as measured from the tube centreline A-A is ϕ_N. The neutral plane is, then, used as a datum from which the angular position of any small element of tube is defined.

A small element (abcda'b'c'd') at an angular position ϕ has a length $R.\delta\theta$, width $r_m.\delta\phi$, and thickness t. The side areas are given by:

$$\delta A_1 = abcd = a'b'c'd' = r_m \cdot \delta\phi \cdot t \qquad 3.8$$

$$\delta A_2 = a'ad'd = b'bcc' = R \cdot \delta\theta \cdot t \qquad 3.9$$

$$\delta A_3 = b'baa' = cc'dd' = R \cdot \delta\theta \cdot r_m \cdot \delta\phi \qquad 3.10$$

where $R = R_o + r_m \cdot \sin(\phi - \phi_N)$

The tube cross-section at an angle $\frac{\delta\theta}{2}$ is shown in figure 3.5. This section is considered to be divided into three different regions; namely A, B and C. The tube material is stressed longitudinally in tension in regions A and B, ie. above the neutral plane N-N and in compression in region C. However, in region A the tube wall is supported internally by the mandrel and externally by the former groove. But in region B, the tube wall is only supported by the internal mandrel.

3.2.2.1 Distribution of stresses in region B

In this region, the longitudinal stress is tensile and its inplane component in the tube section at an angle $\frac{\delta\theta}{2}$ is

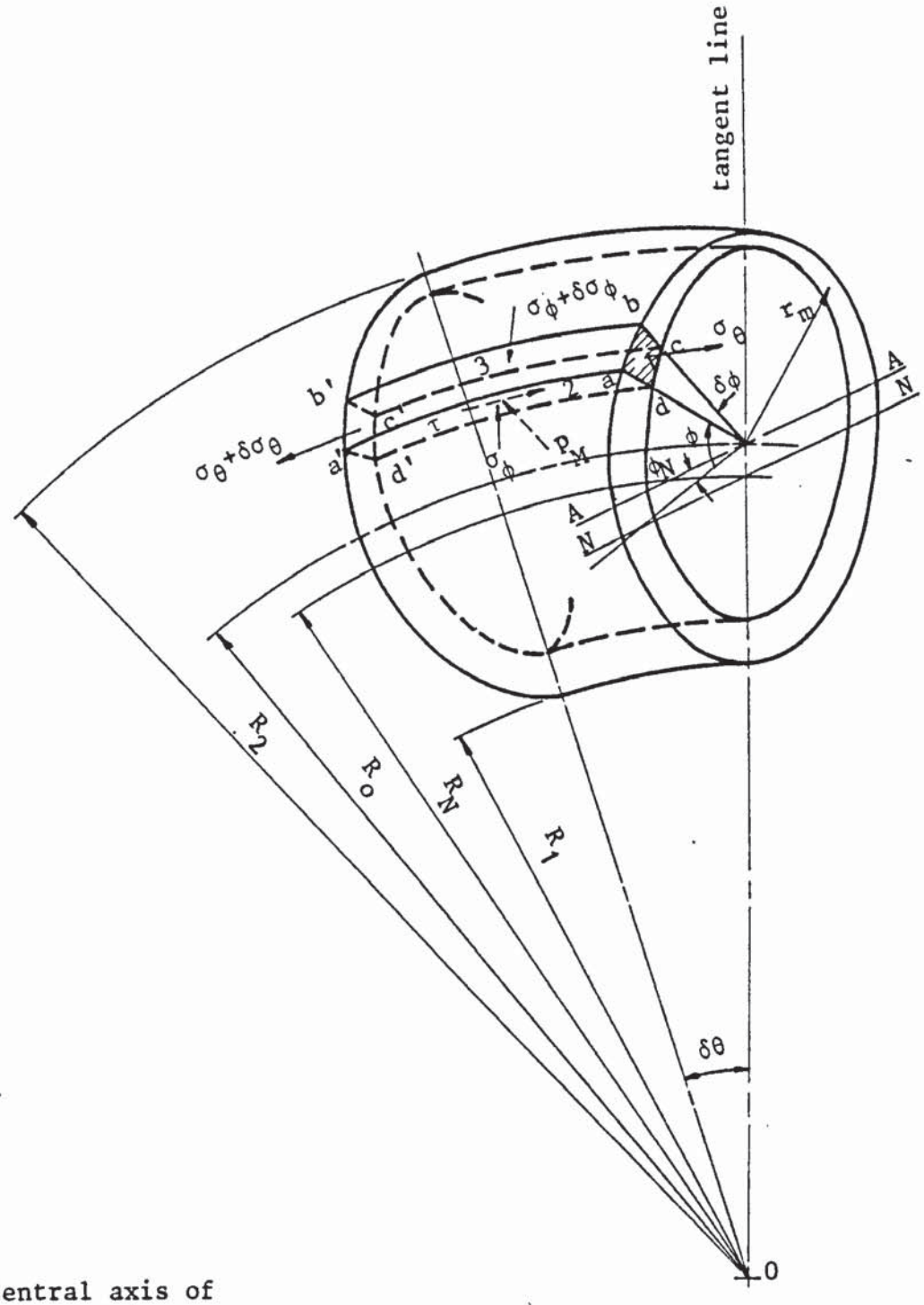

AA : Central axis of tube section

NN : Neutral axis

Figure 3.4: The stresses acting on a three dimensional small element of tube (abcd a'b'c'd') at an angle ϕ in Zone IIb

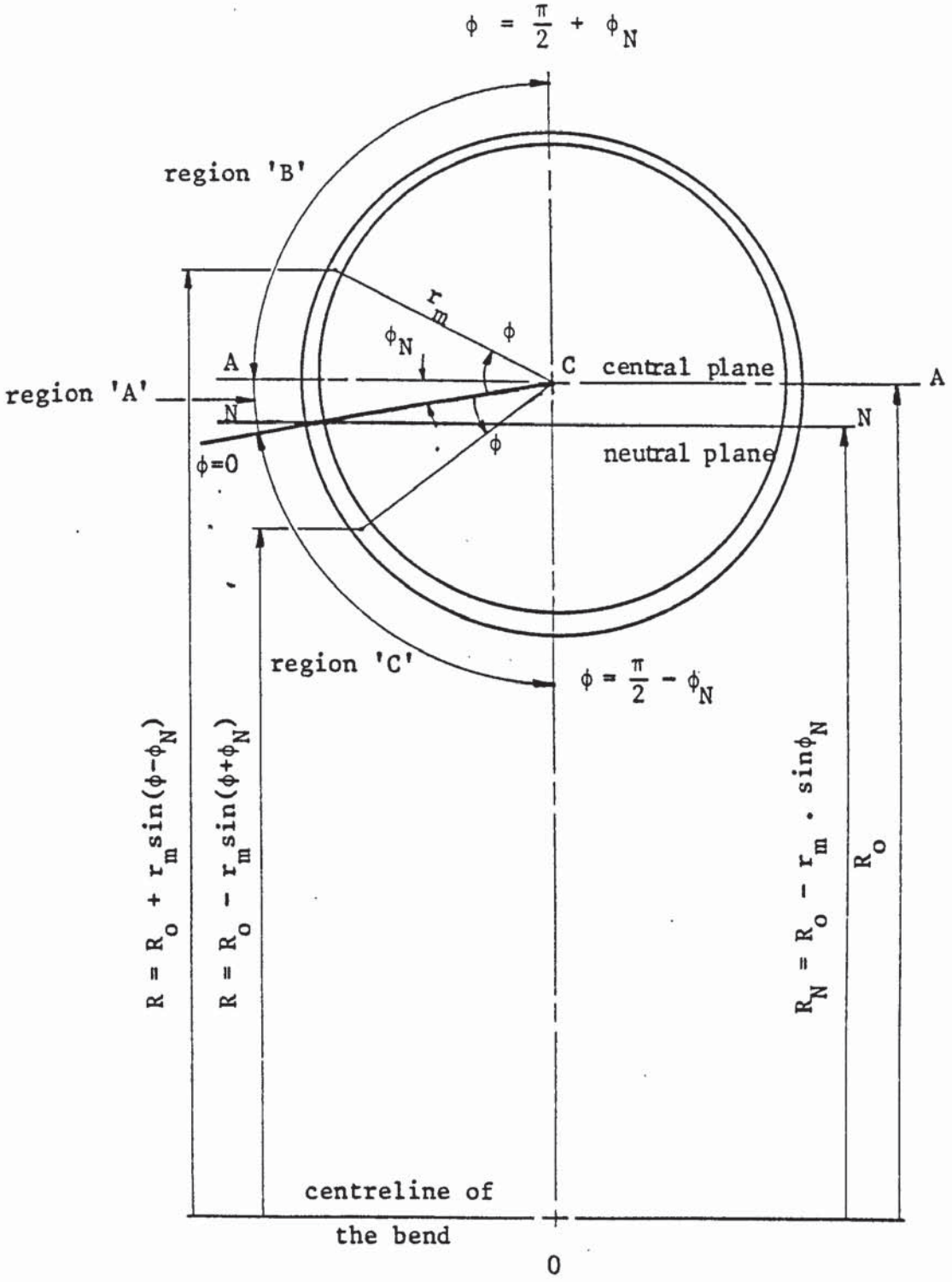

Figure 3.5: The tube section in Zone IIb is considered to be divided into three regions; A, B and C

$$(2\sigma_\theta + \delta\sigma_\theta) \cdot \sin\frac{\delta\theta}{2}$$

as illustrated in figure 3.6. It can be seen also that the hoop stress is assumed to be compressive and the mandrel is exerting an internal pressure p_M on the tube-wall.

(i) Variation of hoop stress with angle ϕ

The equilibrium of forces acting on the small element of tube (b) in the hoop direction, figure 3.6, is expressed as:

$$\sigma_\phi \cdot \delta A_2 \cdot \cos\frac{\delta\phi}{2} - (\sigma_\phi + \delta\sigma_\phi) \cdot \delta A_2 \cdot \cos\frac{\delta\phi}{2} - (2\sigma_\theta + \delta\sigma_\theta) \cdot \delta A_1 \cdot \sin\frac{\delta\theta}{2} \cdot \cos(\phi - \phi_N) = 0 \qquad 3.11$$

Substituting from equations 3.8 and 3.9 in equation 3.11 and since for very small angles $\sin\frac{\delta\theta}{2} = \frac{\delta\theta}{2}$ and $\cos\frac{\delta\phi}{2} = 1$; therefore equation 3.11 reduces to:

$$-\delta\sigma_\phi \cdot R \cdot \delta\theta \cdot t - (2\sigma_\theta + \delta\sigma_\theta) \cdot r_m \cdot \delta\phi \cdot t \cdot \frac{\delta\theta}{2} \cdot \cos(\phi - \phi_N) = 0$$

Dividing by $R \cdot \delta\theta \cdot t$ and ignoring the products of increments; then:

$$\delta\sigma_\phi = -\frac{r_m \cdot \cos(\phi-\phi_N)}{R} \cdot \sigma_\theta \cdot \delta\phi$$

But $R = R_o + r_m \sin(\phi - \phi_N)$; thus:

$$\delta\sigma_\phi = -\frac{r_m \cdot \cos(\phi-\phi_N)}{R_o + r_m \sin(\phi-\phi_N)} \cdot \sigma_\theta \cdot \delta\phi \qquad 3.12$$

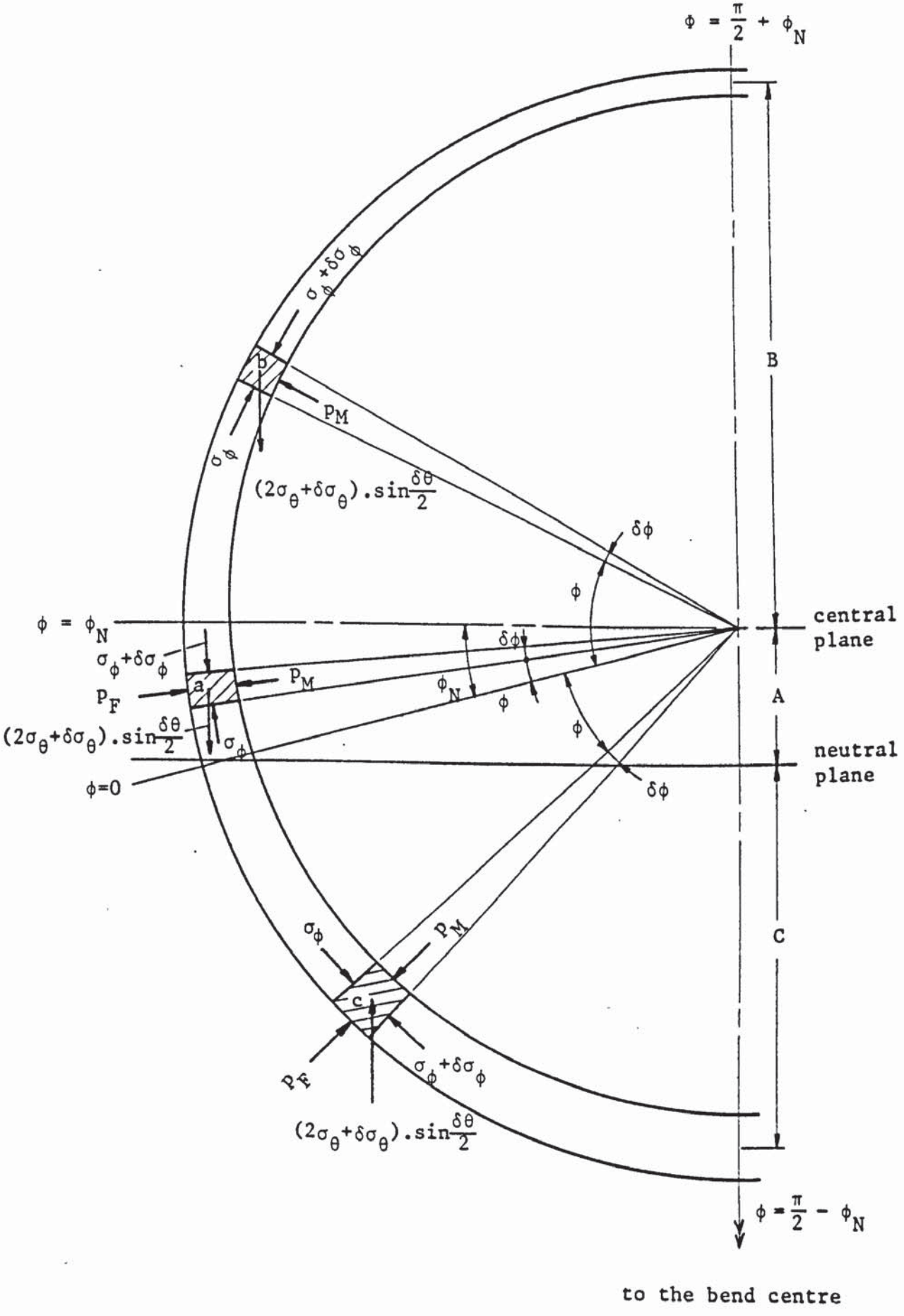

Figure 3.6: The states of stress at different angular positions in the three regions of tube section at an angle $\frac{\delta\theta}{2}$ in the deformation zone IIb.

Equation 3.12 gives the incremental change in the hoop stress for an incremental angle $\delta\phi$ at any angular position ϕ. This equation, however, cannot be integrated due to the variability of σ_θ with the angle ϕ. Nevertheless, equation 3.12 can be used to predict the distribution of the hoop stresses around the periphery of the tube section.

(ii) <u>The relationship between the longitudinal and hoop stresses, and the mandrel pressure</u>

For the same small element (b), figure 3.6, the equilibrium equation of the forces in the radial direction is:

$$p_M \cdot \delta A_3 - (2\sigma_\theta + \delta\sigma_\theta) \cdot \delta A_1 \cdot \sin\frac{\delta\theta}{2} \cdot \sin(\phi - \phi_N) + (2\sigma_\phi + \delta\sigma_\phi) \cdot \delta A_2 \cdot \sin\frac{\delta\phi}{2} = 0 \qquad 3.13$$

Substituting from equations 3.8, 3.9 and 3.10 in equation 3.13; thus:

$$p_M \cdot r_m \cdot R - (2\sigma_\theta + \delta\sigma_\theta) \cdot t \cdot r_m \cdot \frac{1}{2} \cdot \sin(\phi - \phi_N)$$

$$+ (2\sigma_\phi + \delta\sigma_\phi) \cdot R \cdot t \cdot \frac{1}{2} = 0$$

But, $\delta\sigma_\theta$ and $\delta\sigma_\phi$ may be neglected when compared with $2\sigma_\theta$ and $2\sigma_\phi$ respectively, therefore the equilibrium equation becomes:

$$p_M \cdot r_m \cdot R - \sigma_\theta \cdot t \cdot r_m \cdot \sin(\phi - \phi_N) + \sigma_\phi \cdot R \cdot t = 0 \qquad 3.14$$

Dividing by R . t, equation 3.14 reduces to:

$$\sigma_\phi = -K_1 \cdot p_M + K_2 \cdot \sigma_\theta \qquad 3.15$$

$$\text{or} \quad \sigma_\theta = (K_1 \cdot p_M + \sigma_\phi) / K_2 \qquad 3.15a$$

$$\text{where } K_1 = \frac{r_m}{t} \text{ and } K_2 = \frac{r_m \cdot \sin(\phi - \phi_N)}{R_o + r_m \cdot \sin(\phi - \phi_N)}$$

3.2.2.2 Distribution of stresses in regions A and C

Figure 3.6 shows the stresses and the pressures acting on small elements of tube (a) and (c) in the regions A and C. Assuming the hoop stress to be compressive and following the same procedure outlined in section 3.2.2.1, the equilibrium equations in the hoop and radial directions for both regions can be obtained; such that:

for region A

$$\delta\sigma_\phi = -\frac{r_m \cdot \cos(\phi_N - \phi)}{R_o - r_m \cdot \sin(\phi_N - \phi)} \cdot \sigma_\theta \cdot \delta\phi \qquad 3.16$$

and $\sigma_\theta = (K_1 \cdot \Delta p - \delta_\phi) / K2$ 3.17

where $\Delta p = p_F - p_M$

, $K_1 = \frac{r_m}{t}$

and $K_2 = \frac{r_m \cdot \sin(\phi_N - \phi)}{R_o - r_m \cdot \sin(\phi_N - \phi)}$

for region C

$$\delta\sigma_\phi = - \frac{r_m \cdot \cos(\phi + \phi_N)}{R_o - r_m \cdot \sin(\phi + \phi_N)} \cdot \sigma_\theta \cdot \delta\phi \qquad 3.18$$

and $\hat{\sigma}_\theta = (K_1 \cdot \Delta p + \sigma_\phi) / K2$ 3.19

where $\Delta p = p_M - p_F$

, $K_1 = \frac{r_m}{t}$

and $K_2 = \frac{r_m \cdot \sin(\phi + \phi_N)}{R_o - r_m \cdot \sin(\phi + \phi_N)}$

3.2.2.3 The equilibrium between the internal and external forces in the longitudinal direction

The initial friction force (F_o), given by equation 3.7, is considered as the external force applied on the tube section in zone IIb. For the equilibrium in the longitudinal direction, it can be stated that the summation of the internal longitudinal

forces acting on the whole tube section is equal to the external force (F_o), which can be expressed mathematically as:

$$\sum_{\text{tube section}} \sigma_\theta \cdot \delta A_1 = F_o \qquad 3.20$$

It should be emphasised that zone IIb is bounded within a very small angle; hence the effect of friction in this zone is negligible and thus, it can reasonably be assumed that $\delta\sigma_\theta = 0$, see figure 3.4.

3.3 Development of plastic strains in zone IIb

Consider a straight tube element having a small length l_o and a uniform wall thickness t_o is bent to a mean bend radius R_o, as illustrated in figure 3.7. The neutral plane of bend radius R_N, defined as the plane at which the tube material is neither stretched nor compressed, remains unchanged in length, ie. $l_N = l_o$. However, the material above the neutral plane N-N (where $R > R_N$) is stretched and increases in length, while that below N-N shortens and is under compression.

The incremental longitudinal strain can be predicted from the geometrical configuration of the process as follows: at an angle $(\phi - \delta\phi)$ from the neutral plane, the bent-tube element has a length $l_{\phi-\delta\phi}$; where:

$$l_{\phi-\delta\phi} = R_{\phi-\delta\phi} \cdot \delta\theta = [R_o + r_m \cdot \sin(\phi - \delta\phi - \phi_N)] \cdot \delta\theta \qquad 3.21$$

The next element is at an angle (ϕ) and its length l_ϕ can be written as:

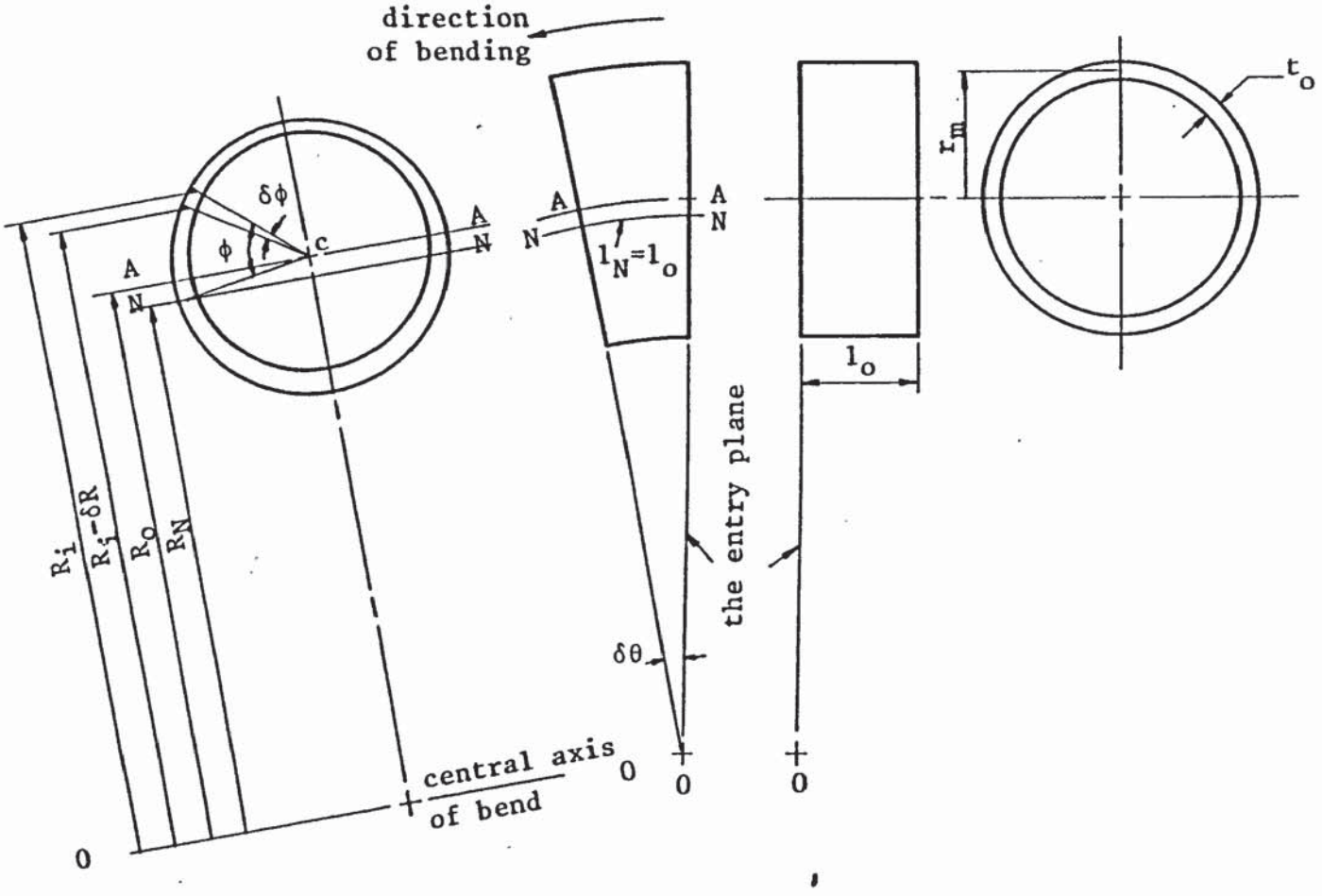

b. the bent tube-element

a. the tube-element before bending

Figure 3.7: An element of tube before bending and just after it has been bent

$$1_{\phi} = R_{\phi} \cdot \delta\theta = [R_o + r_m \cdot \sin(\phi - \phi_N)] \cdot \delta\theta \qquad 3.22$$

Thus, the incremental longitudinal strain at the angular position ϕ may be defined as:

$$\delta\varepsilon_{\theta,\phi} = \frac{\delta 1_{\phi}}{1_{\phi-\delta\phi}} = \frac{1_{\phi} - 1_{\phi-\delta\phi}}{1_{\phi-\delta\phi}} \qquad 3.23$$

Substituting from equations 3.21 and 3.22 in equation 3.23; the incremental longitudinal strain at a general angle ϕ is:

$$\delta\varepsilon_{\theta,\phi} = \frac{r_m [\sin(\phi - \phi_N) - \sin(\phi - \delta\phi - \phi_N)]}{[R_o + r_m \cdot \sin(\phi - \delta\phi - \phi_N)]} \qquad 3.24$$

If the elastic strains are neglected, the developed strains $\delta\varepsilon_{\theta}$, $\delta\varepsilon_{\phi}$ and $\delta\varepsilon_{t}$ can be considered to be the plastic incremental strains in the principal directions. Assuming no change of volume during deformation, the condition of incompressibility at any angular position ϕ on the tube section can be written such that:

$$\delta\varepsilon_{\theta} + \delta\varepsilon_{\phi} + \delta\varepsilon_{t} = 0$$

If the states of stress in the principal directions (σ_{θ}, σ_{ϕ} and σ_{r}) are known at any position, Lévy-Mises[73] equation 3.25 can be applied to predict the other two incremental strains $\delta\varepsilon_{\phi}$ and $\delta\varepsilon_{t}$. The general 'Lévy-Mises' equation is:

$$\frac{\delta\varepsilon_x}{\sigma'_x} = \frac{\delta\varepsilon_y}{\sigma'_y} = \frac{\delta\varepsilon_z}{\sigma'_z} = \frac{\delta\gamma_{yz}}{\tau_{yz}} = \frac{\delta\gamma_{zx}}{\tau_{zx}} = \frac{\delta\gamma_{xy}}{\tau_{xy}} = \delta\lambda \qquad 3.25$$

where σ'_x, σ'_y and σ'_z are the instantaneous deviatoric stresses and τ_{yz}, τ_{zx} and τ_{xy} are the shear stresses. In the present analysis, the stresses and the incremental strains are assumed to be in the principal directions; thus equation 3.25 reduces to:

$$\frac{\delta\varepsilon_\theta}{\sigma_\theta - \sigma_m} = \frac{\delta\varepsilon_\phi}{\sigma_\phi - \sigma_m} = \frac{\delta\varepsilon_t}{\sigma_r - \sigma_m} \qquad 3.26$$

where $\sigma_m = \frac{1}{3}(\sigma_\theta + \sigma_\phi + \sigma_r)$

Equation 3.26 can be written in the form:

$$\frac{\delta\varepsilon_\theta}{2\sigma_\theta - \sigma_\phi - \sigma_r} = \frac{\delta\varepsilon_\phi}{2\sigma_\phi - \sigma_r - \sigma_\theta} = \frac{\delta\varepsilon_t}{2\sigma_r - \sigma_\theta - \sigma_\phi} \qquad 3.26a$$

where $\delta\varepsilon_\phi$ and $\delta\varepsilon_t$ can be obtained as a function of $\delta\varepsilon_\theta$; such that:

$$\delta\varepsilon_{\phi,\phi} = \left[\frac{2\sigma_\phi - \sigma_r - \sigma_\theta}{2\sigma_\theta - \sigma_\phi - \sigma_r}\right] \cdot \delta\varepsilon_{\theta,\phi} \qquad 3.27$$

and

$$\delta\varepsilon_{t,\phi} = \left[\frac{2\sigma_r - \sigma_\theta - \sigma_\phi}{2\sigma_\theta - \sigma_\phi - \sigma_r}\right] \cdot \delta\varepsilon_{\theta,\phi} \qquad 3.28$$

Equation 3.24 together with equations 3.27 and 3.28 can be used to predict the incremental strains at any angular position ϕ on the bent-tube section. The total strains at angle ϕ may be defined as:

$$\varepsilon_{\theta,\phi} = \sum_{i=0}^{\phi} \delta\varepsilon_{\theta,i} \qquad 3.29$$

$$\varepsilon_{\phi,\phi} = \sum_{i=0}^{\phi} \delta\varepsilon_{\phi,i} \qquad 3.30$$

$$\varepsilon_{t,\phi} = \sum_{i=0}^{\phi} \delta\varepsilon_{t,i} \qquad 3.31$$

3.4 Yield criterion

The concept of "equivalent stress" and "equivalent strain" can be used to relate the states of stress and strain at any angle ϕ on the tube section to the stress-strain properties of tube material. Consequently, if the principal stresses σ_θ, σ_ϕ and σ_r represent the state of stress at any point, then the equivalent stress $\bar{\sigma}$ can be defined as:

$$\bar{\sigma} = \sqrt{\tfrac{1}{2}}\,[(\sigma_\theta - \sigma_\phi)^2 + (\sigma_\phi - \sigma_r)^2 + (\sigma_r - \sigma_\theta)^2]^{\frac{1}{2}} \qquad 3.32$$

Also, the incremental equivalent strain $\delta\bar{\varepsilon}$ can be written as:

$$\delta\bar{\varepsilon} = \sqrt{\frac{2}{9}}\,[(\delta\varepsilon_\theta - \delta\varepsilon_\phi)^2 + (\delta\varepsilon_\phi - \delta\varepsilon_t)^2 + (\delta\varepsilon_t - \delta\varepsilon_\theta)^2]^{\frac{1}{2}} \qquad 3.33$$

where $\delta\varepsilon_\theta$, $\delta\varepsilon_\phi$ and $\delta\varepsilon_t$ are the incremental principal strains at any point.

The condition of stress under which the plastic flow proceeds is

assumed to obey the von Mises' yield criterion, which states:

$$(\sigma_1 - \sigma_2)^2 + (\sigma_2 - \sigma_3)^2 + (\sigma_3 - \sigma_1)^2 = 2\bar{\sigma}^2$$

where σ_1, σ_2 and σ_3 are the principal stresses and $\bar{\sigma}$ is the uniaxial stress necessary to cause plastic flow. For a rigid, work-hardening material; $\bar{\sigma}$ is a parameter depending on the amount of pre-strain. The tube material stress-strain relationship is assumed to follow the "Ludwig" empirical equation[73]:

$$\bar{\sigma} = Y + H\bar{\varepsilon}^n \qquad 3.34$$

where Y is the material yield stress; H and n are constants depending on the work-hardening characteristics of the material. The values of Y, H and n are obtained from a uniaxial tensile test for the tube material used.

3.5 Effect of friction on the stresses and the strains in zone IIf

As discussed in section 3.1, the tube material undergoes an additional plastic deformation in zone IIf due to friction as the tube is pulled over the mandrel and around the former. The aim of this section, therefore, is to develop the distribution of stresses and strains as the tube approaches the exit plane.

Figure 3.8 shows a tube element in zone IIf. The stresses applied on a small element, in region B, at an angular position ϕ are also shown. The equilibrium equation in the longitudinal direction can be written as:

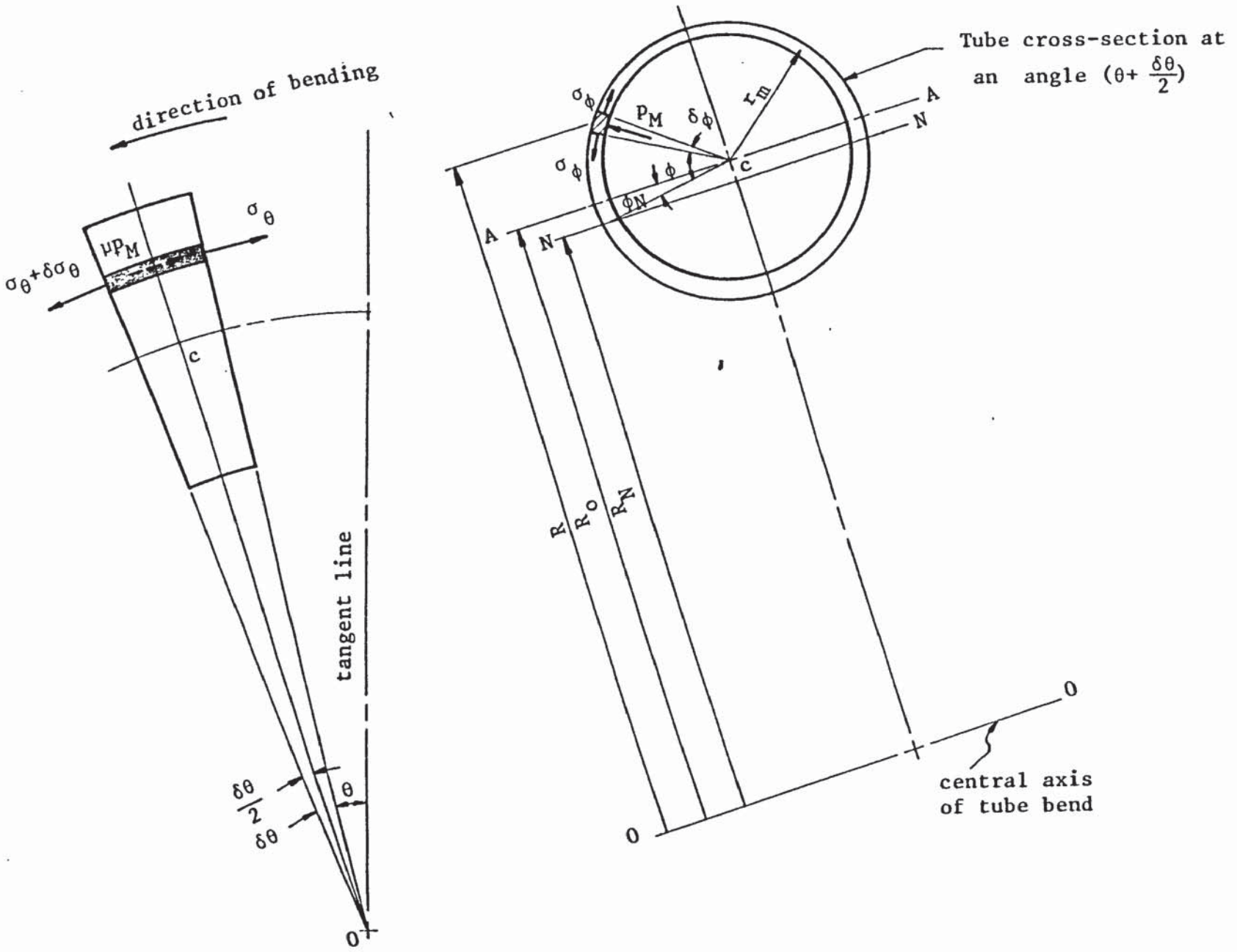

Figure 3.8: Longitudinal, hoop and radial stresses acting on a tube element in zone IIf

$$(\sigma_\theta + \delta\sigma_\theta) \cdot \delta A_1 \cdot \cos\frac{\delta\theta}{2} - \sigma_\theta \cdot \delta A_1 \cdot \cos\frac{\delta\theta}{2} - \tau \cdot \delta A_3 = 0 \qquad 3.35$$

The Coulomb friction model is assumed to apply, ie:

$$\tau = \mu_M \cdot p_M \qquad 3.36$$

Substituting from equation 3.36 in equation 3.35 and replacing δA_1 and δA_3 with their values given in equations 3.8 and 3.10 respectively, the equilibrium equation yields:

$$\delta\sigma_\theta = \mu_M \cdot p_M \cdot \frac{R}{t} \cdot \delta\theta \qquad 3.37$$

where $R = R_o + r_m \cdot \sin(\phi - \phi_N)$

It may be assumed that the radial pressure p_M is uniform over the whole arc of contact between the mandrel and the tube; and μ_M has a constant value. Thus, by integrating equation 3.37 between the limits $\theta = 0$ and $\theta = \theta_1$, the longitudinal stress at the exit plane can be given by:

$$\sigma_{\theta 1} = \sigma_{\theta 0} + \mu_M \cdot p_M \cdot \frac{R_o + r_m \cdot \sin(\phi - \phi_N)}{t} \cdot \theta_1 \qquad 3.38$$

where $\sigma_{\theta 0}$ is the longitudinal stress at the entry plane and θ_1 is the angle contained between the entry and exit planes. In zone IIf, the tube internal surface in regions A and C is not in contact with the mandrel-tip, ie. $p_M = 0$. Similar equations like equation 3.38 can be obtained from the equilibrium of forces in the longitudinal direction such that:

For region A: $$\sigma_{\theta 1} = \sigma_{\theta 0} + \mu_F \cdot p_F \cdot \frac{R_o - r_m \cdot \sin(\phi_N - \phi)}{t} \cdot \theta_1 \qquad 3.39$$

For region C: $$\sigma_{\theta 1} = \sigma_{\theta 0} + \mu_F \cdot p_F \cdot \frac{R_o - r_m \cdot \sin(\phi + \phi_N)}{t} \cdot \theta_1 \qquad 3.40$$

At the exit plane, the state of stress at any angle ϕ on the tube-section is $\sigma_{\theta 1}$, $\sigma_{\phi 1}$ and σ_{r1}. Hence, the equivalent stress at this angle $\bar{\sigma}_1$ can be written as:

$$\bar{\sigma}_1 = \sqrt{\tfrac{1}{2}} \left[(\sigma_{\theta 1} - \sigma_{\phi 1})^2 + (\sigma_{\phi 1} - \sigma_{r1})^2 + (\sigma_{r1} - \sigma_{\theta 1})^2\right]^{\frac{1}{2}} \qquad 3.41$$

And the equivalent strain $\bar{\varepsilon}_1$ can be obtained from the material stress-strain relationship, such that:

$$\bar{\varepsilon}_1 = [(\bar{\sigma}_1 - Y) / H]^{\frac{1}{n}} \qquad 3.42$$

Thus, the increase in the equivalent strain is:

$$\Delta\bar{\varepsilon} = \bar{\varepsilon}_1 - \bar{\varepsilon}_0 \qquad 3.42a$$

where $\bar{\varepsilon}_0$ is the equivalent strain as obtained from zone IIb.

Equation 3.26a can be written as:

$$\frac{\Delta\varepsilon_\theta}{2\sigma_\theta - \sigma_\phi - \sigma_r} = \frac{\Delta\varepsilon_\phi}{2\sigma_\phi - \sigma_r - \sigma_\theta} = \frac{\Delta\varepsilon_t}{2\sigma_r - \sigma_\theta - \sigma_\phi} = \frac{\Delta\bar{\varepsilon}}{2\bar{\sigma}}$$

which can be used to predict the additional straining in the longitudinal, hoop and thickness directions, such that:

$$\Delta\varepsilon_\theta = \frac{\Delta\bar{\varepsilon}}{2\bar{\sigma}_1} \cdot (2\sigma_{\theta 1} - \sigma_{\phi 1} - \sigma_{r1}) \qquad 3.43$$

$$,\Delta\varepsilon_\phi = \frac{\Delta\bar{\varepsilon}}{2\bar{\sigma}_1} \cdot (2\sigma_{\phi 1} - \sigma_{r1} - \sigma_{\theta 1}) \qquad 3.44$$

and $$\Delta\varepsilon_t = \frac{\Delta\bar{\varepsilon}}{2\bar{\sigma}_1} \cdot (2\sigma_{r1} - \sigma_{\theta 1} - \sigma_{\phi 1}) \qquad 3.45$$

3.6 Influence of axial vibration of mandrel on the process

To evaluate the effect of ultrasonic vibration of the mandrel on the mechanics of metal deformation during the bending process; a theoretical analysis which is based on the mechanism of friction vector reversal is considered. The aim of this analysis is to describe, in mathematical terms, that mechanism and to develop expressions which can enable the amount of reduction in the friction forces to be calculated. The theoretical analysis with applied ultrasonic vibrations will be undertaken for the two deformation zones, namely: the initial friction zone I and the final friction zone IIf. Consequently, the initial friction force F_o as well as the distribution of the longitudinal stress at the exit plane, under the vibratory conditions, can be predicted.

Suppose that the mandrel with the mandrel-bar are axially vibrated at a frequency f (kHz) which results in a standing axial vibration-wave of half-wave length $\frac{\lambda}{2}$ to be established. The wave-guide, ie. the mandrel-bar and the mandrel attached at its end, is tuned to resonate at the design frequency f in such a way that a displacement antinode is

situated at the free end of the mandrel. Accordingly, the wave-guide length is, roughly, equal to a number of $\frac{\lambda}{2}$ and the mandrel length, as designed, has a length of $\frac{\lambda}{2}$. Figure 3.9 shows the part of the axial vibration-wave as applied to the mandrel where the maximum amplitudes of vibration are situated at the end faces of the mandrel, ie. at the displacement antinodes. Since the displacement amplitude varies from maximum, A_m, at $x = 0$ to zero at $x = \frac{\lambda}{4}$; therefore an average value for the displacement in this range can be employed as:

$$A_{a1} = \frac{4}{\lambda} \int_{x=0}^{x=\frac{\lambda}{4}} A \cdot dx \qquad 3.46$$

where $A = A_m \cdot \cos \frac{x}{\lambda} \cdot 2\pi$

Substituting with the value of A in equation 3.46 and integrating between the limits; then:

$$A_{a1} = 0.6366\ A_m \qquad 3.47$$

Also, the average displacement amplitude for the range $x = \frac{\lambda}{4}$ to $x = \frac{3}{8}\lambda$ is:

$$A_{a2} = \frac{8}{\lambda} \int_{x=\lambda/4}^{3\lambda/8} A_m \cdot \cos\left(\frac{x}{\lambda} \cdot 2\pi\right) \cdot dx \qquad 3.48$$

Integrating between the limits of x, equation 3.48 yields:

$$| A_{a2} | = 0.3729\ A_m \qquad 3.49$$

Thus, the average displacement amplitude for the vibrations of the

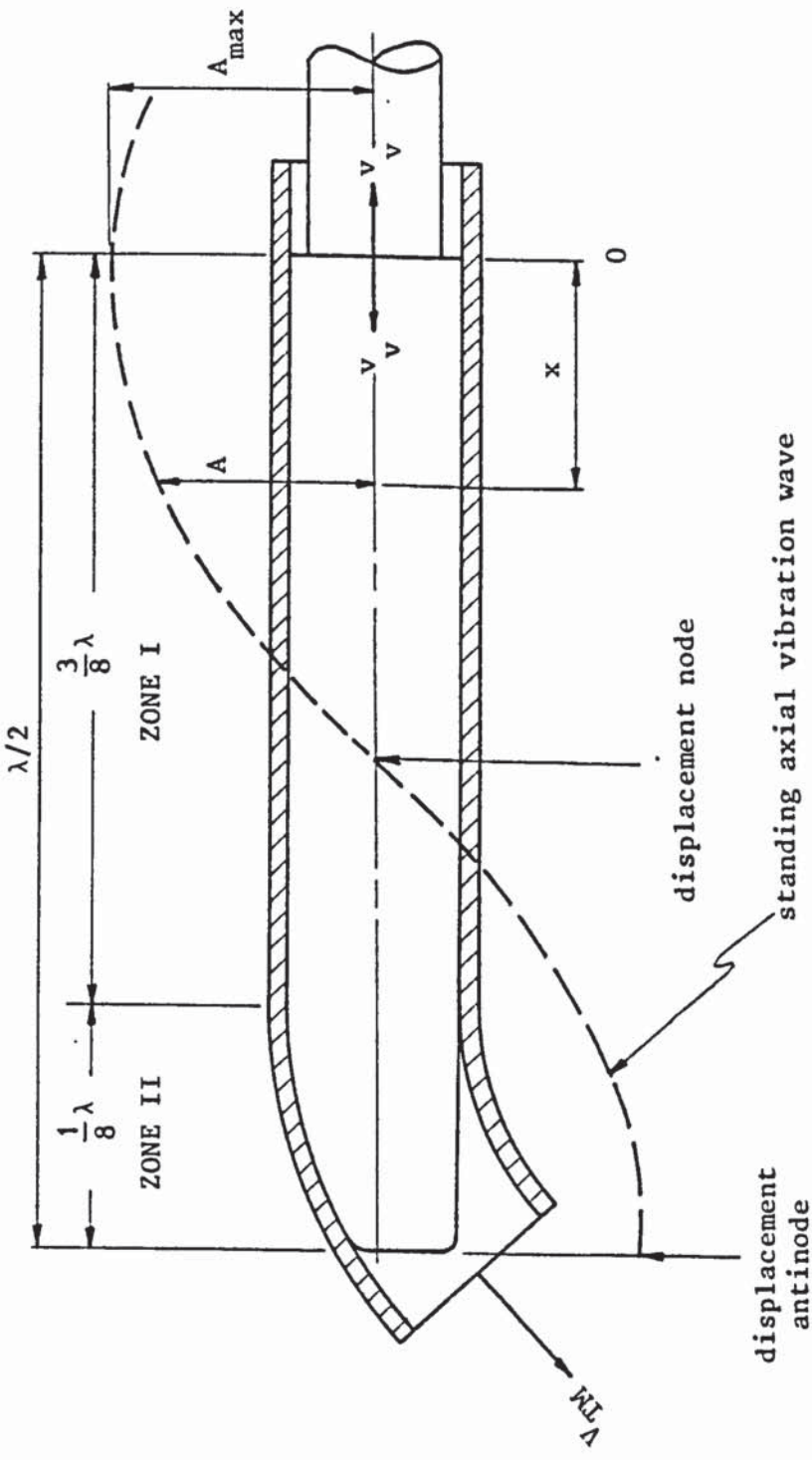

Figure 3.9: Longitudinal section through the deformation area of tube during bending on a solid mandrel axially vibrated at an ultrasonic frequency

mandrel-shank (zone I) can be obtained by combining equations 3.47 and 3.49, such that:

$$A_{aI} = (0.6366\ A_m \times \frac{\lambda}{4} + 0.3729\ A_m \times \frac{\lambda}{8}) \ / \ \frac{3}{8}\lambda$$

which reduces to:

$$A_{aI} = 0.5487\ A_m \qquad 3.50$$

Similarly, for the mandrel-tip (zone II); the average displacement amplitude can be obtained as:

$$A_{aII} = 0.9\ A_m \qquad 3.51$$

3.6.1 Friction vector reversal effect in zone I

Figure 3.10 is a diagrammatic representation showing the friction reversal effect as the tube is pulled over the mandrel-shank in deformation zone I. The displacement curve at any point BI at a distance x is a sine-wave which can be expressed mathematically as:

$$a_v = A_{aI} \cdot \sin \omega t$$

where a_v is the vibration displacement at any time t, and A_{aI} is the average displacement-amplitude as given by equation 3.50. It may be observed that point BI, on the tube bore-mandrel shank interface CI-CI, participates in two movements: advancing in the direction of tube motion with a mean velocity V_{TM} and oscillatory with a velocity v_v; where:

$$V_{TM} = \frac{2\pi N}{60} \cdot R_o$$

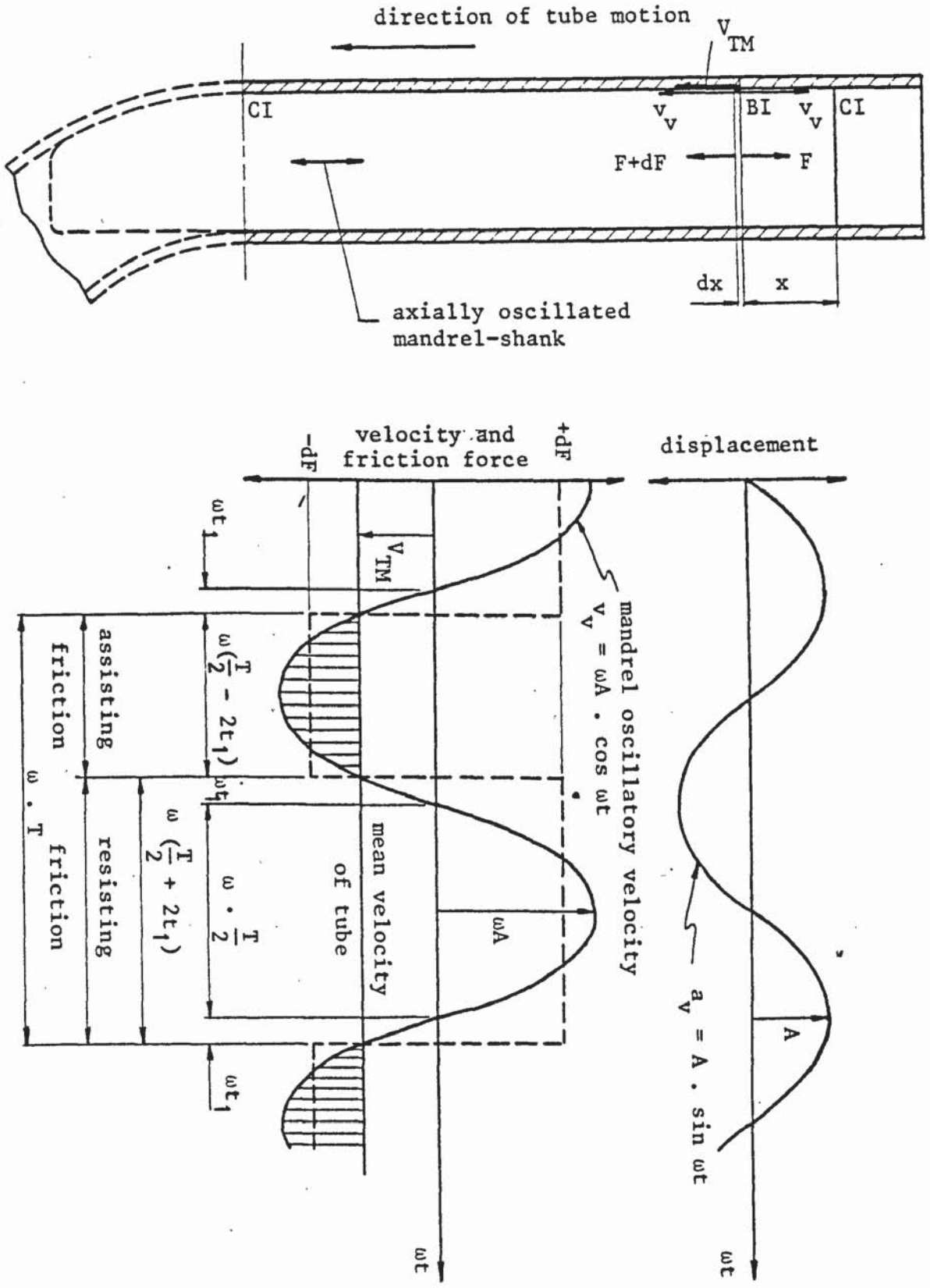

Figure 3.10: Diagram showing the friction reversal effect as the tube is pulled over the mandrel-shank in the deformation Zone I

and $v_v = \omega A_{aI} \cdot \cos \omega t$

N is the speed in rev min^{-1} of the machine shaft during bending. The resultant vector of the relative velocity of point BI on the contact surface changes its direction during the time (T) of a period of oscillation. In a part of that time, ie. $(\frac{T}{2} + 2t_1)$, when the oscillatory velocity is opposite in direction to the advancing velocity of tube, the resultant vector coincides with the direction of the tube motion. During the rest of the time, ie. $(\frac{T}{2} - 2t_1)$, the resultant vector will have an opposite direction to the tube motion if the oscillatory velocity is greater than the advancing velocity of tube. As a result of the changes in the direction of the relative velocity vector, there is a reduction in the effective friction force. This result can be explained mathematically with reference to figure 3.10. It may be seen that the increase in the friction force, dF, is positive during the time $(\frac{T}{2} + 2t_1)$, ie. it resists the motion of the tube, while it is negative during the rest of the time $(\frac{T}{2} - 2t_1)$ and, therefore, it assists the tube motion. Consequently, the ratio between the effective increase in the friction force under the oscillatory conditions, $\overline{dF}$, to that under the non-oscillatory can be written as:

$$k = [\omega(\frac{T}{2} + 2t_1) - \omega(\frac{T}{2} - 2t_1)] \; / \; \omega T$$

which can be simplified such that:

$$k = \frac{4t_1}{T} \qquad 3.52$$

However, it can be seen that the relative movement of point BI, ie.

between the tube-bore and the mandrel-shank is zero when:

$$-V_{TM} = \omega A_{aI} \cdot \cos\left(\omega t_1 + \frac{\pi}{2}\right)$$

which may be rearranged, such that:

$$t_1 = \frac{1}{\omega} \sin^{-1} \frac{V_{TM}}{\omega A_{aI}}$$

Substituting for t_1 in equation 3.52; therefore:

$$k = \frac{4}{\omega T} \sin^{-1} \frac{V_{TM}}{\omega A_{aI}}$$

But $\omega T = 2\pi$

Thus, the value of k can be reduced to:

$$k = \frac{2}{\pi} \sin^{-1} \frac{V_{TM}}{\omega A_{aI}} = \frac{\overline{dF}}{dF}$$

Alternatively, $\overline{dF} = \frac{2 \cdot dF}{\pi} \cdot \sin^{-1} \frac{V_{TM}}{\omega A_{aI}}$ 3.53

Integrating equation 3.53 between $x = 0$ and $x = \frac{3}{8}\lambda$; it yields:

$$\bar{F}_{oM} = \frac{2 F_{oM}}{\pi} \cdot \sin^{-1} \frac{V_{TM}}{\omega A_{aI}}$$ 3.54

where F_{oM} is the force necessary to overcome friction at the tube bore-mandrel shank interface in zone I under the non-oscillatory conditions, and is given by:

$$F_{oM} = \frac{\pi}{2} \cdot \mu_M \cdot F_s \quad \text{(see equation 3.7)}$$

Substituting for F_{oM} in equation 3.54; therefore:

$$\bar{F}_{oM} = \mu'_M \cdot F_s \cdot \sin^{-1} \frac{V_{TM}}{\omega A_{aI}} \qquad 3.54a$$

where μ'_M is the coefficient of friction under the oscillatory conditions. Considering there is no change in friction at the tube-slider interface, thus the initial friction force under oscillatory conditions ($\bar{F}_o$) is:

$$\bar{F}_o = \left(\frac{\pi}{2} \cdot \mu_s + \mu'_M \cdot \sin^{-1} \frac{V_{TM}}{\omega A_{aI}} \right) \cdot F_s \qquad 3.55$$

3.6.2 Friction vector reversal effect in zone IIf

In zone IIf, the bent-tube is pulled over the mandrel-tip with a constant angular speed N rev min^{-1}. But, the tangential velocity V_{TR} of any point on the contact surface, between the tube bore and the mandrel-tip, varies with the bend radius R, and is determined as:

$$V_{TR} = \frac{2\pi N}{60} \cdot R \qquad 3.56$$

Also, the mandrel-form is axially vibrated at an average velocity:

$$v_v = \omega \cdot A_{aII} \cdot \cos \omega t \qquad 3.57$$

where A_{aII} is the average displacement amplitude and is given by equation 2.51. It can be seen from figure 3.11 that while the oscillatory velocity is always in the axial direction, the advancing velocity of tube V_{TR} is acting normal to the tube cross-section and, therefore, its direction varies with the angle θ. Consequently, the resultant vector of the relative velocity of any point on the tube surface in contact with the mandrel-tip depends on the angle θ.

Consider any point BII on the contact surface CII-CII, of bend radius R, as it advances forward at a velocity V_{TR} (equation 3.56) and oscillates at a velocity v_v given by equation 3.57. The direction of the relative velocity vector of point BII, can be opposite to the direction of tube motion, as illustrated in figure 3.11a, if the

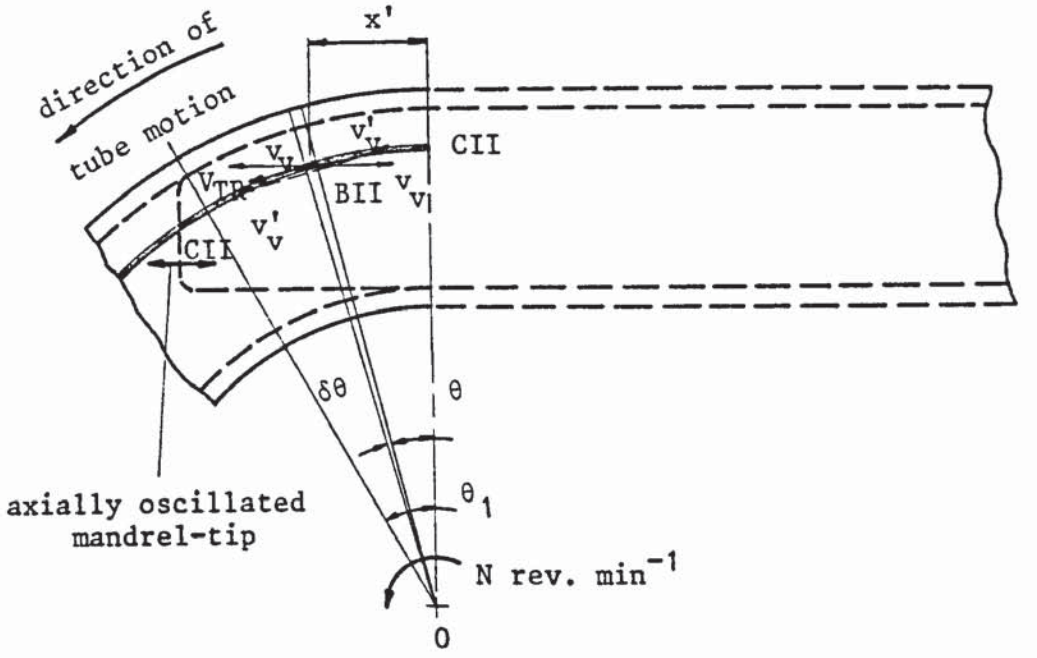

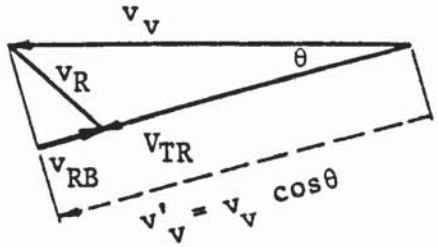

(a)

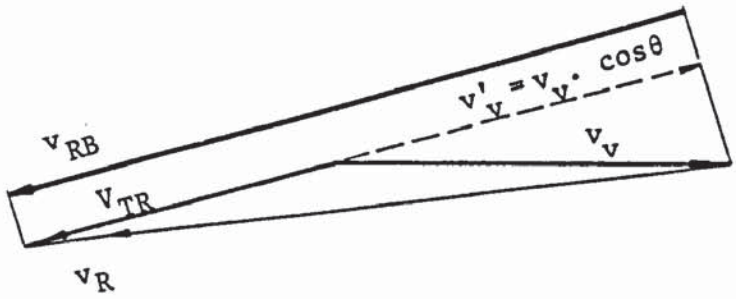

(b)

Figure 3.11: The velocity vector diagrams for point BII on the tube-mandrel interface: (a) when the oscillatory velocity is in the direction of tube motion; (b) when the oscillatory velocity is in an opposite direction to the tube motion

oscillatory velocity is in the forward direction and its component, in the direction of tube motion, has a value greater than that of the advancing velocity. Thus, in this case, the friction force is acting in the direction of tube motion. Conversely, when the oscillatory velocity is in the backward direction, as shown in figure 3.11b, the direction of the relative velocity vector coincides with the advancing motion of tube and, as a result, the friction force is acting in the opposite direction. Figure 3.12 illustrates the friction vector reversal effect as the tube is pulled over the mandrel in zone IIf. It can be seen from this figure that the increase in the friction force δF is negative during the time interval $(\frac{T}{2} - 2t_1)$ of the oscillation period, T, and positive during the rest of the time, ie. $(\frac{T}{2} + 2t_1)$; where t_1 can be obtained as in section 3.6.1, such that:

$$t_1 = \frac{1}{\omega} \sin^{-1} \frac{V_{TR}}{v'_{mv}}$$

where V_{TR} can be obtained from equation 3.56

and $v'_{mv} = \omega A_{aII} \cdot \cos \theta$

Similarly, as in the previous section, the effective increase in the friction force under the oscillatory conditions, $\overline{\delta F}$, can be obtained as:

$$\overline{\delta F} = \frac{2 \cdot \delta F}{\pi} \cdot \sin^{-1} \frac{V_{TR}}{v'_{mv}} \qquad 3.58$$

where δF is the increase in the friction force under the non-oscillatory conditions and is given by:

$$\delta F = \delta\sigma_\theta \cdot r_m \cdot \delta\phi \cdot t \qquad 3.59$$

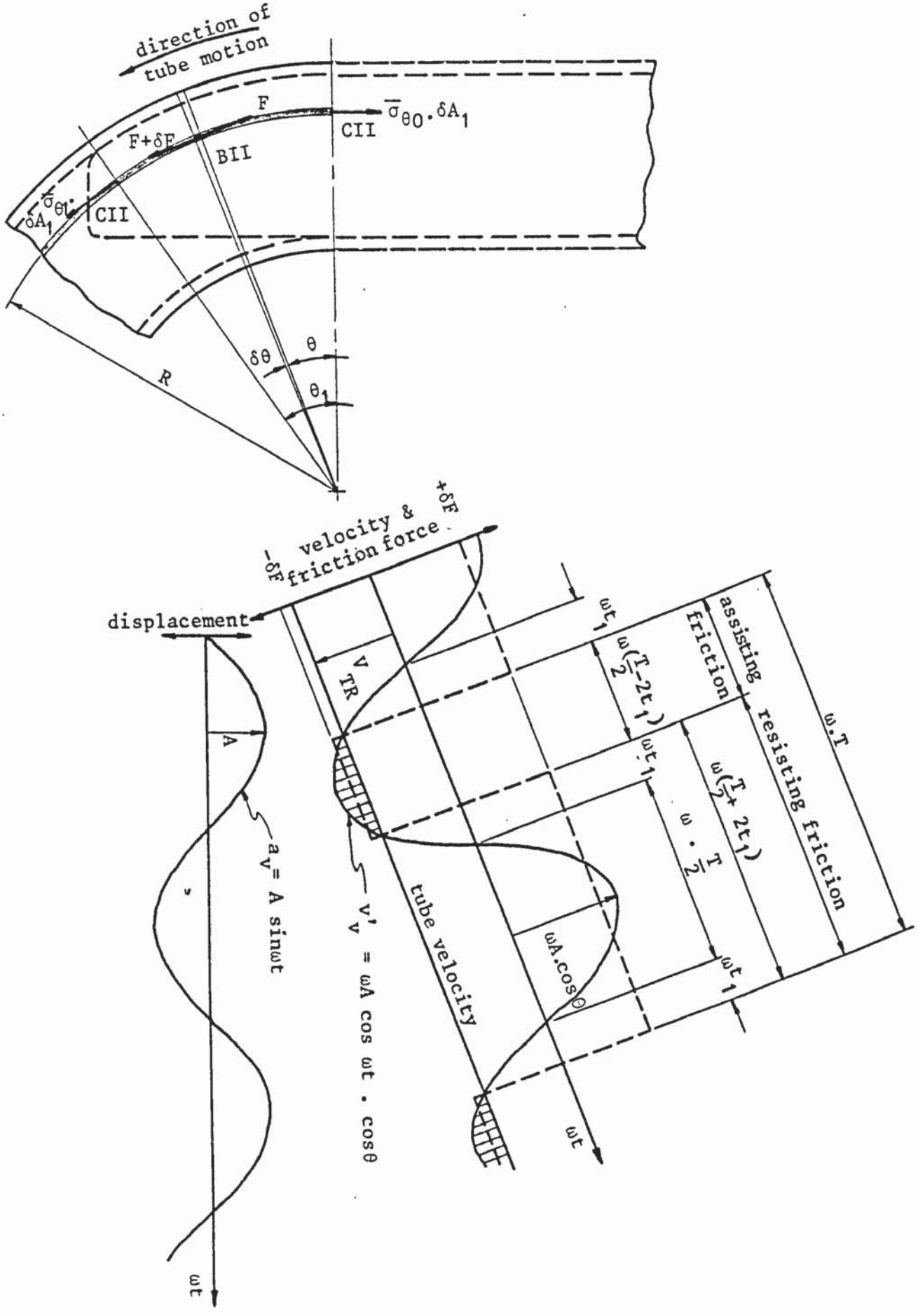

Figure 3.12: A diagram showing the friction reversal effect as the tube is pulled over the mandrel-tip in the deformation zone IIf

Substituting from equation 3.37 in equation 3.59; therefore:

$$\delta F = \mu_M \cdot p_M \cdot R \cdot r_m \cdot \delta\phi \cdot \delta\theta$$

Replacing δF in equation 3.58 with its value; then:

$$\overline{\delta F} = \frac{2}{\pi} (\mu'_M \cdot p_M \cdot R \cdot r_m \cdot \delta\phi \cdot \delta\theta) \cdot \sin^{-1} \frac{V_{TR}}{\omega A_{aII} \cdot \cos\theta} \quad 3.60$$

or $$\overline{\delta\sigma_\theta} = \frac{2}{\pi} (\mu'_M \cdot p_M \cdot \frac{R}{t} \cdot \delta\theta) \cdot \sin^{-1} \frac{V_{TR}}{\omega A_{aII} \cdot \cos\theta} \quad 3.60a$$

where μ'_M is the coefficient of friction under the oscillatory conditions.

Integrating equation 3.60a between the limits $\theta = 0$ and $\theta = \theta_1$ yields:

$$\bar{\sigma}_{\theta 1} = \bar{\sigma}_{\theta 0} + \frac{2}{\pi} (\mu'_M \cdot p_M \cdot \frac{R}{t}) \int_{\theta=0}^{\theta_1} \sin^{-1}\left(\frac{V_{TR}}{\omega A_{aII} \cdot \cos\theta}\right) \cdot d\theta \quad 3.61$$

where $\bar{\sigma}_{\theta_0}$ is the longitudinal stress, under the oscillatory conditons, in zone IIb, ie. just after the entry plane.

However, the integration in equation 3.61 is not easily solved, thus a reasonable approximation can be made in which an average value for v'_{mv} can be obtained such that:

$$v'_{va} = \frac{1}{\theta 1} \int_{\theta=0}^{\theta_1} \omega A_{aII} \cdot \cos\theta \cdot d\theta$$

which can be reduced to:

$$v'_{va} = \frac{\omega \cdot A_{aII} \cdot \sin\theta_1}{\theta_1}$$

and therefore:

$$\overline{\Delta F} = \frac{2.\Delta F}{\pi} \sin^{-1} \frac{V_{TR} \cdot \theta_1}{\omega . A_{aII} \cdot \sin \theta_1} \qquad 3.62$$

where ΔF is the total increase in the non-oscillatory friction force and can be obtained from equation 3.37 as:

$$\Delta F = \mu_M \cdot p_M \cdot R \cdot r_m \cdot \delta\phi \cdot \theta_1$$

Substituting for ΔF in equation 3.62, then:

$$\overline{\Delta F} = \frac{2}{\pi} (\mu'_M \cdot p_M \cdot R \cdot r_m \cdot \delta\phi \cdot \theta_1) \cdot \sin^{-1} \frac{V_{TR} \cdot \theta_1}{\omega A_{aII} \cdot \sin \theta_1}$$

Thus, the final longitudinal stress $\bar{\sigma}_{\theta 1}$, under the oscillatory conditions, can be obtained as:

$$\bar{\sigma}_{\theta 1} = \bar{\sigma}_{\theta 0} + \frac{2}{\pi} (\mu'_M \cdot p_M \cdot \frac{R}{t} \cdot \theta_1) \cdot \sin^{-1} \frac{V_{TR} \cdot \theta_1}{\omega A_{aII} \cdot \sin\theta_1} \qquad 3.63$$

3.7 Development of the final solution

3.7.1 Introduction

The theoretical analysis as described in the previous sections, represents the basis of the final solution to the problem of the

mechanics of tube bending under both vibratory and non-vibratory conditions. In developing the final solution, the principal deformation zones I, IIb and IIf were treated separately and the results of each zone were utilised to arrive at the solution to the next zone. For example, the initial friction force predicted in zone I was used to define the exact position of the neutral plane in the bending zone (IIb). Additionally, the effect of friction in zone IIf was included in the analysis, as friction caused an increase in the longitudinal stresses induced in the tube material during bending. Those longitudinal stresses were predicted from the equilibrium of forces in zone IIb. Further, the final solution included some fundamental assumptions and makes use of the basic equations derived, in the subsequent theoretical analysis.

Due to the complexity of the process and the necessity to assume some of the unknown factors to reach the final solution, a computer programme was written to execute, using an iterative method, the required computations. For instance, to relate the states of stresses and strains developed during bending to the stress-strain properties of the tube material, an iteration procedure was required. Thus a computing loop was used to compare the predicted value of the equivalent strain with the corresponding value obtained from the constitutive equation. Another computing loop was necessary also to compare the internal force with the externally applied force in the bending zone to show the exact position of the neutral plane at which those forces are equal and thus satisfy the equilibrium of forces.

The following sub-sections describe the route which was followed to arrive at the final solution and to predict both i) the distribution of stresses and strains and ii) the bending torque during the process of

tube bending. In addition, the sub-sections illustrate the general theme of the computer programme and the way in which the computational procedures were performed.

3.7.2 General outlines of the solution

The final solution based on the theoretical analysis of the mechanics of tube bending with the use of the "equilibrium of forces approach" may be summarised in the following steps:

1. The initial friction force (F_o) resulting from the friction in zone I is calculated from equation 3.7 for the conventional bending process. This force is assumed to apply on the tube section in zone IIb.

2. The initial position of the neutral plane is assumed, and expressed in terms of the angle 'ϕ_N' measured from the central plane of the tube section. The final (actual, ie. calculated) position of the neutral plane is obtained from the equilibrium between the external force (F_o) and the resultant of the internal forces.

3. It is assumed that the stresses at the neutral plane are those required for the material to exceed the yield point last. Consequently, at $\phi = 0$ the equivalent stress is equal to 'Y' in equation 3.34.

4. The states of stress at the neutral plane, either in region 'A' or in region 'C', can be determined by combining equation 3.17 or

3.19, and equation 3.32 where $\bar{\sigma} = Y$, and by assuming a value of the former pressure (p_F).

5. In region 'A' the mandrel pressure (p_M) being very small, is neglected. It is also assumed that the former does not exert any pressure on the tube wall at the central plane (at $\phi = \phi_N$). Consequently, the hoop stress is also zero at the angular position 'ϕ_N' since the longitudinal stress has no component in the radial direction, see figure 3.6 and equation 3.17.

6. The former pressure (p_F) is assumed to be uniform in region 'C' while it is zero in region 'B'.

7. The tensile and compressive regions of the tube section, ie. above and below the neutral plane respectively, in the deformation zone IIb are related in the solution through a compatability equation. The condition of compatability assumes that the total hoop strains around the periphery of the tube section is equal to zero. This assumption however does not seem unreasonable since the wall-thickness and the length of a tube element being bent in zone IIb are much smaller than the peripheral length of the tube section.

8. The former pressure in region 'C' is given an initial value and the correct pressure is obtained as to satisfy the compatability equation.

9. The peripheral length between the inner and outer peripheries of the bent tube is considered to be divided into a large number of

small elements; each element has a peripheral angle ($\delta\phi$) measured from the centre of the tube section. A small angular element $\delta\phi$ equal to 0.01 rad was chosen to enable the distribution of the stresses and the strains to be predicted with greater accuracy.

10. In the bending zone IIb, having predicted the states of stresses and strains at any angular position (ϕ), the stresses and the strains at the next angular position ($\phi + \delta\phi$) can be obtained as follows:

(a) The change in the hoop stress is obtained from equations 3.12, 3.16 or 3.18 for the regions 'B', 'A', or 'C' respectively.

(b) The magnitude of the former pressure or the mandrel pressure is assumed in region 'A' or regions 'B' and 'C' respectively. The exact value of pressure is obtained through an iteration procedure which compares the predicted value of the incremental equivalent strain with the corresponding value on the material stress-strain curve.

(c) The longitudinal stress is calculated from equations 3.15a, 3.17 or 3.19 in regions 'B', 'A' and 'C' respectively.

(d) The incremental longitudinal strain is calculated from equation 3.24 while the incremental values of the hoop and thickness strains are obtained from equations 3.27 and 3.28.

(e) The predicted value of the incremental equivalent strain can be obtained by substituting the values obtained in step (d) in equation 3.33.

(f) The equivalent stress is calculated from equation 3.32, while the equivalent strain may be obtained from the stress-strain relationship of the tube material (equation 3.34).

(g) The incremental increase in the equivalent strain on the stress-strain curve is calculated by subtracting the value of the equivalent strain at the angular position (ϕ) from the corresponding value as obtained in (f).

(h) The incremental equivalent strains from (f) and (g) are then compared. If proved unequal, another pressure value is assumed and the iteration procedure repeated starting from step (b).

11. In the final friction zone (IIf), the increase in the longitudinal stresses may be obtained from equation 3.37 by substituting the value of the mandrel pressure as predicted in zone IIb and by assuming a reasonable value for the coefficient of friction. The longitudinal stresses at the exit plane are calculated from equations 3.38, 3.39 and 3.40 for regions 'B', 'A' or 'C' respectively.

12. The equivalent stresses and strains at the exit plane are obtained from equations 3.41 and 3.42 respectively. The increase in the equivalent strain can then be calculated (equation 3.42a) and consequently, the additional straining of the tube material in the longitudinal, hoop and thickness directions can be obtained from equations 3.43, 3.44 and 3.45 respectively.

13. In zone IIb, the longitudinal, hoop and thickness strains at any angular position (ϕ) are obtained by summing all the incremental strains between $\phi = 0$ and the required angular position. The tube wall-thickness at any angle (ϕ) is calculated as:

$$t_{\phi} = t_{\phi-\delta\phi} \cdot (1 + \delta\varepsilon_{t,\phi})$$

where $t_{\phi-\delta\phi}$ is the tube wall-thickness at the preceding element having an angular position $(\phi - \delta\phi)$.

14. The bending torque in zone IIb is obtained from the following expression:

$$Q_0 = \sum_{\text{tube section}} \sigma_{\theta 0} \cdot t \cdot r_m \cdot \delta\phi \cdot R \qquad 3.64$$

while the bending torque at the exit plane is calculated as:

$$Q_1 = Q_0 + Q_f \qquad 3.65$$

where Q_f is the torque required to overcome friction as the tube is pulled over the mandrel-tip and around the former, which may be obtained using the following formula:

$$Q_f = \Sigma \delta W_f \cdot t \cdot r_m \cdot \delta\phi \cdot R \qquad 3.66$$

δW_f is the frictional work per unit volume at any angular position (ϕ) and is given by:

$$\delta W_f = \tfrac{1}{2} (\bar{\sigma}_0 + \bar{\sigma}_1) \cdot \Delta\bar{\varepsilon}_f \qquad 3.67$$

and $\Delta\bar{\varepsilon}_f$ is equal to $\Delta\bar{\varepsilon}$ in equation 3.42a.

15. If the supporting mandrel is axially vibrated during the bending

process, then the initial friction force can be calculated from equation 3.55. Also, the longitudinal stress at the exit plane is obtained from equation 3.63.

3.7.3 The computer programme "UTB-INI"

The theoretical solution as outlined in the previous sub-section was translated to a computer programme. This new programme was written in BASIC language to execute the computational procedures and to print-out the obtained results which provide useful information regarding the distribution of stresses and strains and also the bending torque.

Figure 3.13 represents a flow chart of the computer programme "UTB-INI", which summarises the basic structure of the programme. A complete listing of the computer programme together with a sample of the output results are shown in Appendix A.

Generally, the "UTB-INI" programme consists of the main programme and a number of subroutines principally utilised in executing the iteration procedures. The main programme is divided into a number of sections regarding deformation zones I and IIb and also regions 'A', 'B' and 'C'. While a number of the subroutines were written to execute the iteration procedures, other subroutines were used for performing the computations in zone IIf and for printing-out the necessary results.

It may be seen from the example given in Appendix A that by feeding the required data: the tube dimensions, the stress-strain characteristics of the tube material, the mean bend radius and the frictional conditions into the computer programme, useful information regarding the mechanics of tube bending may be obtained. Furthermore, the programme was extended to include the influence of applied vibrations on the bending process.

Figure 3.13: A flow-chart of the computer programme "UTB-INI"

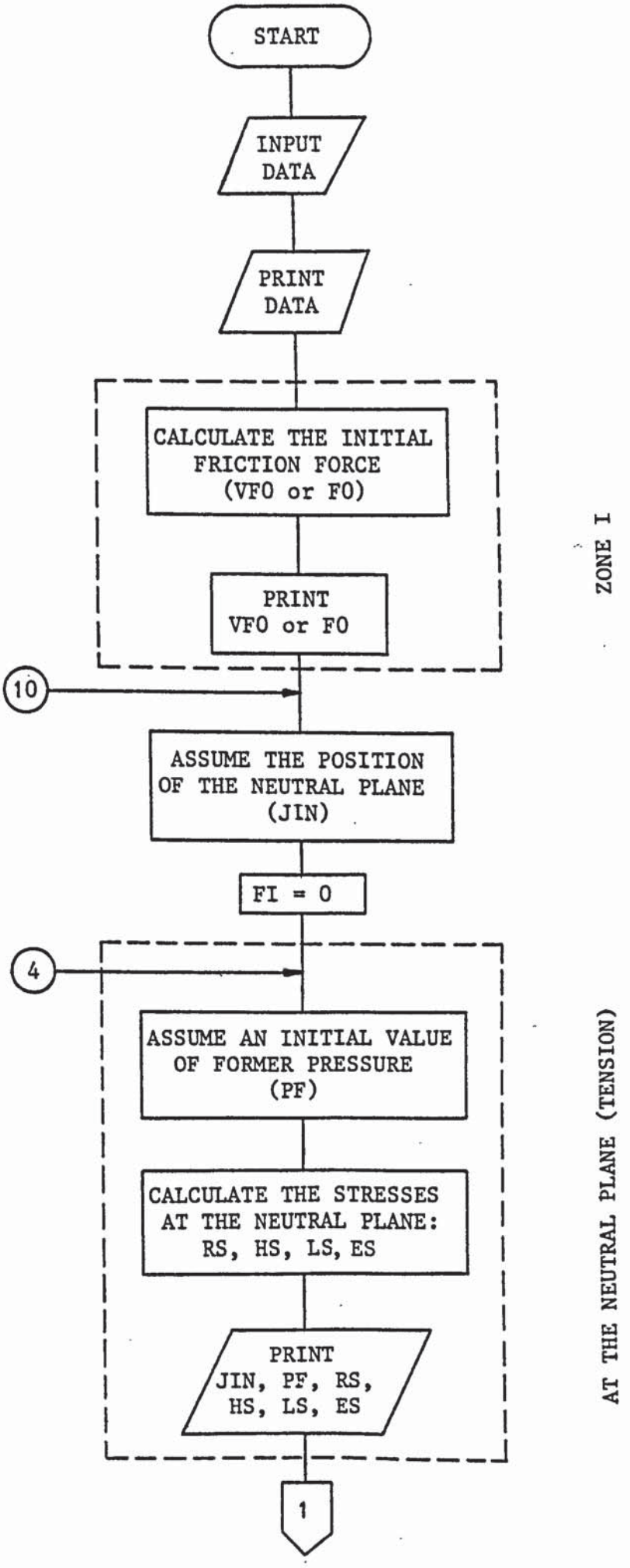

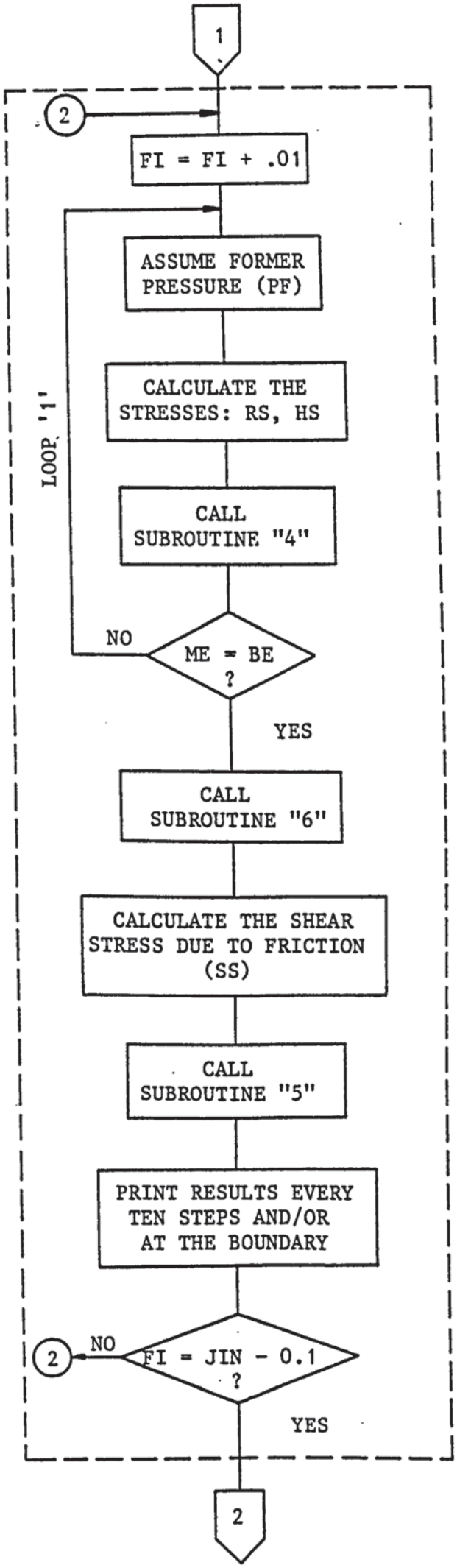
1
2
FI = FI + .01
ASSUME FORMER PRESSURE (PF)
CALCULATE THE STRESSES: RS, HS
CALL SUBROUTINE "4"
NO
ME = BE ?
YES
CALL SUBROUTINE "6"
CALCULATE THE SHEAR STRESS DUE TO FRICTION (SS)
CALL SUBROUTINE "5"
PRINT RESULTS EVERY TEN STEPS AND/OR AT THE BOUNDARY
2
NO
FI = JIN - 0.1 ?
YES
2
LOOP '1'
REGION "A"

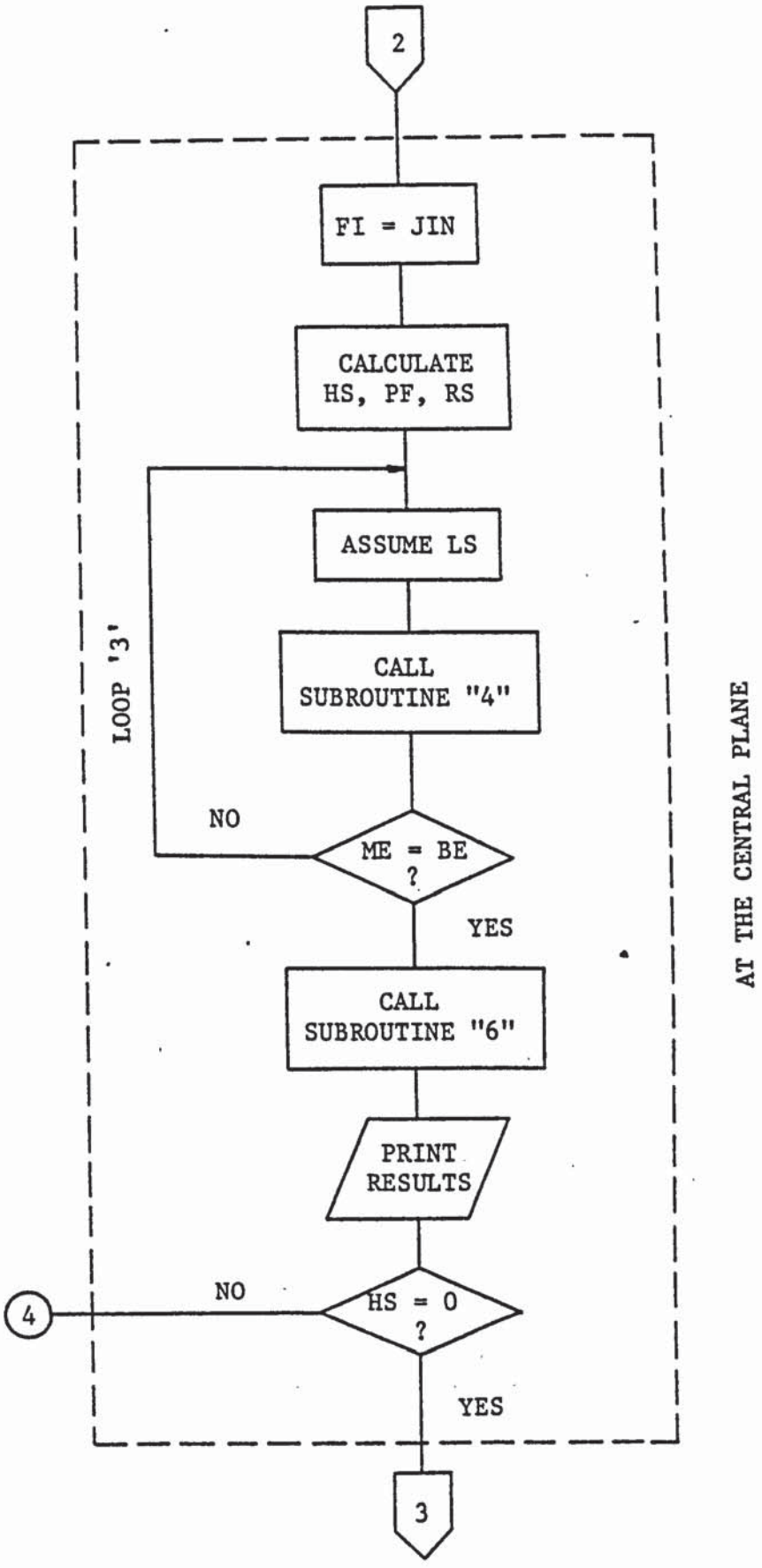
2
FI = JIN
CALCULATE HS, PF, RS
ASSUME LS
CALL SUBROUTINE "4"
NO
ME = BE ?
YES
CALL SUBROUTINE "6"
PRINT RESULTS
4
NO
HS = 0 ?
YES
3
LOOP '3'
AT THE CENTRAL PLANE

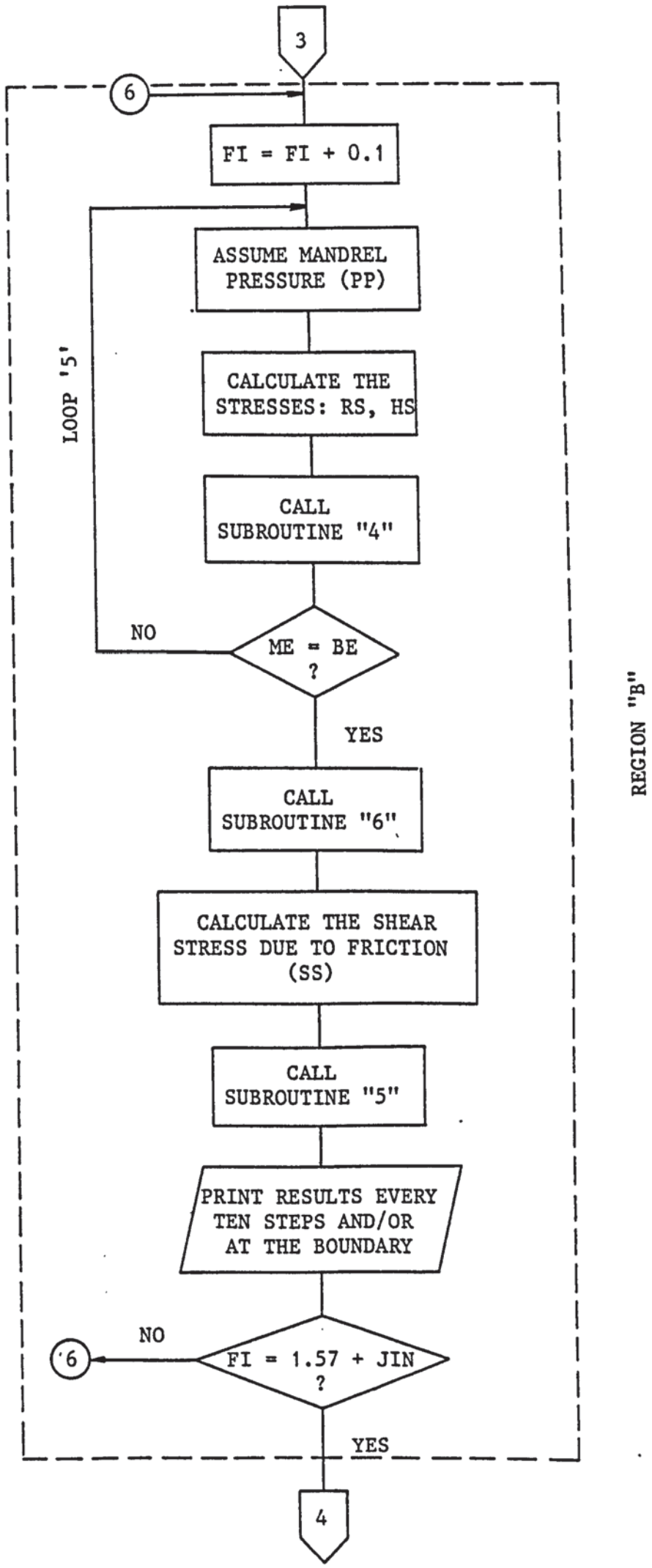
3
6
FI = FI + 0.1
ASSUME MANDREL PRESSURE (PP)
CALCULATE THE STRESSES: RS, HS
CALL SUBROUTINE "4"
NO
ME = BE ?
YES
CALL SUBROUTINE "6"
CALCULATE THE SHEAR STRESS DUE TO FRICTION (SS)
CALL SUBROUTINE "5"
PRINT RESULTS EVERY TEN STEPS AND/OR AT THE BOUNDARY
NO
6
FI = 1.57 + JIN ?
YES
4
LOOP '5'
REGION "B"

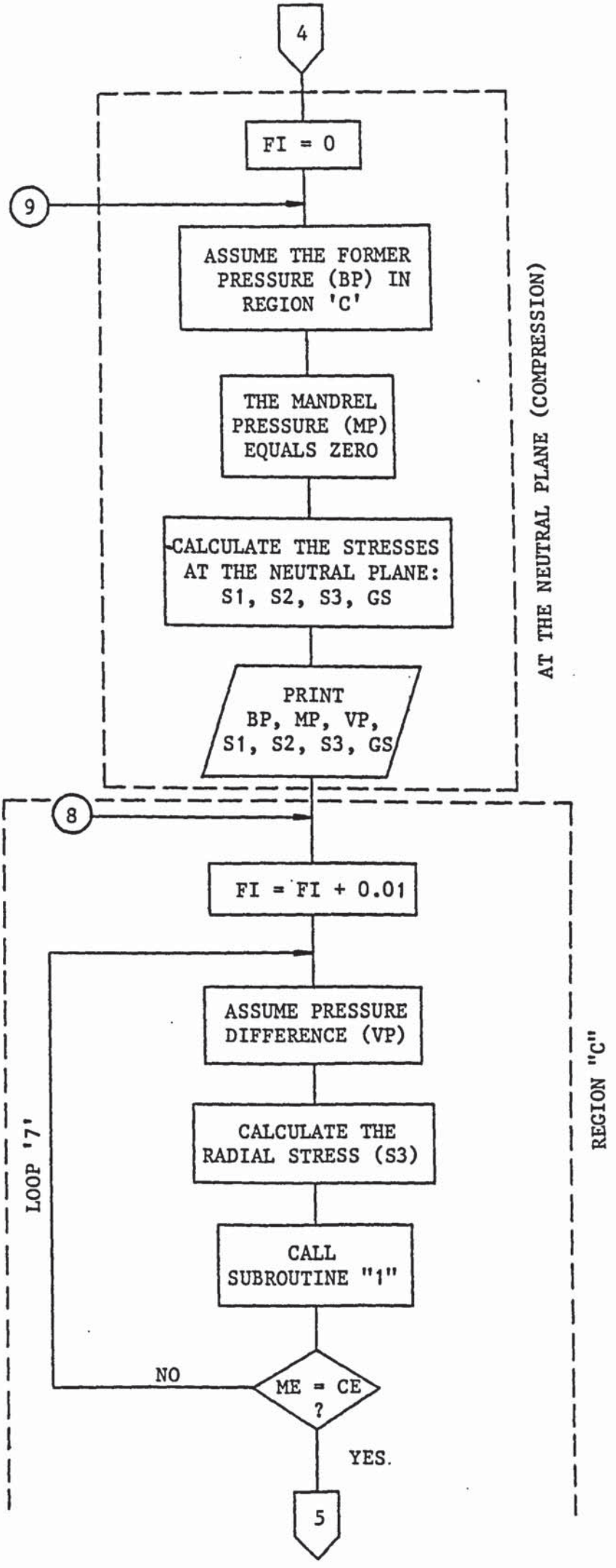
4
FI = 0
9
ASSUME THE FORMER PRESSURE (BP) IN REGION 'C'
THE MANDREL PRESSURE (MP) EQUALS ZERO
CALCULATE THE STRESSES AT THE NEUTRAL PLANE: S1, S2, S3, GS
PRINT BP, MP, VP, S1, S2, S3, GS
AT THE NEUTRAL PLANE (COMPRESSION)
8
FI = FI + 0.01
ASSUME PRESSURE DIFFERENCE (VP)
CALCULATE THE RADIAL STRESS (S3)
CALL SUBROUTINE "1"
LOOP '7'
NO
ME = CE ?
YES.
5
REGION "C"

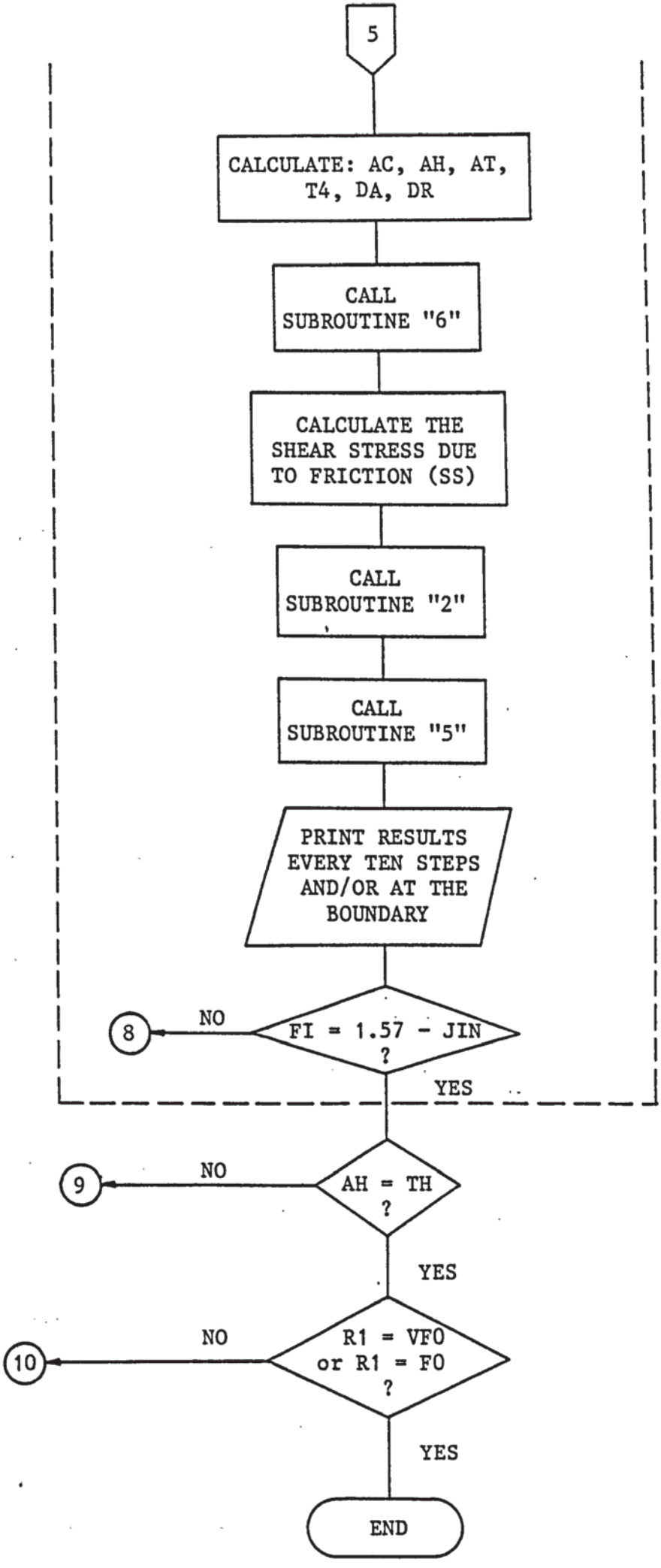
5
CALCULATE: AC, AH, AT, T4, DA, DR
CALL SUBROUTINE "6"
CALCULATE THE SHEAR STRESS DUE TO FRICTION (SS)
CALL SUBROUTINE "2"
CALL SUBROUTINE "5"
PRINT RESULTS EVERY TEN STEPS AND/OR AT THE BOUNDARY
FI = 1.57 - JIN ?
NO
8
YES
AH = TH ?
NO
9
YES
R1 = VF0 or R1 = F0 ?
NO
10
YES
END
REGION "C" (Cont'd)

CHAPTER FOUR

EQUIPMENT AND INSTRUMENTATION

4.1 Conventional Bending Equipment

4.1.1 The tube bending machine

Since the current research is concerned with bending tubes to small bend radii, a bending machine of the rotary-draw type has been used. A 'Mark 13' bender which is mechanically powered and manually operated, was supplied by Brookes (Oldbury) Ltd. According to the machine data, a mild steel tube of 1 in outside diameter and 0.064 in wall thickness can be bent to a maximum centreline bend radius of 7 inches. The minimum bending radius to the centreline of tube is 1.25 in on 0.50 in outside diameter tube. The machine has two bending speeds of 10 and 15 rev min^{-1} and also two return speeds of 15 and 22 rev min^{-1}. A bending angle of up to 180 degrees is possible and can be determined by the position of the cam on the indexing plate. Full specifications of the bending machine and also the sequence of its operation are reported in Appendix B.1.

Several arrangements have been made for the tube bender either to add more facilities to it or to fix the measuring equipment. A wiper die holder was manufactured and fixed on the top of the slider support. This holder was designed in such a way to ensure proper adjustment of the wiper die with respect to the former and the other bending tools.

Consequently, the tip of the wiper die can be advanced as far as the tangent line and also the rake angle between the tube and the wiper die can be adjusted for minimum drag and for maximum support to the inner periphery of the bend. Although the previously mentioned method of mounting the wiper die holder may not be most satisfactory it was the only possible and practical way of fitting a wiper die. It seems however that the 'Mark 13' machine was not made to produce such tight bends and hence the employment of a wiper die was not required.

The research programme necessitated the measurement of the gripper and slider forces. Therefore, modifications were made for the gripper and slider assemblies in order to fit the new load cells. Further, a load cell for measuring the bending torque was installed between the driving shaft and the driven bending arm and a specially made support for the torque-meter was fixed to the bending machine. Figure 4.1 shows the tube bender together with the necessary arrangements which have been made. Also, the .detailed descriptions and mechanical drawings of those arrangements are shown in Appendix B.2.

4.1.2 The bending tools

The main design features and the basic requirements of the bending tools have been described in Chapter Two. The tooling required for the present work were particularly designed and manufactured to suit the bending machine and also to cover a wide range of tube outside diameters, wall thicknesses and mean bend radii. In addition to the basic tools, ie. the former, the gripper and the slider, a form-mandrel and a wiper die were used also throughout the experiments. A complete set of tooling during the bending operation is shown in figure 4.2.

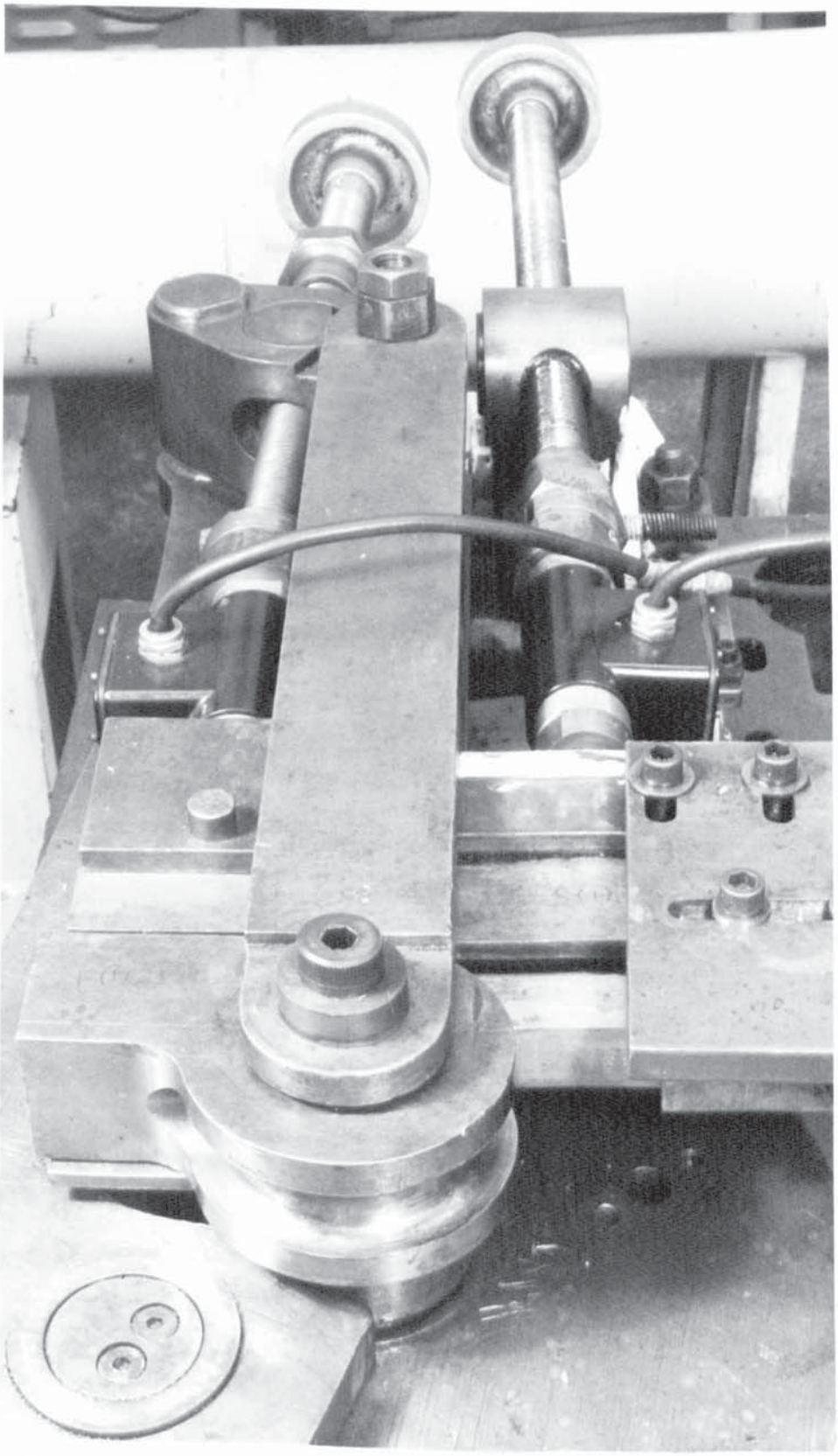

Figure 4.1: A close-up of the bending machine with the necessary arrangements

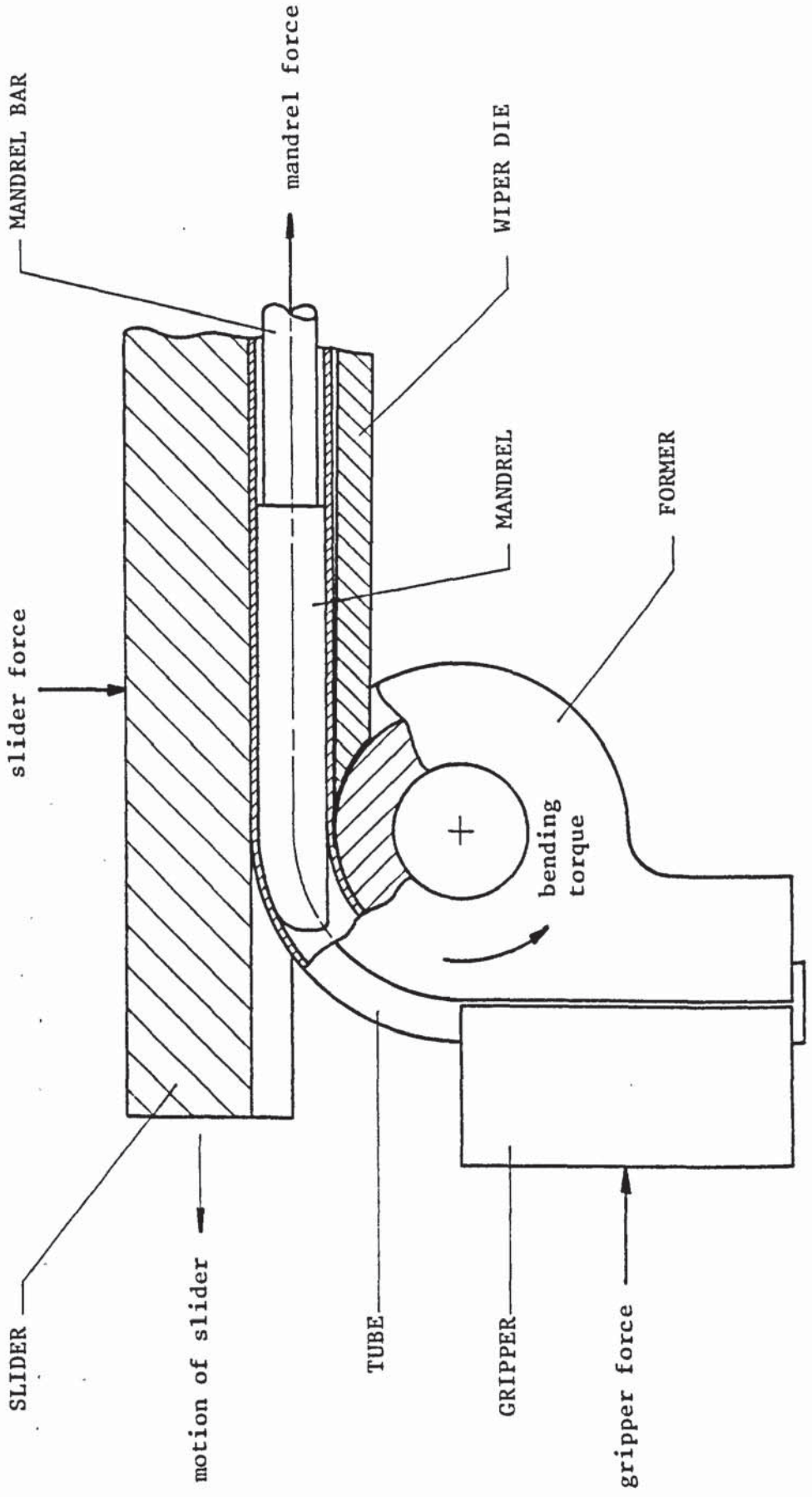

Figure 4.2: A complete set of tooling during the draw-bending of tube

Generally, the machine requires a new set of bending tools if the tube outside diameter changes. But if the bend radius alone differs from a bend already produced, only additional former, wiper die and form-mandrel are needed. Similarly, if all the dimensional parameters are identical with a previous component except the tube bore, only one extra mandrel is required. The specifications, the full dimensions and the working drawings of the bending tools are given in Appendix B.3.

4.2 Ultrasonic equipment

The equipment for the ultrasonic system has been designed in order to produce a standing axial vibration wave in the mandrel bar-mandrel assembly at a nominal resonant frequency of 20 kHz. The generation of such an axial mode of mandrel vibration at the desired amplitudes required very special equipment which would function satisfactorily at the appropriate ultrasonic frequencies. Essentially, the ultrasonic system consists of two parts, namely: the mechanical system and the electrical system. The latter implies the use of a high-power generator with a built-in frequency controller, which is connected to a piezoelectric transducer matchbox, while the mechanical system includes the piezoelectric transducers, the coupling horn and the mandrel bar as a wave-guide. Figure 4.3 shows the various components of the integral mechanical system. Also, a schematic layout of the electrical system is illustrated in figure 4.4.

4.2.1 The electrical system

(a) The power generator and the frequency controller

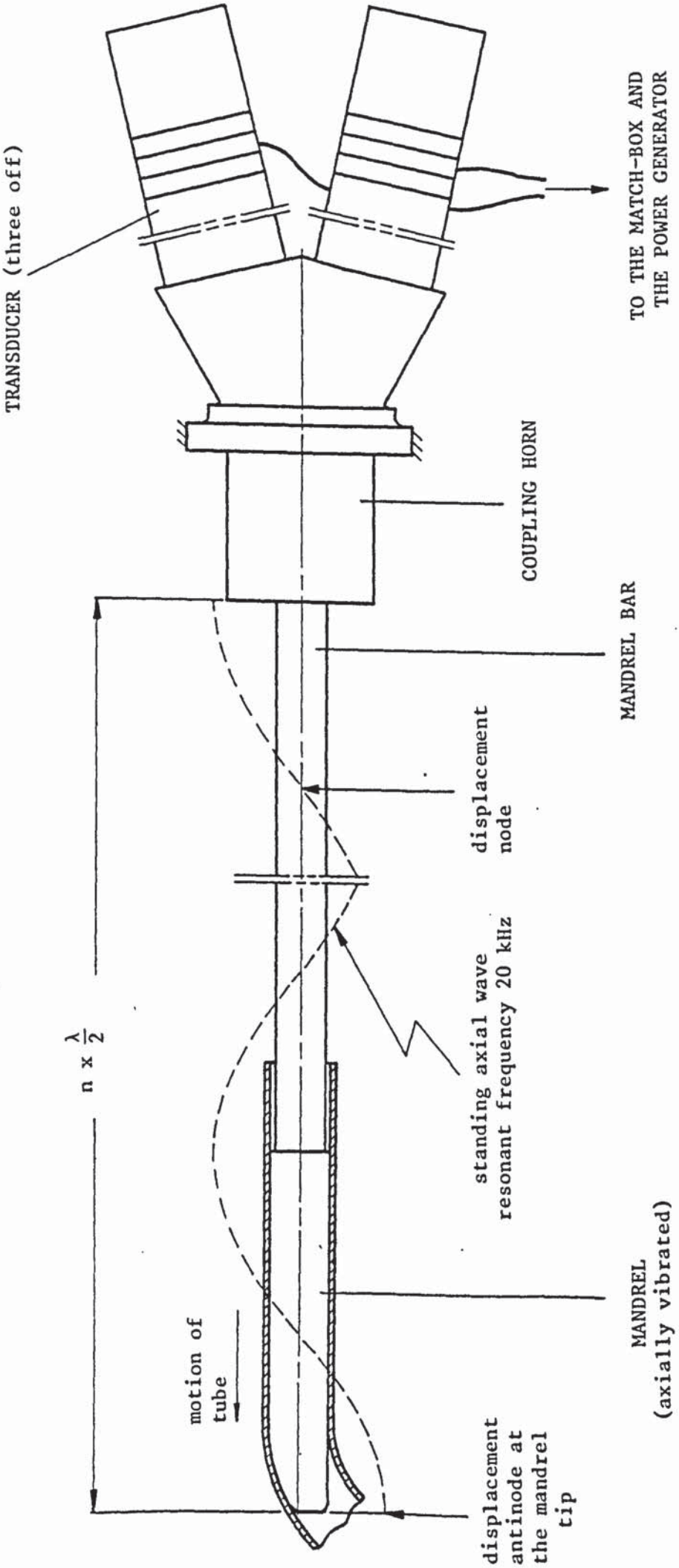

Figure 4.3: The integral mechanical system of the ultrasonic equipment

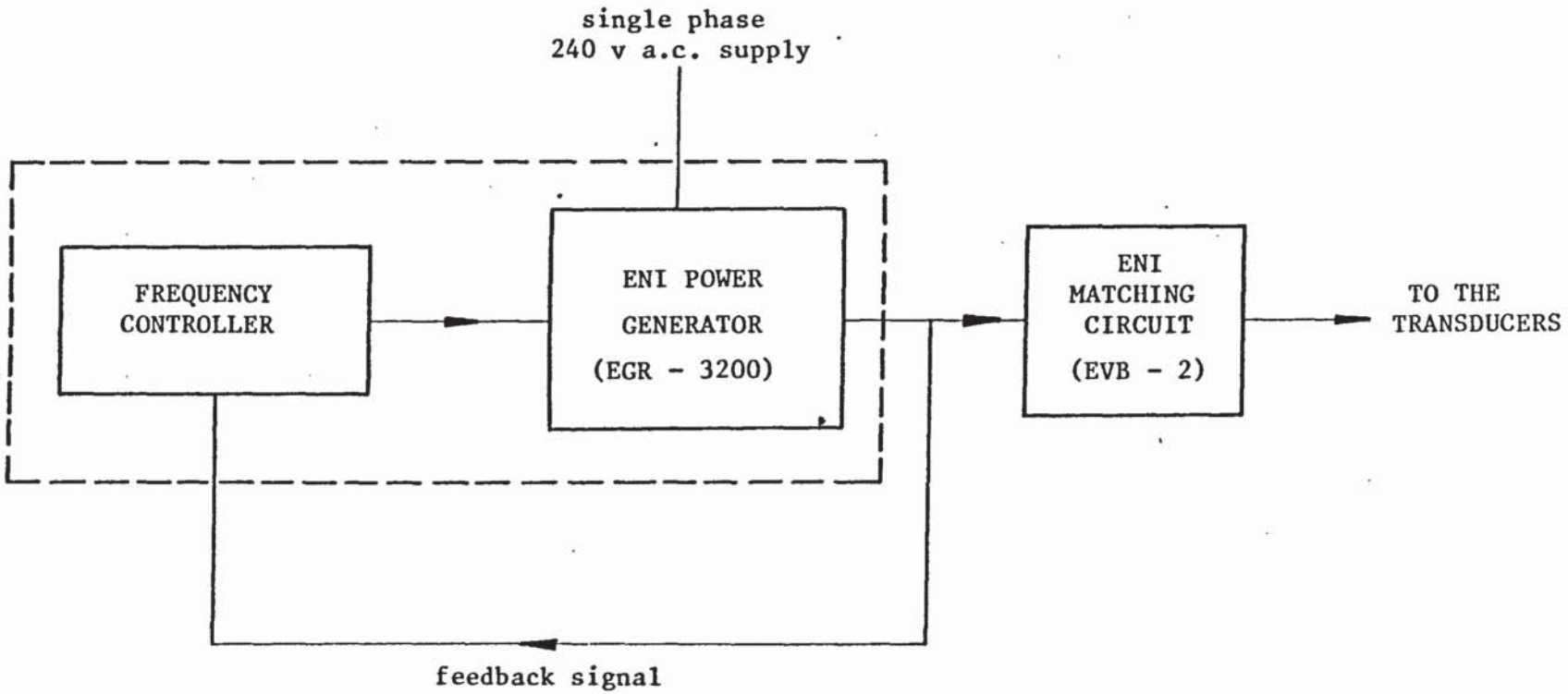

Figure 4.4: A schematic layout of the electrical system

The power generator which is manufactured by ENI Power Systems Ltd is a solid state broad band amplifier driven by an internal oscillator. In the low level oscillator-linear power amplifier shown in figure 4.5 the operating frequency is determined by the frequency setting of the oscillator and its output power is dependent solely on the gain setting of the power amplifier. The model ENI EGR-3200 generator gives an output rating of 3000 watt over a frequency range of 14 to 79 kHz. It is one of the most versatile and electronically robust generators of this kind available commercially.

The generator has an output impedence of 50 ohm and an external matching circuit is provided to ensure effective coupling to the electrical load presented by the transducers. Also, the EGR-3200 is protected against an impedence mismatch, tolerating 700 watt of power reflected from the load. Instantaneous overload protection is provided should the load impedence exceed allowable limits. This minimises the risk of overheating and consequential failure of the power transistors.

The power meter which uses the principle of directional coupling in a transmission line, enables the forward and reverse power waves to be independently monitored. A computing circuit allows switched selection of both the forward and load powers on the meter face. This gives an immediate assessment of the matching efficiency between the generator and the load. When the load impedence is equal to 50 ohm the reverse power wave is zero and hence the load power is equal to the forward power. The ratio of the load power to forward power is an indication of the degree of match of the load to the power generator. Generally, for good operating efficiency, this ratio should be equal to or greater than 0.9. The details of the EGR-3200 specifications and the tune-up procedure are given in Appendix B.4.

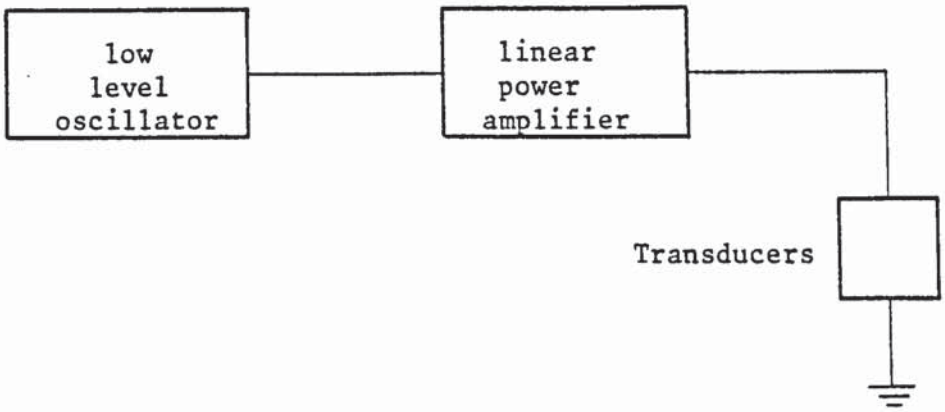

Figure 4.5: A block diagram of the oscillator-amplifier power generator

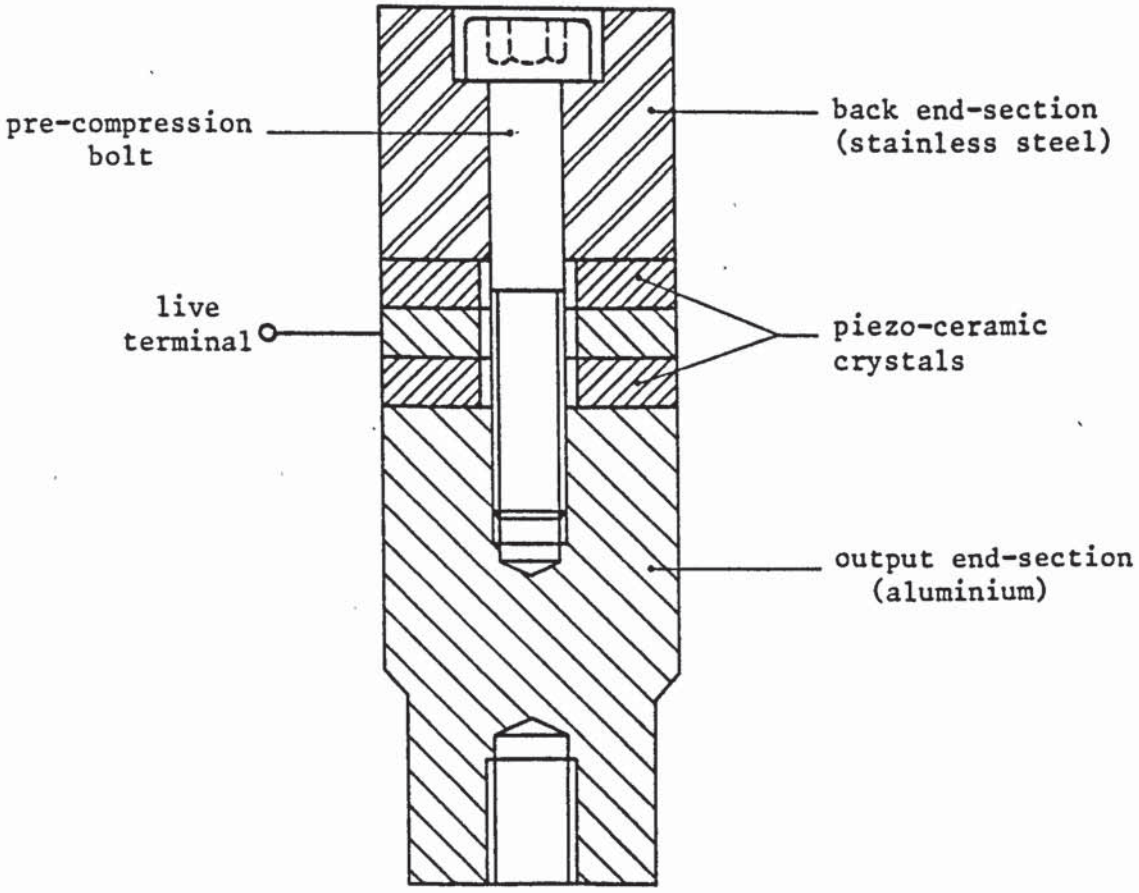

Figure 4.6: A longitudinal section of the sandwich piezo-electric transducer

Normally, during the bending operation, the resonant frequency of the mechanical system changes due to load variations which affect the stiffness and mass of the system and also due to heating effects which may alter the elastic properties of the various elements. Therefore, unless the generator can be made to follow any shift of frequency quickly and accurately, the load impedence will become mismatched with the generator. As a result, the load power will considerably decrease and also the generator might 'trip-out' due to an excessive amount of reflected power. In order to avoid this and thus to keep the load power at its optimum level irrespective of any load variations, a phase-lock loop circuit has been designed, which continuously monitors and compares the phase relationship between the load current and a reference voltage at the oscillator output.

For resonance to occur and thus an optimum amount of load power to be delivered, there should be no phase shift between the output current and the voltage. However, when the load frequency varies in relation to the generator frequency, the phase angle between the current and the voltage changes. This change in the phase angle is used to generate a feedback d.c. signal which is applied to the frequency control circuit automatically correcting the generator frequency to match that of the load. Thus, the generator will restore the correct phase relationship between the output current and the voltage and consequently the load power remains at its optimum level.

(b) <u>The matching circuit</u>

In the ultrasonic system, the elctrical matching between the power generator and the load is of prime importance. This can be accomplished by adding an in-series inductance to cancel the transducer

capacitance and by transforming the resistive load impedence to 50 ohm in order to match the generator output impedence. For this purpose, an ENI Power Systems Model EVB-2 "Piezoelectric Transducer Matchbox" is used.

The matching circuit is designed to convert virtually any piezoelectric transducer or array of piezoelectric transducers in the 9 kHz to 50 kHz frequency range to a purely resistive 50 ohm. It consists of two multi-tap transformers and a multi-tap air cored inductor. High power switches permit the actual tuning operation to be carried out under the actual transducer operating conditions while the generator is set at low power level. By observing the ratio of the load power to forward power on the generator meter, the appropriate switches can be rotated until the ratio is as close to unity as possible. At that point, the load impedence is correctly matched to the 50 ohm power generator. The specifications and the operation procedure of the EVB-2 matchbox are written in more detail in Appendix B.4.

4.2.2 The mechanical system

(a) The ultrasonic power transducers

Three PZT (lead zirconate titanate) sandwich transducers have been used. They have the ability of converting the electrical power to mechanical vibrations at the design frequency. These transducers are capable of operating effectively and tolerating a frequency variation of ± 500 Hz to the nominally tuned unloaded frequency. Furthermore, they are very powerful and their efficiency when correctly matched to the mechanical load is better than 95 per cent.

The transducers which are a half-wavelength in length, were made to vibrate axially at a resonant frequency of 20 kHz. Each transducer has the capacity of transmitting an amount of ultrasonic power equal to 1000 watt. As shown in figure 4.6, the sandwich transducer consists of two piezo-ceramic crystals compressed by a pre-loading central bolt between stainless steel and aluminium masses. In addition, the transducer has a sandwiched aluminium ring placed between the piezo-crystals serving as a live terminal. The transducers are earthed to the machine base. Generally, dissimilar combinations of materials such as stainless steel and aluminium are used in the arrangement, since the latter when connected to the output end will vibrate at larger amplitudes due to its small density (ρ) and Young's modulus (E). The velocity amplification, M, which can be obtained using two such materials is approximately given as:

$$M = \left[\frac{\rho_1 E_1}{\rho_2 E_2} \right]^{\frac{1}{2}}$$

where $\rho_1 E_1$ of stainless steel is greater than $\rho_2 E_2$ of aluminium.

(b) The coupling horn and its mount

The specially designed horn shown in figure 4.7 is attached to the three transducers to produce high ultrasonic power densities. The horn which has been made to resonate at a nominal frequency of 20 kHz provides an accurate acoustic impedence-match between the transducers and the mandrel bar to ensure maximum energy transmission to the load. The coupling horn has a length equivalent to half-wavelength of the vibration wave and is mounted at its nodal flange of zero displacement amplitude. This can prevent energy dissipation to the machine frame

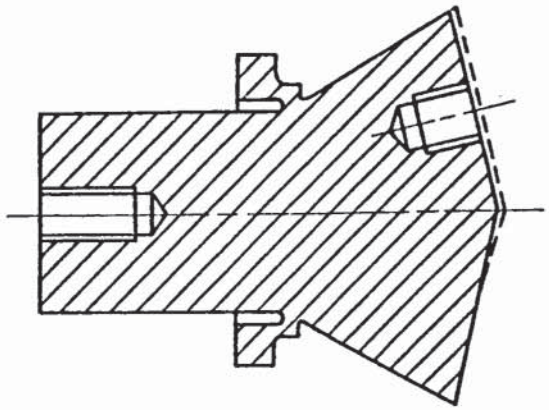

SECTION A-A

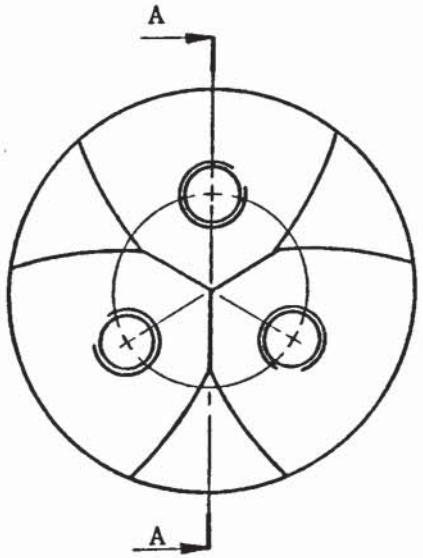

Figure 4.7: The coupling horn

and thus the optimum utilisation of the ultrasonic energy can be achieved. In addition to its main fuction as an energy coupler, the horn amplifies the output wave displacement and therefore it may be called an 'acoustic concentrator' or 'velocity transformer'.

It is essential that the coupling horn is fixed firmly to the machine body at its nodal flange. So, a holding system was produced in which the horn flange is clamped tightly around its periphery by an annular clamping ring, attached to a heavier section annular ring which is fixed on the machine frame by four bolts. This arrangement does not only ensure an effective mounting of the horn but also facilitates the correct adjustment of the mandrel bar and the mandrel with respect to the other bending tools. Details of the mounting assembly are shown in Appendix B.5.

(c) The ultrasonic wave-guide

The coupling horn is attached, at its smaller end, to the mandrel bar which works as a wave-guide. The mandrel bar shown in figure 4.8 was made from 321-stainless steel which proved to be of high acoustic properties. The tool, ie. the form-mandrel, was made from hardened tool steel, and it was fixed to the working end of the mandrel bar. The joints in the oscillatory mechanical system, which were necessary for practical purposes, may result in undesirable effects such as loss of vibration energy in the form of heat, stress concentration and fatigue effects. However, flat end faces and very tight fittings can provide a means of minimising such effects. Screw-thread attachments were the only practical laboratory possibility for the construction of the mechanical system because of the necessity to dismantle the mandrel bar and the mandrel for tool changing purposes.

ALL DIMENSIONS IN INCHES

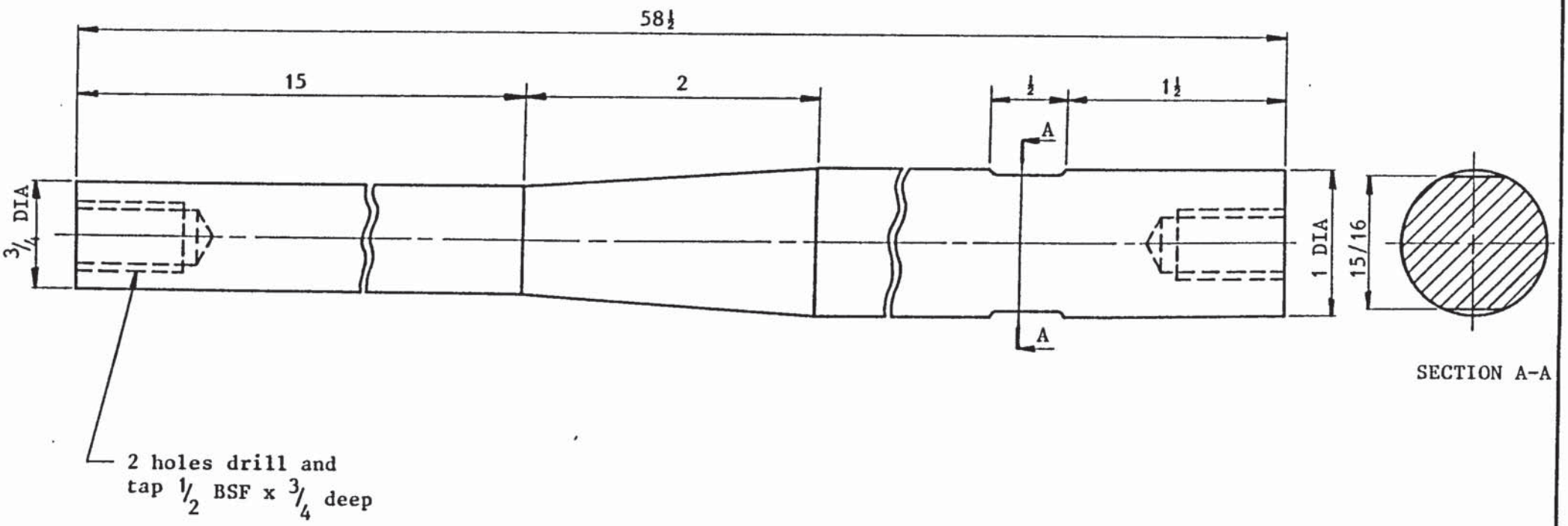

SECTION A-A

SCALE: Full	MATERIAL: 321-Stainless Steel	DRN	I N IBRAHIM	Mandrel Bar	DRG NO: 4.8
TOLERANCES: LIMITS UNLESS OTHERWISE SPD FRAC. ± 1/64" DEC. ± 0.010" ANG. ± 15'		DATE	14.2.1983		
	PART NO:	APP		UNIV. OF ASTON IN BIRMINGHAM PROD. TECH. DEPT. G. ALEX. LABS.	
	No. REQ: 1	DATE			

In order to achieve the optimum effect of the application of ultrasonic vibrations, the length of the mandrel bar and the mandrel must complete an integral number of half-wavelengths in the wave-guide for resonance to occur at the design frequency. This can ensure that a standing axial vibration wave is established along the mandrel-mandrel bar assembly with a displacement antinode at the free end of the mandrel. However, due to some factors such as the change in the wave velocity as a result of using different materials for the tool and wave-guide, a correction had to be made by reducing the mandrel bar length from the theoretical one. This experimental correction to the length of the wave-guide was necessary to maintain resonance at the design frequency of 20 kHz. This tuning procedure is explained in more detail in the next section.

4.2.3 Tuning of the oscillatory mechanical system

Since the piezoelectric transducers were made to vibrate at a resonant frequency of 20 kHz, it became necessary for the efficient operation of the ultrasonic system that each part of the oscillatory mechanical system was accurately tuned to resonate at the same frequency as the transducers. The exact tuning of various parts, ie. the transducers, the coupling horn and the mandrel bar was essential to adjust their post-manufacture resonant frequencies to the specified frequency.

The first part to be tuned was the coupling horn. Its resonant frequency, prior to tuning was lower than 20 kHz because it had to be manufactured with its length slightly greater than the theoretically calculated value. For tuning, material was removed from the small end

of the horn because as the length becomes shorter the resonant frequency increases. However, attention had to be paid to the amount of metal removal since it was critical that the resonant frequency should not be increased above 20 kHz. The horn was shortened by turning in a lathe with the use of a special adaptor made to mount the horn in the chuck. The tuning operation was carried out by detecting the corresponding mechanical resonance of the horn with the use of a piezo-ceramic crystal attached to the small end of the horn. When applying low power from the connected generator, the signal from the piezo-crystal was observed on an oscilloscope, with the maximum amplitude being obtained at resonance. The amount of removed metal and the resonant frequency were recorded to show the progress of tuning.

After monitoring the resonant frequency, the coupling horn was again mounted on the lathe and more metal was removed. The procedure was repeated as the tuning operation continued. However, as the resonant frequency becomes closer to the design frequency the amount of metal removed had to be decreased since a slight decrease in the horn length produces a considerable change in the resonant frequency. Having completed the horn tuning, its measured frequency at resonance was as close as is practically possible to 20 kHz. In the final stages of tuning, changes in temperature of the component make significant differences to the resonant frequency.

The next part to be tuned was the mandrel bar which was made of greater length than the calculated size, ie. a complete number of half-wavelengths of the vibration wave plus an allowance for the tuning purpose. The same procedure of tuning the coupling horn was adopted for tuning the mandrel bar to reach a resonant frequency of almost 20 kHz.

The final test of tuning was performed for the complete assembly of the ultrasonic system. It was observed that the resonant frequency of the system was very close to the design value (20,040 kHz). However, as the system parts warmed up it was observed that the resonant frequency decreased and reached an operating minimum value of 19.980 kHz.

It is emphasised that the correct design and accurate tuning of the mechanical system together with the perfect matching of the electrical system and the tightness of joints, all contributed significantly to the excellent performance of the ultrasonic system. This was of great importance for the transmission of the acoustic energy down to the mandrel with minimum energy loss or reverse back to the power generator.

4.3 Instrumentation and calibration

4.3.1 The gripper and slider load cells

The research programme necessitated the measurement of the gripper and slider forces prior to and during the bending operation. The reasons for that were: first, to assess the magnitude of the proper initial forces required for each bend and secondly, to examine the effect of applied ultrasonic vibrations on the increase of the forces while bending proceeds. Therefore, two identical load cells supplied by Novatech Ltd were used and arrangements have been made to install the load cells in the gripper and slider assemblies, as discussed earlier in section 4.1.1.

The gripper and slider load cells have capacities of 3 tonf and 1 tonf respectively. They are of cylindrical shape and can be attached

at their ends with screws. The circuit diagram of the load cells are shown in figure 4.9.

4.3.2 The torque-meter load cell

The bending torque was measured during bending under both vibratory and non-vibratory conditions. For this purpose, a specially made meter was installed on the bending machine. The torque-meter consists of a ring-type load cell, a fixed head and a free head. The load cell is attached to the two heads with cylindrical pins, see figure 4.10. While the fixed head is clamped firmly to the driven bending arm, the other head is free to adjust itself correctly, once bending starts, to a support fixed to the driving shaft of the bending machine, as illustrated diagrammatically in figure B.9.

The load cell used for measuring the bending force was supplied by Ether Ltd and it has the capacity of withstanding a maximum compressive force of 5000 lbf. Having measured the bending force, the torque can be calculated by multiplying that force by the normal distance to the centre of machine shaft. Figure 4.11 shows the bridge circuit of the torque-meter load cell.

4.3.3 The mandrel load cell

As illustrated in figure B.16, a load cell was located between the faces of the nodal flange of the horn and the holding plate which is fixed to the machine body. This load cell which is compact and annular, was used to measure the axial force on the mandrel during bending.

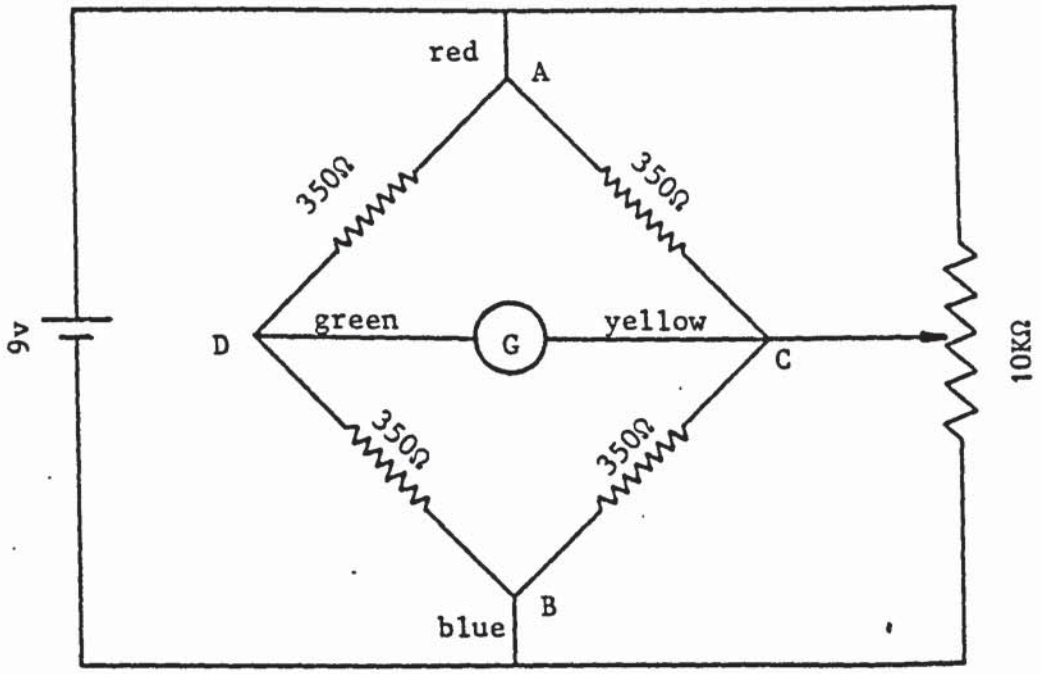

Figure 4.9: The circuit diagram of the gripper and slider load cells

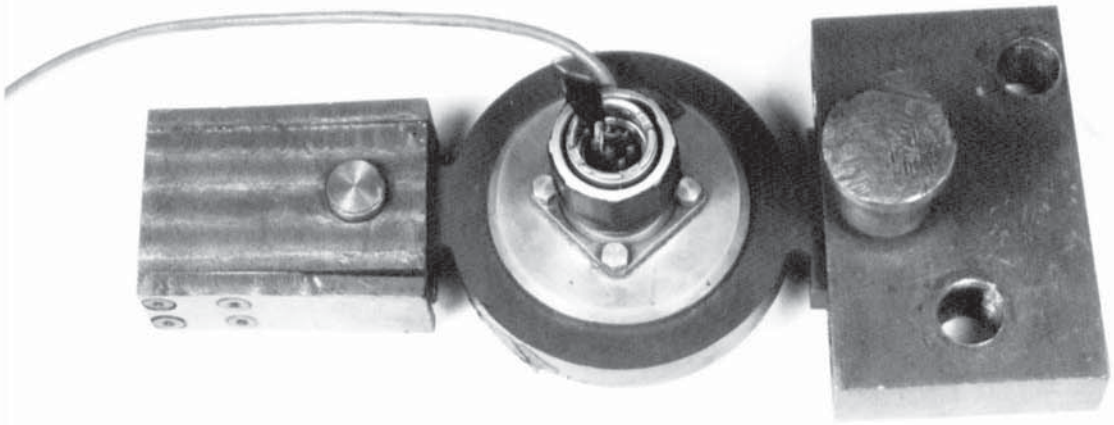

Figure 4.10: The load cell for measuring the bending torque

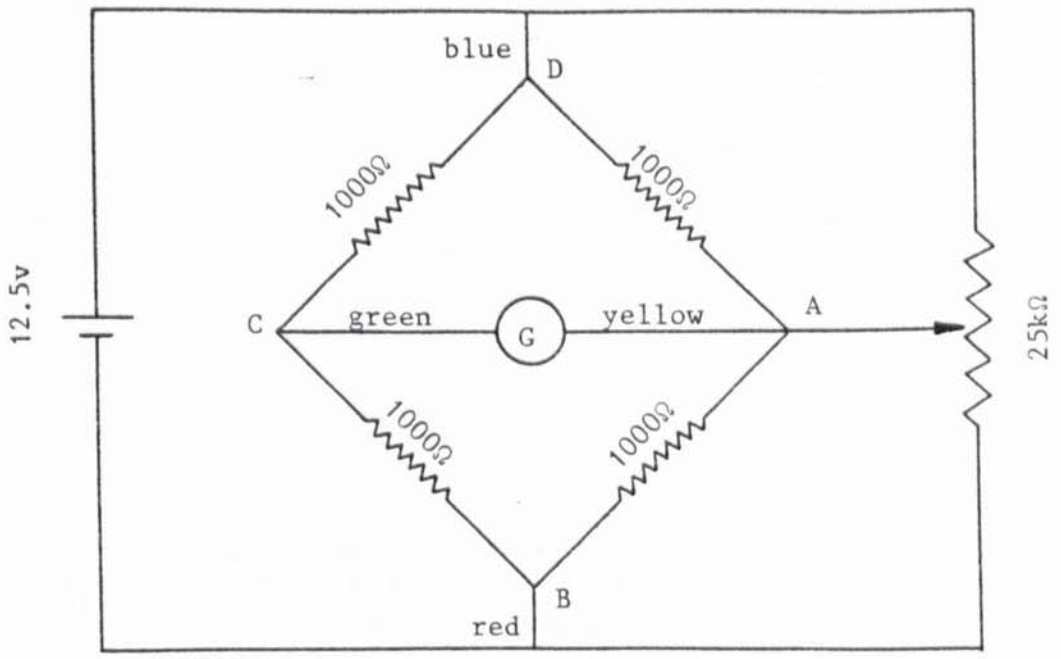

Figure 4.11: The circuit diagram of the torque-meter load cell

The mandrel load cell was designed for a maximum compressive axial load of 2 tonf. It consists of a continuous ring of rectangular cross-section. On one side, see figure 4.12, are four integral sectoral supports equally spaced, and on the other side there is a similar number of equi-spaced supports placed in positions equal to half the pitch. The ring is thus formed from a continuous series of circumferentially shaped beams which strain in bending and torsion when subjected to an axial thrust. The stress and strain distributions, and the stiffness of this type of load cell is discussed elsewhere in detail by Basily[74].

The active strain gauges, which were bonded in positions of maximum bending moments, ie. on the side opposite to the sectoral supports, respond to a tensile bending strain when loaded under axial compression. Also, inactive gauges were bonded on the inner and outer peripheral surfaces in the circumferential direction in positions of zero bending moment. Those inactive gauges were adopted to compensate for temperature variations and any other distortion than that caused by axial thrust. The circuit diagram of the mandrel load cell is shown also in figure 4.12.

4.3.4 Calibration of the load cells

Each of the four load cells was calibrated by compressing it between the two plattens of a recently calibrated 50 tonf 'Denison' hydraulic testing machine. Before the calibation was started, it was necessary to stabilise the equipment by having the instruments switched on for about an hour. The load cell was first loaded to the maximum desired value and the voltage of the d.c. supply, or the span of the

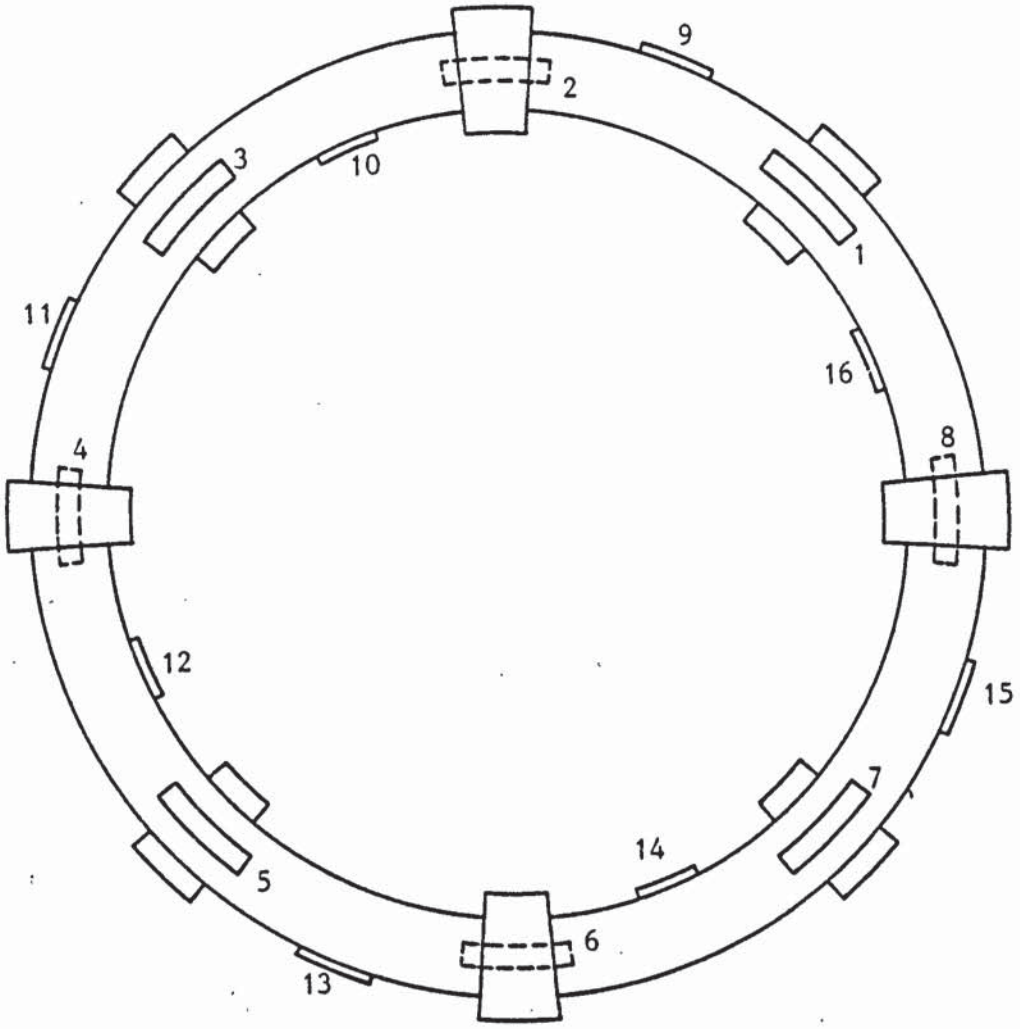

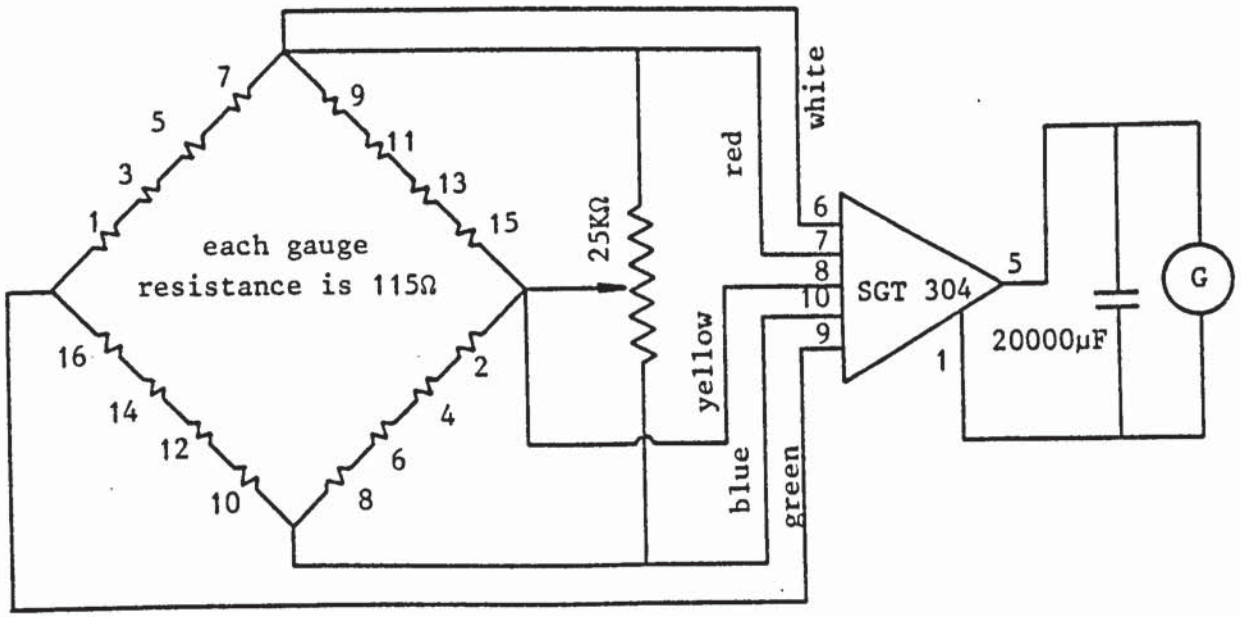

Figure 4.12: The strain gauge arrangement and the circuit diagram of the mandrel load cell

amplifer in case of the mandrel load cell, was adjusted to make use of the full range of the ultra-violet recorder. The load cell was loaded between zero and the maximum load at incremental load of 0.1 tonf (0.25 tonf for the gripper load cell). At each increment, the load was held for a short time while the paper of the u.v. recorder was switched on and off. The readings of the galvanometer deflection and the compressive load, were taken for both the increasing and decreasing loads.

The calibration procedure was repeated twice to ensure reproducible results. Also, the load cells were calibrated for different values of maximum load by changing either the reference d.c. voltage or the amplifier span. This was important in order to choose the suitable working range of the load cells for the best response on the u.v. recorder. The calibration charts of the four load cells, for the ranges used in the bending tests, are shown in Appendix B.6.

4.3.5 Measurement of vibration amplitude

The maximum amplitude of axial vibration of the mandrel, ie. at its end face, was measured using a 'Distec' displacement transducer. This device is a non-contact sensor operating on the eddy current loss principle, which gave a voltage signal directly proportional to the relative displacement of the sensor from the mandrel end face. The 'Distec' position from the vibrating surface was adjusted until a reference output voltage was obtained. This ensured that the datum point was within the output range of the sensor. When the power generator was dwitched on, an alternating voltage was obtained. An

oscilloscope was used to display the output signal and peak-to-peak measurements were taken at different levels of the ultrasonic power from the generator.

In order to relate the recorded peak-to-peak measurements to the actual displacement, a means of calibration was necessary. This was performed by measuring the static displacement of the sensor, using an accurate dial gauge, for the range being considered. The operational procedure consisted of disconnecting the mandrel from the mandrel bar and gripping it in a lathe chuck. The Distec was mounted on the machine carriage together with a dial gauge of a resolution of 0.0001 in. The values of the sensor output on the oscilloscope were recorded against the readings of the dial gauge, see Figure B24. This calibration procedure enabled the maximum amplitude of mandrel vibration to be determined at any value of the output power from the generator, as shown in figure 4.13.

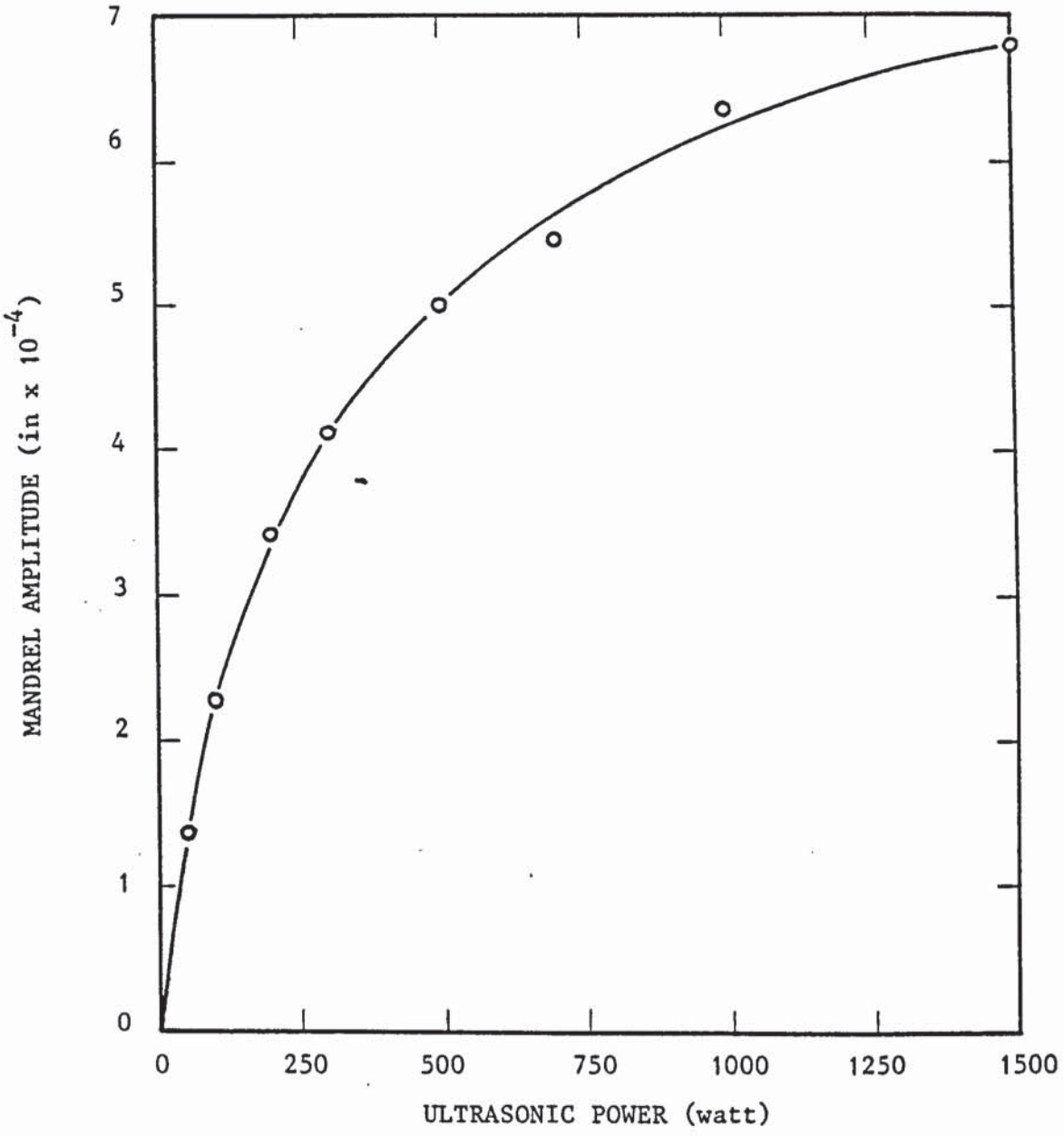

Figure 4.13: The relationship between the ultrasonic power delivered from the generator and the mandrel amplitude

CHAPTER FIVE

EXPERIMENTAL TECHNIQUE AND PROCEDURE

5.1 General description

The current research programme was undertaken to study experimentally the mechanics of tube draw-bending process with and without applied ultrasonic axial vibrations to the supporting mandrel. Additionally, the investigation aimed at examining the influence of varying the amplitude of mandrel vibration on the bending forces and torque, and also on the strains developed during the process.

To achieve these objectives, thin-walled mild steel tubes of different diameter to thickness ratios were bent to mean bend radii varying between 1.5 and 2 times the tube outside diameter. Bends were made under both oscillatory and non-oscillatory conditions. The ultrasonic power and the amplitude of vibrations were varied for each series of oscillatory bending tests. The bending torque, the mandrel force and also the slider and gripper forces were recorded during the bending operation. A grid was scribed on the tube surface in order to enable the longitudinal and hoop strains to be measured after deformation. Each tube bend was carefully sectioned and the variation of tube wall-thickness was accurately measured.

In the following sections, the details of the experimental procedure will be discussed. In addition to reviewing the process parameters, the test procedure and the method of measuring the strains, also the

other experimental preparations will be described.

5.2 The process parameters

The principal parameters in the bending process, namely: the tube diameter to thickness ratio (d/t) and the mean bend radius (R_o), were taken into account in the experimental work. The aims were not only to investigate the influence of those variables on the mechanics of metal deformation during the conventional bending but also to establish the conditions under which the application of ultrasonic oscillations can be more beneficial. Furthermore, for the oscillatory tests, the parameters included the amount of input ultrasonic power (the amplitude of mandrel vibration).

Table 5.1 summarises the number of bending tests which were carried out and shows the details of the process parameters being considered.

The tube diameter to thickness ratios were in the range from 15 to 26. The nominal wall-thicknesses were .036, .048 and .064 in, while the tubes had a constant outside diameter of 1 in. For each d/t ratio, a set of experiments was conducted by changing both the mean bend radius and the mandrel amplitude. Results were obtained for the effect of varying the d/t ratio on the bending forces and the strains under oscillatory and non-oscillatory conditions.

The values of the mean bend radii were selected to be 1.5 and 2 times the tube outside diameter, which may be considered as tight bends. It was also planned to conduct tests on tighter bends having a mean radius equal to the tube diameter, and so, bending tools were designed and manufactured for this purpose, see Appendix B.3. However, as a result of the difficulties associated with gripping the tubes and with

d_o (in)		1				
$\frac{d_o}{t_o}$		15	21	26		
$\frac{R_o}{d_o}$	2.0	B1	B6	B11	0 (0)	Ultrasonic power, watt (vibration amplitude, in x 10^{-4})
			B7	B12	250 (3.8)	
			B8	B13	500 (5.0)	
					750 (5.8)	
			B10	B15	1000 (6.3)	
	1.5	B16	B21	B26	0 (0)	
		B17			250 (3.8)	
		B18	B23	B28	500 (5.0)	
		B19	B24	B29	1000 (6.3)	
		B20			1500 (6.8)	

TABLE 5.1: The number and specifications of bent tubes with and without applied ultrasonic vibrations

using an obsolete and mechanically controlled bender and also because of the length of time taken during the experimental procedure, those tests were left for future work.

The amplitude of mandrel oscillations was varied by changing the output ultrasonic power from the generator. So, oscillatory tests were carried out at different levels of ultrasonic power having various values from 250 watt to 1500 watt, and the corresponding mandrel amplitudes varied between 3.8×10^{-4} in and 6.8×10^{-4} in. In most cases, however, the maximum power was limited to 1000 watt. Because it was difficult to measure the mandrel amplitude during the bending operation, the oscillatory power as observed on the generator meter, provided a satisfactory measure of the values of the amplitude. These two variables, ie. the generator power and the mandrel amplitude were related to each other under no-load conditions through the procedure described in section 4.3.5.

Other process parameters which could have been considered in the experiments would have included the tube outside diameter, the bending speed and the tube material. However, the pressure of time and material expense suppressed a wider consideration of those parameters. It was proposed that tubes having a constant diameter to thickness ratio but of varying outside diameters would be bent to a tight mean bend radius conventionally and with applied oscillations. Bending tools were made for 0.75 in and 1.25 in tube sizes, which are shown in Appendix B.3. A fixed bending speed of 10 rev. min^{-1} was used throughout the experiments, but it is believed that changing the speed would have an effect on the oscillatory bending results. Lower speeds can have advantageous effects but higher values may require larger amplitudes of mandrel vibration to achieve the same reductions of forces

and strains. Some tests were performed in collaboration with Hilmor Limited for bending stainless steel tubes with and without applied ultrasonic vibrations.

5.3 Experimental preparations

Before each series of experiments, certain arrangements were made, notably the proper set-up of bending tools and the correct adjustment of the oscillatory equipment. Also, a number of tube specimens were cut and prepared. On the surface of each specimen, a grid was accurately scribed.

5.3.1 Machine set-up for bending

Setting-up the bending machine correctly for producing good quality bends was one of the most difficult and time consuming tasks in the experimental procedure. Essentially, for each change of the mean bend radius, the machine had to be reset and the bending tools were readjusted precisely relative to each other. Consequently, trials were made for each tooling set-up which were followed by the necessary corrections depending on the problems or faults which may have arisen. Although the right bending tools may have been employed, an incorrect tooling set-up can result in bend faults such as: heavy or little wrinkles on the inside surface of a bend, excessive flattening of the tube section, a hump at the end of bend and marks or scratches on the tube surface. Some industrial publications[75] provide useful information regarding some improvements to the tooling set-up for correcting poorly bent tubes. However, most of the setting-up task relies heavily on the

individual judgement of the operator. In general, after the initial set-up of tools, the bend produced was studied in order to determine what tools should be readjusted to achieve a better quality bend. It was also important to make only one adjustment for each trial unless a second adjustment was obviously necessary.

The former, the gripper and the slider were accurately set relative to each other so that their grooves were at the same level. Also, the slider was adjusted parallel to the gripper in order to exert a uniform pressure on the straight part of tube during bending. Much attention was paid to the setting of the mandrel and the wiper die, and their correct locations were found by trial and error. The considerations given to the tooling set-up are discussed in more detail in section 2.1.

Tubes were bent through 180 degrees and this was also achieved by trial and error and by using the cam on the indexing plate inside the bending machine. An over-bend was necessary to compensate for the tube springback which was largely affected by the mean radius of bend.

5.3.2 Adjustment of oscillatory equipment

To achieve the full utilisation of the ultrasonic energy, the electrical equipment of the oscillatory system was accurately adjusted before each set of experiments. This included the correct matching between the power generator and the ultrasonic transducers, and the best tuning of the oscillatory system. Details of the matching and tuning procedures are written in Appendix B.4.

The adjustment of the oscillatory equipment was necessary for

resonance to be obtained at the right frequency and for the displacement antinode to be at the free end of the mandrel. Resonance was obtained when the ratio of the load power to the forward power was at its maximum value. However, additional signs can help the operator to recognise resonance such as the sound made by the oscillatory system at resonance which is distinctly different from the off-resonant sound, and the complete disappearance of the normal metallic feeling at resonance with the highest amplitude giving rise to a 'glassy' feeling when touched.

Having achieved resonance, the frequency controller was switched on before the oscillatory tests. This ensured a steady load power during the bending operation.

5.3.3 Preparation and gridding of test tubes

Each tube specimen of specific diameter and wall-thickness was cut to a certain length. The required tube length varied with changing the mean radius of bend. The approximate length was as: $L = R_o \cdot \theta + 2L_s$, where θ is the total angle of bend, and L_s is the length of the end straight parts. Since θ was chosen to be 180 degrees and L_s had a value of 4 in, so the tube length was approximately: $\pi R_o + 8$ in. Thus, for the mean bend radii of 1.5 in and 2 in, the lengths of test tubes were about 13 and 14.5 in. Having cut the tubes, the edges were deburred and the internal and external surfaces were cleaned with trichlorethylene to remove any dirt or grease which might affect the surface conditions.

A square grid, having divisions of 0.1 in each, was scribed on the external surface of the initially straight tube. The details

of the grid are shown in figure 5.1. Light lines were scribed on the surface along the tube length and around its periphery. The objective was to measure the longitudinal and hoop strains in bent tubes at different current angles of bend and at various points on the tube cross-section. The design of the grid was such that the strains could be measured on the outer and inner peripheries and also on the central plane. However, since the accurate measurement of strains, see section 5.5, was a laborious and time consuming job, more attention was paid to measuring the strains on the bend outer periphery. This was most important to show the beneficial effects of applied ultrasonic oscillations in reducing the maximum amount of wall-thinning as a result of the reduction in the longitudinal tensile strains developed during bending.

The longitudinal lines of the grid were scribed by holding the tube in an indexing head and a short plug was fitted into the tube end to prevent its collapse. The free end of the tube was supported by a tail stock as illustrated in figure 5.2. The tube specimen was then rotated through the required angles, and lines were carefully scribed using a height-gauge. To scribe the hoop lines, ie. around the tube periphery, the tube was located horizontally between two central supports fixed on the carriage of the universal measuring machine shown in figure 5.3. The lines were made using a scriber clamped in the machine head. This was achieved by moving the machine carriage to specified positions and the tube was then rotated through 360 degrees against the scriber.

Having scribed the grid, the lengths of divisions were optically checked on the universal measuring machine, and the tube and the lines were labelled. The final lengths of the distorted

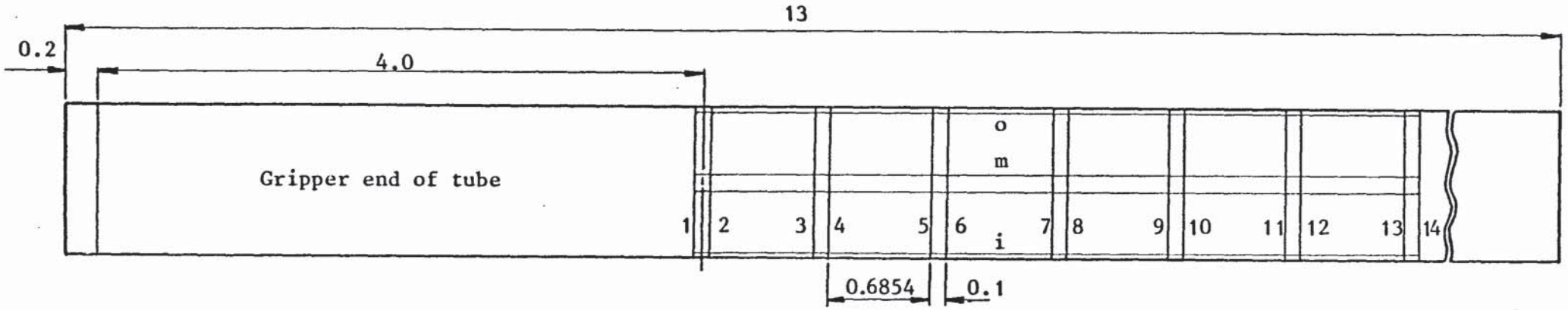

corresponding angle of bend 0° 30° 60° 90° 120° 150° 180°

DIMENSIONS IN INCHES

o, m and i refer to the outer, middle and inner peripheries of the bent tube

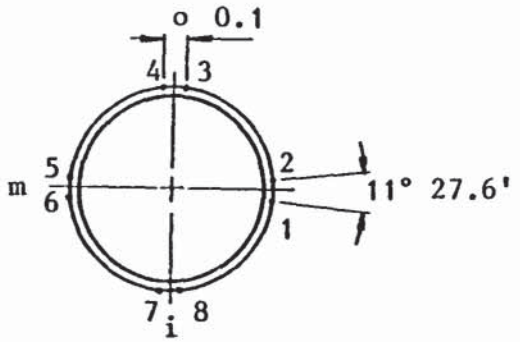

A tube cross-section

Figure 5.1: A diagrammatic drawing showing the details of grid scribed on the tube surface for $d_o = 1$ in and $\frac{R_o}{d_o} = 1.5$

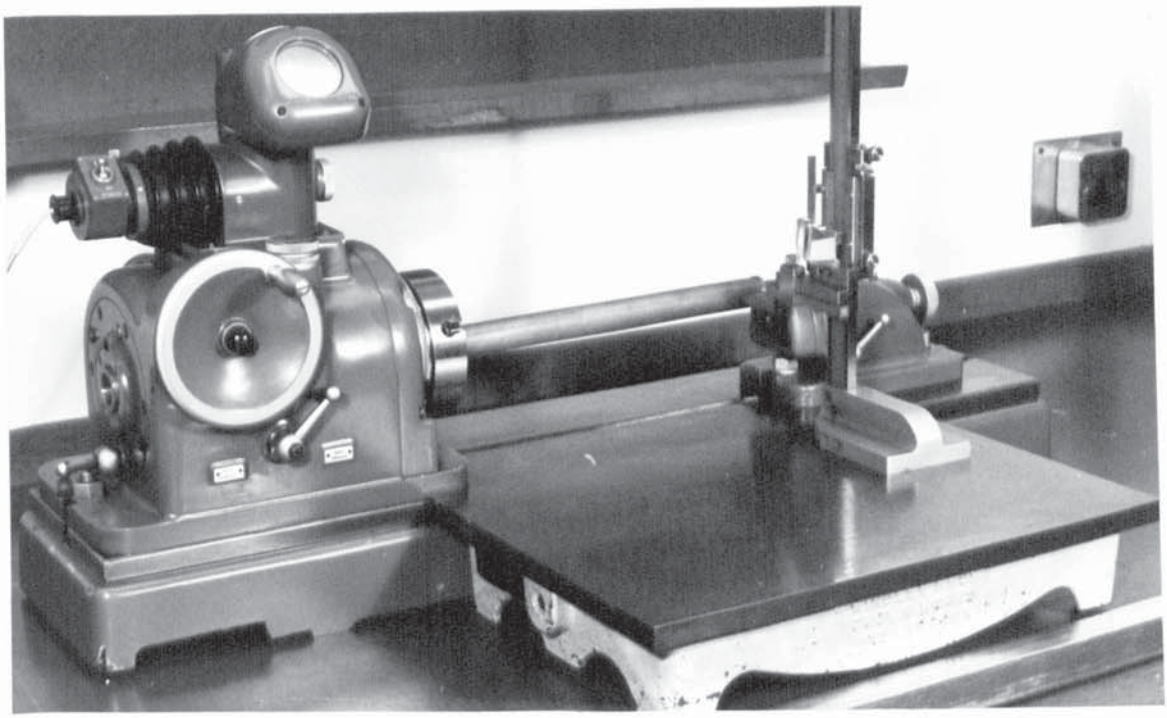

Figure 5.2: The set-up for scribing the longitudinal lines of a grid on the tube surface

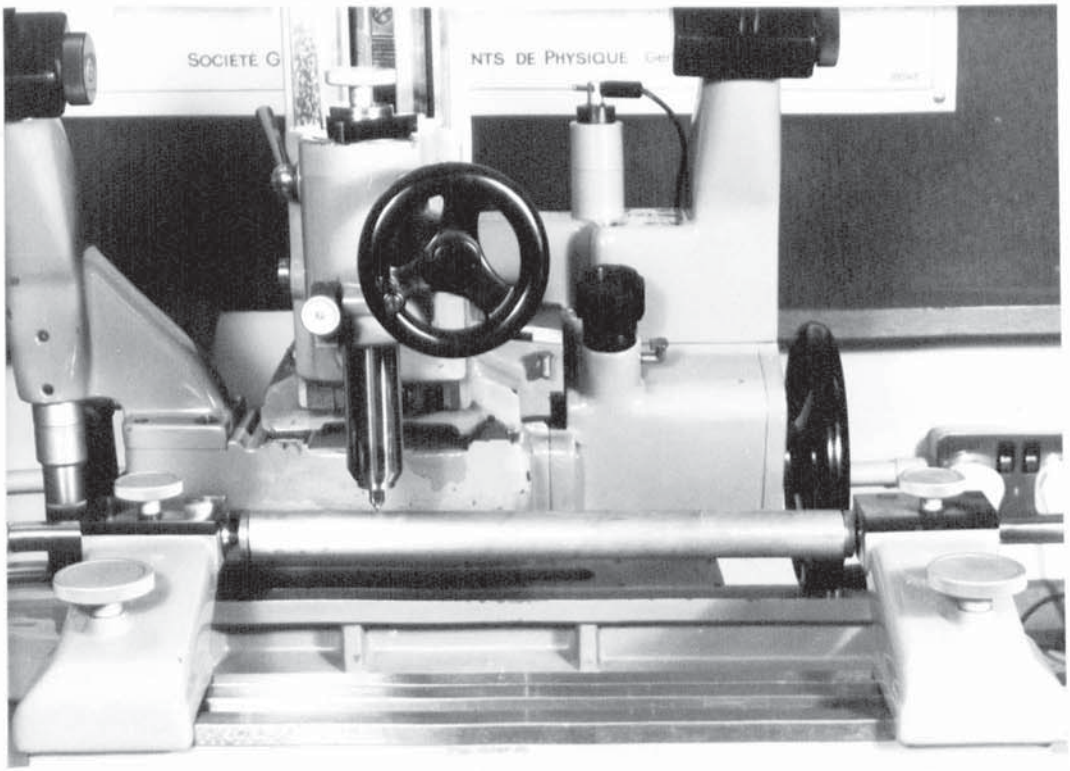

Figure 5.3: Scribing grid lines around the tube periphery using the 'universal measuring machine'

grid on the bent-tube surface were measured using the same machine. The method which was adopted for measuring the longitudinal and hoop strains is described in more detail in section 5.5. A diagrammatic representation of the ideally distorted grid is shown in figure 5.4.

5.4 Test procedure

Before the start of each experimental session, the instruments were allowed to warm up for about one hour in order to ensure the stability of all the electrical circuitry. The balance of the load-cells bridge circuits was checked using a highly sensitive optical galvanometer and any out-of-balance was rectified by adjusting the potentiometers connected to the bridge circuits. Also, the supply voltage of each load cell was checked against a digital voltmeter.

The bending tools, having been correctly set-up, were cleaned and degreased with trichlorethylene before each test. The oscillatory equipment was also adjusted before each set of experiments as discussed in section 5.3.2. For the oscillatory tests, the level of ultrasonic power was varied; and this was achieved by adjusting a power control on the generator front panel.

The test tubes were well lubricated before bending. Two lubricants were recommended by the manufacturers for heavy duty and high performance metalworking. 'Curtagil 90' and 'TD45' which have nearly the same properties and are highly viscous non-volatile fluids, were supplied by Curtagil Limited and Edgar Vaughan Limited respectively. The lubricant was poured into the bore of the tube which was then left for about ten minutes allowing the excess oil to drain away and to give

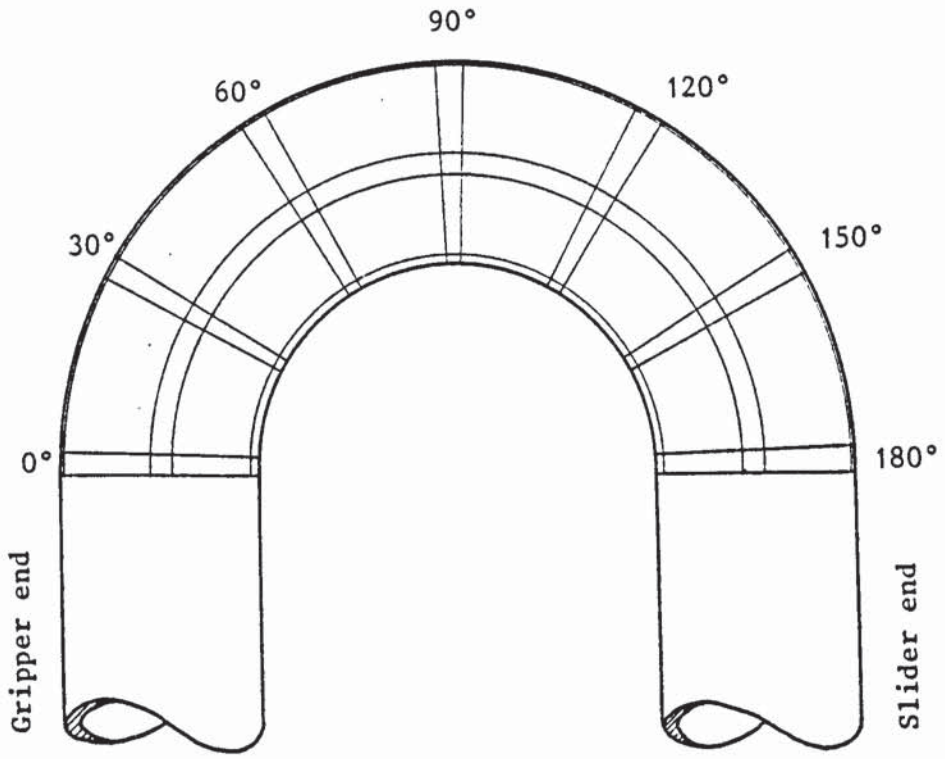

Figure 5.4: A diagrammatic representation of the ideally distorted grid on tube surface

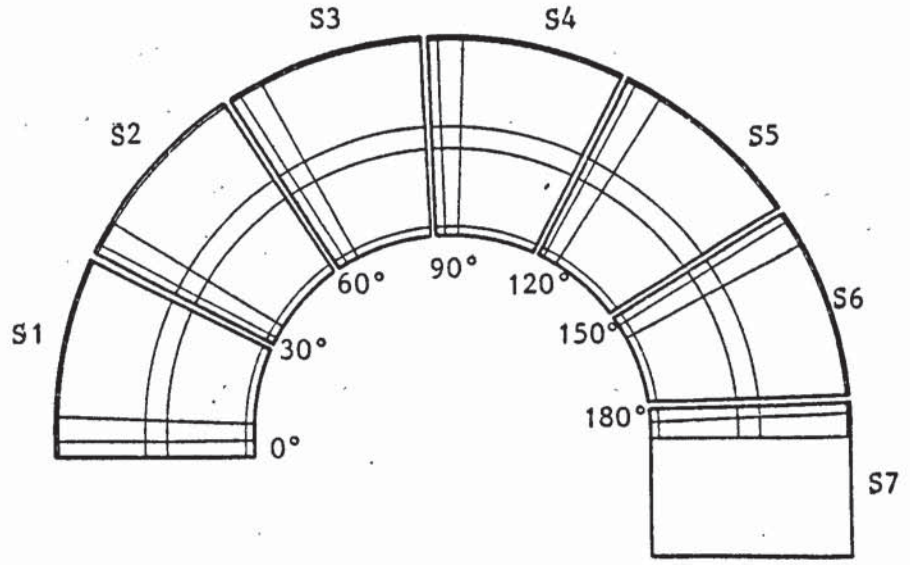

Figure 5.5: The sectoral sections of a bent tube after being cut for strain measurement

a uniform lubricant film. The external surface of a tube was again cleaned.

The lubricated tube was pushed onto the mandrel to a specified position. For very thin-walled tubes, a plug was used to support the tube end in the gripping area. The pedal of the bending machine was depressed and the initial forces on the gripper and the slider were applied. These forces considerably affected the quality of bend and their magnitudes were determined by trial and error. However, the experiments showed that the mean bend radius and also the tube wall-thickness were decisive factors in determining the initial gripper and slider forces which were observed on an ultra-violet recorder. The switch of the bending machine was put on the forward stroke, ie. the direction of bending. The u.v. recorder was started followed by the start of bending operation when the push-button for the required bending speed was switched on. The sequence of bending operation is described in Appendix B.1.

During bending, all the data were recorded on the u.v. recorder with the exception of the ultrasonic frequency which was displayed on a digital frequency counter. The recorded data included the progress of the bending torque, the mandrel force and also the slider and gripper forces in relation to the current angle of bend. On completion of the bending operation the bent tube was removed, checked and cleaned. In addition, all the information regarding the bend number, the specifications of tube and bend, the amount of ultrasonic power and the quality of bend produced were recorded on a data sheet. These records proved invaluable for reference and identification of the products.

The bent tube was carefully cut into sections, figure 5.5, using a thin cutting wheel on a grinding machine in order to enable the

longitudinal, hoop and thickness strains to be measured.

5.5 Measurement of strains

Great care was taken in measuring the final lengths of the distorted grid on the bend surface, as they were used for calculating the longitudinal and hoop strains. Each section of bend was held in an adjustable vice fixed on the carriage of the universal measuring machine, as shown in figure 5.6, such that the grid divisions which were measured by the vernier microscope were nearly horizontal. Different readings were taken over a narrow range of setting angles with the greatest value selected to represent the measured length in the horizontal plane. This procedure was used for measuring the grid divisions in both the longitudinal and the hoop directions.

The thickness strains were also measured at the periphery of bend and at various points on the tube cross-section. The average initial thickness of the original tubes and the final thicknesses of the bent tubes were carefully measured. This was also done on the universal measuring machine but using a probe having a spherical head, figure 5.7, which proved to be more accurate and reliable. The method adopted for measuring the grid divisions was also used for measuring the wall thickness. However, the true thickness was taken as the minimum recorded value.

5.6 Tensile testing of tube material

The tube material used in the experiments was mild steel, standardised as BS 980: 1950, CDS-1. The tubes were cold drawn

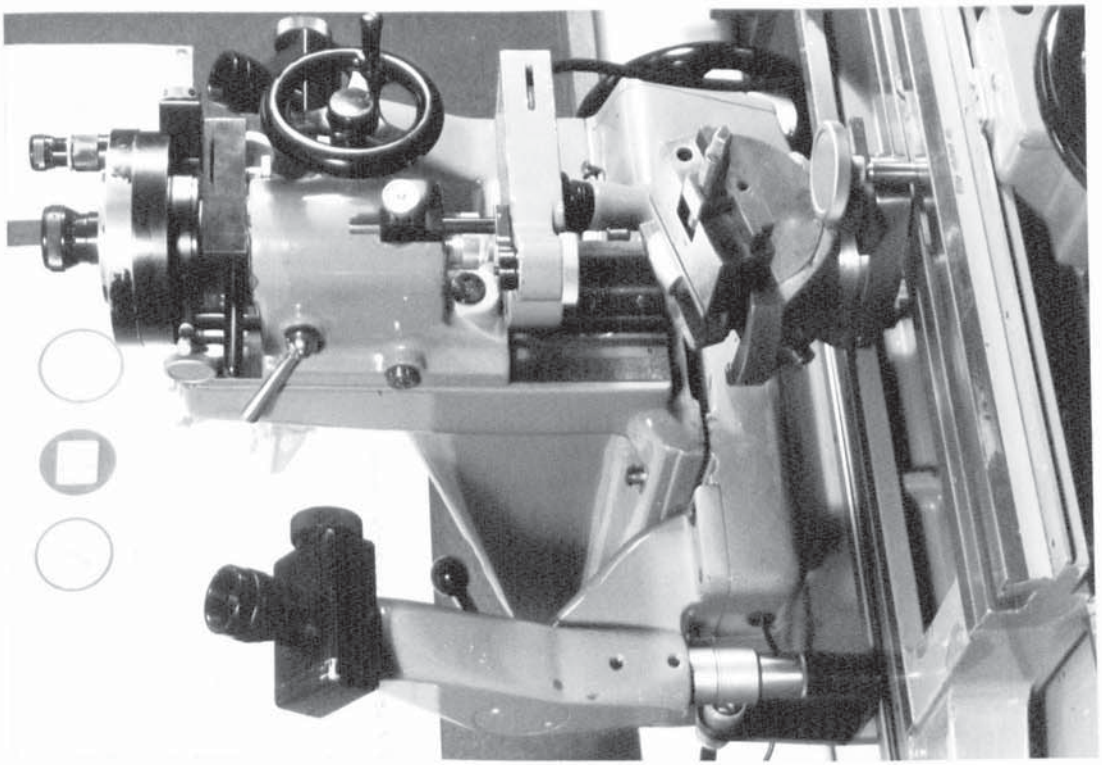

Figure 5.6: Measurement of final length of the grid in the longitudinal and hoop directions

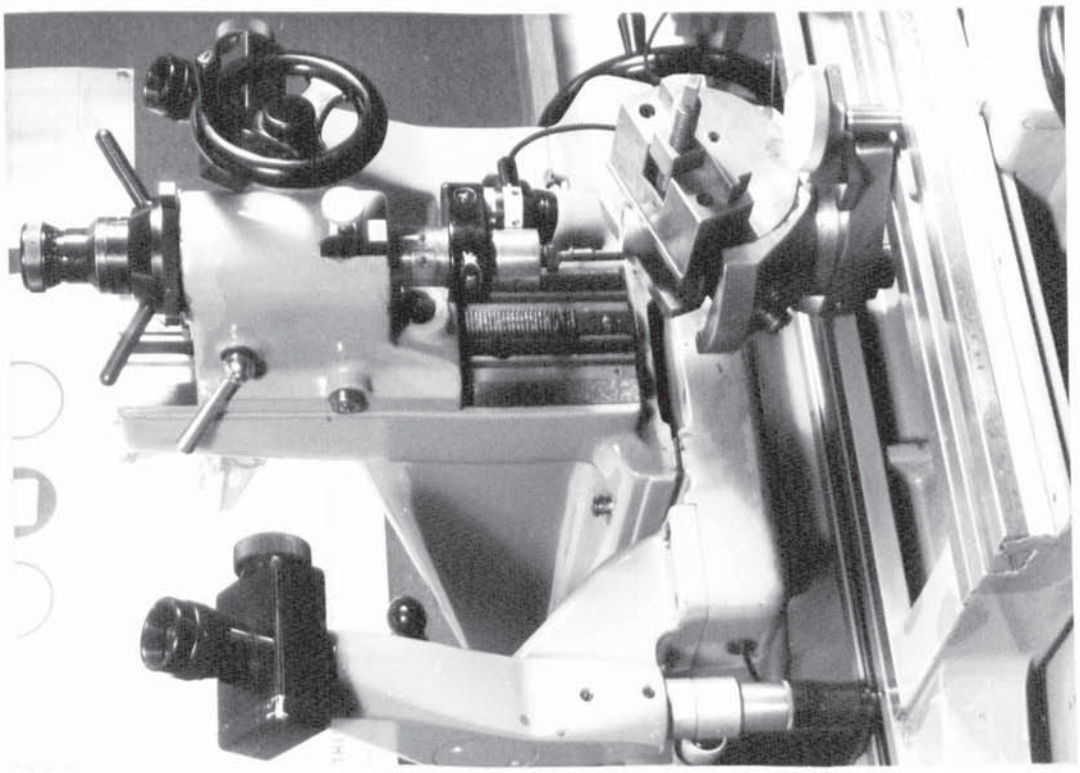

Figure 5.7: Measurement of the variation of the tube wall-thickness in a bent tube using the probe of a universal measuring machine

seamless and fully annealed. The whole batch of tubes was supplied by Le Bas Tube Company Limited in random lengths. The tube size and wall-thicknesses are written in section 5.2.

The material was tested under simple tension. The uniaxial stress-strain tests were carried out on full sections of the tube using an Avery universal testing machine. Plugs were inserted inside the ends of the tubular specimens in order to support them when gripped between the machine jaws. During testing, a graph of the load-extension relationship was obtained. The process was repeated for a few specimens of different wall-thicknesses and the average values were taken to represent the material load-extension relationship which was converted to a true stress-true strain curve.

The relationship between the true stress and the true strain, shown in figure 5.8, was expressed in the form: $\bar{\sigma} = Y + H\bar{\varepsilon}^n$, which can be rewritten as:

$$\ln(\bar{\sigma} - Y) = \ln(H) + n \cdot \ln(\bar{\varepsilon}) \qquad 5.1$$

The curve representing $\ln(\bar{\sigma} - Y)$ vs $\ln(\bar{\varepsilon})$ when plotted gives a linear relationship. The slope of the line is the strain hardening exponent 'n' and the material yield stress is 'Y'. The value of 'H' can be obtained as the intersection of the extrapolated line with the $\ln(\bar{\sigma} - Y)$ axis. However, since the theoretical solution, developed in Chapter Three, required an accurate determination of the stresses and the strains, so the curve representing equation 5.1 was divided into three regions as shown in figure 5.9. The line in the third region was extrapolated to higher strains than those obtained from the tensile tests.

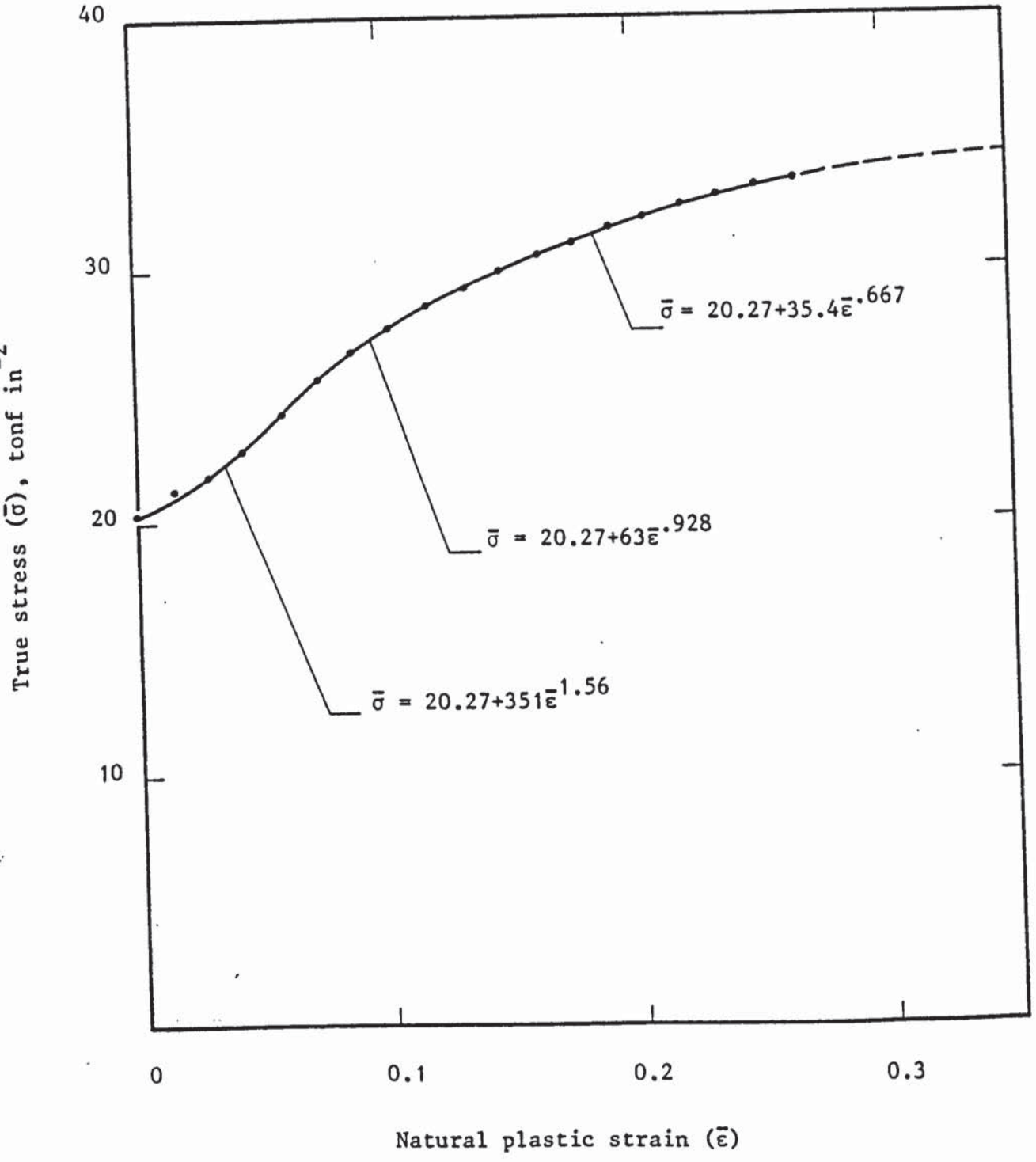

Figure 5.8: The true stress-natural strain diagram for the mild steel tubes under the uniaxial tension

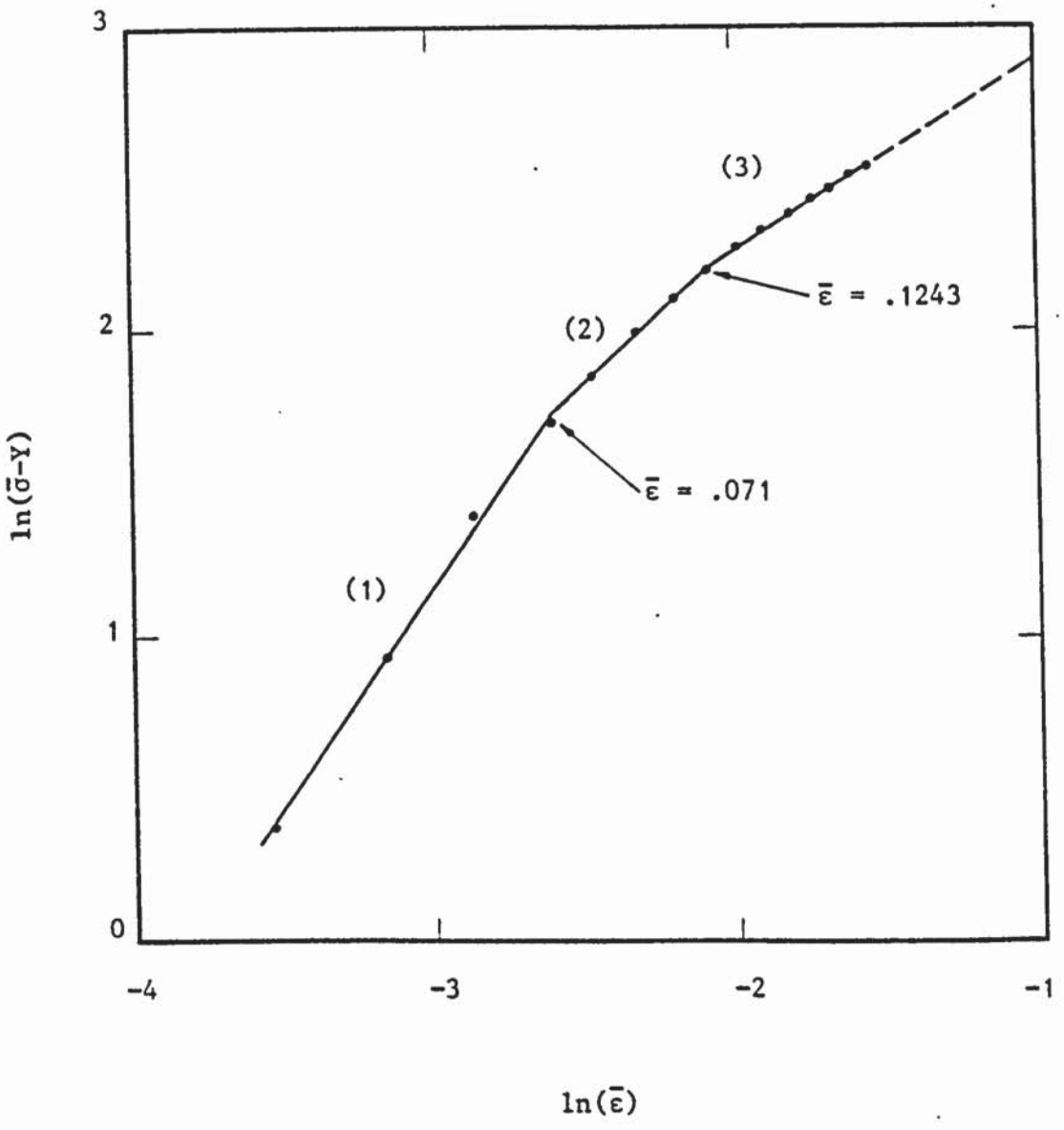

Figure 5.9: The curve representing $\ln(\bar{\sigma}-Y)$ vs $\ln(\bar{\varepsilon})$ for the tube material (derived from Fig.5.8)

CHAPTER SIX

GRAPHICAL THEORETICAL RESULTS

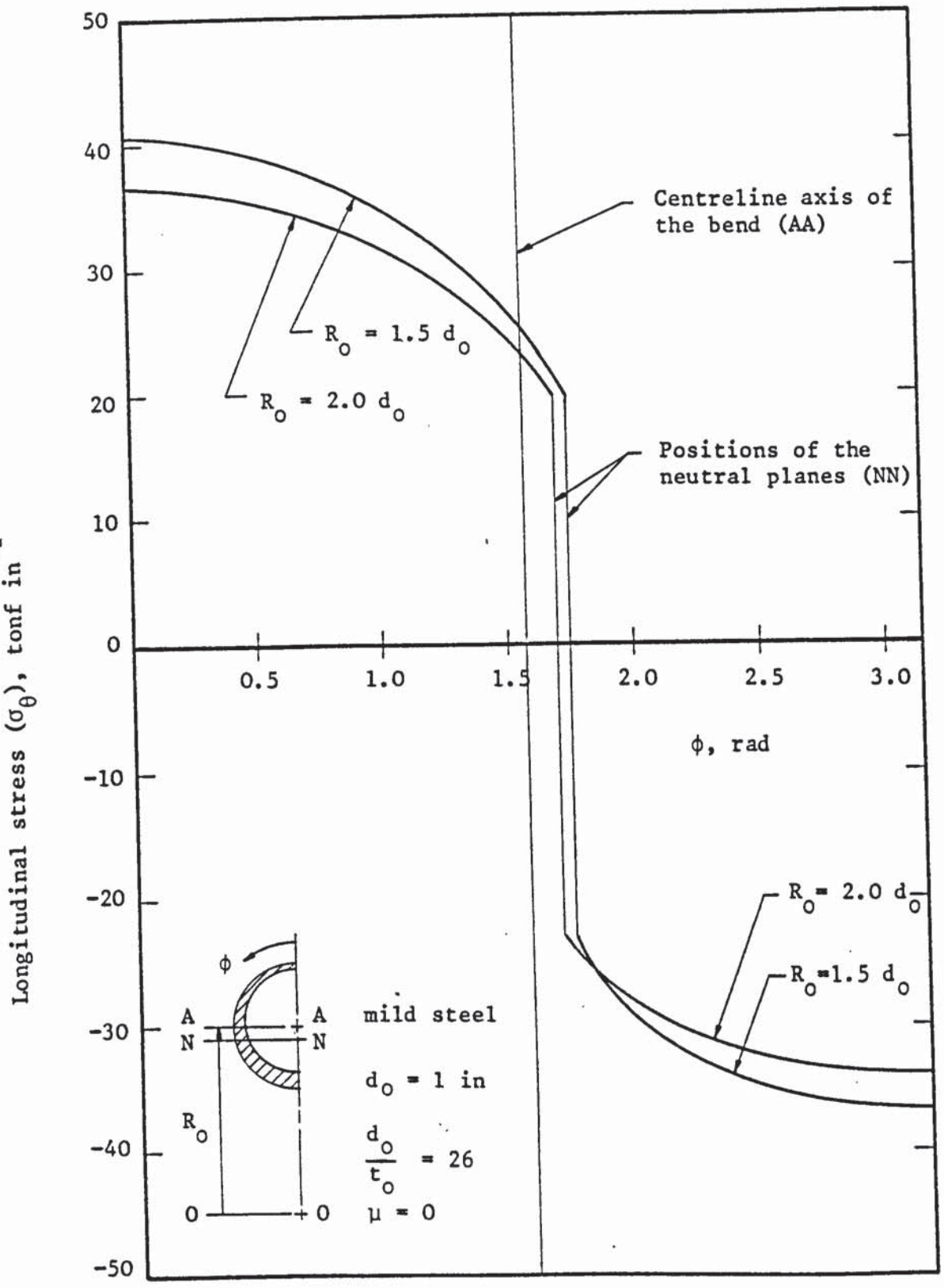

Figure 6.1: Distribution of the longitudinal stress (σ_θ) around the periphery of the tube-section (eqns. 3.15a, 3.17 and 3.19) for various values of mean bend radii under frictionless conditions

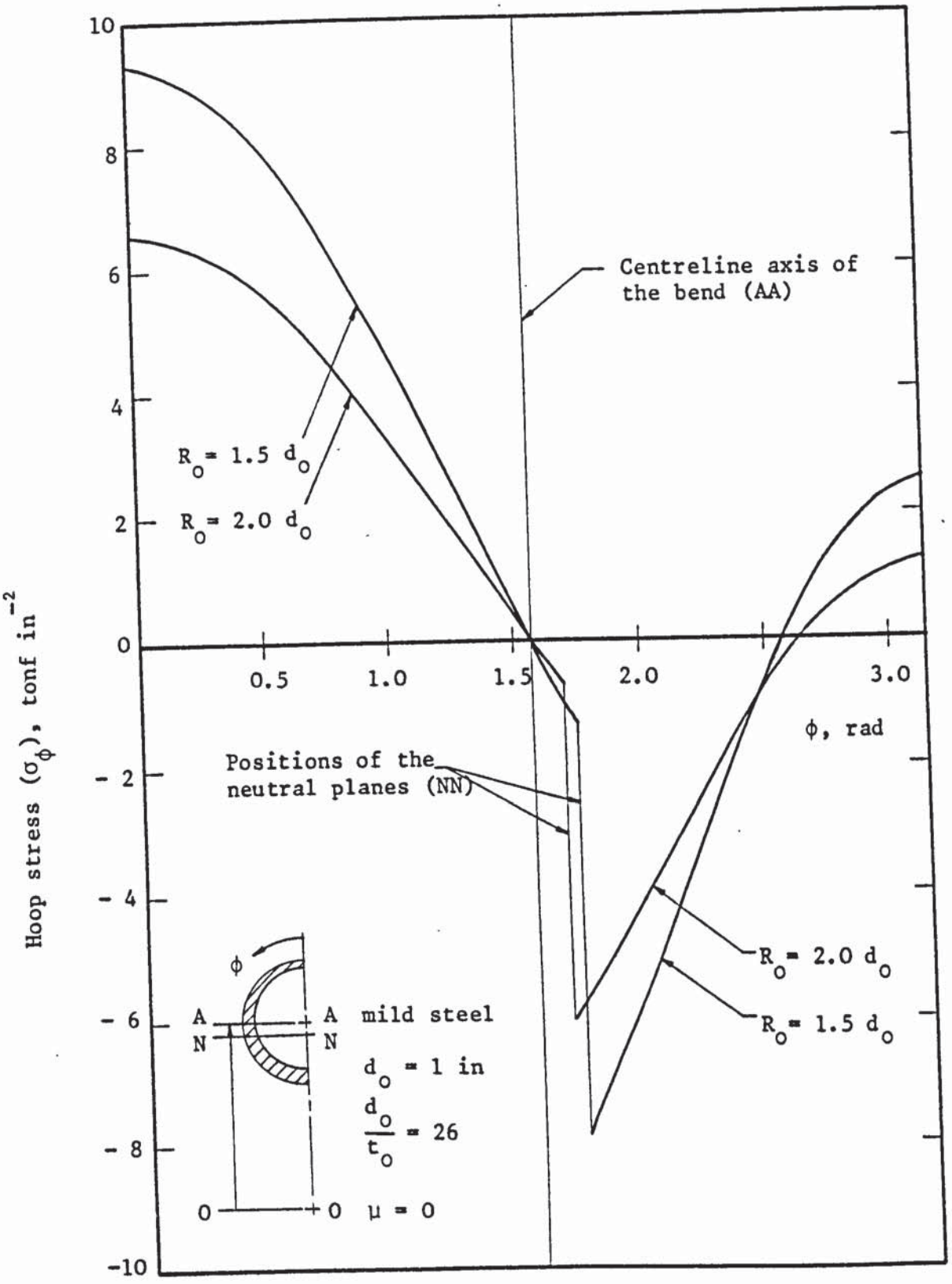

Figure 6.2: Distribution of the hoop stress (σ_ϕ) around the periphery of the tube-section (eqns. 3.12, 3.16 and 3.18) for various values of mean bend radii under frictionless conditions

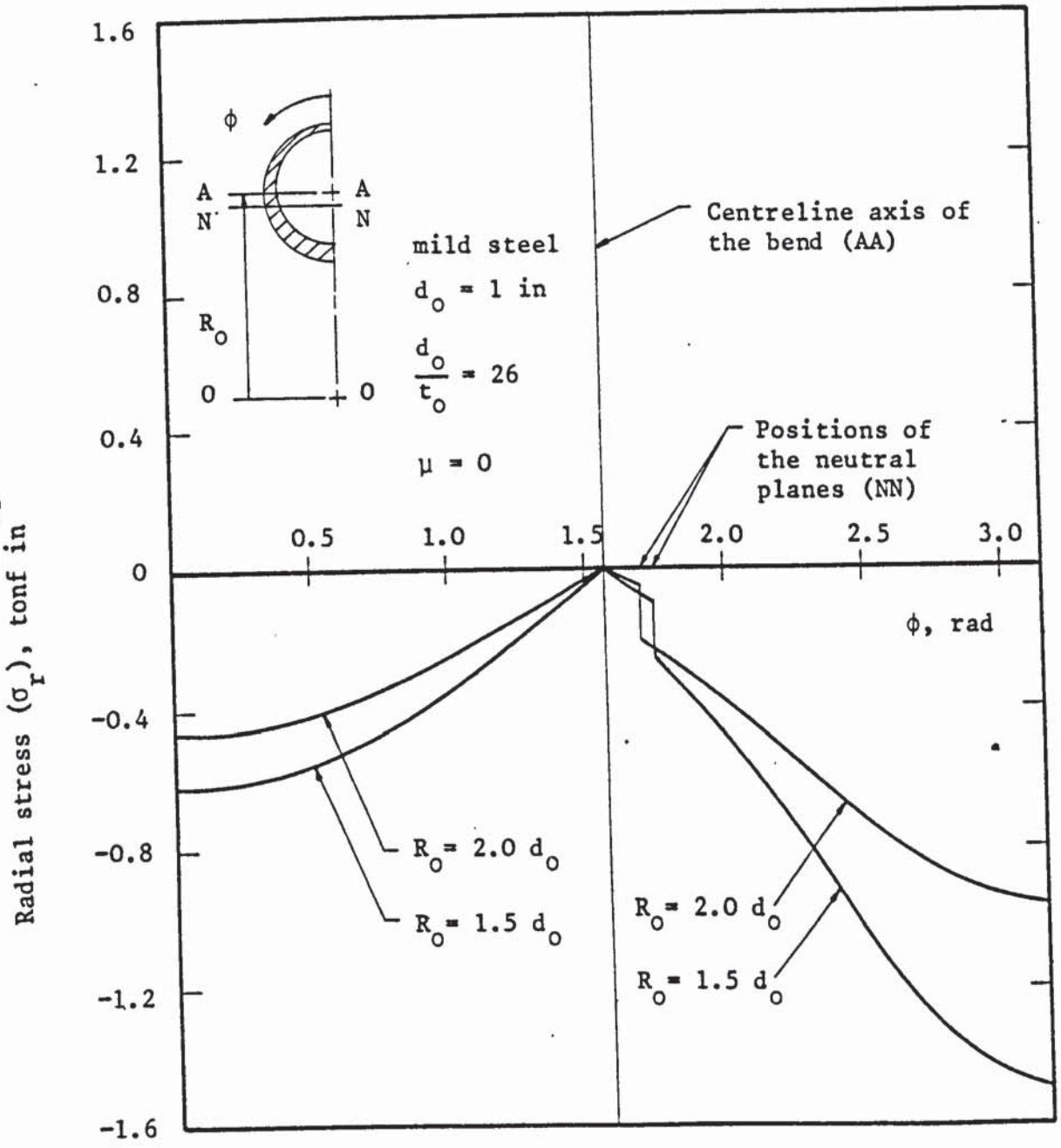

Figure 6.3: Distribution of the radial stress (σ_r) around the periphery of the tube-section in the bending zone (IIb) for various values of mean radii under frictionless conditions

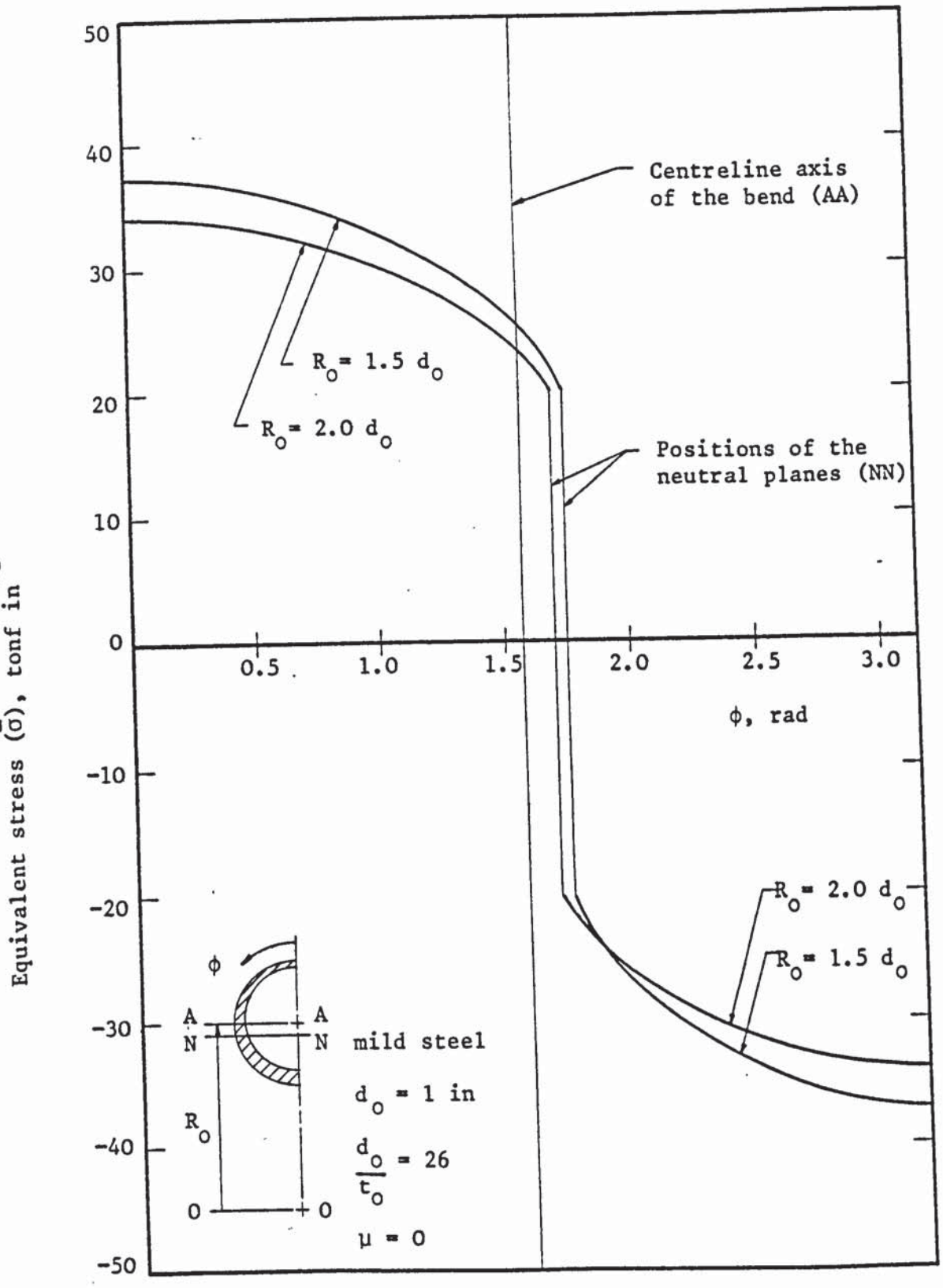

Figure 6.4: Distribution of the equivalent stress ($\bar{\sigma}$) around the periphery of the tube-section (eqn. 32) for various values of mean bend radii under frictionless conditions

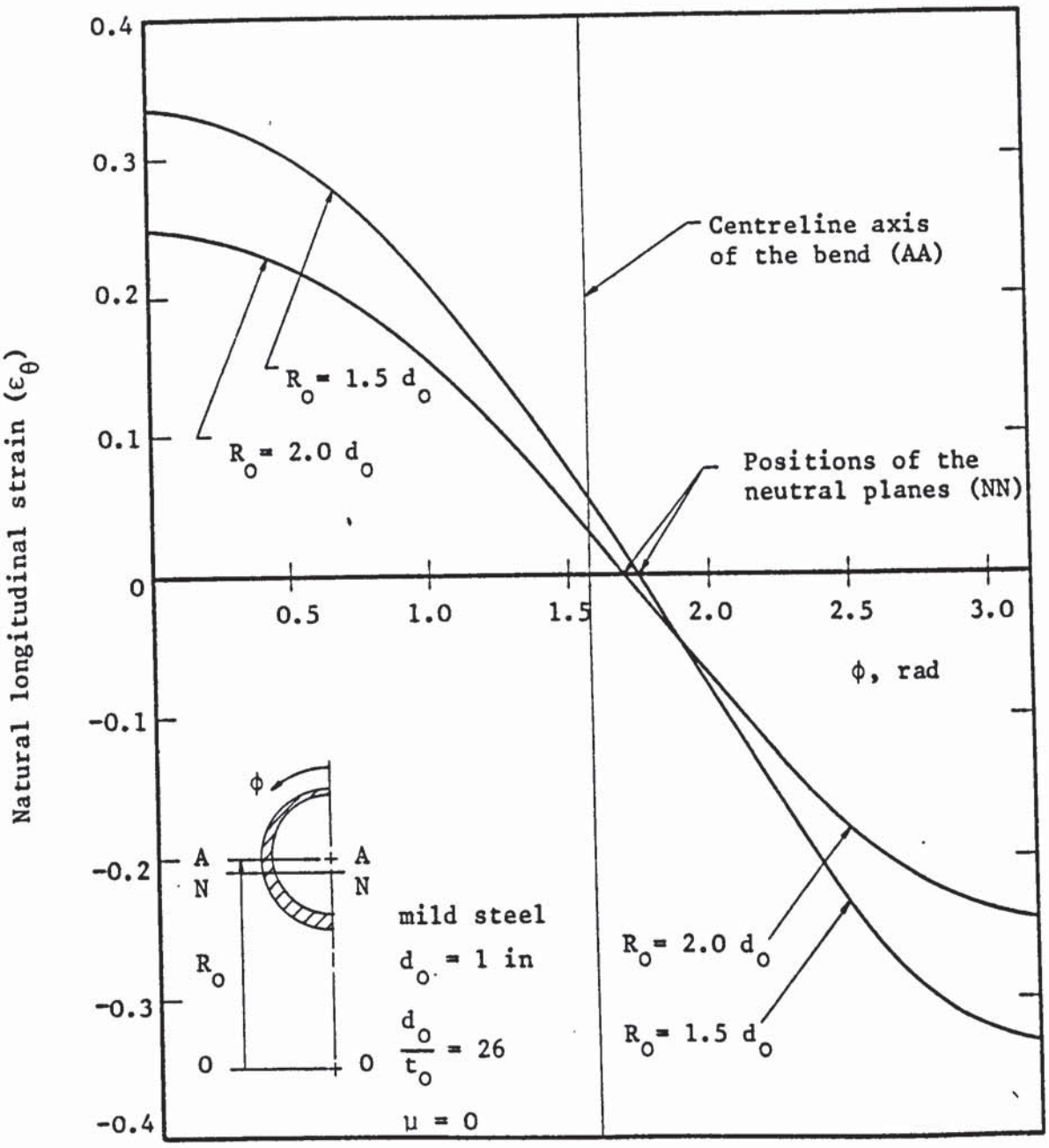

Figure 6.5: Distribution of the longitudinal strain (ε_θ) around the periphery of the tube-section (eqns. 3.23 and 3.29) for various values of mean bend radii under frictionless conditions

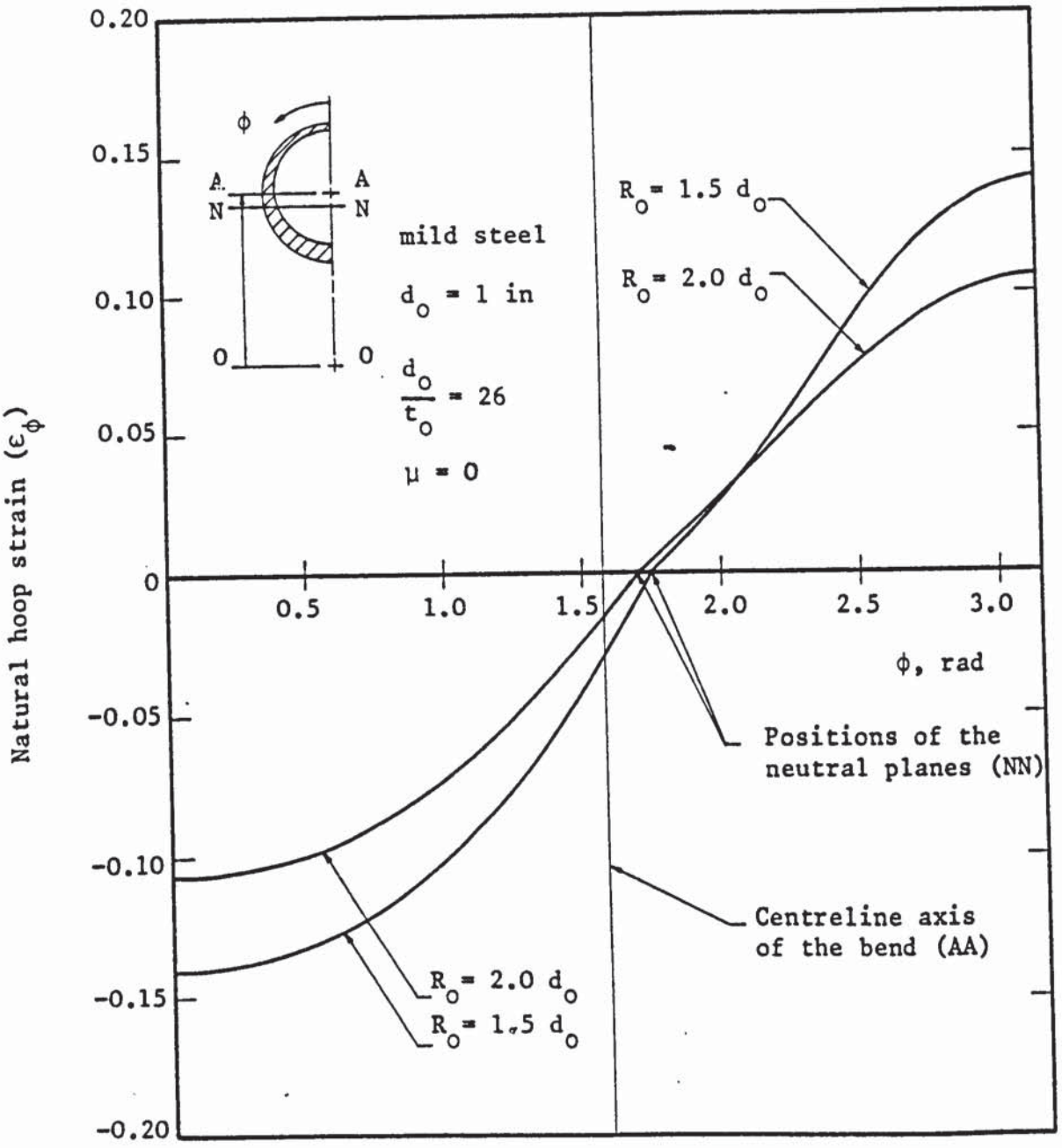

Figure 6.6: Distribution of the hoop strain (ε_ϕ) around the periphery of the tube-section (eqns. 3.27 and 3.30) for various values of mean bend radii under frictionless conditions

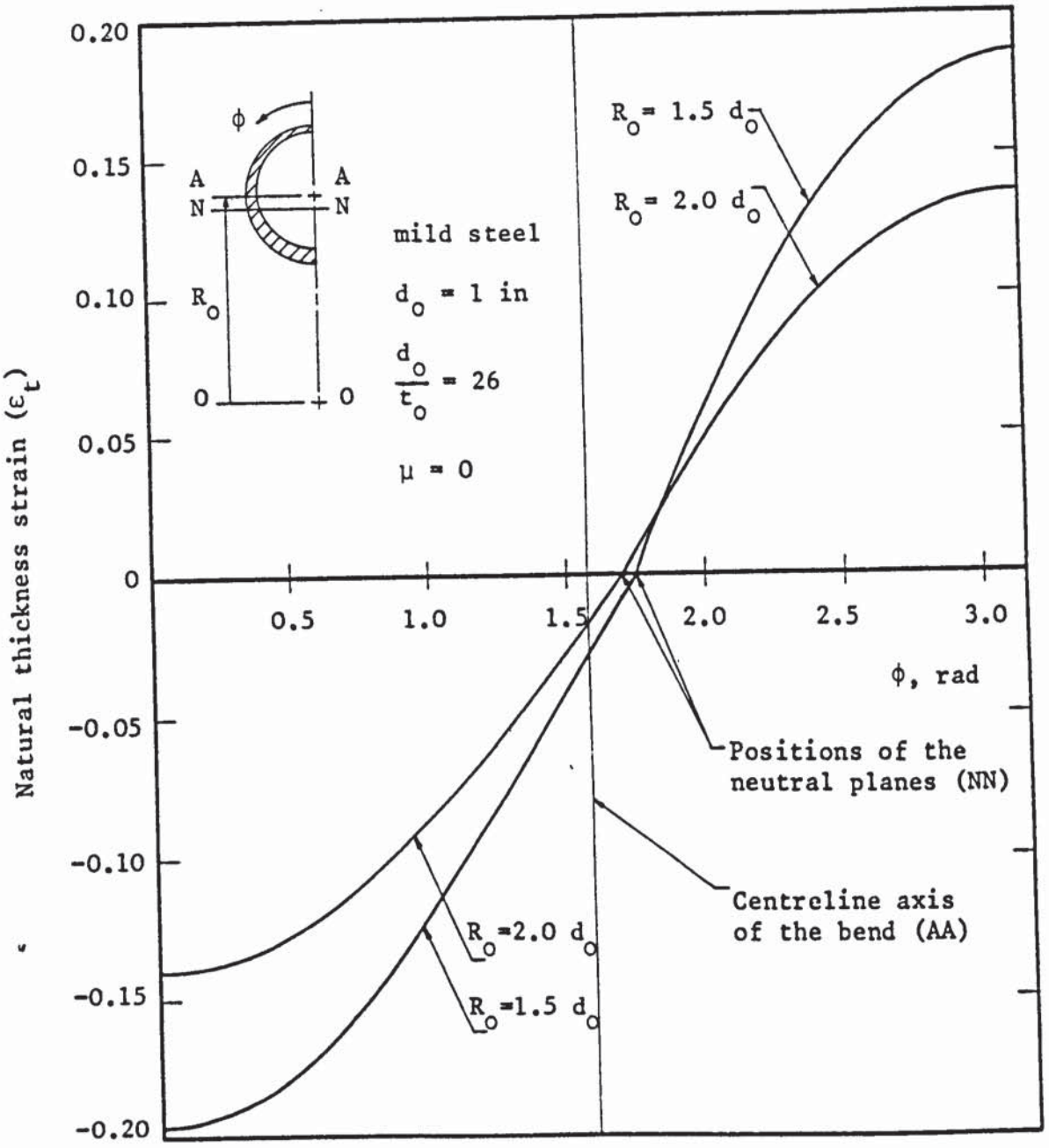

Figure 6.7: Distribution of the thickness strain (ε_t) around the periphery of the tube-section (eqns. 3.28 and 3.31) for various values of mean bend radii under frictionless conditions

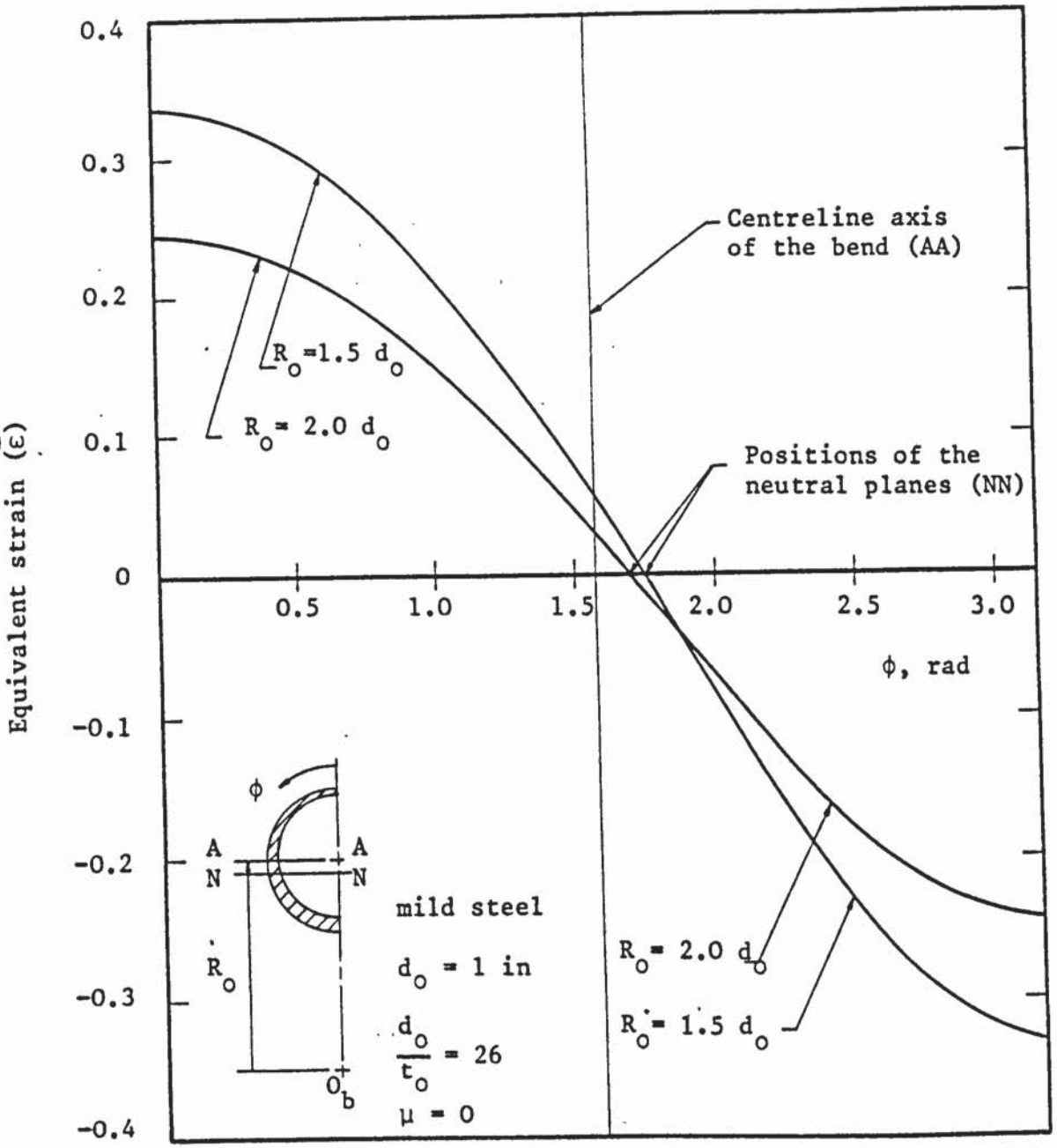

Figure 6.8: Distribution of the equivalent strain ($\bar{\varepsilon}$) around the periphery of the tube-section (eqn. 3.34) for various values of mean bend radii under frictionless conditions

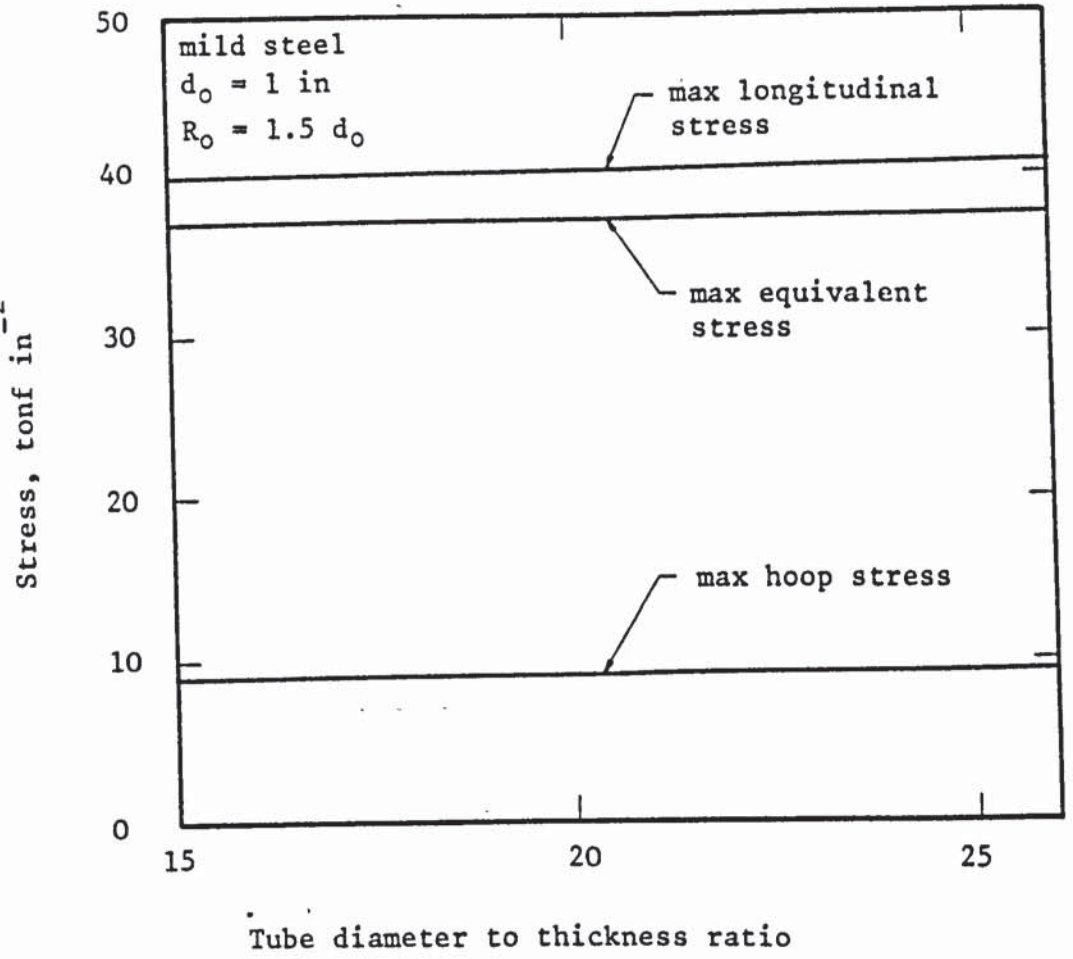

Figure 6.9: Effect of tube diameter to thickness ratio on the longitudinal, hoop and equivalent stresses at the outer periphery of the bend, for R_o = 1.5 d_o

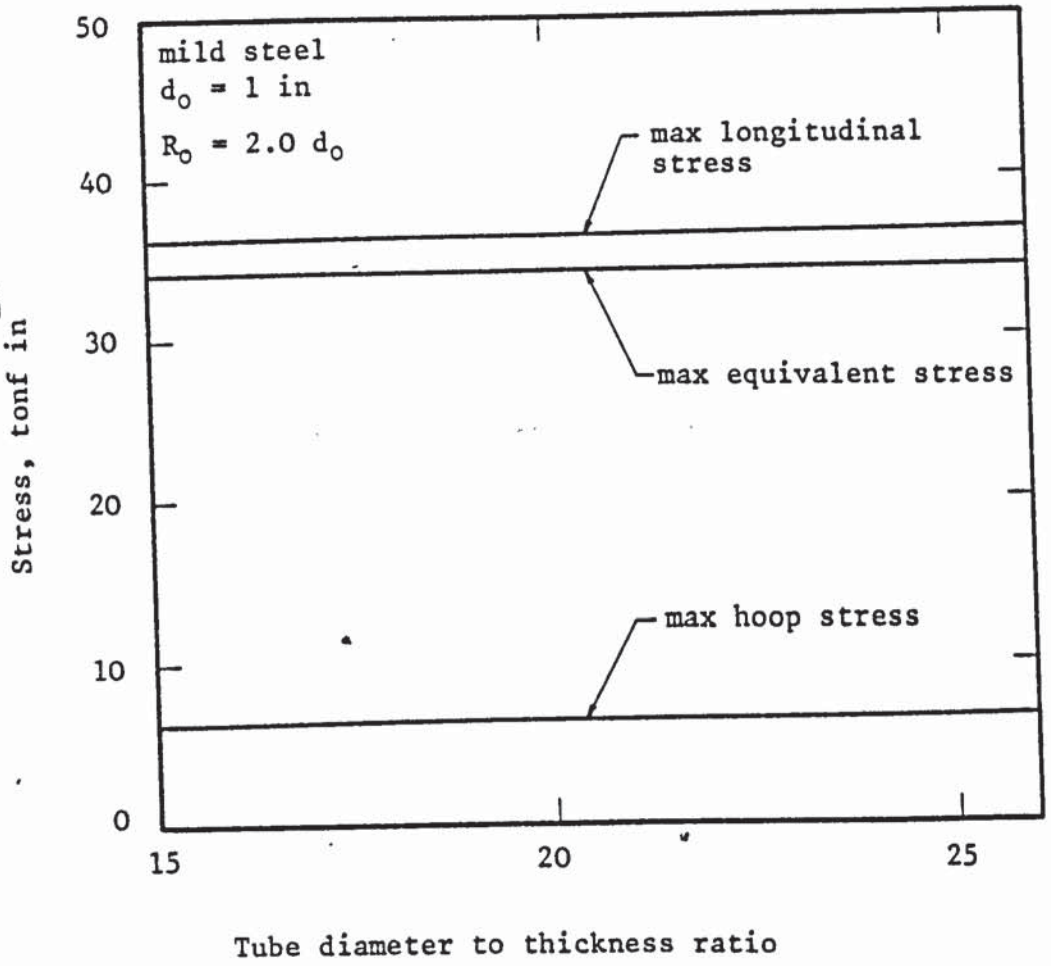

Figure 6.10: Effect of tube diameter to thickness ratio on the longitudinal, hoop and equivalent stresses at the outer periphery of the bend, for R_o = 2.0 d_o

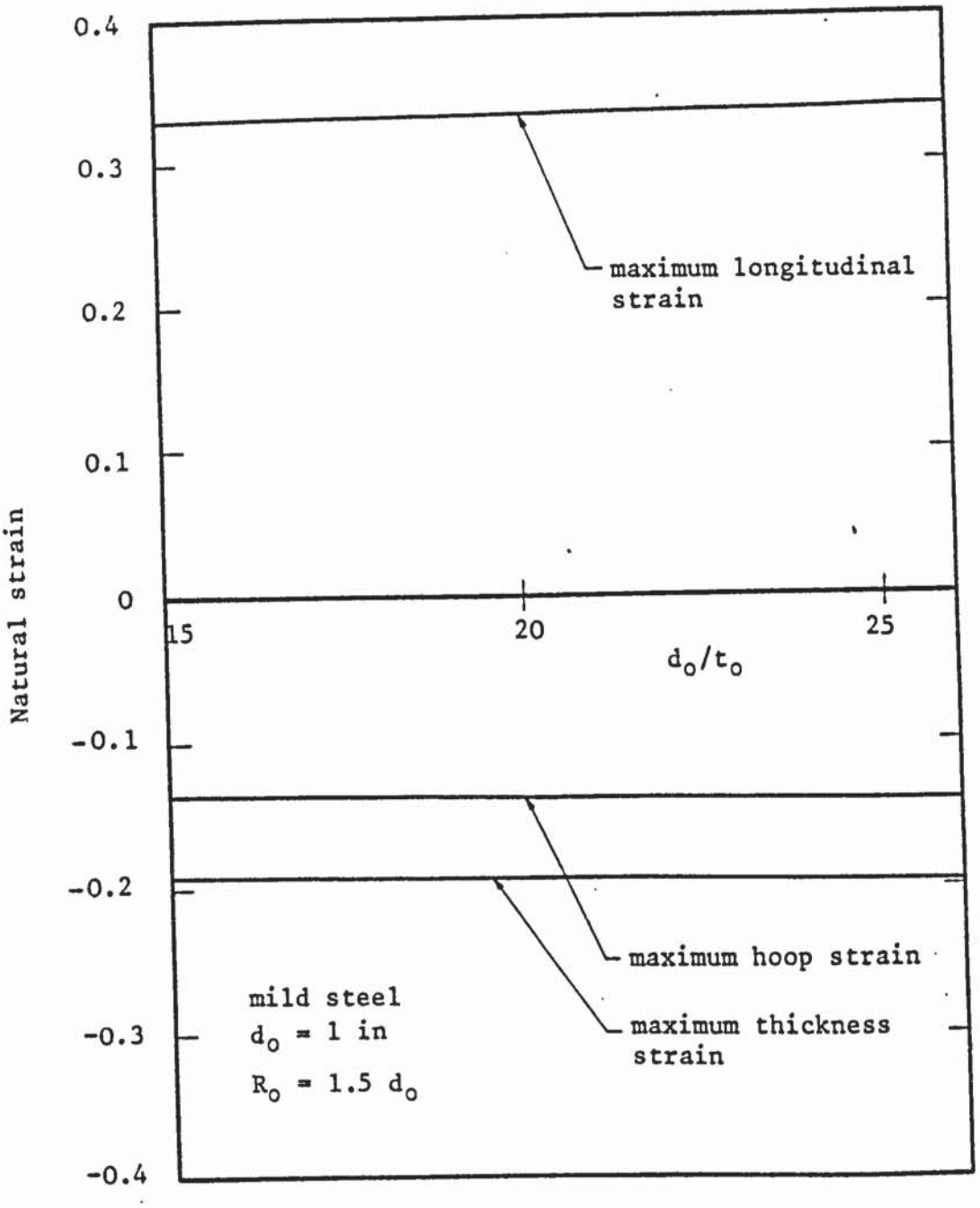

Figure 6.11: Effect of tube diameter to thickness ratio (d_o/t_o) on the longitudinal, hoop and thickness strains at the outer periphery of the bend, for R_o = 1.5 d_o

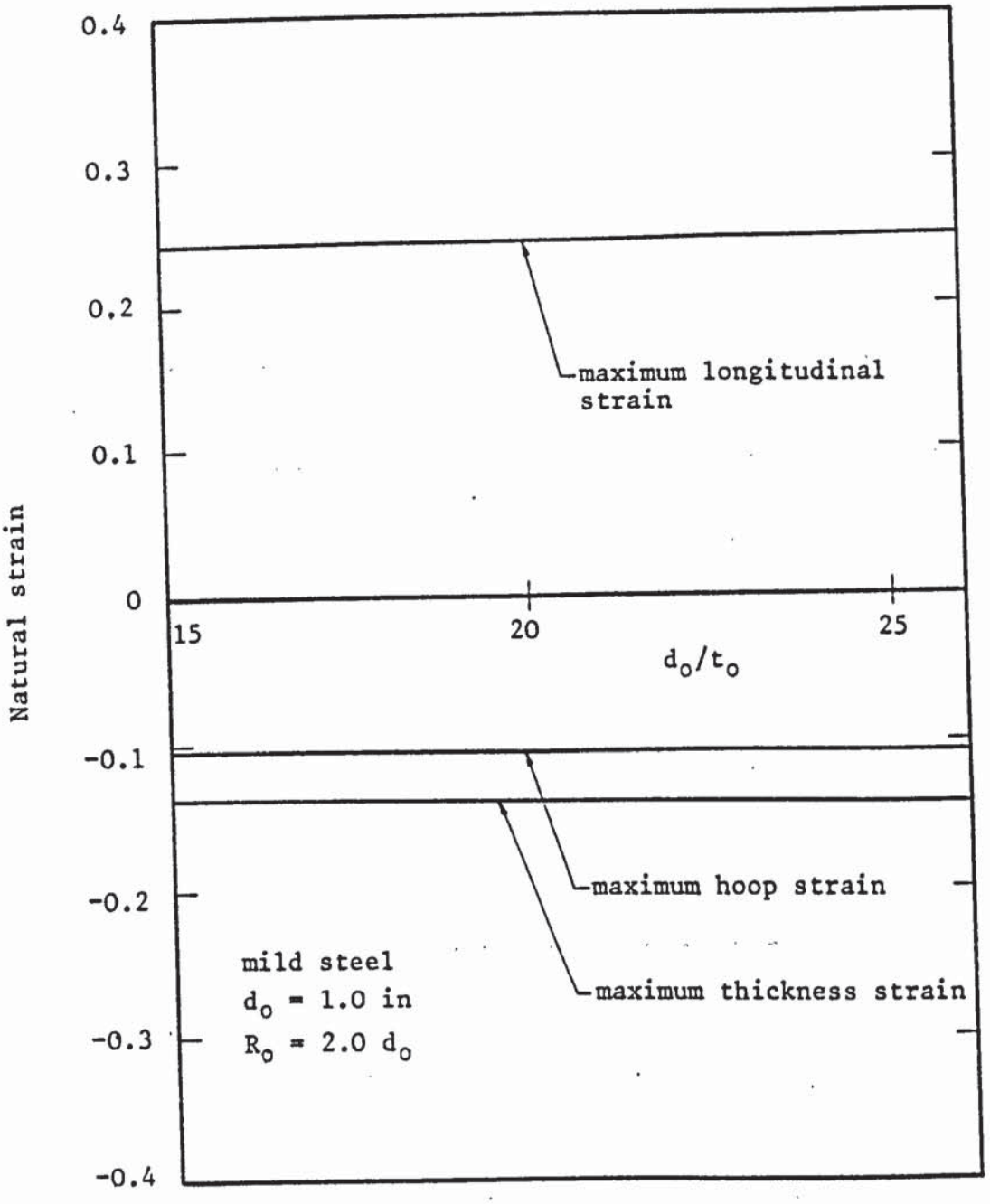

Figure 6.12: Effect of tube diameter to thickness ratio on the longitudinal, hoop and thickness strains at the outer periphery of the bend for R_o = 2.0 d_o

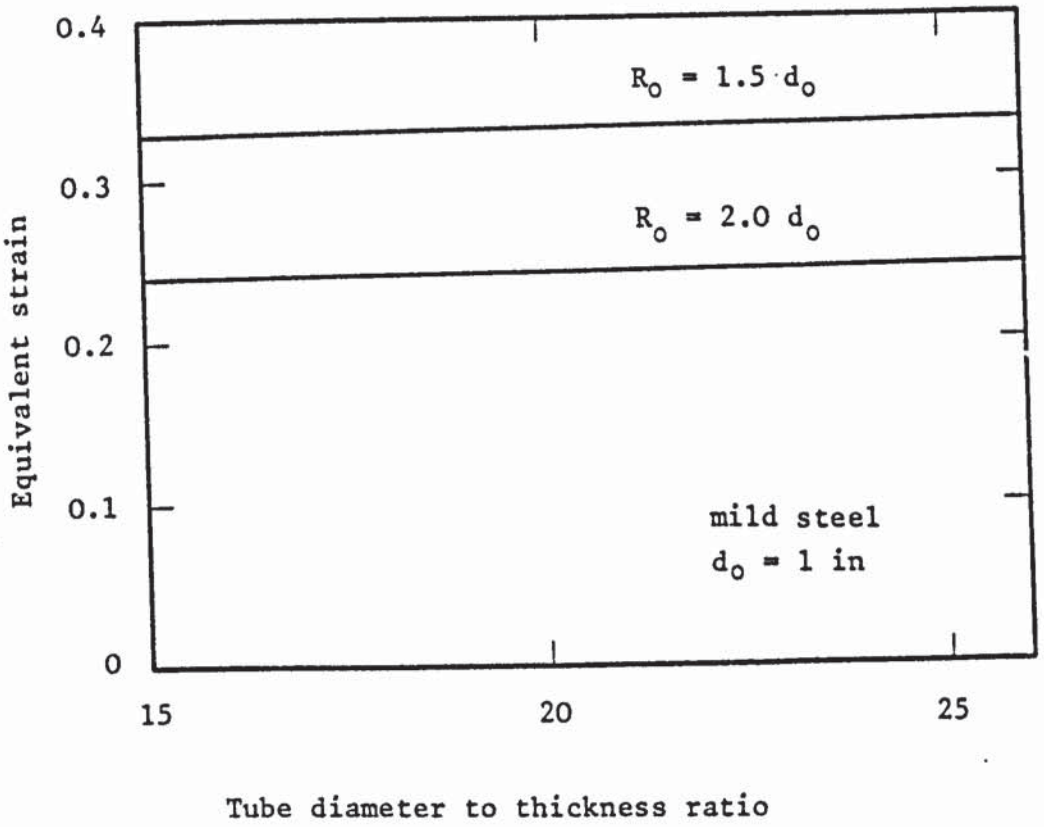

Figure 6.13: Effect of tube diameter to thickness ratio on the equivalent strain at the outer periphery of the bend for various values of mean bend radii

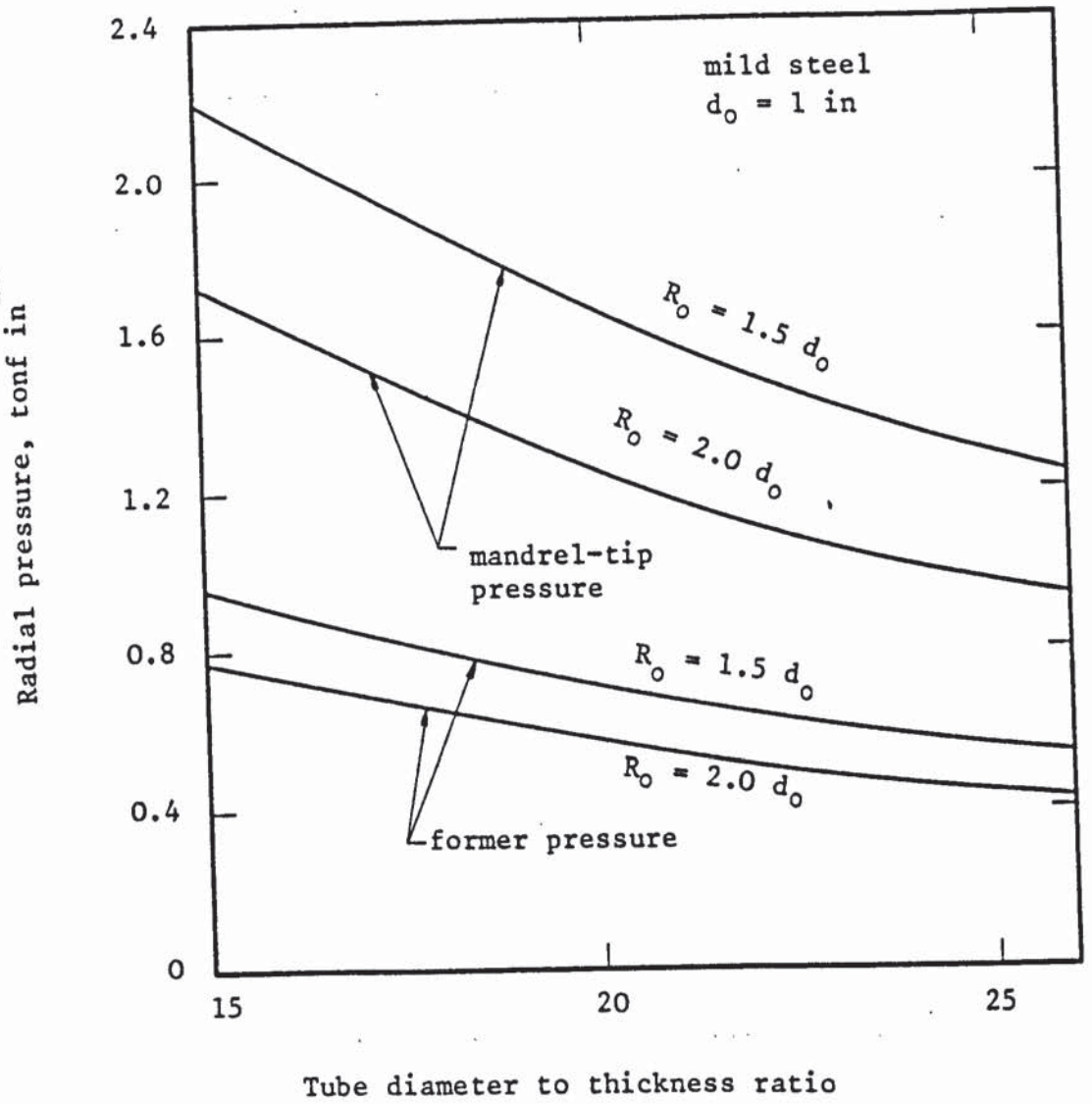

Figure 6.14: Effect of tube diameter to thickness ratio on the pressures of former and mandrel-tip for various values of mean bend radii

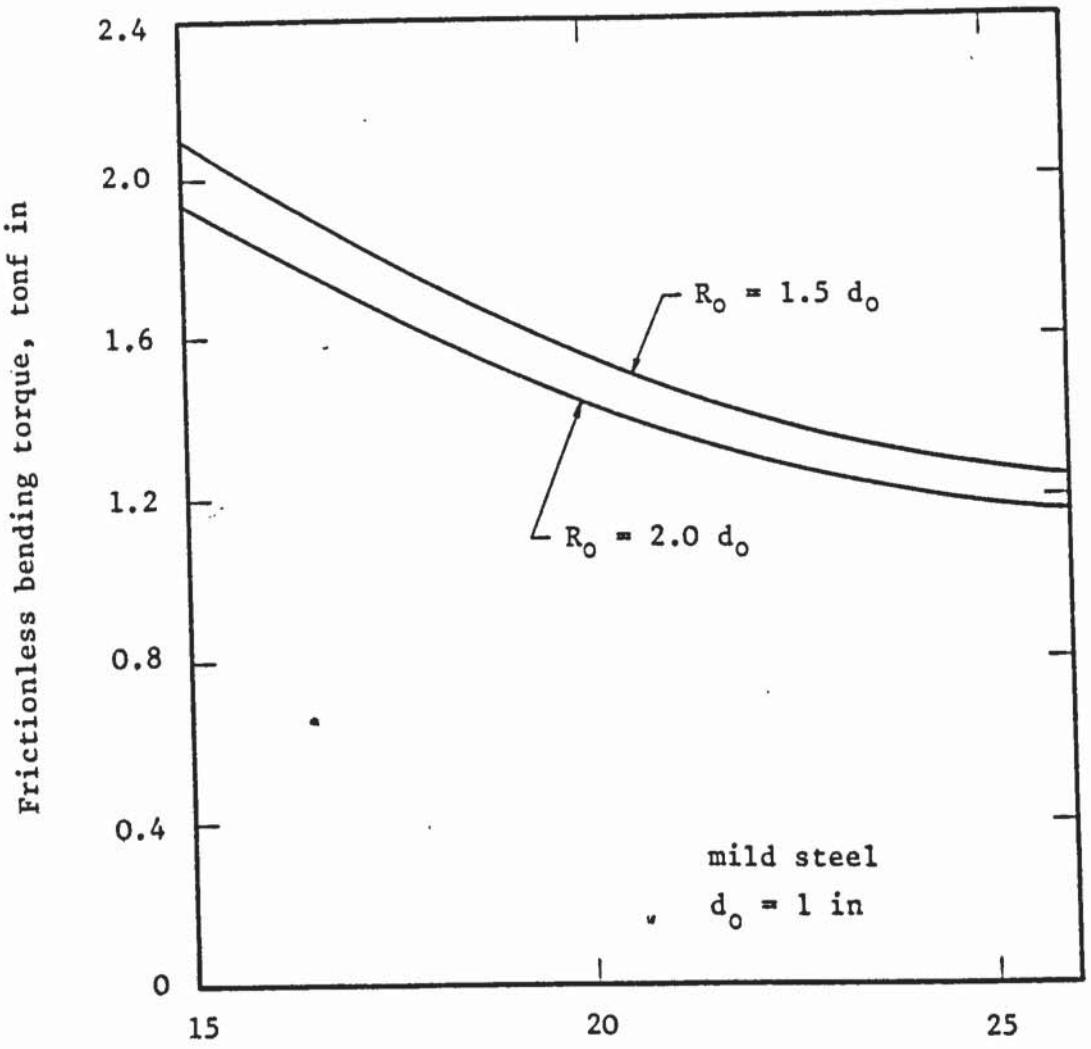

Figure 6.15 Effect of tube diameter to thickness ratio on the frictionless bending torque for various values of mean bend radii

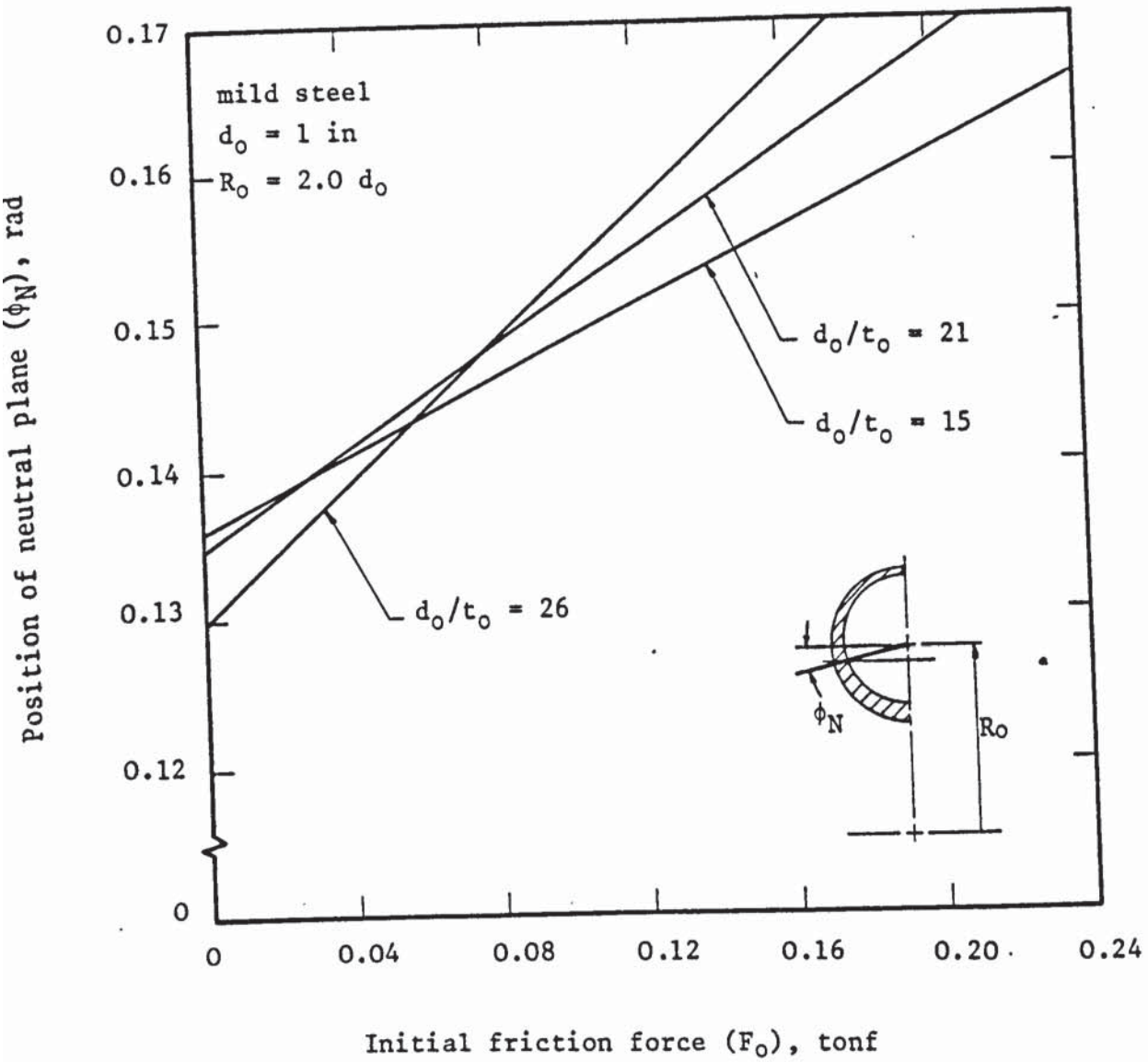

Figure 6.16: Effect of the initial friction force (F_o) on the position of the neutral plane (ϕ_N) in the bending zone 'IIb' for various tube diameter to thickness ratios

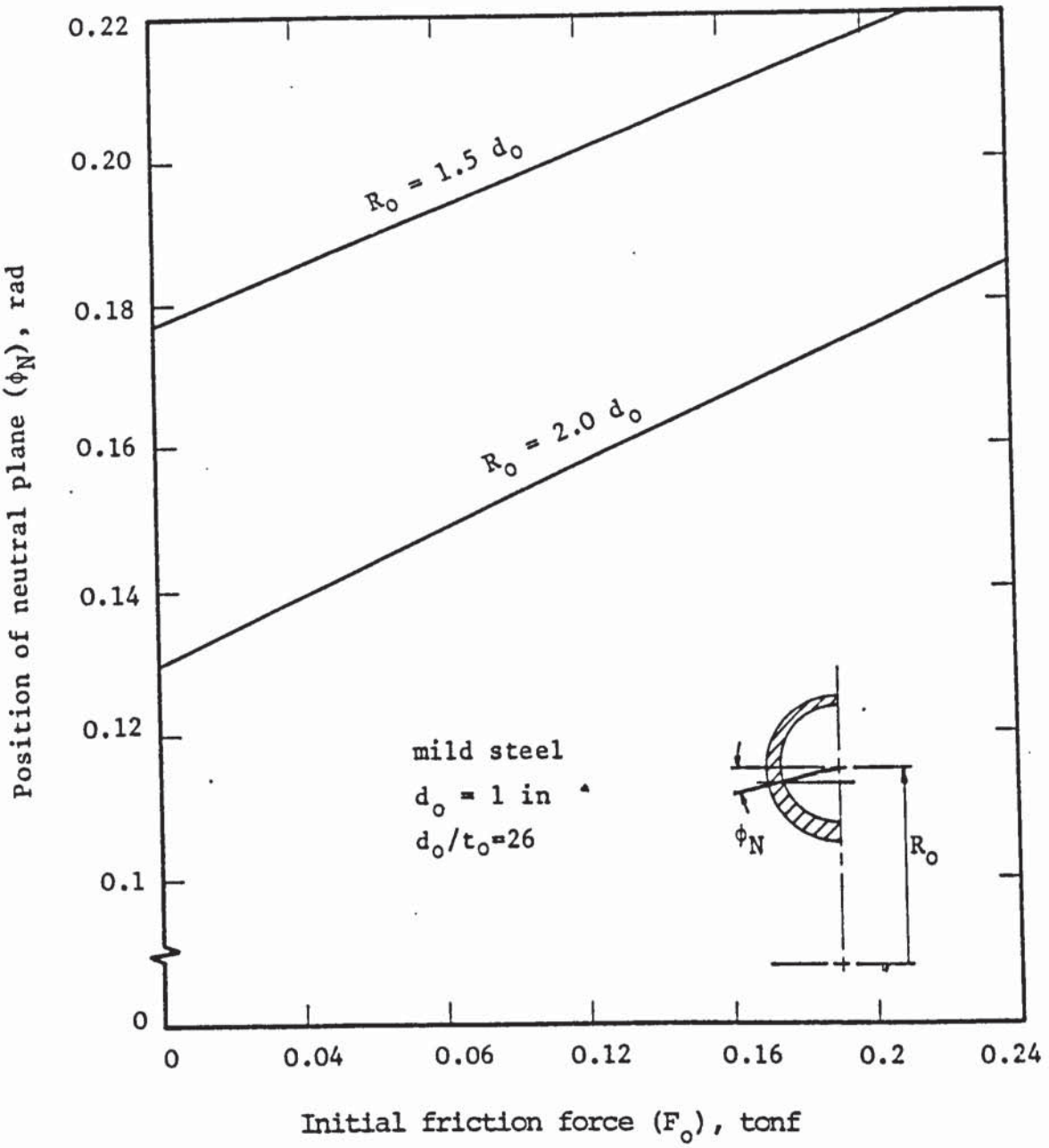

Figure 6.17: Effect of the initial friction force (F_o) on the position of the neutral plane (ϕ_N) in the bending zone 'IIb' for various mean bend radii

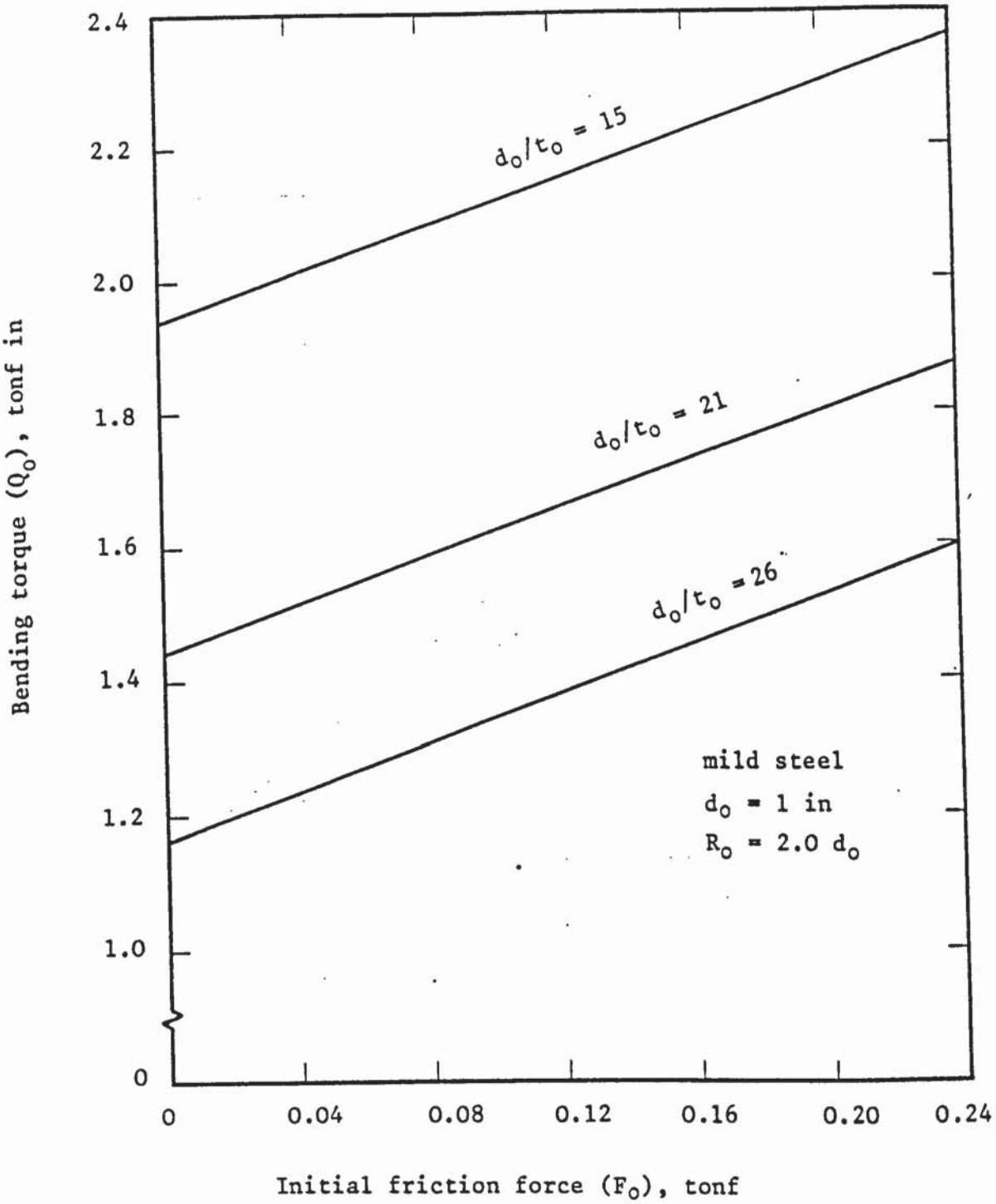

Figure 6.18: Effect of the initial friction force (F_o) on the bending torque (Q_o) in the bending zone 'IIb' for different tube diameter to thickness ratios

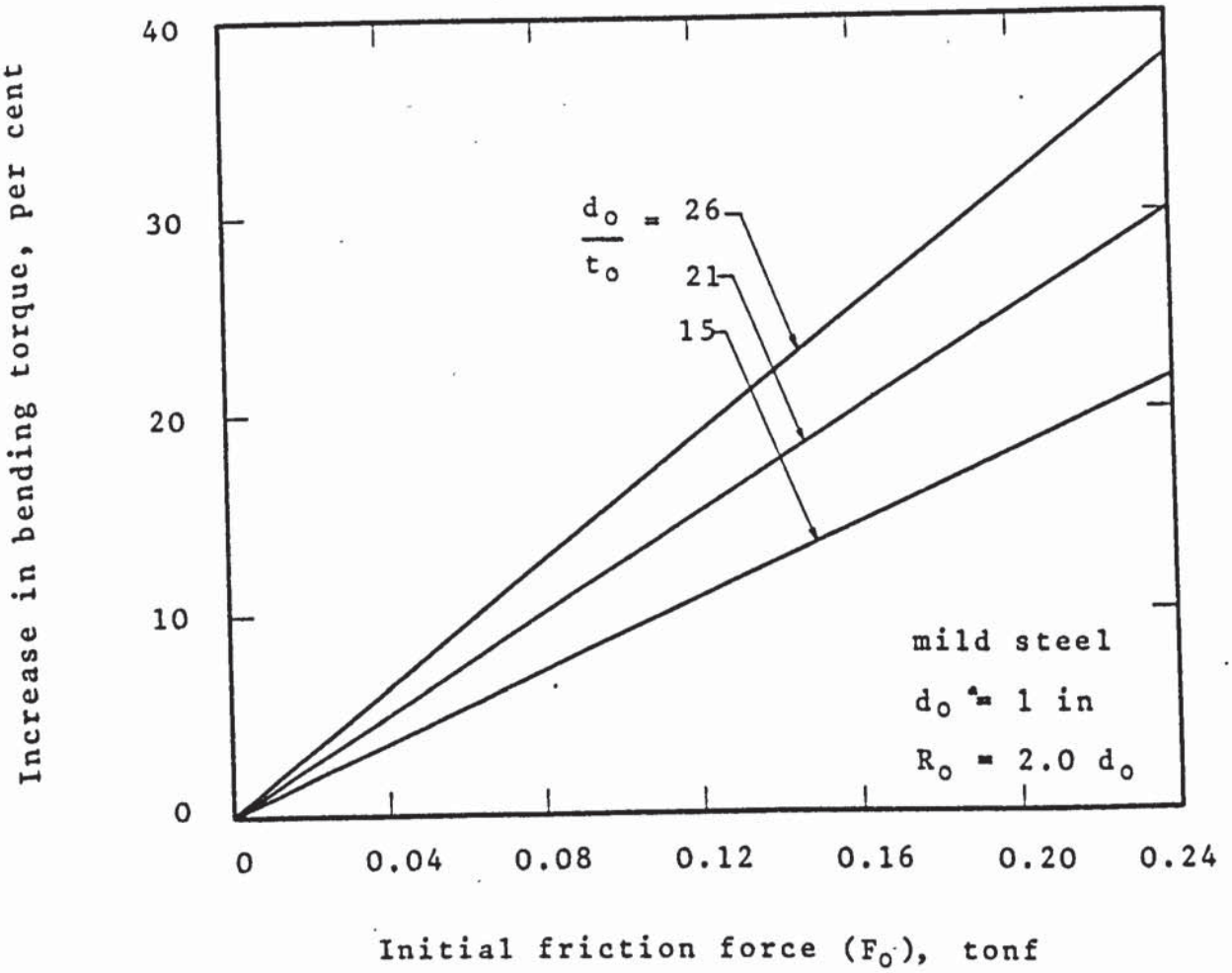

Figure 6.19: Effect of the initial friction force on the percentage increase in the bending torque (Q_o) in zone 'IIb' for different tube diameter to thickness ratios

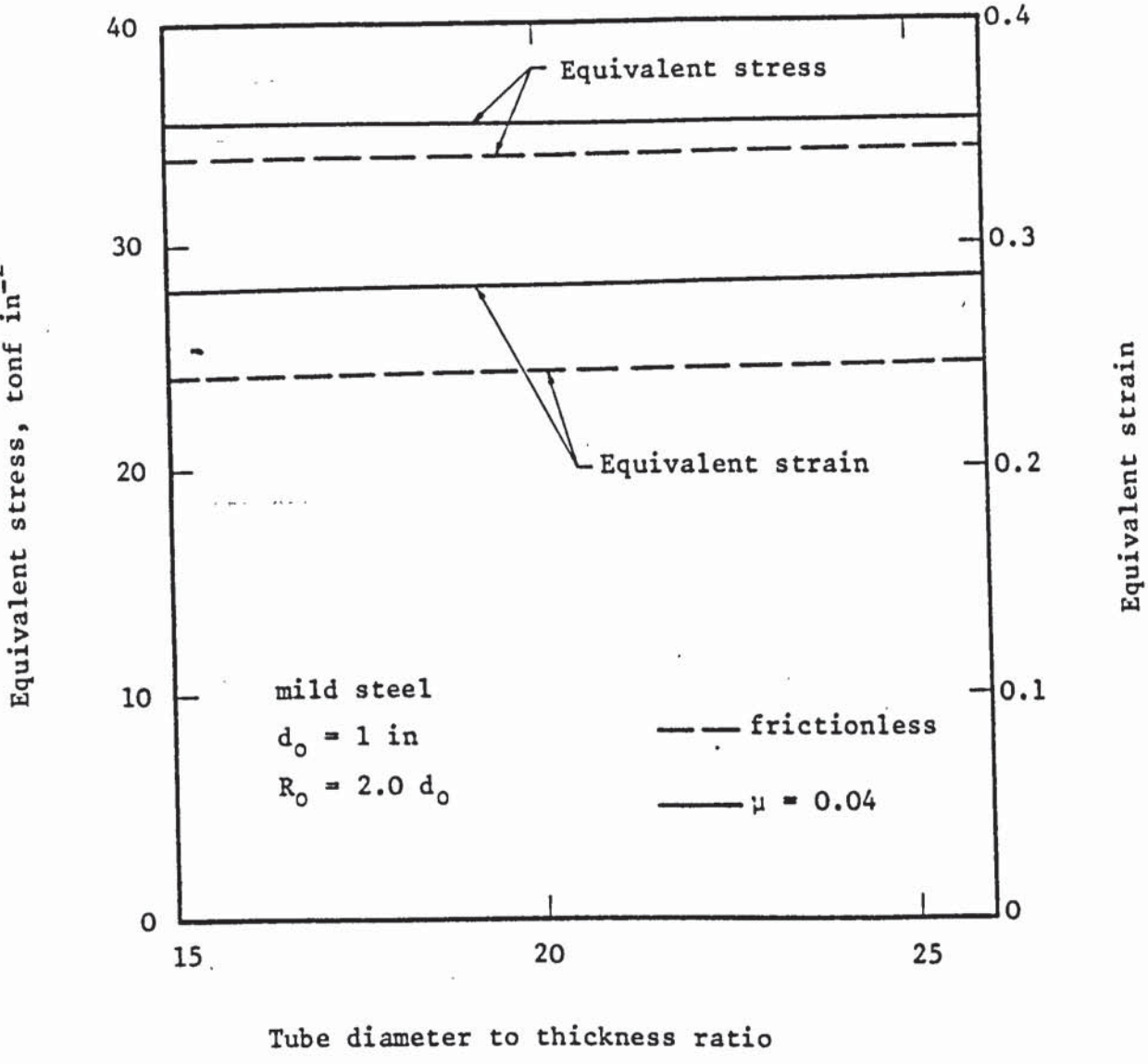

Figure 6.20: Effect of friction on the equivalent stress and the equivalent strain on the outer periphery of the bend for different tube diameter to thickness ratios

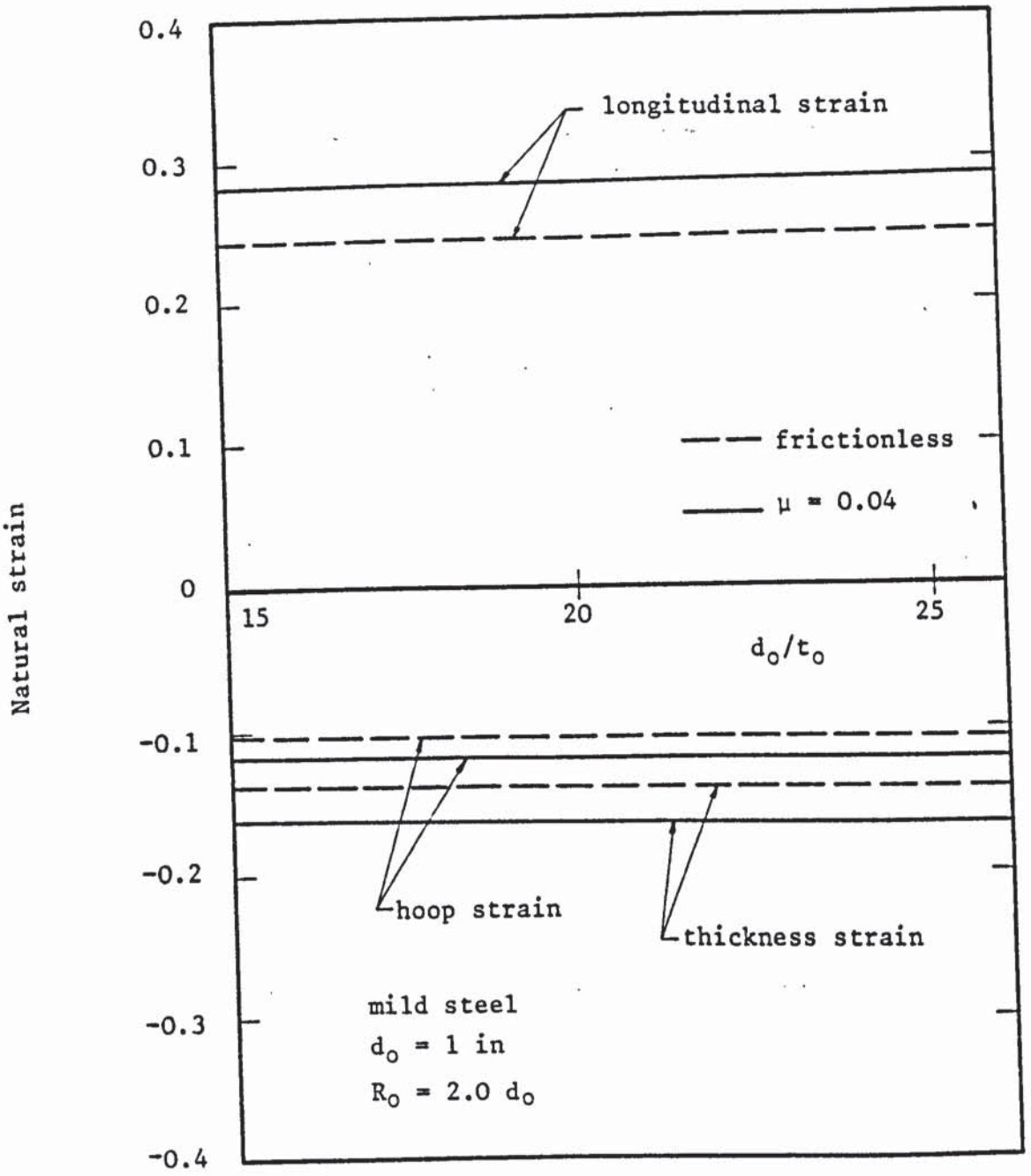

Figure 6.21: Effect of friction on the longitudinal, hoop and thickness strains on the outer periphery of the bend for different tube diameter to thickness ratios

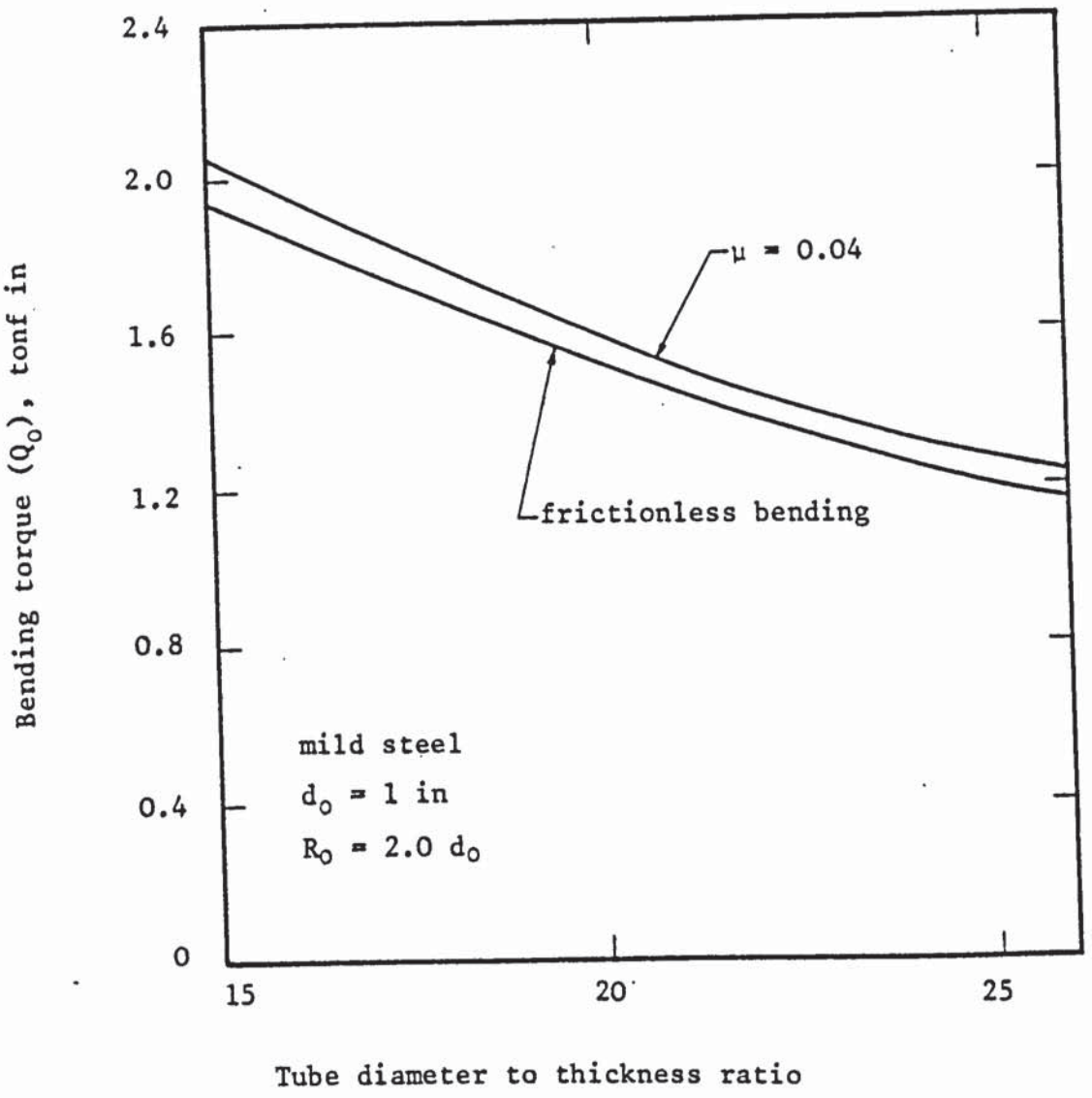

Figure 6.22: Effect of the initial friction force on the bending torque (Q_o) in zone 'IIb' at the steady state (at about 180 degree) for different tube diameter to thickness ratios (equation 3.64)

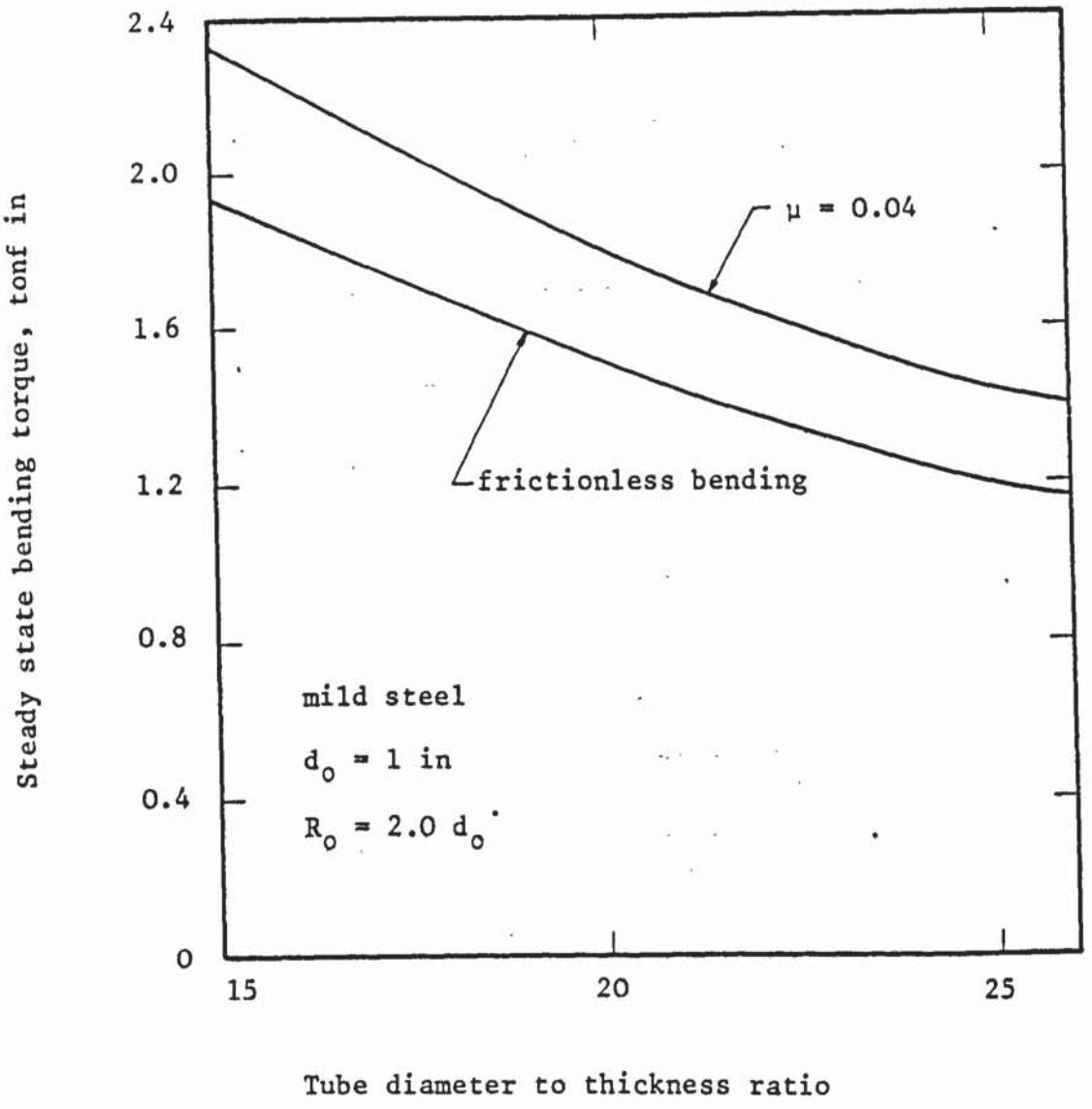

Figure 6.23: Effect of friction on the steady state bending torque, Q_1, (at about 180 degree) for different diameter to thickness ratios (equation 3.65)

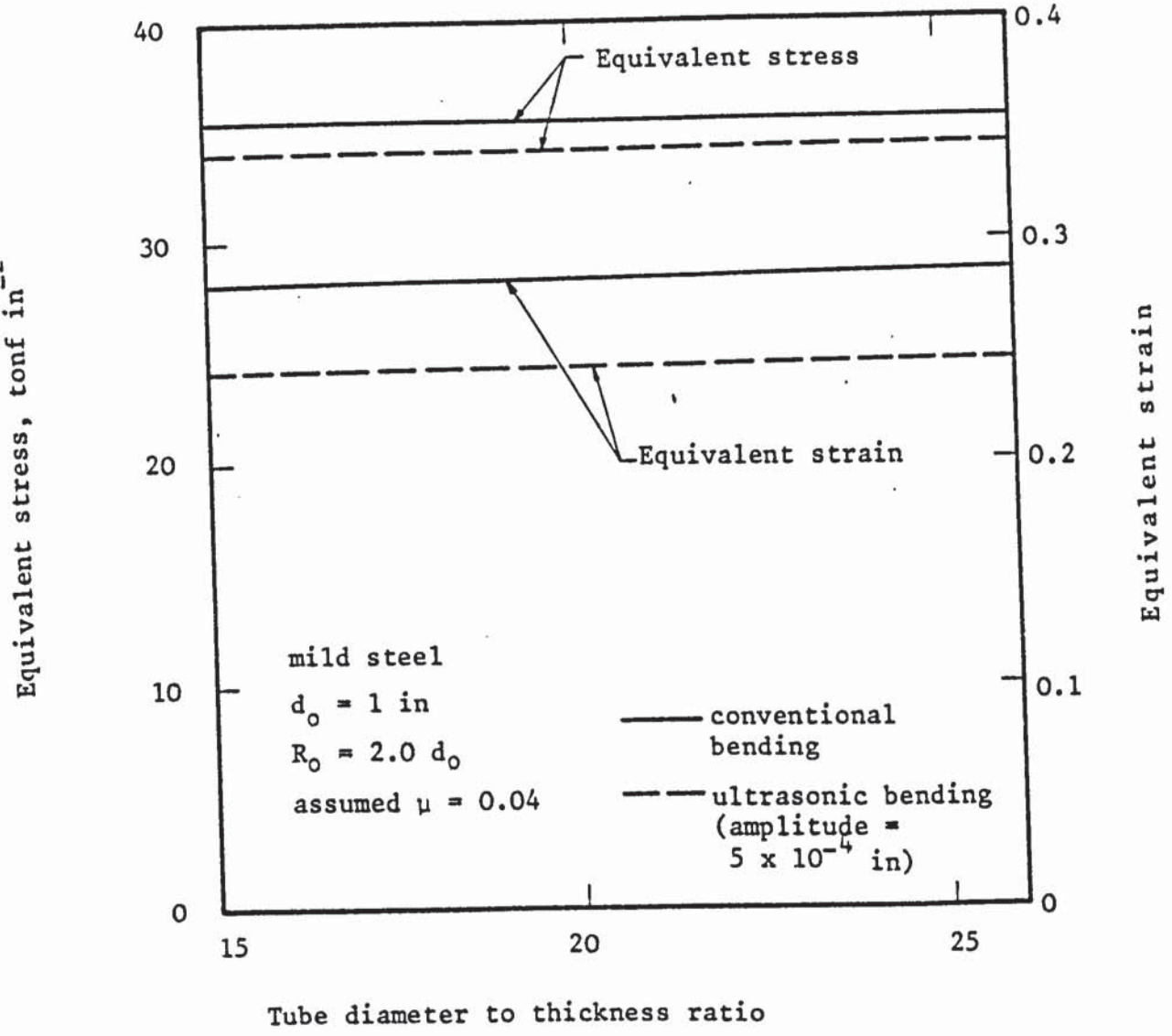

Figure 6.24: Effect of mandrel vibration on the equivalent stresses and the equivalent strains at the outer perphery of the bend for different tube diameter to thickness ratios

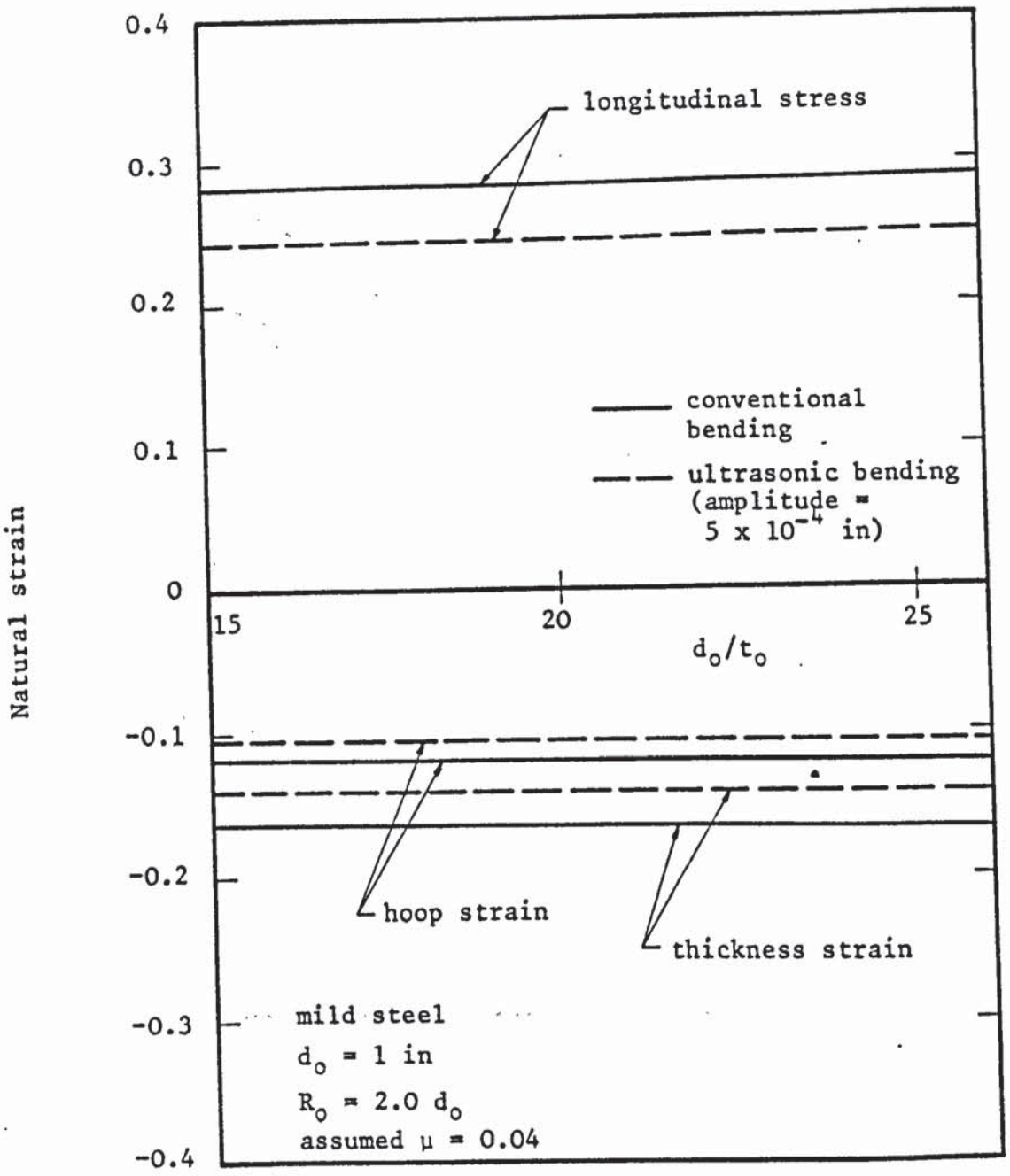

Figure 6.25: Effect of mandrel vibration on the longitudinal, hoop and thickness stains at the outer periphery of the bend for different tube diameter to thickness ratios.

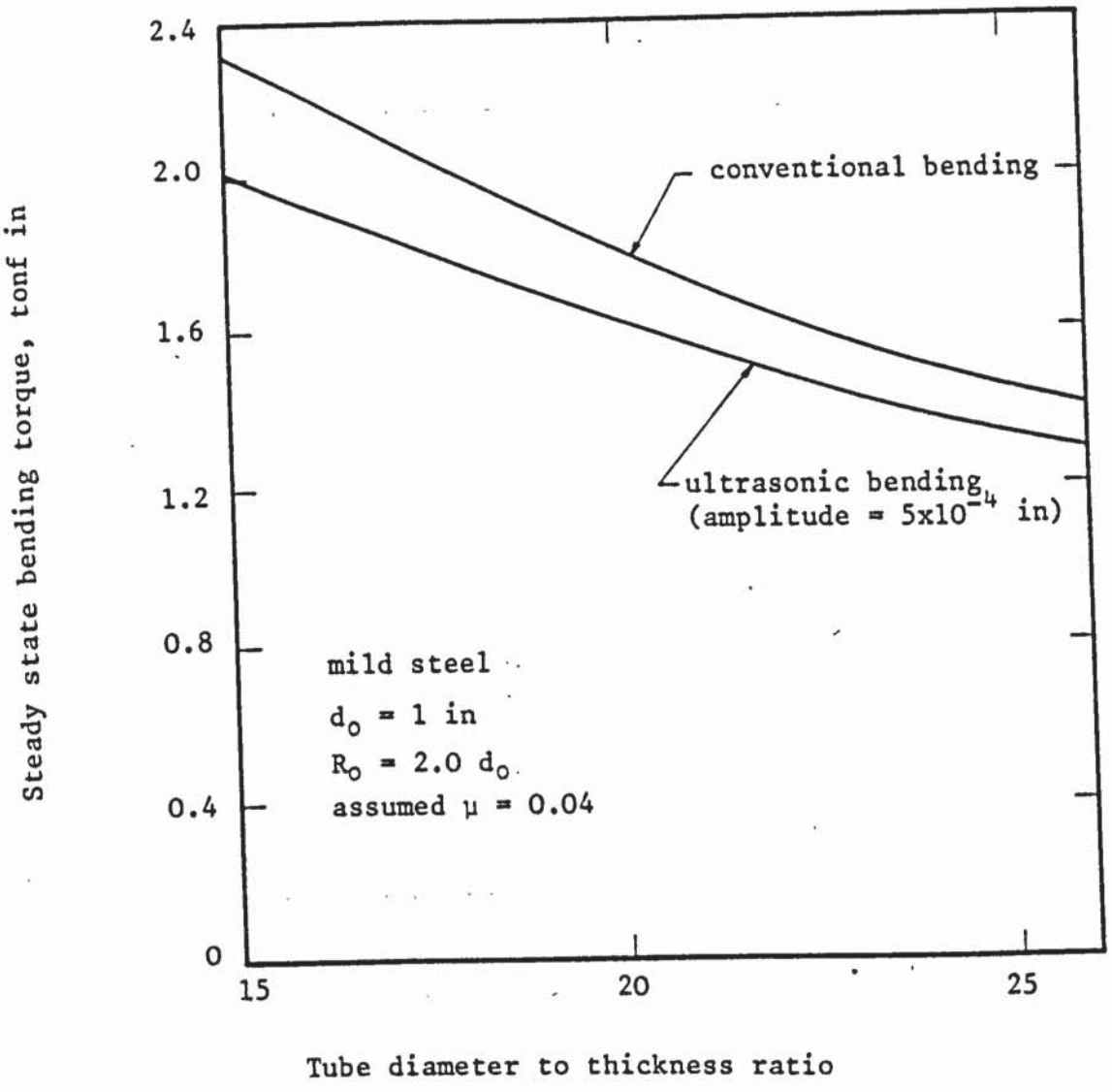

Figure 6.26: The variation of the steady state benching torque (at about 180 degree) with the tube diameter to thickness ratios for vibratory and non-vibratory conditions

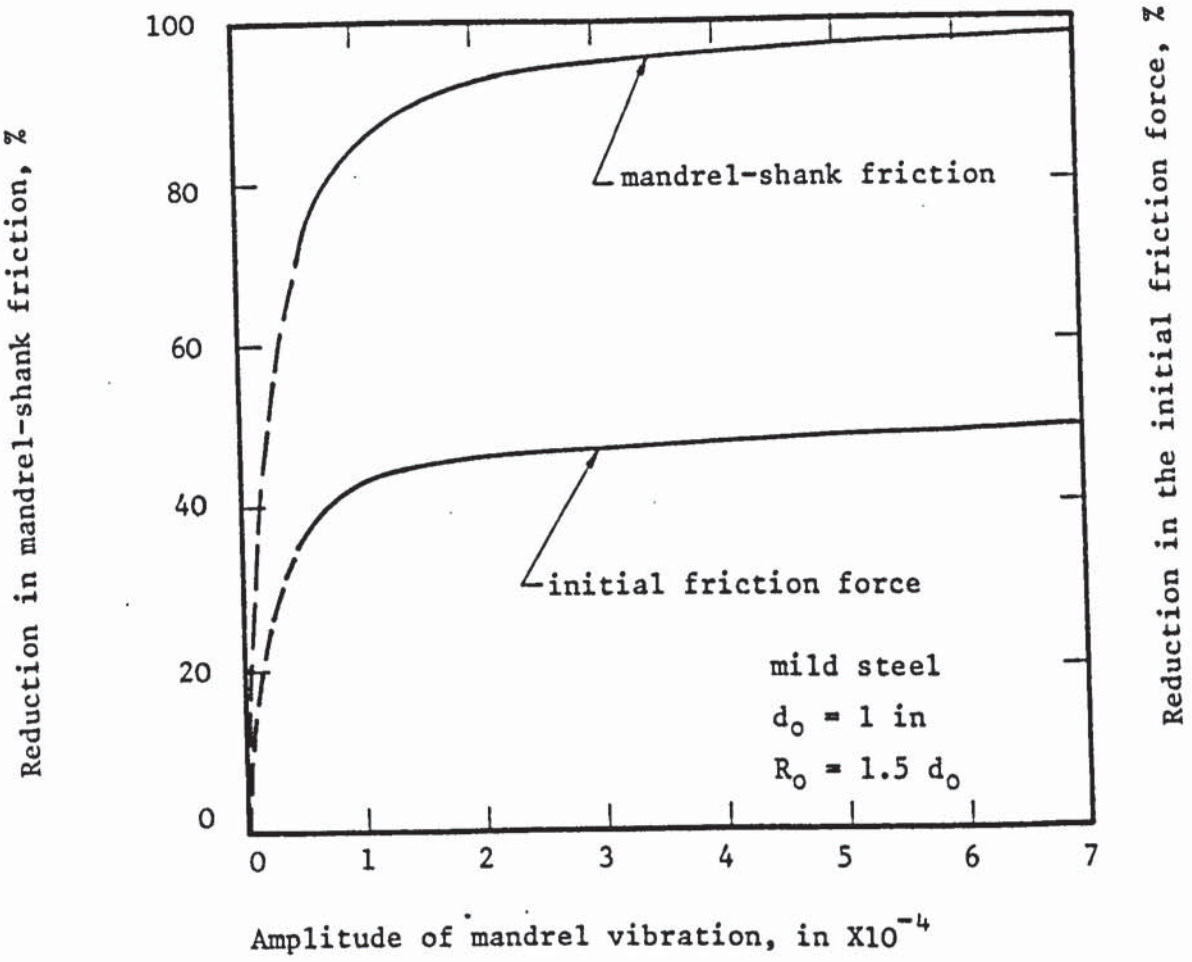

Figure 6.27: Effect of varying the amplitude of mandrel vibration on the percentage reduction of friction at the tube bore-mandrel shank interface and the initial friction force

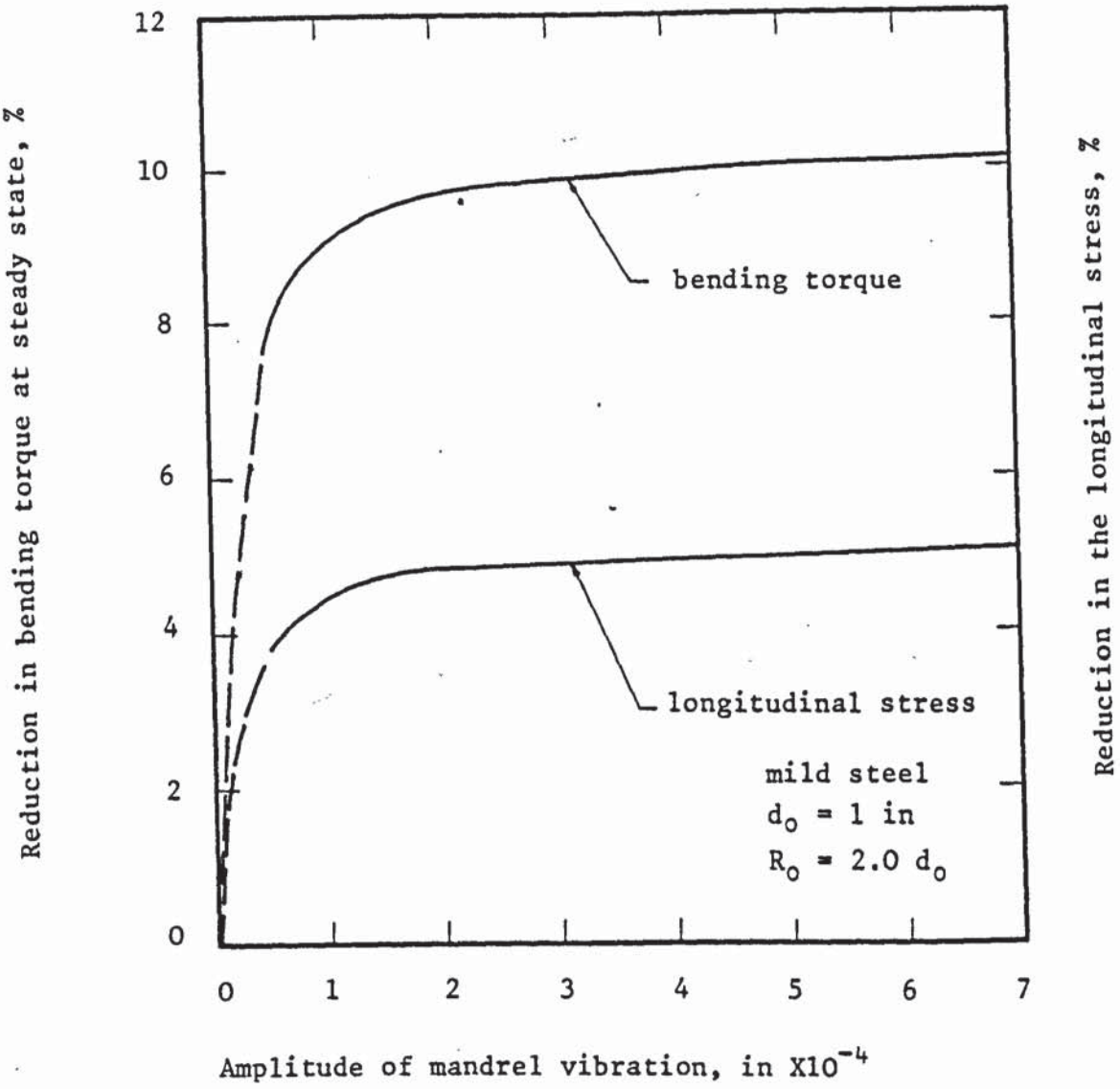

Figure 6.28: Effect of varying the amplitude of mandrel vibration on the percentage reduction in the steady state bending torque (at about 180 degree) and in the longitudinal stress at the outer periphery of the bend

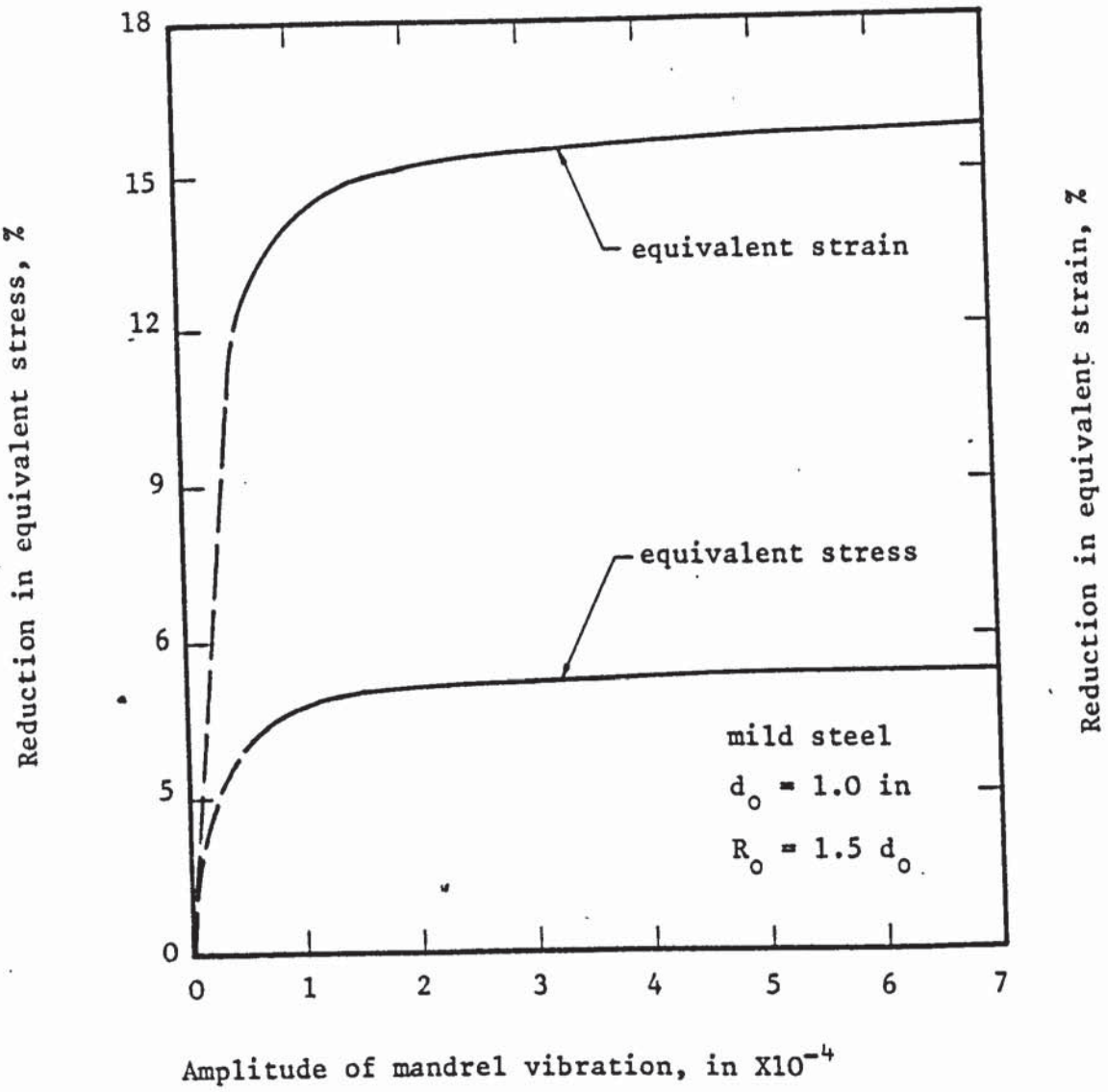

Figure 6.29: Effect of varying the amplitude of mandrel vibration on the percentage reduction in the equivalent stress and in the equivalent strain at the outer periphery of the bend

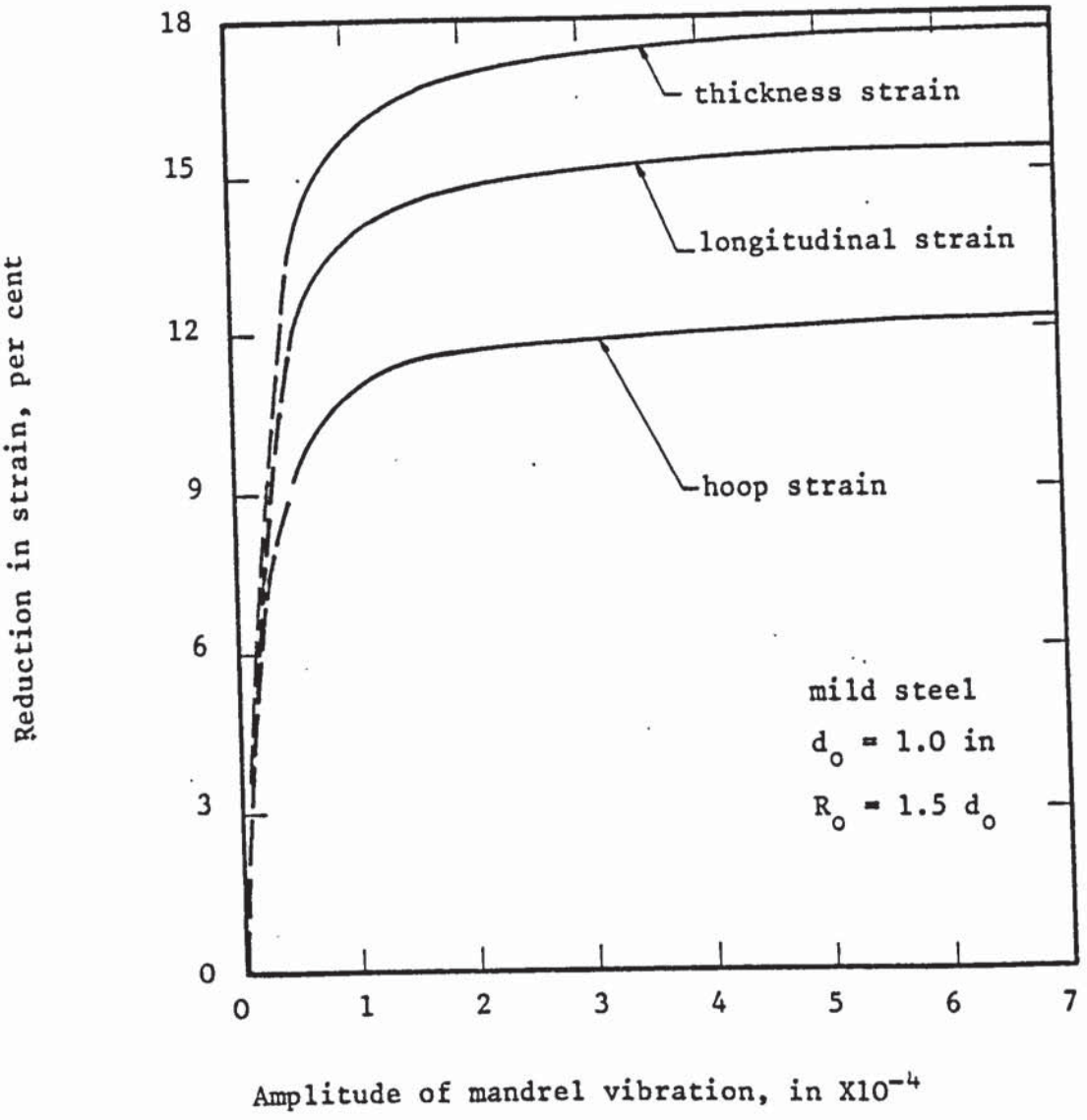

Figure 6.30: Effect of varying the amplitude of mandrel vibration on the percentage reduction in the longitudinal, hoop and thickness strains at the outer periphery of the bend

CHAPTER SEVEN

DISCUSSION OF RESULTS

7.1 Discussion of the theoretical results

Utilising the theoretical analysis developed in Chapter Three and with the aid of the computer programme "UTB-INI", theoretical results for bending mild steel tubes having a constant outside diameter of 1 in with and without applied ultrasonic vibrations were obtained. A number of tube bends were theoretically analysed, which covered a wide range of tube diameter to thickness ratios, mean bend radii and amplitudes of mandrel vibration. The results also provided useful information for discussion regarding the influence of friction on the stresses, strains and bending torque developed during the bending process. Furthermore, the beneficial effects of axially vibrating the supporting mandrel on the mechanics of metal deformation during bending were theoretically studied.

In addition to the above mentioned objectives, the theoretical results aimed to establish an adequate understanding of the mechanics of tube draw-bending which was largely unexplored. Also, the results can help to explain some of the experimental results obtained under both the vibratory and non-vibratory conditions. The graphical theoretical results are shown in Chapter Six and the tabulated results are given in Appendix C.

7.1.1 The mechanics of frictionless tube-bending

Figures 6.1 to 6.4 represent the distribution of the longitudinal, hoop, thickness and equivalent stresses around the periphery of tube section during the bending operation in the absence of friction. The results were obtained for a tube having an outside diameter (d_o) of 1 in and a diameter to thickness ratio (d_o/t_o) of 26. Two values of mean bend radii (R_o) equal to 1.5 and 2.0 times the tube diameter were considered. The figures show that the neutral plane (NN) has moved away from the central plane of the tube-section (AA) and closer to the centre of the bend (OO). The change in the position of the neutral plane can be explained by the thinning and thickening of the outside and inside tube-wall respectively due to bending as illustrated diagrammatically in the figures. This satisfies the equilibrium of forces in the longitudinal direction, equation 3.20, with the value of F_o being equal to zero. As figure 6.1 shows, the tube material therefore is subjected to higher tensile and less compressive longitudinal stresses on the outer and inner peripheries of the bend respectively. It is also evident that as the mean bend radius becomes smaller, the displacement of the neutral plane towards the centre of the bend increases.

During bending the angular positions $\phi = 0$ and $\phi = \pi$ represent the points of maximum tensile and compressive stresses respectively. At these points the tube material does yield first and as the stresses increase yielding progresses towards the neutral plane at which the material is just yielding. This led to the assumption that the equivalent stress at the neutral plane is equal to the yield strength of the material for the plastic deformation of the whole tube-section to be

complete. Due to the work-hardening characteristics of the tube material, the equivalent stress which is minimum at the neutral plane progressively increases reaching its maximum values at the outer and inner peripheries of the bend as demonstrated in figure 6.4. The figure also shows that the equivalent stresses are higher for sharper bend radii which is attributable to the fact that the tube material is strained more as the mean radius of bend becomes smaller, see figure 6.8. It can be seen from figure 6.1 that the longitudinal stress reverses from tension to compression at the position of the neutral plane while figures 6.2 and 6.3 show discontinuities of the hoop and radial stresses at the same position. The states of stresses at both sides of the neutral plane were obtained by assuming certain values of the former pressure to fulfil both the conditions of compatability and of zero radial stress at the central plane and also to satisfy the yielding criterion, as explained in more detail in section 3.7. The distribution of the hoop stresses around the tube periphery as shown in figure 6.2 indicates that the hoop stresses are mostly tensile above the neutral plane where the material is stretched in the longitudinal direction while it shortens in the hoop direction. Conversely, the hoop stresses are largely compressive in the part of tube-section below the neutral plane. More significantly the figures 6.1 to 6.4 demonstrate the effect of the mean bend radius on the stresses induced in the tube material during bending, which are markedly higher for small bend radii. This may prove, as would be expected, that producing sharper bends is more difficult than bending tubes to large radii.

The distributions of the longitudinal, hoop, thickness and equivalent strains around the periphery of the tube-section are shown in figures 6.5, 6.6, 6.7 and 6.8 respectively. It can be seen that the

strains are minimum at the neutral plane (NN) and maximum at the outer and inner peripheries of the bend, ie. at $\phi = 0$ and π respectively. The definition of the neutral plane is that plane which undergoes no change in length as a result of bending and the assumption that the material has just yielded without any plastic straining led to zero strain values at the position of the neutral plane. The tube material on the outside of the bend is stretched longitudinally resulting in positive longitudinal strains which are accompanied by negative values of both the thickness and hoop strains with consequential thinning of the tube-wall and shortening of the tube periphery on the bend outside. The figures show also the opposite effects occurring on the bend inside as the tube material shortens longitudinally under compression. However, due to the displacement of the neutral plane closer to the centre of the bend, the maximum longitudinal and thickness strains at the bend outer periphery are slightly higher than the corresponding values at the inner periphery; the difference is more pronounced for the smaller bend radii. The effect of varying the mean bend radius on the developed strains is clearly demonstrated in the figures 6.5 to 6.8. It can be seen that the strains considerably increase with decreasing the bend radius and that the greatest increase of the strain values is at the outer and inner peripheries of the tube bend which correspond to the maximum stress points.

The theoretical analysis was applied to the bending of thin-walled tubes having various values of diameter to thickness ratio in the range from 15 to 26 to investigate its effect on the stresses, strains and bending torque. In figures 6.9 and 6.10, the maximum values of the longitudinal, hoop and equivalent stresses at the outer periphery of bend were plotted against the tube diameter to thickness ratio for

different values of mean bend radii. While the bend radius has a considerable influence on the stresses, the d_o/t_o ratio, in the range considered, seems to have little effect on the maximum stresses. Although the graph shows a slight increase in the longitudinal, hoop and equivalent stresses at the bend outer periphery, this increase is considered insignificant when bending thin-walled tubes. A similar conclusion may be drawn regarding the maximum values of the strains on the outer periphery of the bend as illustrated in figures 6.11, 6.12 and 6.13.

The effect of the tube diameter to thickness ratio and the mean radius of bend on the former and mandrel-tip pressures and on the bending torque is illustrated in figures 6.14 and 6.15. It may be seen from figure 6.14 that the mandrel-tip pressure is considerably higher than the former pressure, also that the pressures are greatly affected by both the mean bend radius and the diameter to thickness ratio. Generally, the radial pressures on the outside and inside tube-walls are significantly higher when bending thicker-walled tubes to tighter bend radii and obviously those pressures have a considerable effect on the frictional forces as the tube is pulled over the mandrel-tip and around the former during the actual bending operation. Figure 6.15 shows that the tube diameter to thickness ratio has the greatest influence on the frictionless bending torque while the mean radius of bend has less significant influence. Referring to equation 3.64, the frictionless bending torque increases with increasing the longitudinal stresses, the tube cross-sectional area and the mean bend radius. Since the diameter to thickness ratio has little effect on the longitudinal stresses, the torque required to bend a thicker-walled tube is obviously higher than that needed to bend a thinner-walled tube to the same radius. On the

other hand, for the same tube diameter to thickness ratio the frictionless bending torque generally increases as the mean bend radius becomes smaller, figure 6.15. However, this is entirely dependent on the product of the bend radius and the longitudinal stresses, and indeed on the work-hardening characteristics of the tube material.

7.1.2 The mechanics of conventional tube-bending

As previously described in Chapter Three, friction has a considerable effect on metal plastic deformation during the process of draw-bending tube over a mandrel. The variation of the position of the neutral plane in the bending zone with the initial friction force is illustrated in figures 6.16 and 6.17. It may be seen that the movement of the neutral plane closer to the centre of the bend proportionally increases with the increase in the initial friction force. Figure 6.16 also shows that at high friction forces and for the same mean bend radius, the angle ϕ_N is greater for thinner-walled tubes. This may be explained by the fact that the internal forces in zone IIb are less for the higher values of tube diameter to thickness ratio. This also explains the slightly higher rate of increase in ϕ_N when bending the same tube to larger bend radii, figure 6.17. Practically however the initial friction force is largely influenced by the slider force which varies with both the mean bend radius and the tube diameter to thickness ratio.

In figure 6.18, the bending torque in zone IIb is plotted against the initial friction force for different tube diameter to thickness ratios. The figure clearly shows an increase in the bending torque as the friction force increases, and shows that the rate of increase is

largely independent on the diameter to thickness ratio. However, since the torque required to bend thinner-walled tubes is relatively small, the friction in zone I has a more significant influence on such bends. Figure 6.19 represents the percentage increase in the bending torque vs. the initial friction force and shows a greater rate of increase with higher values of tube diameter to thickness ratio.

Theoretical results were obtained for bending mild steel tubes having various values of diameter to thickness ratio to mean bend radius equal to 2.0 times the tube diameter. A value of the coefficient of friction ($\mu = 0.04$) was assumed to represent the frictional conditions in the bending process. Figures 6.20, 6.21, 6.22 and 6.23 demonstrate the effect of friction on the stresses and the strains at the outer periphery of bends, also on the bending torque. The figures compare the predicted values when friction is taken into account with the results under frictionless conditions.

As shown in figure 6.20, the equivalent stress increases due to the frictional effect with the increase being principally attributable to the longitudinal stresses rather than the hoop or radial stresses. Equation 3.38 indicates that an additional force in the longitudinal direction is needed to overcome friction as the tube is pulled over the mandrel-tip in zone IIf. Additionally, the movement of the neutral plane closer to the centre of bend in zone IIb also results in higher stresses at the bend outer periphery. Moreover the figure shows a more significant increase in the equivalent strains developed in the tube material because of the frictional work. This may be explained by reference to the stress-strain properties of mild steel, figure 5.8. Since the strain-hardening rate of the material is relatively small, an additional increase in the stress level can result in a fairly large

consequential increase in the strain.

The additional straining of the tube material at the outer periphery of the bend in zones IIb and IIf due to friction results in a consequential increase in the maximum values of the longitudinal, hoop and thickness strains as illustrated in figure 6.21. It may also be seen that the greatest influence of friction is on the thickness strains (about 18 per cent increase). This can lead to a greater wall-thinning than that which occurs under frictionless conditions.

Figure 6.22 shows the increase in the bending torque in zone IIb as a result of the increase in the initial friction force. This may be explained by the movement of the neutral plane close to the centre of bend which causes an increase in the tensile stresses while reducing the compressive stresses in the longitudinal direction, equation 3.64. Consequently, the amount of increase in the bending torque is largely dependent on the slider force and the frictional conditions. In figure 6.23, the steady state bending torque, ie. at an angle of bend equal to 180 degrees, in the conventional bending operation shows an additional increase due to friction as the tube is pulled over the mandrel and around the former in zone IIf. The figure also shows that the smaller the diameter to thickness ratio the greater the amount of increase in the bending torque. This may be explained partly by the higher pressures from the mandrel-tip and the former on the tube wall for a constant bend radius, and partly by the larger cross-sectional area. However, the percentage increase in the bending torque to overcome friction could be greater when bending thinner-walled tubes.

7.1.3 The influence of mandrel vibration on the process

The effect of friction reversal on the mechanics of the draw-

bending of tubes with the supporting mandrel vibrating axially at an ultrasonic frequency is discussed in section 2.6. With the aid of the computer programme "UTB-INI", the distribution of the stresses and the strains, and the bending torque were predicted when bending mild steel tubes under vibratory conditions. While constant values of tube outside diameter (1 in) and mean bend radius ($2d_o$) were considered, tube diameter to thickness ratios were varied between 15 and 26. The ultrasonic frequency was 20 kHz and the amplitude of mandrel vibration was selected to be 5×10^{-4} in which corresponds to 500 watt of ultrasonic power delivered from the generator. The results were obtained assuming there is no change in the coefficient of friction which was taken to be the same as in the case of conventional bending ($\mu = 0.04$).

Figure 6.24 illustrates the effect of mandrel vibration on the equivalent stresses and the equivalent strains at the outer periphery of bend. It is shown that the mandrel vibration reduces the equivalent stresses and strains developed during bending and that the amount of reduction is apparently equal for the considered range of the tube diameter to thickness ratios. The figure clearly indicates that when the mandrel vibrates, the tube material at the outer periphery of bend is strained to a point on the material stress-strain curve, which is well below the corresponding point during conventional bending. This result is primarily due to a substantial reduction in frictional work and this may be explained by the friction vector reversal effect. It is interesting to observe that the percentage reduction in the equivalent strain (13%) is much greater than the corresponding reduction in the equivalent stress, which is only 4 per cent.

The longitudinal, hoop and thickness strains at the outer periphery

of bend under both the vibratory and non-vibratory conditions are shown in figure 6.25. It may be seen that the values of strains are considerably reduced as a result of mandrel vibration and that the maximum reduction occurs in the thickness strain (about 17 per cent). The significance of this result is that with applied ultrasonic vibrations the maximum amount of tube wall-thinning can be considerably less than the corresponding amount resulting from the conventional process. Indeed such an effect has its practical advantages in many industrial uses of bent tubes. The friction reversal effect may also explain the reduction in the bending torque with applied ultrasonic vibrations as illustrated in figure 6.26. It is also quite clear that the amount of reduction in the steady state bending torque becomes greater as the diameter to thickness ratio decreases. This may be attributable to the higher pressures exerted on the tube-wall and consequently to the greater friction forces arising while bending thicker-walled tubes. However, the percentage reduction in the bending torque as compared with its conventional value could be higher for thinner-walled tubes.

Comparing figures 6.24, 6.25 and 6.26 with their corresponding counterparts for conventional bending (figures 6.20, 6.21 and 6.23), it is interesting to notice that the results obtained under vibratory conditions are nearly the same as those obtained conventionally under frictionless conditions. This is an indication that the effect of friction is negligible when bending tubes with applied vibrations to the supporting mandrel. In other words, the reversed friction which occurs during ultrasonic tube bending cancels the resisting frictional forces at the considered values of frequency and amplitude of vibrations.

In order to show the effect of vibration amplitude on the mechanics

of deformation during the process of ultrasonic tube-bending, theoretical results were obtained for various amplitudes in the range from 0.5×10^{-4} in to 7×10^{-4} in. Mild steel tubes having 1 in outside diameter and of a diameter to thickness ratio equal to 26 were bent with applied vibrations to a mean bend radius equal to 1.5 times the tube diameter. The frequency of vibrations was 2×10^{4} Hz and the bending speed had a constant value of 10 rev min^{-1}. The percentage reductions in the frictional forces, the bending torque, the stresses and the strains against the amplitude of mandrel vibration are shown in figures 6.27, 6.28, 6.29 and 6.30 respectively.

It can be seen from figure 6.27 that at relatively low amplitudes of mandrel vibration there is a rapid rate of reduction in both the mandrel-shank friction and the initial friction force. The trend also shows a slower rate of increase in the amount of friction reduction as the vibration amplitude increases beyond 3×10^{-4} in after which the relationship is almost linear. It is interesting to observe that friction at the tube-mandrel interface is negligible with applied vibrations at relatively high amplitudes. This result is attributable to the effect of the friction vector reversal, assuming there is no change in the coefficient of friction. With reference to figure 3.10 and equation 3.54, it may be seen that the reduction in frictional forces in zone I is a function of the velocity ratio, ie. the ratio between the tube velocity and the vibratory velocity. Since in the analysis both the frequency of vibration and the bending speed were kept constant, the friction reduction is only dependent on the amplitude of mandrel vibration with the assumption that both the slider force and the coefficient of friction remain unchanged. It can be concluded therefore that, under these conditions, as the vibration amplitude

increases the vibratory initial friction force decreases since the term $\sin^{-1} \frac{V_{TM}}{\omega A_{aI}}$ (see section 3.6.1) becomes smaller and consequently the period over which the mandrel velocity exceeds the tube velocity becomes greater.

In addition to a reduction in friction in zone I, friction at the tube-mandrel tip interface (zone IIf) is also reduced as a result of the friction vector reversal which is described in more detail in figures 3.11 and 3.12 and in section 3.6.2. As previously explained the tensile longitudinal stresses do increase as the tube is pulled over the mandrel-tip in order to overcome the frictional resistance and apparently the increase in the stresses is considerably less with the application of ultrasonic vibrations. The amount of reduction in the longitudinal stresses and the bending torque depends on the amplitude of mandrel vibration as illustrated in figure 6.28 and shows similar trends to those curves in figure 6.27.

Figure 6.29 demonstrates the effect of vibration amplitude on the reduction in the equivalent stress and the equivalent strain at the outer periphery of the bend. It is seen that the amount of reduction increases with increasing the amplitude of mandrel vibration. This may be explained by a more pronounced reduction in the frictional work and thus the tube material at the outer periphery is stretched to a point on the stress-strain curve of the material which is below that occurring at lower values of mandrel amplitude. The figure also shows a significant reduction in the equivalent strain, which can be related to the strain-hardening characteristics of the tube material as previously discussed in section 7.1.2.

Similar results were obtained for the effect of the amplitude of mandrel vibration on the longitudinal, hoop and thickness strains at the

outer periphery of the bend. Figure 6.30 shows identical trends to those in figures 6.27, 6.28 and 6.29. However, while the results indicate that the hoop strain is less influenced by applying ultrasonic vibrations, the thickness strain is significantly reduced under vibratory conditions. This can prove that ultrasonic tube-bending is most advantageous in minimising the amount of tube wall-thinning at the outer periphery of bend which is greatly appreciated in many practical applications of bent tubes.

7.2 Discussion of the experimental results

The experimental programme previously described in Chapters Four and Five was undertaken to investigate the tube-bending process with and without ultrasonic vibrations. In addition to studying the influence of the basic process parameters on the mechanics of conventional bending, particular attention was given to exploring the advantageous effects of axially vibrating the supporting mandrel at an ultrasonic frequency.

The experimental results reported were obtained for bending mild steel tubes at a variety of tube diameter to thickness ratios, mean bend radii and amplitudes of mandrel vibration. Bending tests were carried out under oscillatory and non-oscillatory conditions, also a few interrupted oscillatory tests, in which the ultrasonic power was switched on and off during bending, were performed to explore the immediate effects of vibrations on the bending forces and torque. The graphical experimental results are shown at the end of this chapter (see section 7.4) and the tabulated results are given in Appendix D.

7.2.1 Non-oscillatory bending

Tube bends of good quality were made under conventional conditions, ie. without vibrating the supporting mandrel. The accurate set-up of bending tools particularly the mandrel and the wiper die, and also the correct initial gripper and slider forces were considered essential elements in producing bends with minimum flattening and free from wrinkles. For example, the experiments demonstrated the necessity of increasing the amount of advance of the mandrel-tip for larger bend radii. This was essential to reduce the amount of tube ovality during bending and to exert adequate pressure on the internal tube-wall surface. It was found also that a higher initial slider force should be applied when bending thinner-walled tubes to smaller radii in order to help prevent the formation of wrinkles on the inside of the bend and to reduce the amount of springback.

Figures 7.1, 7.2, 7.3 and 7.4 illustrate the progress of the bending forces and torque with the current angle of bend for various values of the tube diameter to thickness ratio and mean bend radius. It may be seen that during the process of draw-bending of tubes, the forces and the torque do increase progressively with the angle of bend. This may be due to frictional effects since the slider force, which influences the initial friction force as the tube is pulled over the mandrel-shank while being supported externally by the slider and the wiper die, is not constant. However, in the circumstances in which the slider force approaches a constant value, the gripper and mandrel forces as well as the bending torque tend to taper off to a constant level. The figures clearly show that the bending forces are significantly higher for thicker-walled tubes and/or smaller bend radii, which may

indicate that it is more difficult to bend tubes having larger values of diameter to thickness ratio to sharper radii.

In figure 7.1 the slider force, which represents the radial reaction from the straight part of tube on the moving slider during the bending operation, shows a higher rate of increase with the current angle of bend for the mean radius of bend equal to 1.5 times the tube diameter. The figure, on the other hand, shows a less significant effect of the tube diameter to thickness ratio on the slider force except in case (a) which may be explained by the tight clearance between the tube bore and the supporting mandrel. Generally, the value of the clearance lies between 10 and 15 per cent of the tube wall-thickness but in this particular case the clearance was only 4 per cent because of a greater wall-thickness (.0675 in) of the supplied tubes by comparison with a nominal thickness of 0.064 in.

The slider force had a considerable effect on the frictional forces; they were monitored by measuring the mandrel force, as illustrated in figure 7.2. Comparing the results of (b) and (c) in figures 7.1 and 7.2 it may be concluded that, the higher the rate of increase in the slider force, the greater the effect would be on the mandrel force due to friction. As previously mentioned, friction takes place in two zones: first, as the tube is pulled over the mandrel-shank it is compressed from the outside by the slider and by the tip of the wiper die adjacent to the former, and secondly as the tube, having been bent, is pulled over the mandrel-tip and around the former. The measured axial force on the mandrel is a summation of two components: (a) the frictional component which is tensile, and (b) the axial component of the force resulting from the tube pressure on the mandrel-tip which is compressive. The tensile mandrel forces shown in figures

7.2(b) and 7.2(c) may then be explained by the greater frictional forces compared with the compressive forces on the mandrel-tip. Also, since the mandrel-tip pressure is largely unaffected by the bending angle the observed increase in the mandrel force is principally attributable to the increase in the frictional forces in zone I as a result of a marked increase in the slider force.

The mandrel force for bending tubes to a mean bend radius equal to $2d_o$ showed negative values, ie. compression, figures 7.2(b) and 7.2(c). The reasons for this can be higher pressure on the mandrel-tip as a result of greater advance of the mandrel beyond the tangent line and a smaller rate of increase in the slider force, figures 7.1(b) and 7.1(c). It is interesting to note that in those cases, the mandrel force reached a maximum compressive value and then started to decrease due to the increase in friction, and the rate of decrease has proved to be dependent on the rate of increase in the slider force. This also may explain the variation of the mandrel force with the current angle of bend in figure 7.2(a). The upper curve shows that the frictional forces are greater than the force resulting from the pressure on the mandrel-tip; by contrast the lower curve indicates a much higher pressure due to bending thick-walled tube to a small bend radius.

Figure 7.3 shows that the gripper force increases continuously with the current angle of bend and that the rate of increase is affected by both the mean bend radius and the tube diameter to thickness ratio. Also, comparing this figure with figure 7.1 indicates a dependency of the gripper force on the frictional forces.

The progress of the bending torque with the current angle of bend is demonstrated in figure 7.4 which shows that the bending torque considerably increases with the decrease in the tube diameter to

thickness ratio. The mean bend radius however shows a less significant effect. As previously explained in section 7.1.2 the bending torque is a function of the product of the mean bend radius and the longitudinal stresses for the same diameter to thickness ratio; the longitudinal stresses are largely influenced by the mean bend radius and the frictional conditions. Figures 7.4(a), 7.4(b) and 7.4(c) demonstrate three different trends of the variation in the bending torque. Figure 7.4(a), for example, shows an increase in the bending torque with the increase in the bend radius, which is not generally expected. However this may be explained by reference to figure 7.2(a) which shows higher frictional forces for the larger bend radius. Consequently the tensile longitudinal stresses and thus the bending torque will be greater. Furthermore, figures 7.4(a), (b) and (c) show a higher initial bending torque for the larger mean bend radius which may be explained as a result of greater advance of the mandrel-tip beyond the tangent line. Consequently the tube material is stretched more on the outside of the bend resulting in higher tensile longitudinal stresses. However, as bending progresses, the rate of increase in the bending torque appears to be largely influenced by the frictional forces (comparing figures 7.4(b) and 7.4(c) with figures 7.2(b) and 7.2(c) respectively); this explains the three different trends in figure 7.4. It may be concluded therefore that the mean bend radius has little effect on the bending torque which is greatly influenced by the frictional conditions and the position of the mandrel relative to the tangent line.

The distribution of strains along the bend length for different values of the tube diameter to thickness ratio and the mean bend radius are shown in figures 7.5 to 7.8. The longitudinal strains at the outer, central and inner peripheries of the bend are plotted against the

current angle of bend, as illustrated in figure 7.5. It can be seen that the strain values are minimum at the angles 0 and 180 degrees, ie. nearest to the gripper and slider straight parts of tube respectively. However the strain values at those positions could not be taken as representative of the developed longitudinal strains in a bent tube since one half of the corresponding grid division was on the unbent part of the tube. Also the tube material near the gripper part or the slider part was not fully strained either because the frictional forces were not high enough at the start of bending or because the tube had not passed fully over the mandrel-tip and around the former. Moreover, figure 7.5 shows that the longitudinal strains reach a steady state in the middle part of the bend although the tensile strains show a slight increase with the angle of bend which may be due to the increase in the slider force and therefore in the initial friction force. It is clearly seen also that the longitudinal strains are tensile at the central plane, this an indication of the displacement of the neutral plane closer to the centre of the bend. But it can be seen that the maximum tensile and compressive longitudinal strains are almost equal. This may be explained by reference to the strain values being calculated from the natural logarithm of the ratios between the bend radii at the outer and inner peripheries and that of the neutral plane.

Figures 7.6 and 7.7 describe the distribution of the longitudinal, hoop and thickness strains at the outer and inner peripheries of the bend respectively. It can be seen that the thickness strains are considerably greater than the hoop strains, however as the mean bend radius increases the difference between the thickness and hoop strains becomes smaller as illustrated in figure 7.8. It is likely therefore that the draw-bending process may approach uniaxial stress for

considerably large bend radii; this condition obviously does not arise for small bend radii. It may be seen also from figures 7.6 and 7.7 that the compressive and tensile hoop strains at the outer and inner peripheries of bend are nearly equal, ie. the total hoop strains around the periphery of the tube section are almost zero.

The distribution of the longitudinal, hoop and thickness strains at the outer periphery of a bend having a mean bend radius equal to 2.0 d_o is shown in figure 7.8 with the results plotted for different tube diameter to thickness ratios. Although the longitudinal and thickness strains show a slight increase with the decrease in the tube wall-thickness, it is apparent that the diameter to thickness ratio has an insignificant effect on the developed strains for a constant mean bend radius. Comparing figures 7.6 and 7.8 for different bend radii, clearly indicates that the longitudinal and thickness strains significantly increase as the mean radius of bend becomes smaller.

7.2.2 Interrupted oscillatory bending tests

In order to examine the immediate effects of applying ultrasonic oscillations axially to the supporting mandrel during the draw-bending of tubes, a limited number of tests were carried out with the oscillations only applied intermittently. In the tests the ultrasonic power was switched on and off while the tube was being bent. Figure 7.9 represents typical ultra-violet recorder traces which show the changes in the bending torque and the mandrel force during an interrupted oscillatory test. It can be seen that with the application of oscillatory power both the mandrel force and the bending torque drop abruptly, only to increase immediately to higher levels when the power

is switched off. The part of figure 7.9 relating to the bending torque shows that while the non-oscillatory torque (broken curve) increases continuously, the oscillatory curve is almost flat. Furthermore, the applied oscillations can be seen to cause the mean mandrel force to reverse its direction from tension to compression. Thus when the power is on the mandrel is clearly assisting the tube motion instead of resisting it, as occurs during the non-oscillatory bending.

As previously discussed, the total work done to draw-bend a tube consists of two parts: a first part which is the deformation work, ie. the work needed to deform the tube plastically in the absence of friction, and a second part required to overcome friction (principally between the surface of the tube bore and the supporting mandrel). The frictional component of the total work results in higher bending forces and torque than would otherwise be necessary to perform the bending operation. This explains the continuous increase in the bending torque and also the higher levels of the non-oscillatory mandrel force as bending progresses; these can be attributed to an increase in the frictional forces during the process (see figure 7.9). When the mandrel is axially vibrated at an ultrasonic frequency, it is believed that the frictional work diminishes not only due to a reduction in the coefficient of friction between the mandrel and the tube bore but also to the reversal of the friction vector.

It is likely that a reduction in the coefficient of friction occurred under the oscillatory conditions. This can result from the mandrel oscillatory motion helping to pump the lubricant into the tube-mandrel interface and thus compelling the presence of a thicker film of lubricant between the contacting surfaces. Further, a real reduction in friction may have arisen from the energy dissipated in the cyclic

relative motion of the surfaces in contact, inducing a rise in temperature and a reduction in the shear yield stress of the tube surface asperities. It is also possible that as a result of such a relative motion at ultrasonic frequencies there may have been a softening or melting of the asperities.

The mechanism of the friction vector reversal may be explained by appreciating that when the mandrel is stationary and a tube is moved slowly over it, the friction acting in the conventional direction always opposes the tube motion. However, when the mandrel is axially vibrated the resultant vector of the relative velocity of any point on the tube contact surface changes its direction during the time of an oscillation period; this is explicitly demonstrated in figures 3.10, 3.11 and 3.12. In a part of that time when the oscillatory velocity is in the forward direction and has a value greater than that of the tube forward velocity, the resultant vector is in a direction opposite to the tube motion. Therefore, the frictional force then acts in the bending direction, ie. assisting the process. During the rest of the oscillation period, the mandrel moves backwards and the relative velocity vector coincides with the tube velocity. The friction during this time is resisting the tube motion, however its magnitude cannot exceed the friction force under the conventional conditions. This is because the friction force is equal to the product of the coefficient of friction and the normal reaction between the parts in contact, and the coefficient of friction is actually less than it would have been if the mandrel was stationary, for the reasons previously stated.

The reversal of the mean mandrel force, shown in figure 7.9, is a real indication of the reduction in friction. As explained earlier in section 7.2.1, the axial force on the mandrel is a resultant of two

forces: the tensile frictional force, and the compressive force caused by the pressure exerted from the tube on the mandrel-tip. Since such a pressure is largely unaffected by the mandrel vibration, it can be concluded that any reduction in the conventional tensile mandrel force or its reversal to compression, as demonstrated in figure 7.9, is solely due to a reduction in the frictional force. This interesting result is very significant in the sense that the vibrated mandrel can be employed to assist the bending machine by pushing the tube forward and therefore causing a substantial reduction in the bending torque as observed in the figure. Moreover, it may be seen that the ultrasonic vibrations can be more effective with higher frictional forces. This explains the greatly increasing bending torque due to an increase in friction as the non-oscillatory bending proceeds while under oscillatory conditions little increase was recorded.

It is important to emphasise that the measured mandrel force shows only the mean effect of applied ultrasonic vibrations. As previously mentioned, the mandrel force can be expressed as a wave form varying between a positive value which represents the conventional tensile force and a negative value equal to the oscillatory force; this variation occurs at an ultrasonic frequency. However, as a result of the ultra-violet recorder galvanometer being unable to respond to this rapid variation in the mandrel force, it recorded only the mean value. Because the compressive component was greater than the tensile component, the resultant mean force on the mandrel showed a negative value when the ultrasonic vibrations were applied, figure 7.9.

7.2.3 Bending with the mandrel vibrating at an ultrasonic frequency

An extensive investigation of the process of draw-bending tubes with the supporting mandrel axially vibrating at an ultrasonic frequency was undertaken. Good quality bends were made under vibratory conditions and the results related to the bending forces, torque and strains were compared with those obtained using the conventional bending method. For each bend, the set-up of the bending tools and also the initial gripper and slider forces were kept constant throughout the oscillatory and non-oscillatory tests.

Figures 7.10 to 7.16 represent a set of experimental results obtained for bending mild steel tubes having an outside diameter of 1.0 in and a diameter to thickness ratio of 15. The mean bend radius was 1.5 times the tube outside diameter. The amplitude of mandrel vibration during the oscillatory test was 5×10^{-4} in which corresponds to an output power from the generator equal to 500 watt.

The progress of the slider force during the bending operation is illustrated in figure 7.10. It can be seen that the slider force increases continuously with the current angle of bend and that the mandrel vibration has an insignificant effect on the increase in the slider force. Thus it may be concluded that any changes in the mandrel force with applied vibrations are due to other effects and not to a significant change in the slider force. These changes are recorded in figure 7.11 which represents the variation of the mandrel force with the current angle of bend during the oscillatory and non-oscillatory tests.

As illustrated in figure 7.11, the mandrel force is generally compressive when bending thick-walled tubes to small bend radius, which can be explained by the greater compressive axial force resulting from the high pressure exerted on the mandrel-tip. However, it can be seen clearly that the non-oscillatory curve approaches a maximum negative

value at a small angle of bend and then starts to increase in the reverse direction, which indicates an increase in the tensile frictional force. At small angles, the tube has not passed completely over the mandrel-tip and therefore the compressive force due to the pressure from the tube-wall is less than its maximum value which occurs at approximately 30 degrees. It is likely then that the maximum compressive force would remain unchanged and thus the decrease in the compressive mandrel force observed in figure 7.11 can only be explained by an increase in the slider force with its consequential higher initial friction force. The oscillatory curve of the mandrel force, on the other hand, reached its maximum negative value, which is numerically greater than the corresponding non-oscillatory value, and remained constant thereafter. This interesting observation indicates that friction at the tube-mandrel interface almost disappeared when the mandrel was axially vibrated.

Considering the friction vector reversal as a result of the axial vibration of the mandrel (see section 3.6 and figures 3.10 and 3.12), it may be appreciated that at a low bending speed and a high amplitude of mandrel vibration, almost 100 per cent reduction in mandrel friction can be achieved. This is presumably possible, if for an oscillation period, the time during which the mandrel velocity exceeds the tube velocity is half the total oscillation time, then a reduction in friction of 100 per cent is achievable. It may be concluded that at 500 watt of ultrasonic power, the vibration amplitude was high enough to result in a substantial reduction in friction between the tube bore and the supporting mandrel.

The consequential effects of the reduction in friction during the bending operation can be seen in figures 7.12 and 7.13 which compare the

progress of the oscillatory gripper force and bending torque with those recorded under conventional conditions. The figures demonstrate that the non-oscillatory curves are higher than those obtained when the mandrel was oscillated. Furthermore, the non-oscillatory curves show a greater rate of increase with the angle of bend than that of the oscillatory curves. The results may be explained by referring to figures 7.10 and 7.11 whch indicate the increase in the frictional force with the increase in the angle of bend and a substantial reduction in the mandrel friction as a result of applied ultrasonic oscillations.

The effect of mandrel vibration on the strains developed in the bent tubes are shown in figures 7.14, 7.15 and 7.16. It is clearly seen from figure 7.14 that the maximum longitudinal strains at the outer and central peripheries of the bend were reduced under the oscillatory conditions. However, the oscillatory curve representing the distribution of the strains at the inner periphery of the bend shows higher values of the maximum strains than those observed under the conventional conditions. These results may be explained by a reduction in the initial friction force when the mandrel is axially vibrated, and consequently the movement of the neutral plane towards the centre of the bend is less than that which occurs during the non-oscillatory bending. In addition, a considerable reduction in friction as the tube is pulled over the mandrel-tip while being vibrated can also account for a reduction in the maximum longitudinal strains at the outer periphery of the bend, figure 7.14.

Figures 7.15 and 7.16 illustrate the distribution of the longitudinal, hoop and thickness strains at the outer and inner peripheries of the bend with and without axial vibration of the mandrel. It can be seen that while the mandrel vibration caused the strains at

the outer periphery to decrease, figure 7.15, it also resulted in an increase in the strains at the inner periphery as shown in figure 7.16. The friction reduction occurred under the oscillatory conditions, therefore, caused the tube material on the bend outside to stretch less, and on the bend inside to contract more than that taking place during the conventional bending process. The consequential effects are, thus, a reduction in the tube wall-thinning and an increase in the amount of wall-thickening on the outside and inside of the bend respectively. The significance of such a result is that a stronger bend can be produced with applied ultrasonic vibration than is possible by the conventional methods.

Bends were made with the mandrel axially vibrated at different amplitudes in the range from 3.8×10^{-4}in to 6.3×10^{-4}in which corresponded to levels of ultrasonic power between 250 watt and 1500 watt. The objective was to investigate the effect of varying the amplitude of mandrel vibration on the reduction in the bending torque and on the strains developed at the outer periphery of the bend.

Figures 7.17 and 7.18 show that the reduction in the steady state bending torque (at about 180 degrees) increases with increasing the ultrasonic power (vibration amplitude) and that the amount of reduction does not seem to be influenced significantly by the variation in the tube diameter to thickness ratio. For a constant bending velocity, as the mandrel amplitude increases, the reduction in the frictional force, correspondingly increases since the period over which the mandrel velocity exceeds the tube velocity becomes greater. Figure 7.18 and 7.19 also illustrate a large rate of increase for the reduction in the bending torque at relatively low ultrasonic power. However, as the power increases, the rate of torque reduction slows down. This

observation is also illustrated in figures 7.19 and 7.20 which represent the percentage reduction in the steady state bending torque vs. the ultrasonic power. It can be seen from the figures that as the tube diameter to thickness ratio increases, the percentage reduction in the bending torque becomes greater. Thus the use of ultrasonic oscillations can prove to be more advantageous for bending thin-walled tubes since the frictional component as a percentage of the total work done increases as the tube-wall becomes thinner. This result is also demonstrated in figure 7.21 which clearly shows that the percentage reduction in the bending torque increases (almost linearly) with the tube diameter to thickness ratio. It can be seen also that the rate of torque reduction is higher at greater ultrasonic power, ie. vibration amplitude.

The effect of varying the amplitude of mandrel oscillation on the strains developed in the bent tubes is summarised in figures 7.22 and 7.23. The figures represent the distribution of the longitudinal, hoop, thickness and equivalent strains at the outer periphery of the bend under the oscillatory and non-oscillatory conditions. The tube diameter to thickness ratio and the mean bend radius to tube diameter were 26 and 2.0 respectively. It can bee seen once more that the mandrel oscillation reduced the maximum values of strains and that the amount of reduction is most significant for the thickness strains (about 15 per cent).

As has been predicted from the theoretical analysis, at higher amplitudes of mandrel vibration, a greater amount of reduction in the strains at the outer periphery of the bend may be achieved. This is due to a greater reduction in friction at the tube-mandrel interface. However, figures 7.22 and 7.23 show little effect of the vibration

amplitude on the strains, which may be due to the small experimental step taken in the vibration amplitude although the ultrasonic power was doubled. The theoretical results indicate (see figures 6.27 and 6.30) that extra reduction in the frictional forces and the strains is not significant in this range of the vibration amplitudes. Moreover, in addition to a slight variation of the original tube wall-thickness around the periphery, the difficulty of measuring the lengths of the grid divisions and the wall-thicknesses very accurately using the available equipment made the slight variations in the strains not easily detected.

It may be concluded, therefore, that under the experimental conditions investigated, an input ultrasonic power in the range from 250 watt to 500 watt is sufficient to achieve a satisfactory reduction in the strains. However higher power, ie. greater amplitudes of mandrel vibration, may be necessary for bending other tube materials, eg. stainless steel or for tubes having bigger sizes. Using faster bending speeds may also require higher vibration amplitudes to achieve the same reduction in friction and consequently in the strains (this is directly related to the velocity ratio).

7.3 Correlation between the theoretical and experimental results

It is the objective of this section to show the degree of correlation between some of the experimental results relating to the strain distribution and the bending torque, and the corresponding values predicted from the theory developed in Chapter Three. The results are plotted for bending mild steel tubes having an outside diameter of 1.0 in and a diameter to thickness ratio of 26 to a mean bend radius equal

to 2.0 times the tube diameter. A family of theoretical curves was obtained assuming various values for the coefficient of friction in the range from 0 to 0.04. Figures 7.24 to 7.29 illustrate the results of tube-bending under both vibratory and non-vibratory conditions. The amplitude of mandrel vibration was selected to be 5.0×10^{-4}in which corresponds to 500 watt of ultrasonic power.

Figures 7.24 and 7.25 represent the variation of the longitudinal, hoop, thickness and equivalent strains with the current angle of bend at steady state during conventional bending. It can be seen that the predicted longitudinal, thickness and equivalent strains show good agreement with the experimental data. The experimental curves may be seen to lie between the theoretical curves corresponding to an assumed coefficient of friction having values between 0.01 and 0.02. Although the measured strains showed a slight increase with the current angle of bend, the theoretical trends indicate an insignificant increase in the strains. The explanation of this may lie in the underestimation of the initial friction force which influences the position of the neutral plane and therefore the strain values at the bend outer periphery in deformation zone IIb. It is likely that the increase in the slider force results in a greater increase in the initial friction force than the predicted values. Practically, the friction between the wiper die and the tube external surface, and between the mandrel and the tube bore in the vicinity of the entry plane (the tangent line) could also have affected the initial friction force. Ignoring this effect would, of course, lead to an underestimation of the influence of the increase in the slider force on the displacement of the neutral plane and the consequential increase in the strains at the bend outer periphery. It can also be seen from figure 7.24 that there is a slight difference

between the predicted and measured values of the hoop strain which proved to be the most difficult to measure very accurately.

The effect of axial ultrsonic vibration of the mandrel on the distribution of the longitudinal, hoop, thickness and equivalent strains at the outer periphery of the bend is demonstrated in figures 7.26 and 7.27. It can be clearly seen that the best agreement between the theory and the experimental results is for the longitudinal and equivalent strains, while the predicted hoop strains showed the greatest deviation from the measured values. It is interesting to notice that, when vibrating the mandrel, the friction has little effect on the developed strains. This result may be attributed to the fact that the amplitude of mandrel vibration was high enough so that, for the process conditions, the frictional force was nearly eliminated. This is a result of the reversal of the friction vector between the mandrel and the tube bore. The significance of this conclusion is that a poor lubricant can be used in the oscillatory bending operation without having an effect on the developed strains, bearing in mind the likely reduction in the coefficient of friction with applied ultrasonic oscillations for the reasons previously mentioned. Once more the experimentally determined strains under the oscillatory conditions show a slight increase with the current angle of bend, which is markedly less than the corresponding increase during conventional bending, figures 7.24 and 7.25.

The progress of the bending torque with the current angle of bend under both vibratory and non-vibratory conditions is described in figures 7.28 and 7.29. It may be seen that the predicted bending torque shows a reasonable correlation with the experimental data although there is some deviation. As can be observed from the figures,

the theory predicts nearly the same value of the initial bending torque, ie. at the start of the bending operation. Also, it may be seen that the general trend of both the experimental and theoretical curves is the same, however the rate of increase in the bending torque with the bend angle observed experimentally was underestimated. This latter result may be explained by the fact that the theory underestimates the friction forces and so the increase in the bending torque. The experiments showed a reduction in the bending torque of more than 20 per cent for mandrel vibration, while the theory estimated only 12 per cent reduction. As previously discussed, the slider force has a dictating influence on the progress of the bending torque due to its considerable effect on the initial friction force (see figures 6.18 and 6.19). In the theoretical analysis, the friction at the slider-tube and the mandrel-tube interfaces was taken into account while the friction between the wiper die and the tube and between the mandrel and the tube bore in the vicinity of the tangent line was not considered. It may be reasonable therefore to assume that the latter friction could have a significant effect on the initial friction force and consequently on the bending torque. Furthermore, since the mandrel was slightly advanced forward beyond the tangent line for that bend, a fact which was not taken into consideration in the theoretical analysis, the pressure exerted on the mandrel-tip could have been higher than its predicted value. Consequently, the final friction force was likely to be greater than the theoretical value.

During the oscillatory bending tests, it was observed that some of the ultrasonic energy was transmitted through the tube-wall, in particular when high power was used, which may have resulted in a reduction in friction at the wiper die-tube and slider-tube interfaces.

This in addition to a substantial reduction in the mandrel friction may explain the higher reduction in the bending torque, particularly at greater frictional forces, than the values predicted theoretically, figures 7.28 and 7.29.

Section 7.4: Graphical experimental results

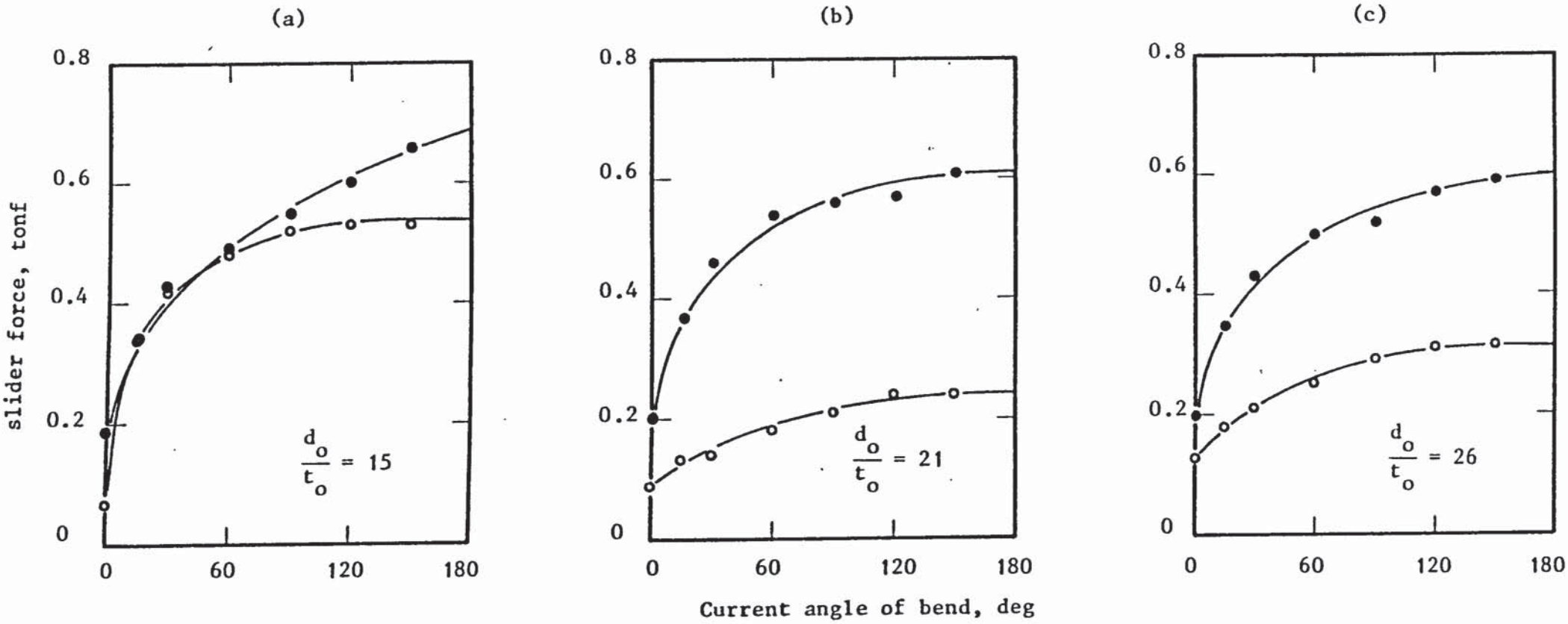

Figure 7.1: The progress of the slider force with the current angle of bend during the conventional process of tube draw-bending for various values of tube diameter to thickness ratios and mean bend radii

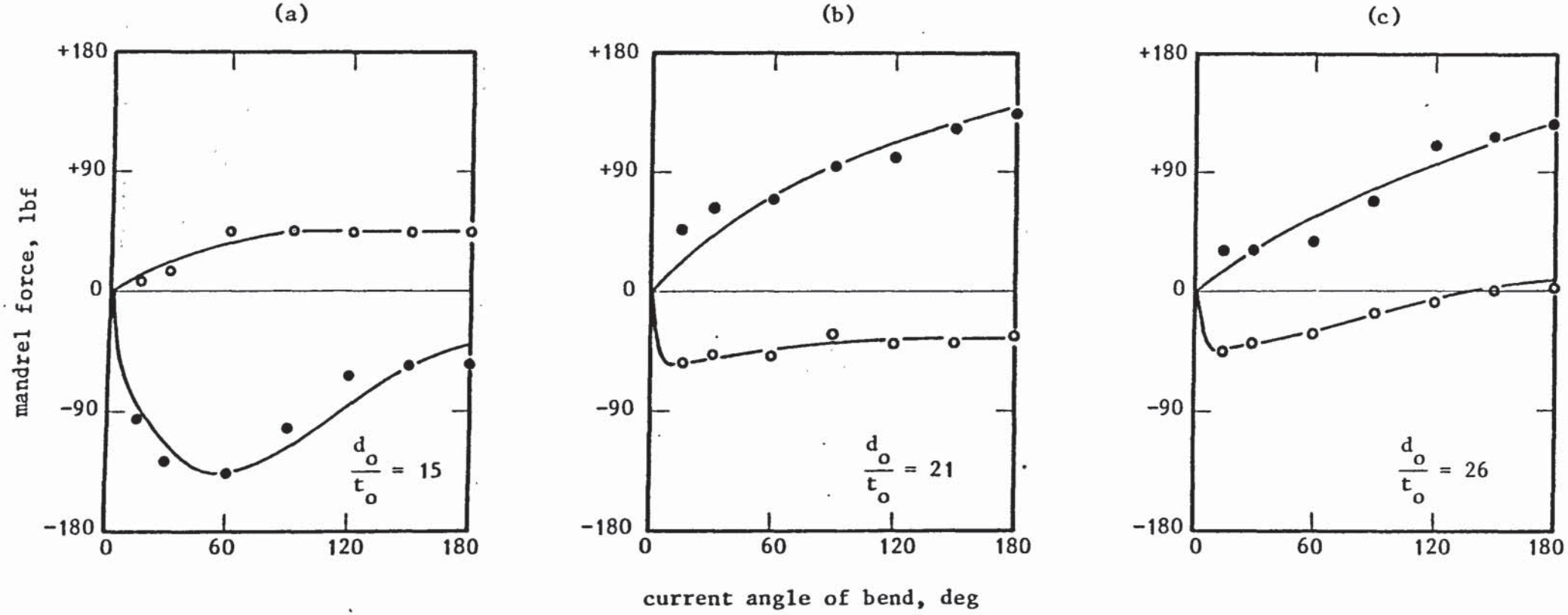

Figure 7.2: The variation of the mandrel axial force with the current angle of bend during the conventional process of draw-bending for various values of tube diameter to thickness ratios and mean bend radius

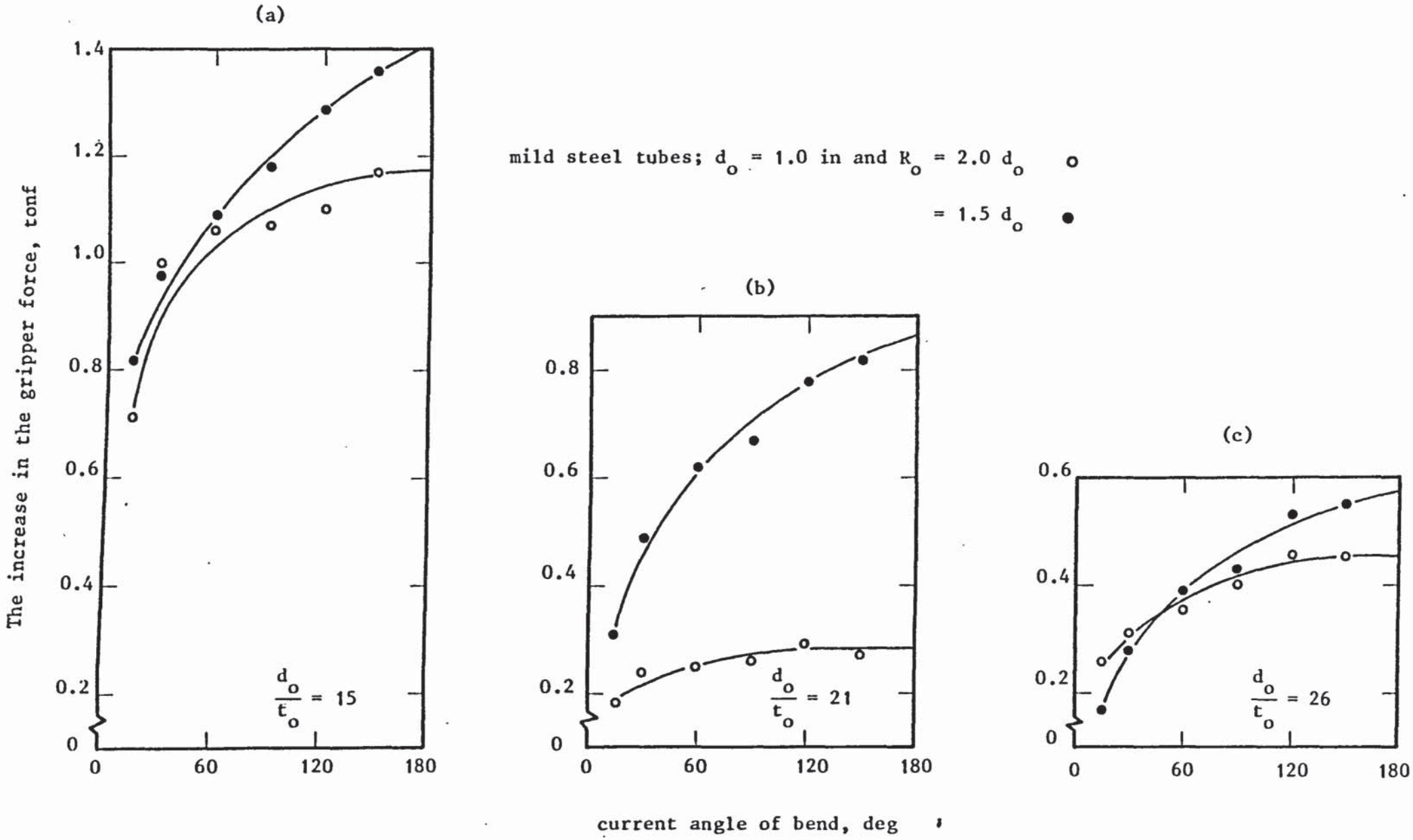

Figure 7.3: The increase in the gripper force vs. the current angle of bend during the conventional process of tube draw-bending for various values of tube diameter to thickness ratios and mean bend radii

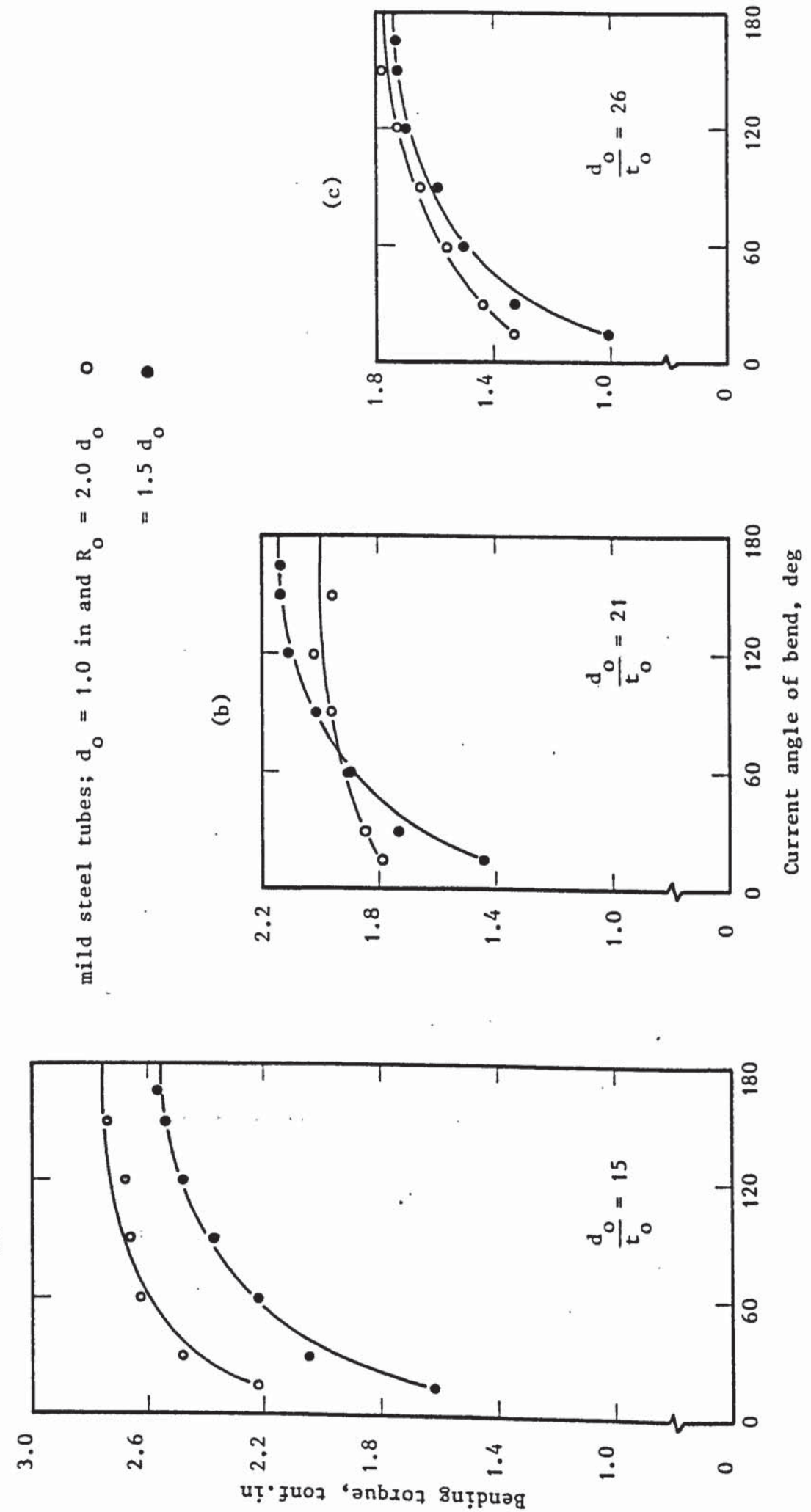

Figure 7.4: The progress of the bending torque with the current angle of bend during the conventional process of tube draw-bending for various values of tube diameter to thickness ratios and mean bend radii

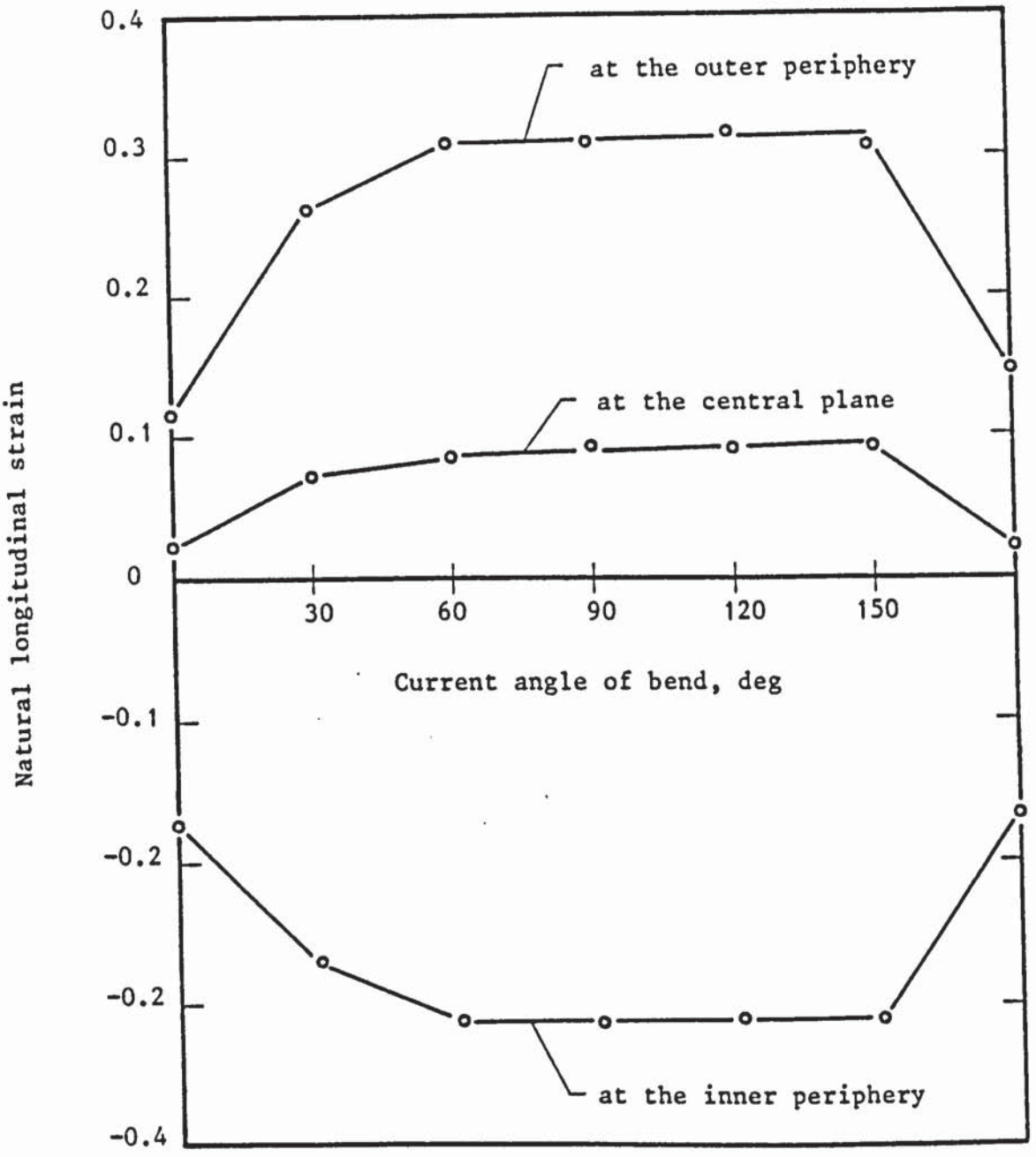

Figure 7.5: Distribution of the longitudinal strains along the bend length on the tube external surface (mild steel tube; d_o = 1.0 in, d_o/t_o = 15 and R_o = 1.5 d_o)

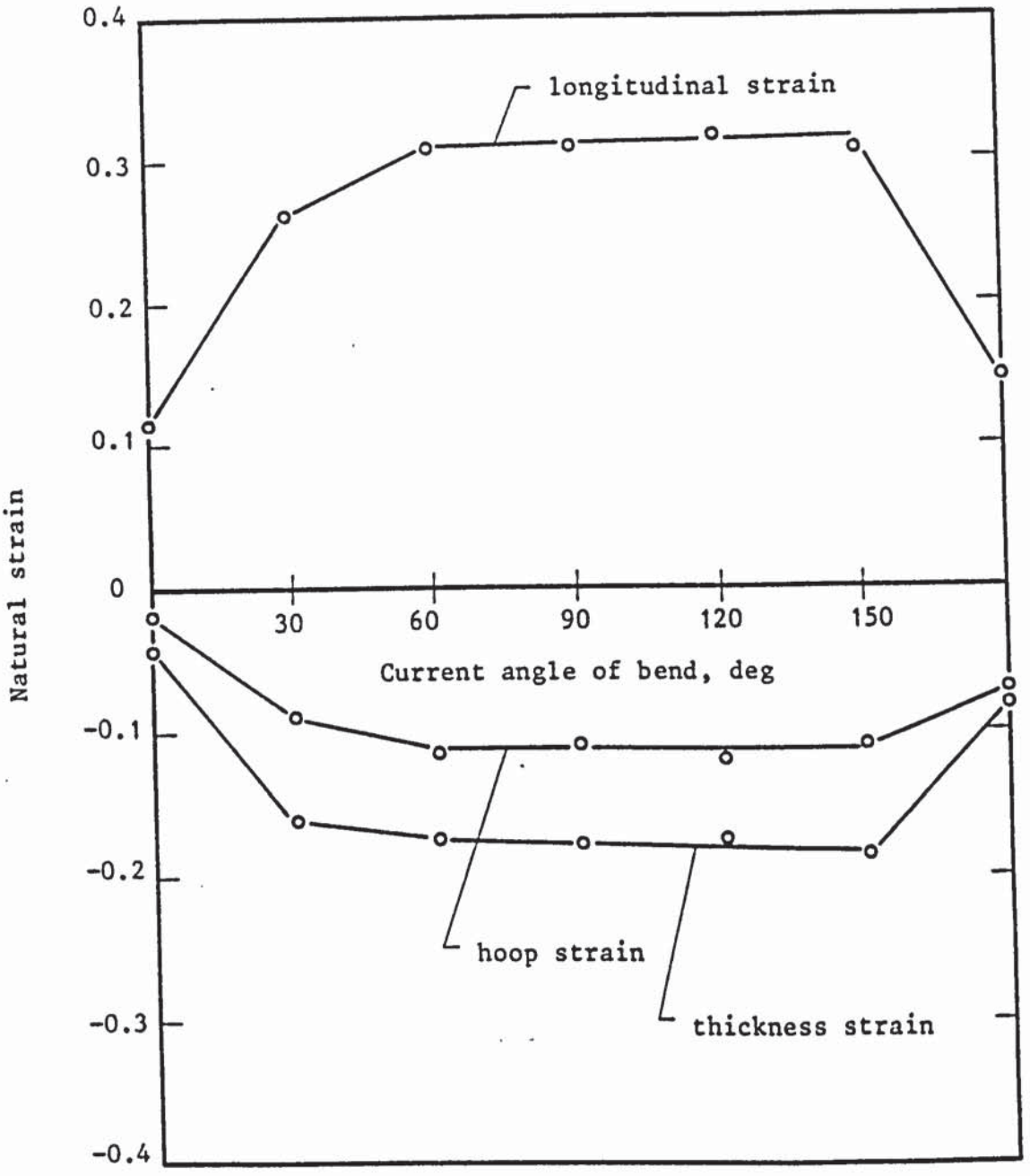

Figure 7.6: Distribution of the longitudinal, hoop and thickness strains at the outer periphery of the bend (mild steel tube; d_o = 1.0 in, d_o/t_o = 15 and R_o = 1.5 d_o)

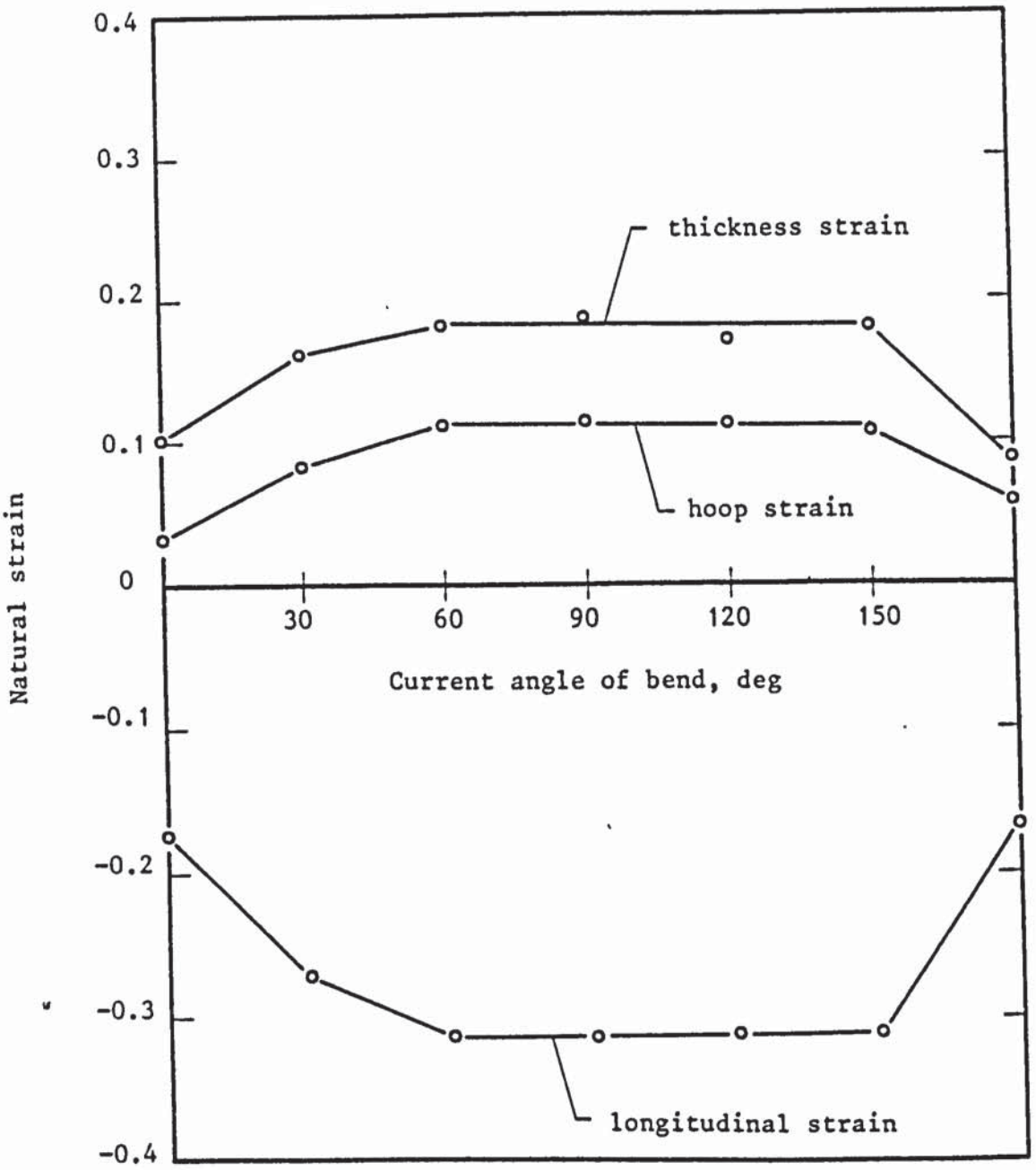

Figure 7.7: Distribution of the longitudinal, hoop and thickness strains at the inner periphery of the bend (mild steel tube; d_o = 1.0 in, d_o/t_o = 15 and R_o = 1.5 d_o)

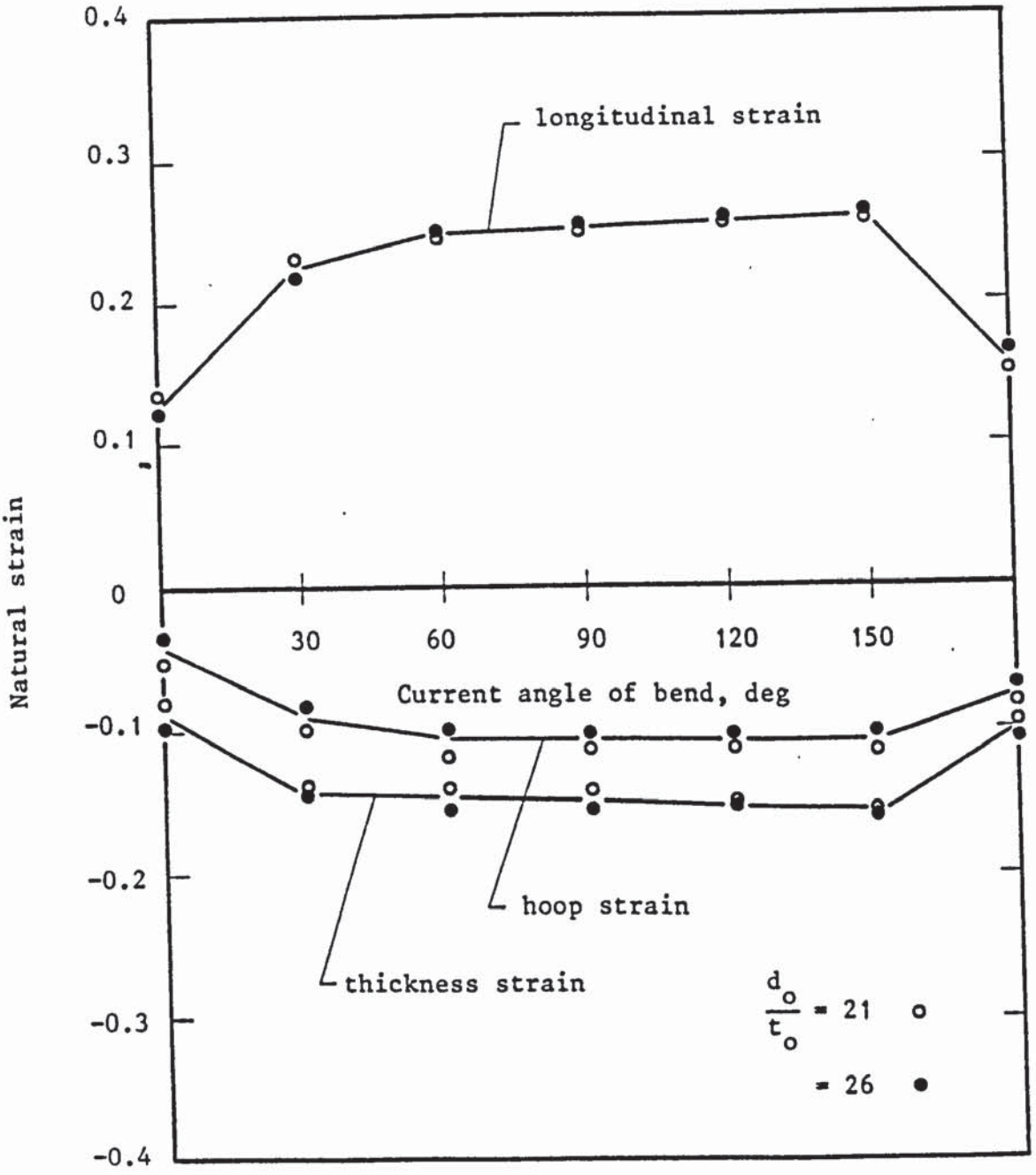

Figure 7.8: Effect of the tube diameter to thickness ratio on the distribution of the longitudinal, hoop and thickness strains at the outer periphery of the bend (d_o = 1.0 in and R_o = 2.0 d_o)

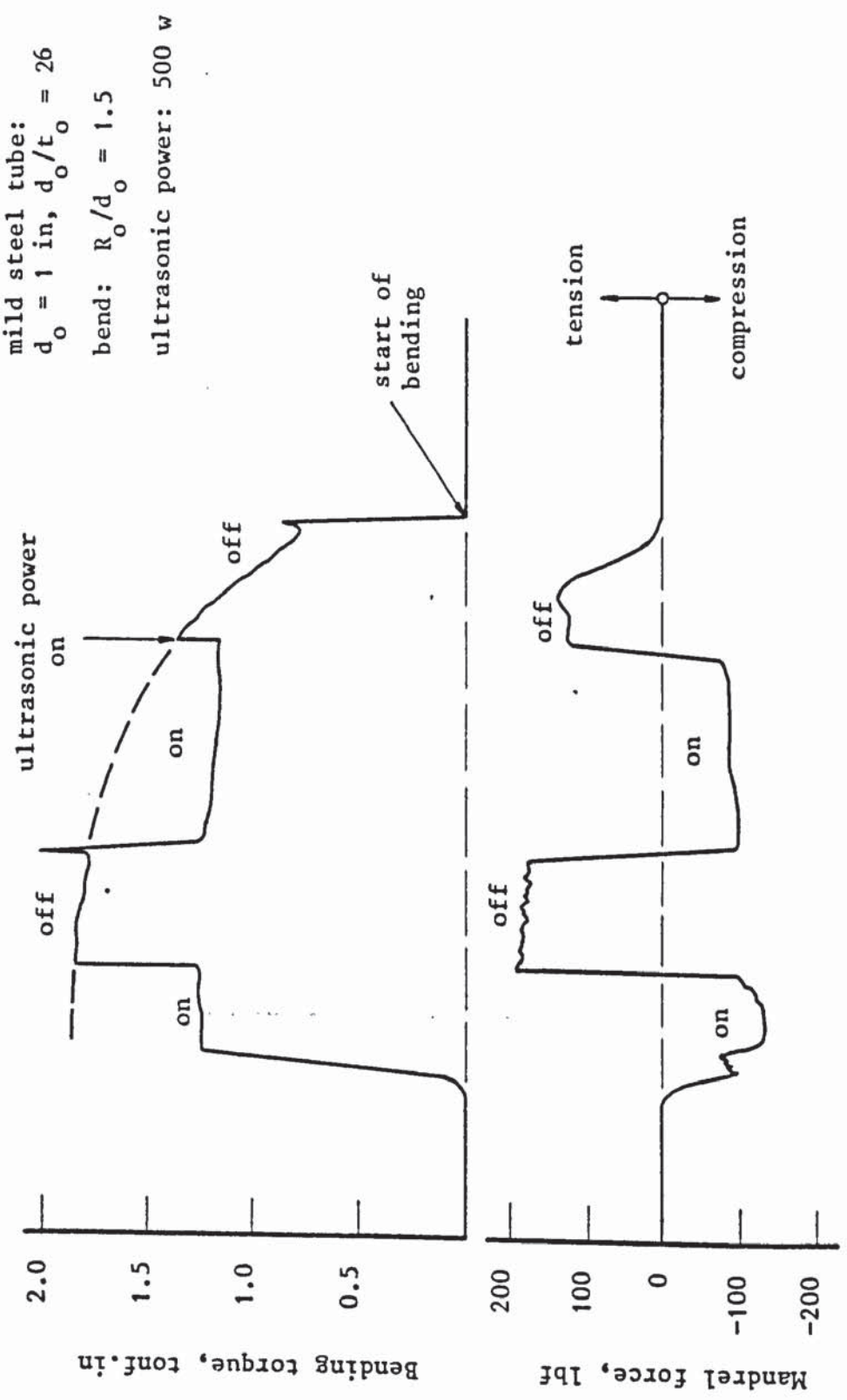

Figure 7.9: Typical traces of u.v. recorder showing the changes in bending torque and mandrel force during an interrupted oscillatory test

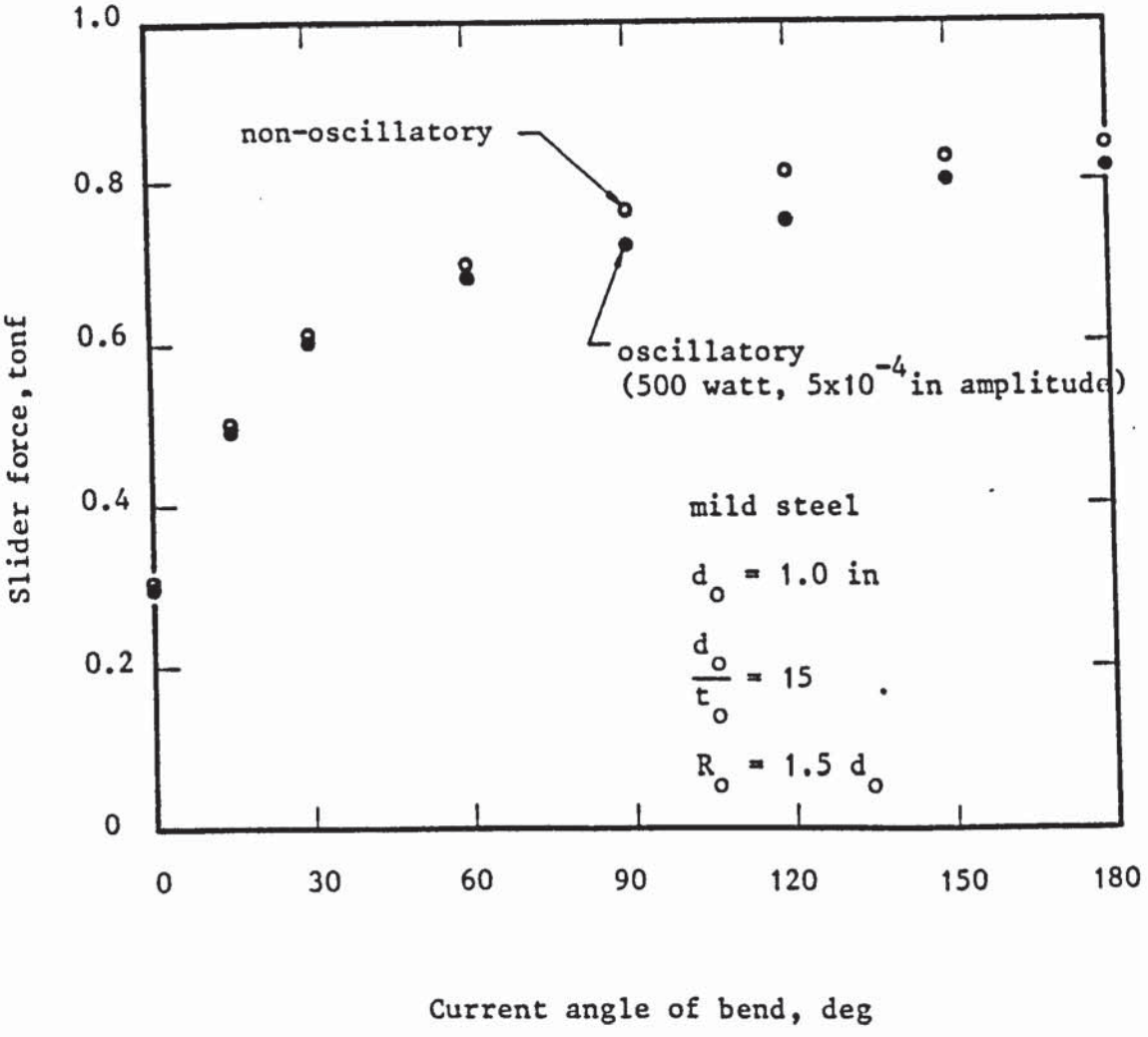

Figure 7.10: The slider force vs. the current angle of bend under oscillatory and non-oscillatory conditions

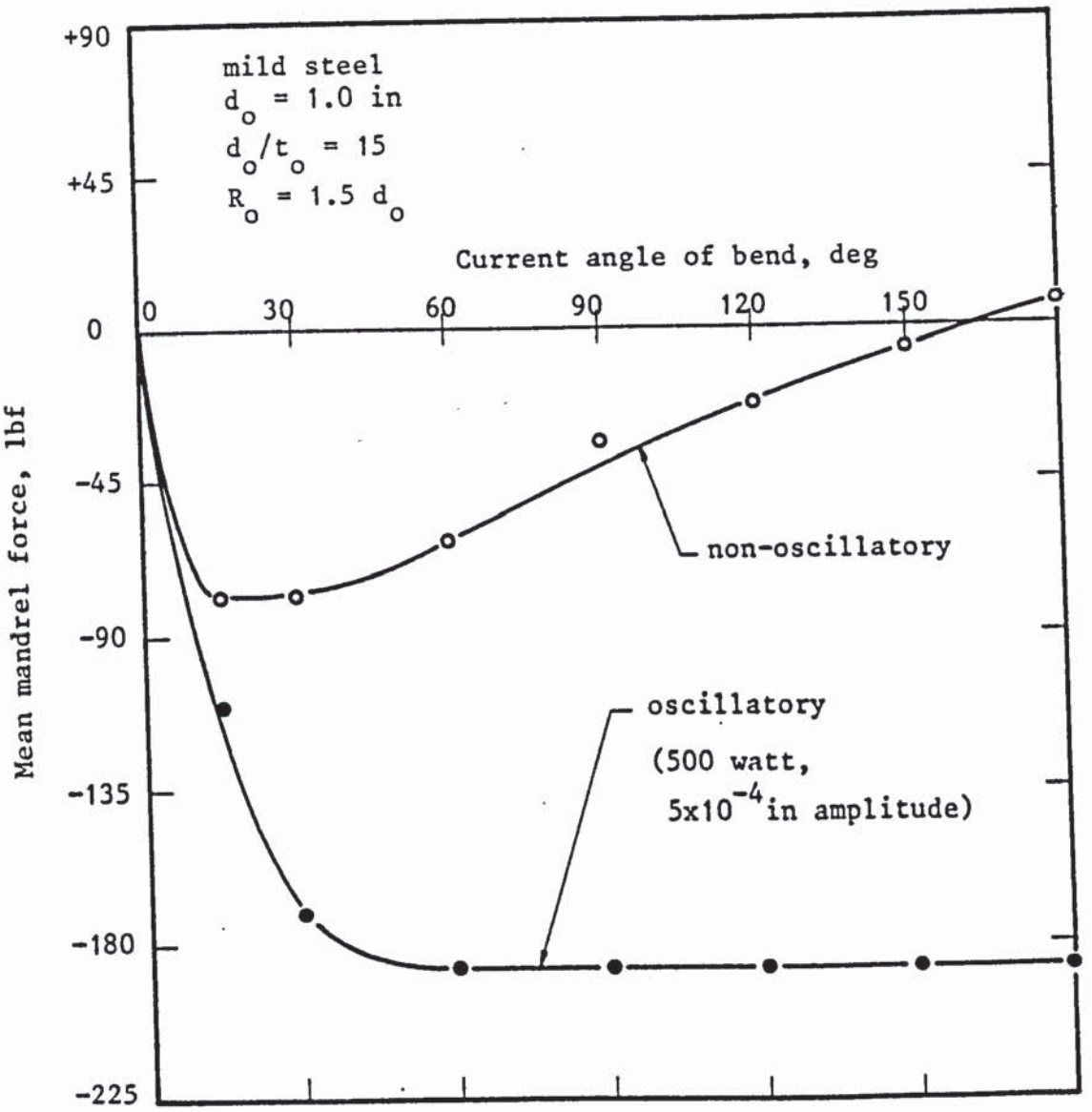

Figure 7.11: The variation of the mean mandrel force with the current angle of bend under both oscillatory and non-oscillatory conditions

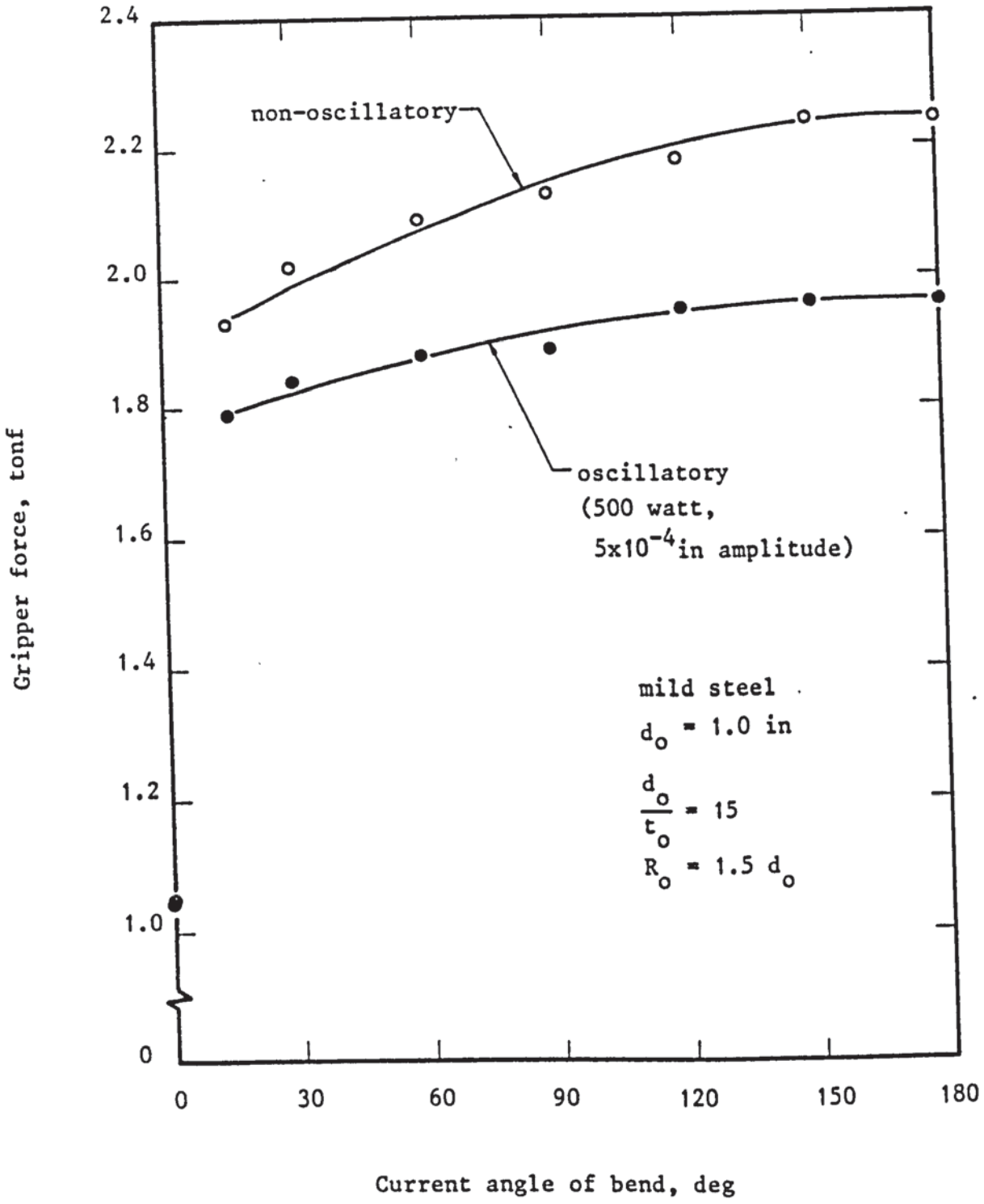

Figure 7.12: The gripper force vs. the current angle of bend under oscillatory and non-oscillatory conditions

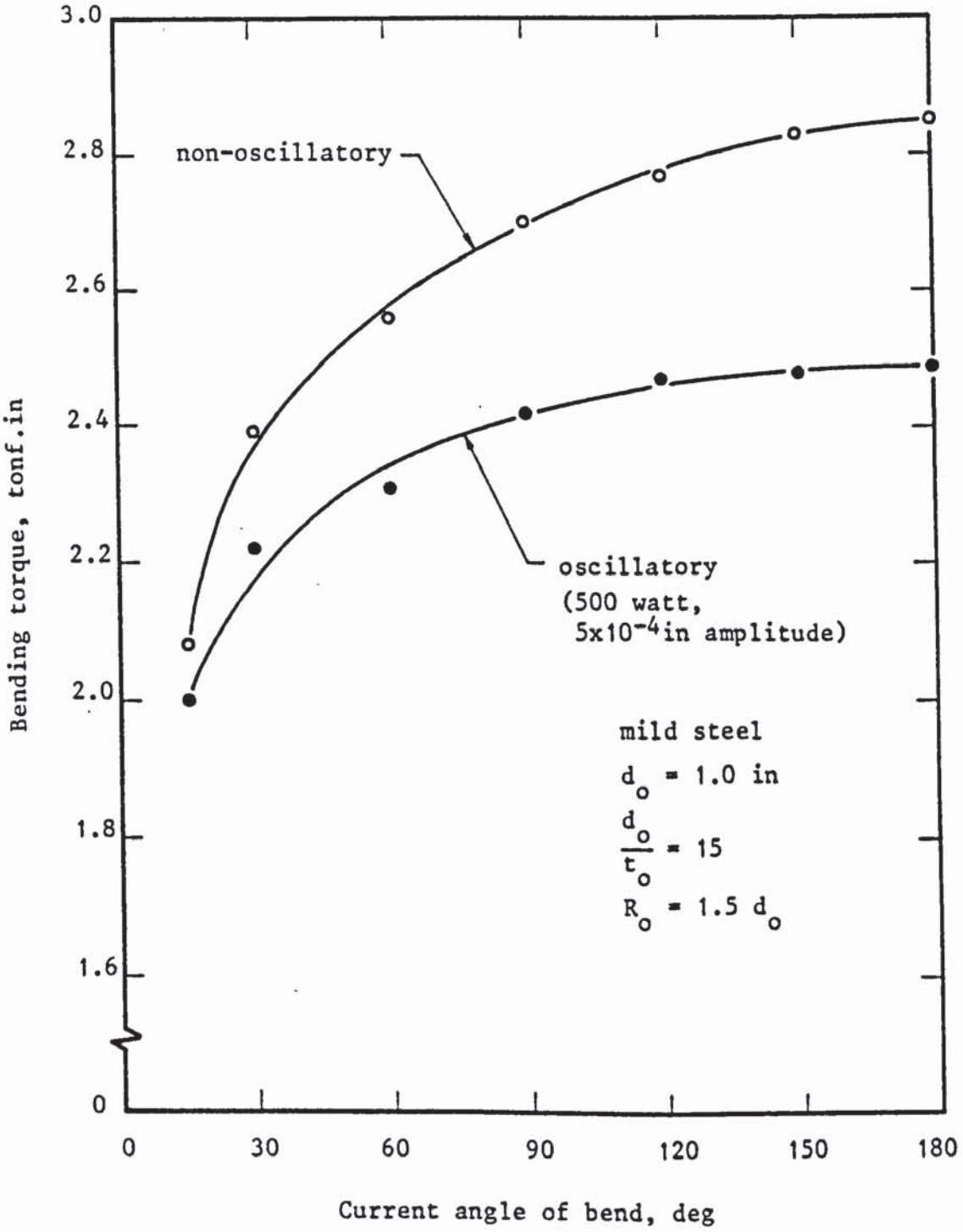

Figure 7.13: The progress of the bending torque with the current angle of bend with and without mandrel axial vibration at an ultrasonic frequency

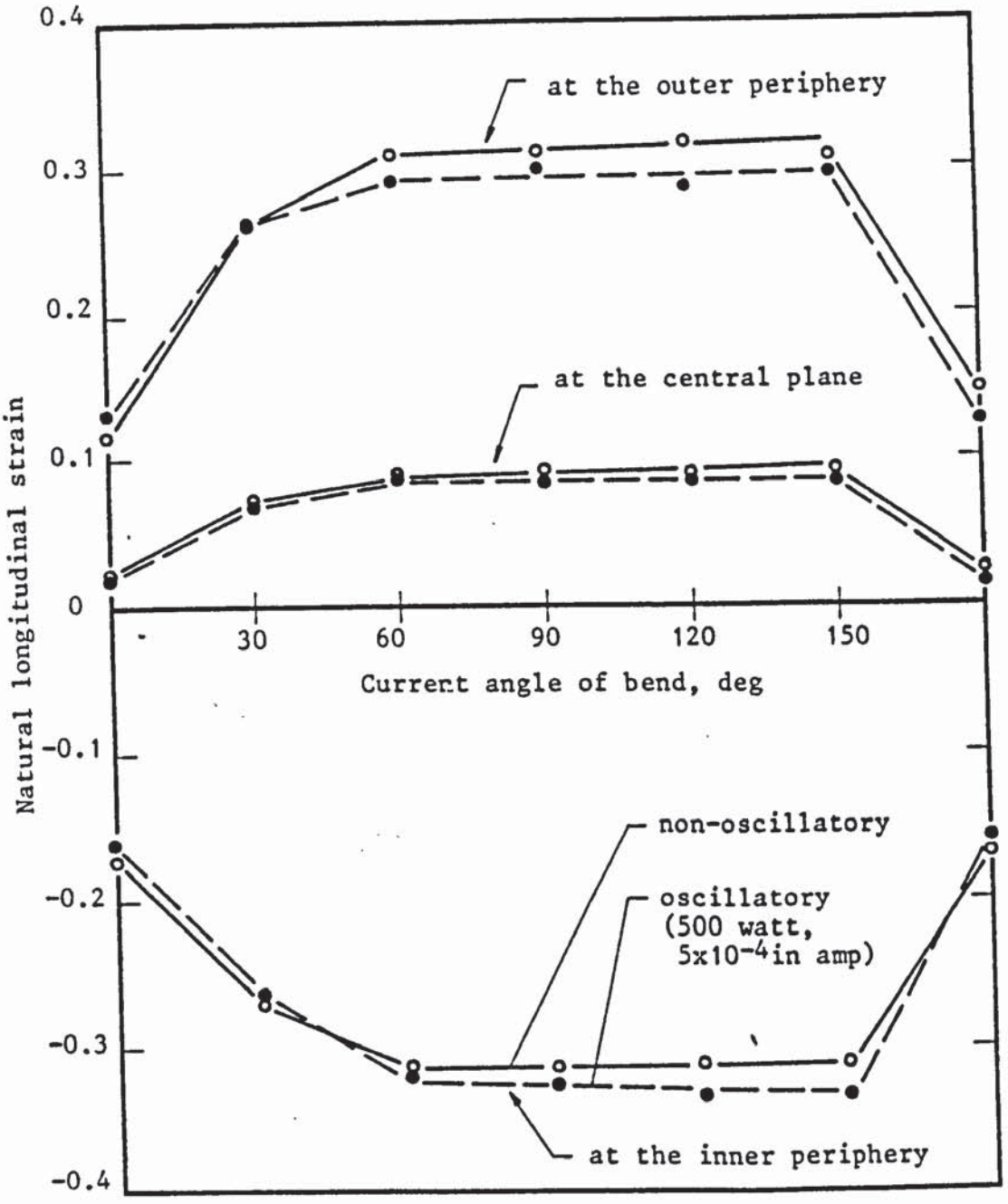

Figure 7.14: Effect of applying ultrasonic oscillations on the distribution of the longitudinal strains on the tube external surface (mild steel tubes; d_o = 1.0 in, d_o/t_o = 15 and R_o = 1.5 d_o)

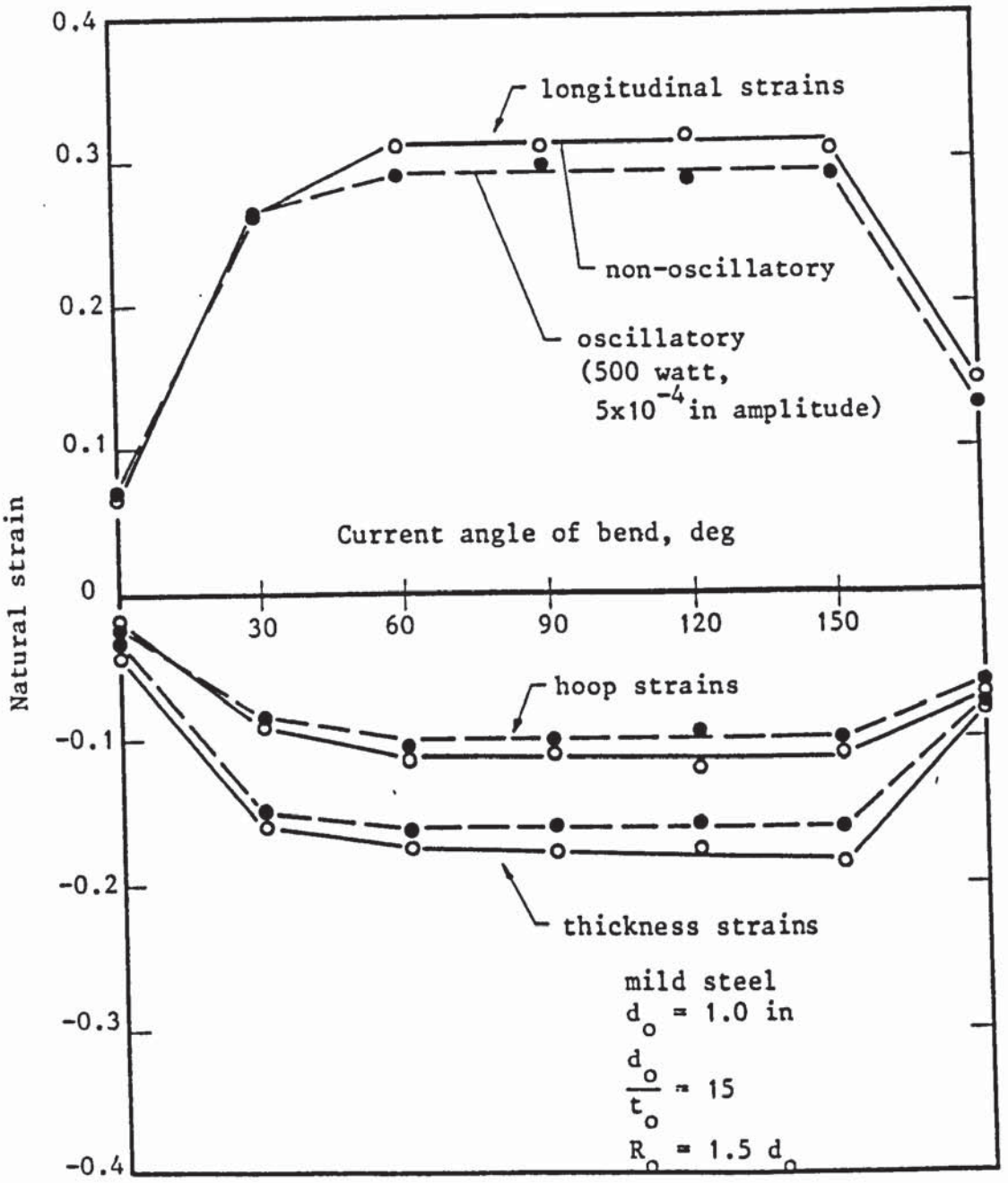

Figure 7.15: Effect of applying ultrasonic vibrations on the distribution of strains at the outer periphery of the bend

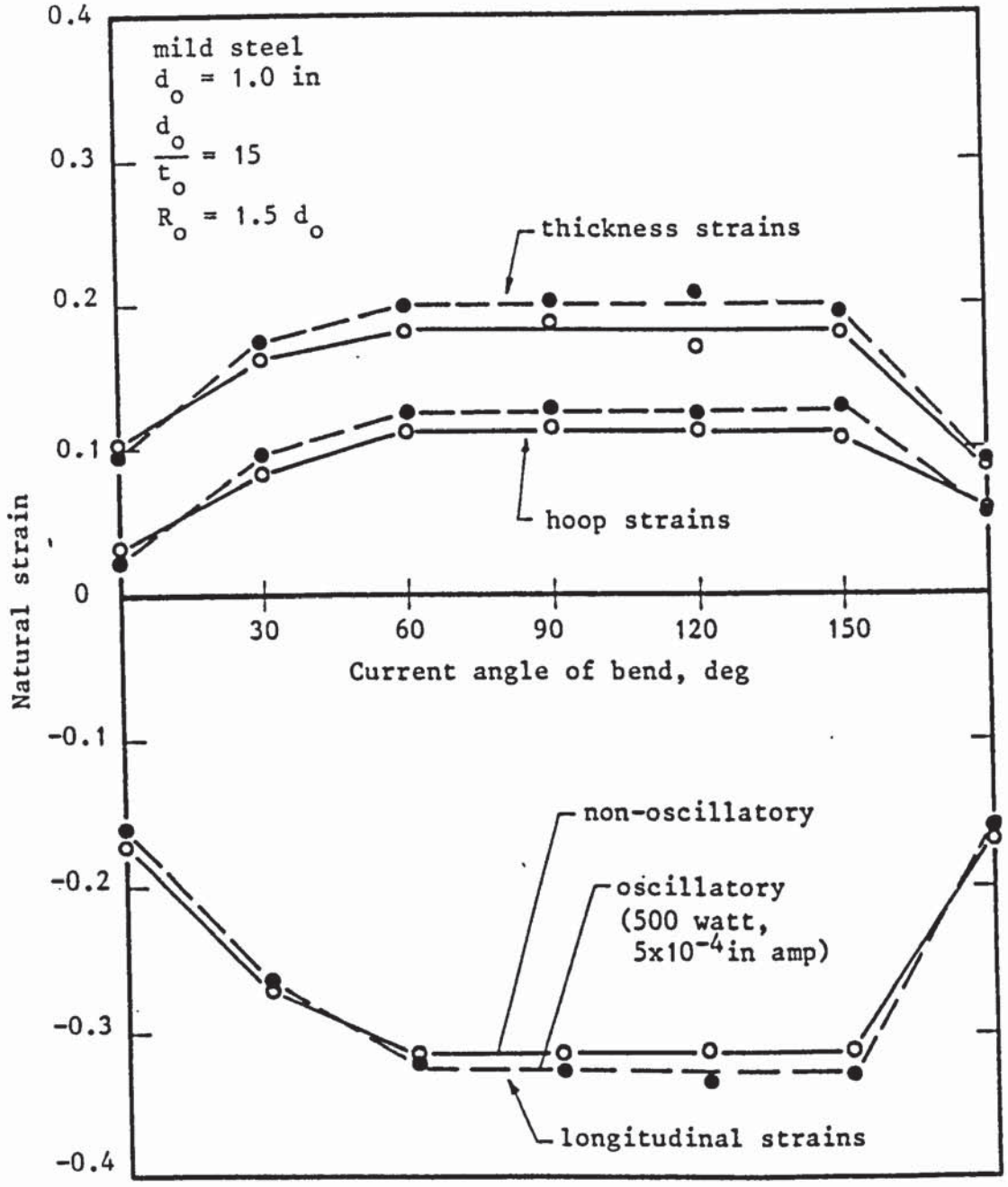

Figure 7.16: Effect of axial vibration of the mandrel on the distribution of strains at the inner periphery of the bend

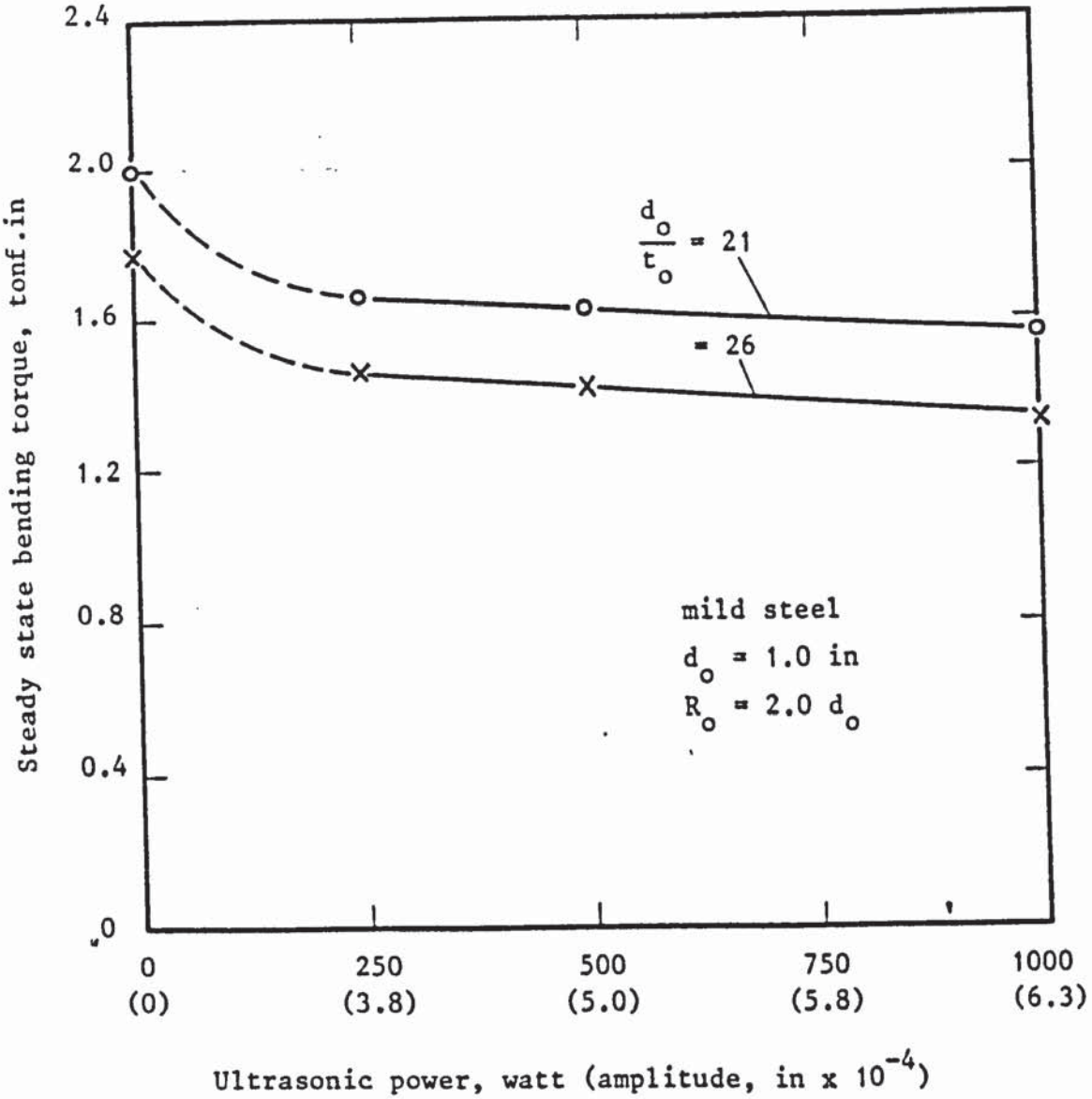

Figure 7.17: Effect of vibration amplitude of the mandrel on the steady state bending torque (at about 180 degrees) for different tube diameter to thickness ratios (d_o/t_o)

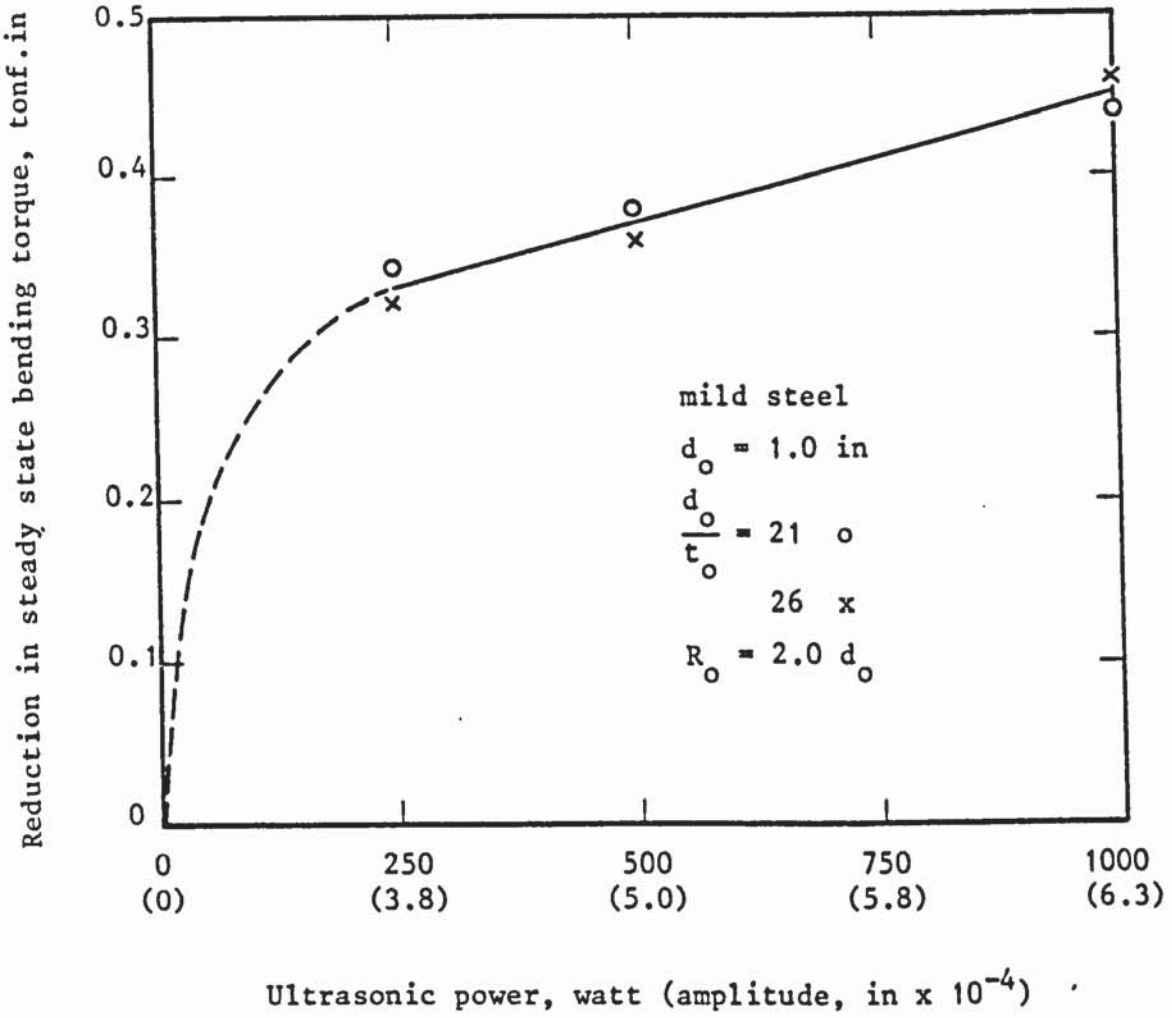

Figure 7.18: Effect of vibration amplitude of the mandrel on the reduction in the steady state bending torque (at about 180 degrees) for different tube diameter to thickness ratios (d_o/t_o)

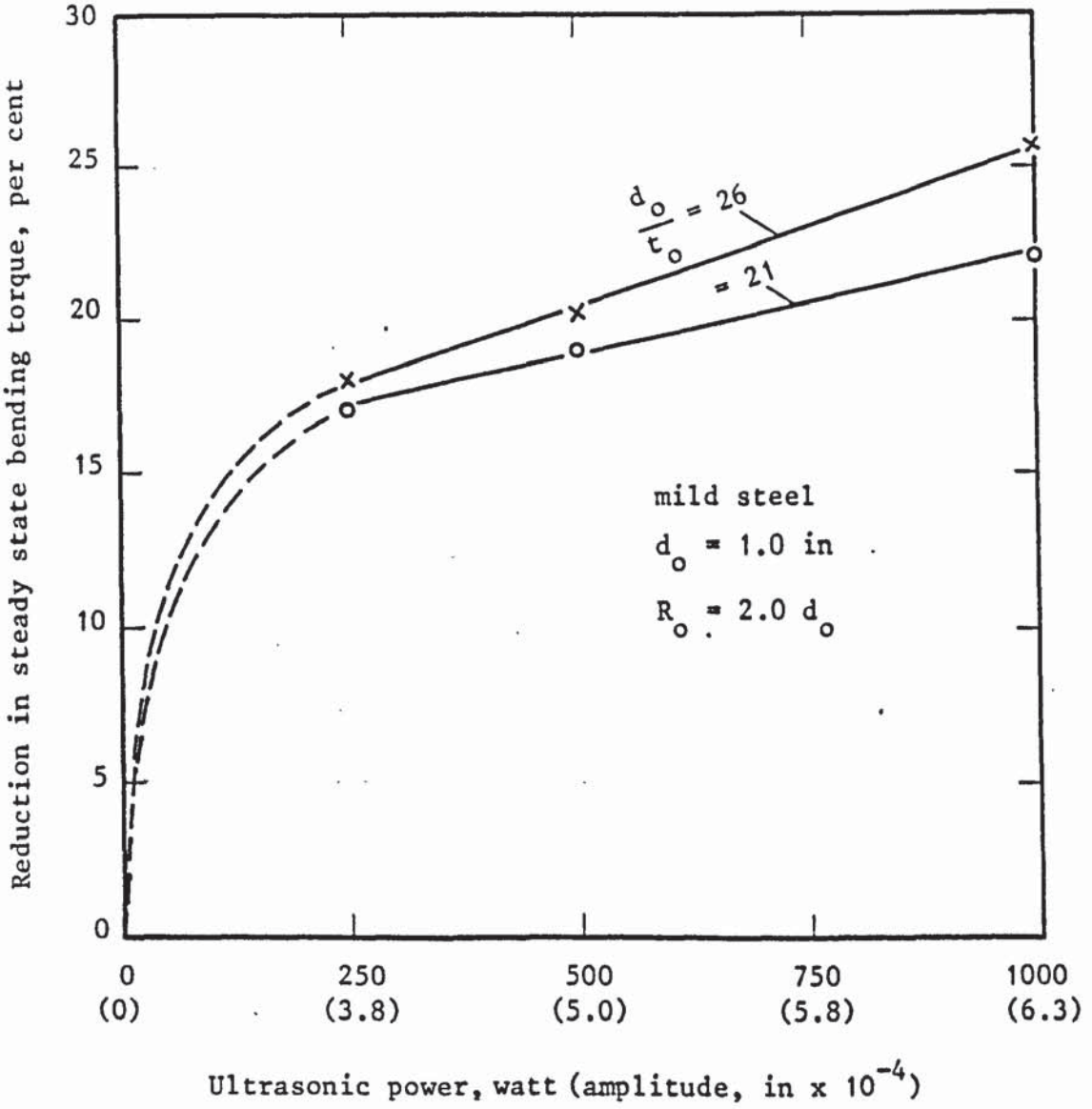

Figure 7.19: Effect of vibration amplitude of the mandrel on the percentage reduction in the steady state bending torque (at about 180 degrees) for different tube diameter to thickness ratios (d_o/t_o)

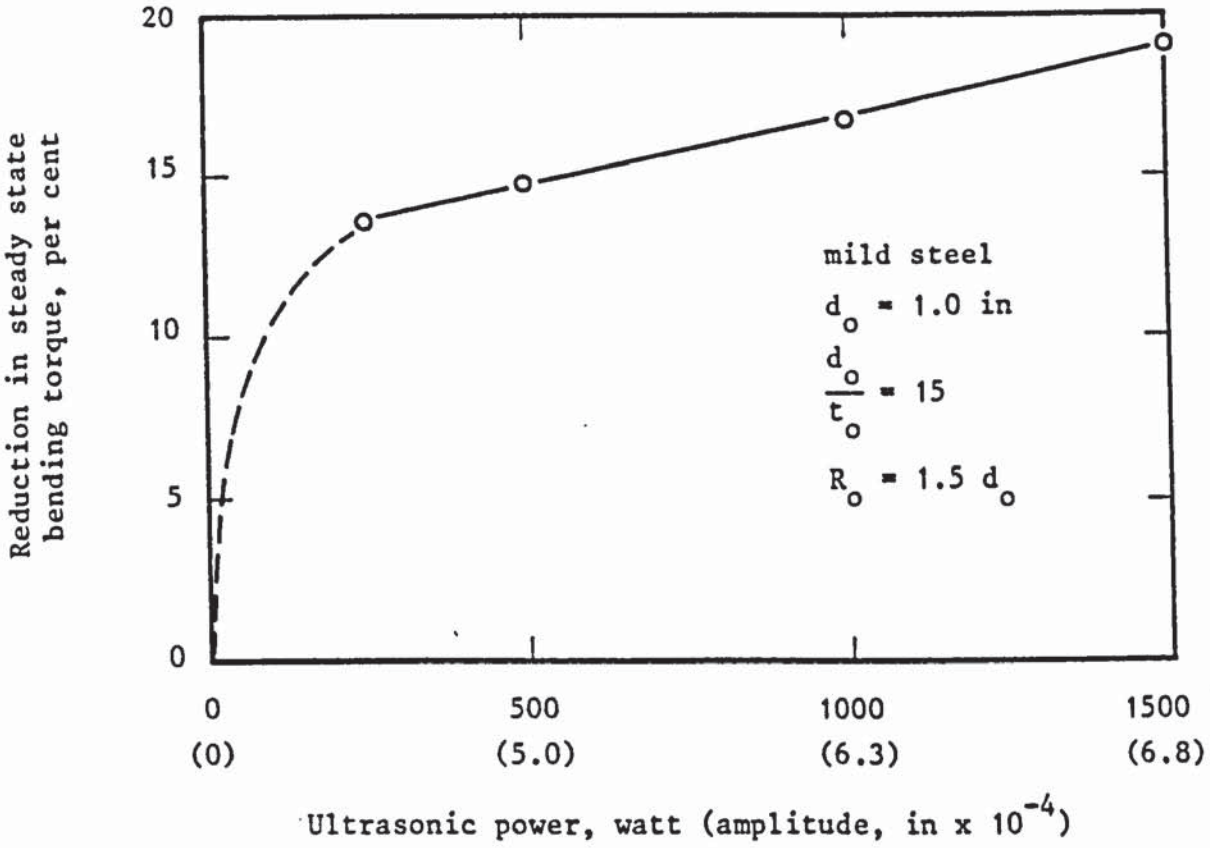

Figure 7.20: Effect of vibration amplitude of the mandrel on the percentage reduction in the steady state bending torque (at about 180 degrees) for a mean bend radius equal to 1.5 times the tube diameter

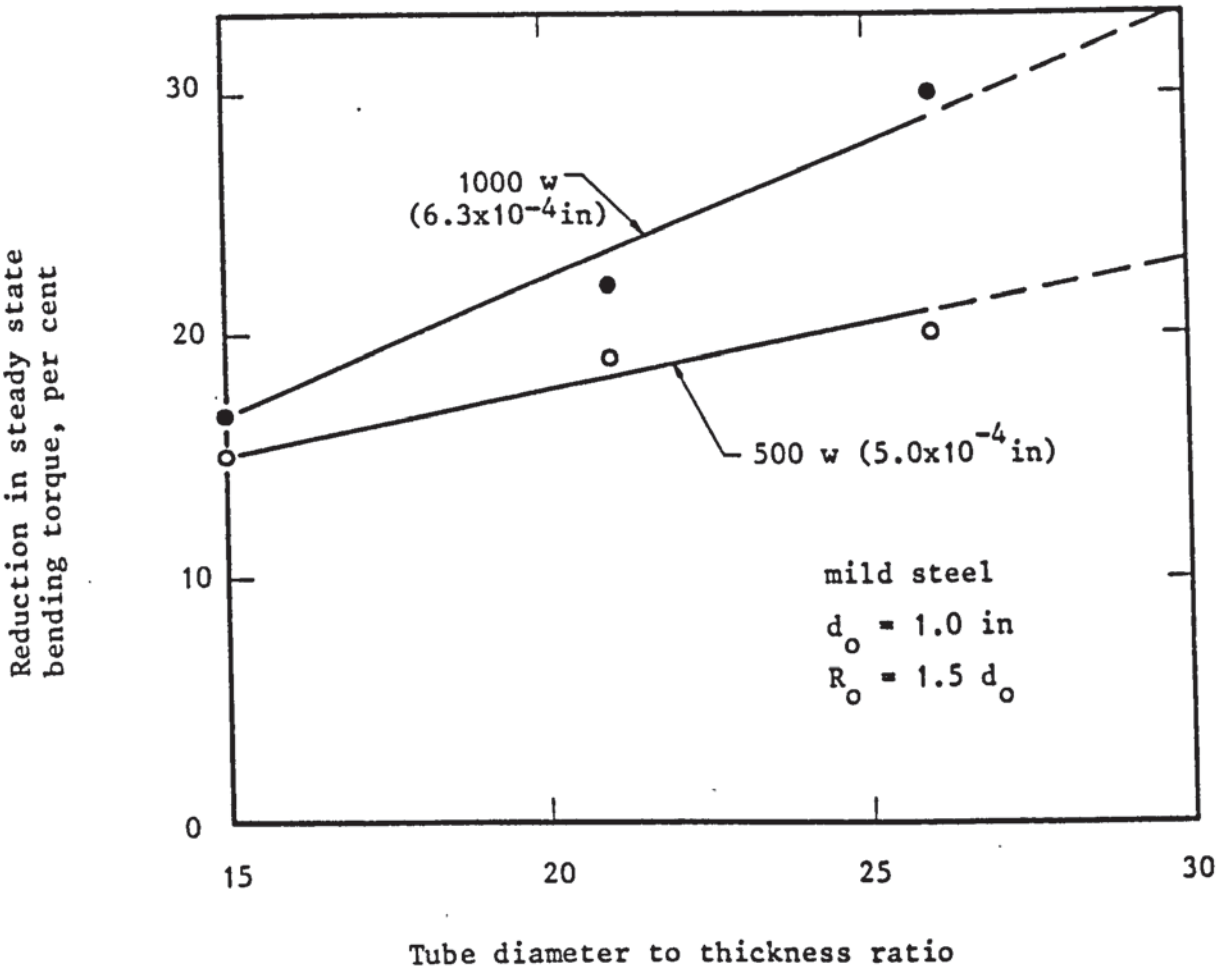

Figure 7.21: The reduction in the steady state bending torque (at about 180 degrees) vs. the tube diameter to thickness ratio for various levels of ultrasonic power (amplitudes of mandrel vibration)

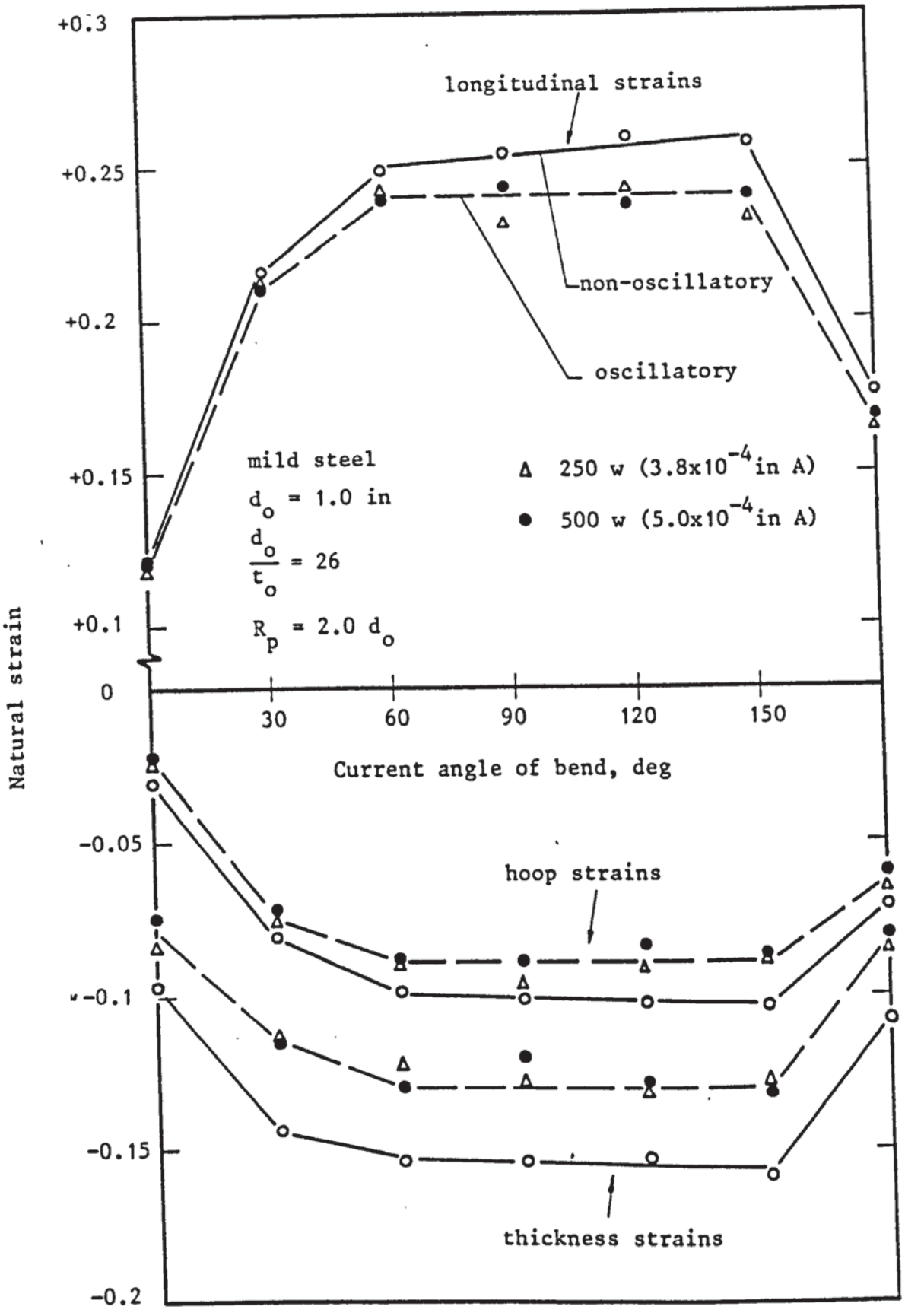

Figure 7.22: Distribution of longitudinal, hoop and thickness strains at the outer periphery of the bend with and without mandrel vibration at an ultrasonic frequency for different levels of power (amplitudes)

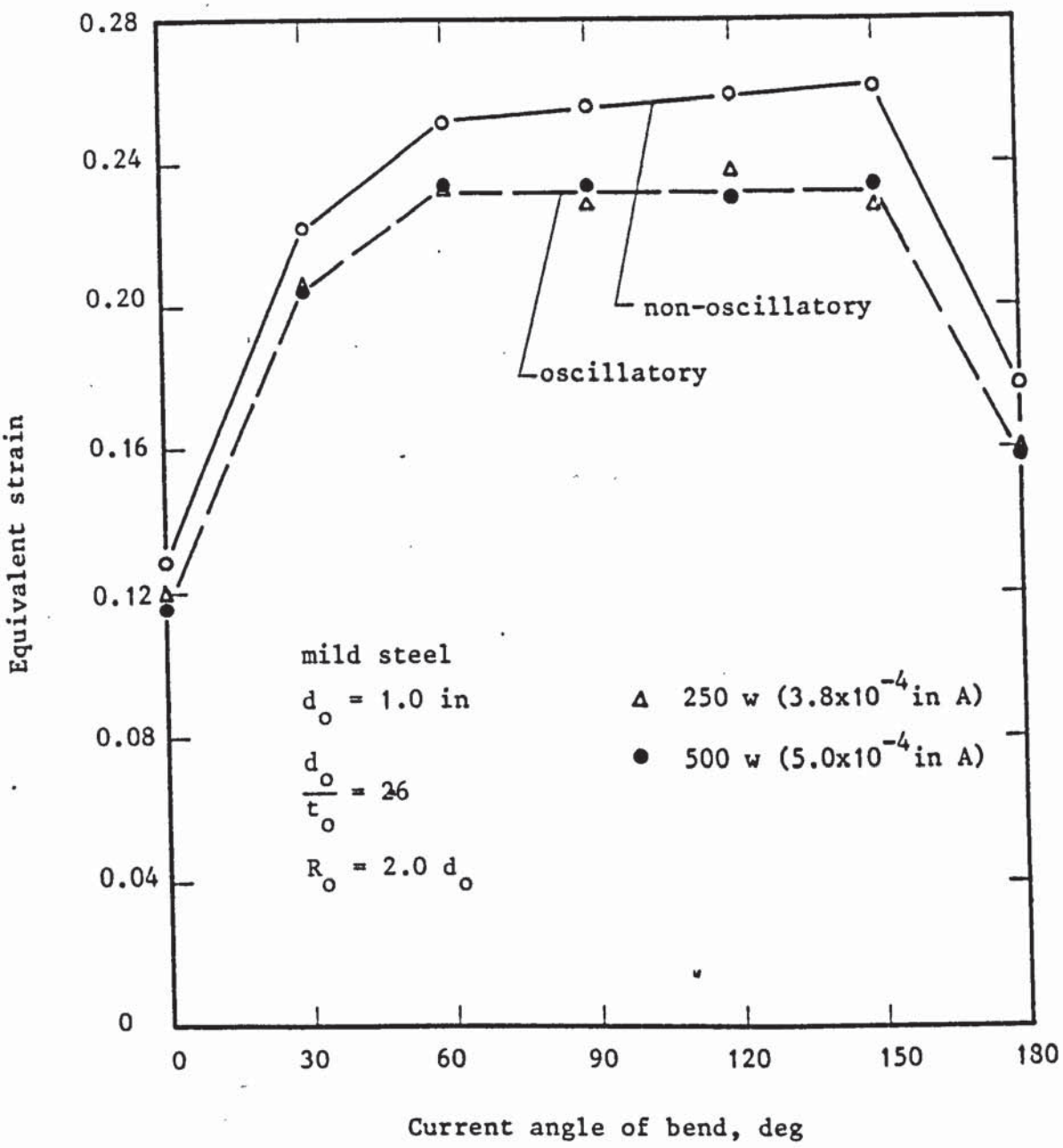

Figure 7.23: Distribution of equivalent strains at the outer periphery of the bend with and without mandrel vibration at an ultrasonic frequency for different levels of power (amplitudes)

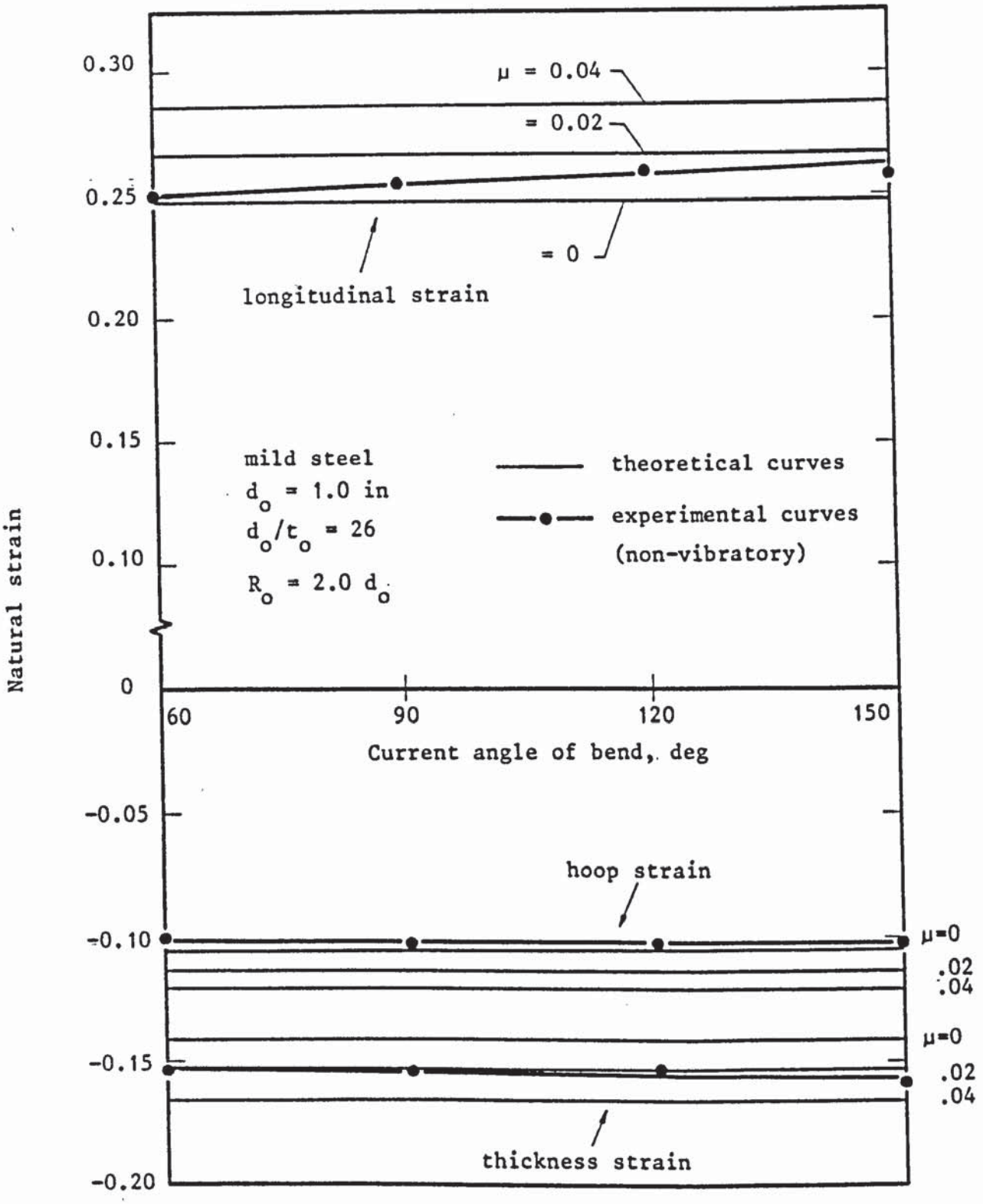

Figure 7.24: The variation of the longitudinal, hoop and thickness strains at the outer periphery of the bend with the current angle of bend under non-vibratory conditions

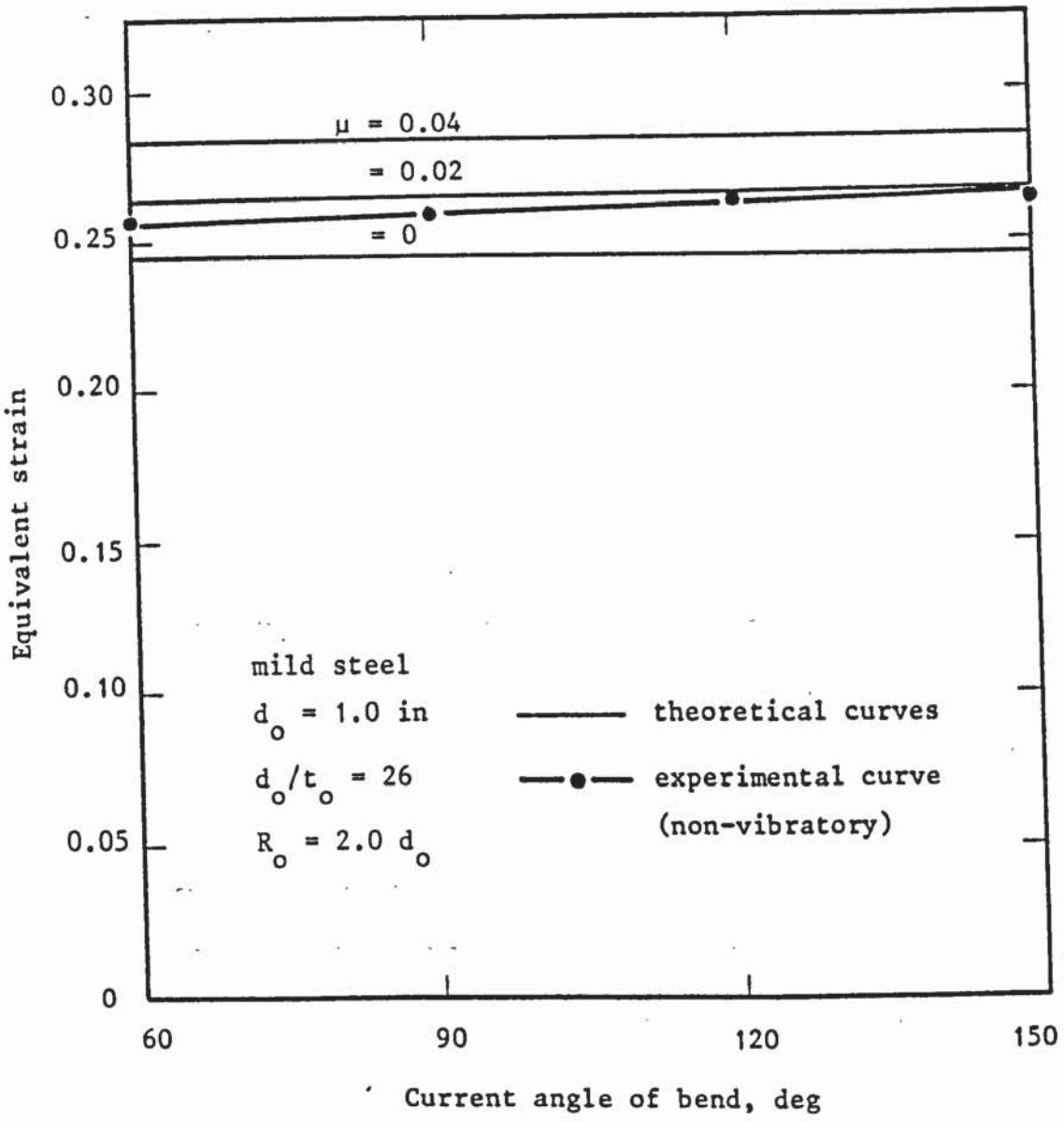

Figure 7.25: The equivalent strain on the outer periphery of the bend vs. the current angle of bend under non-vibratory conditions

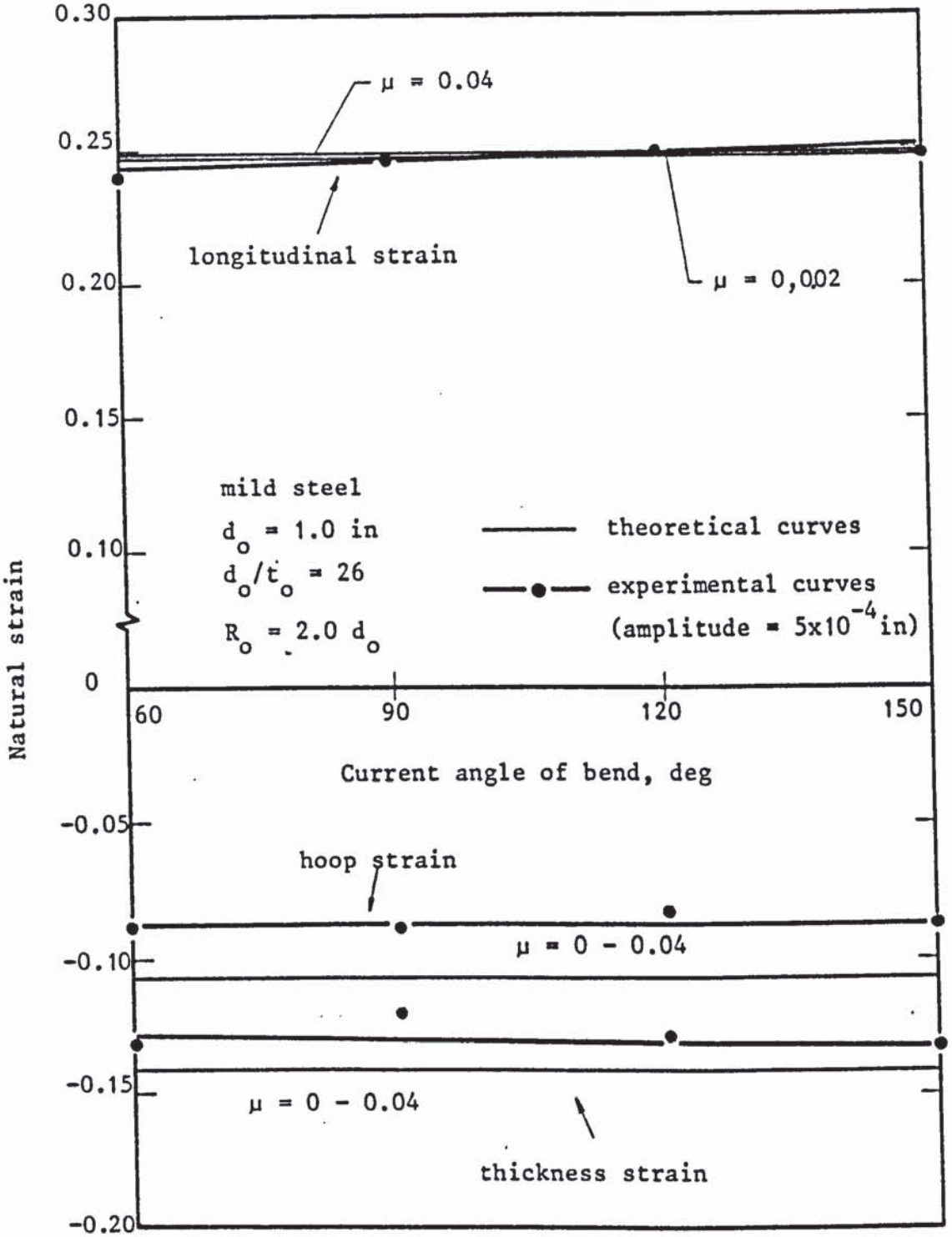

Figure 7.26: The variation of the longitudinal, hoop and thickness strains at the outer periphery of the bend with the current angle of bend under vibratory conditions

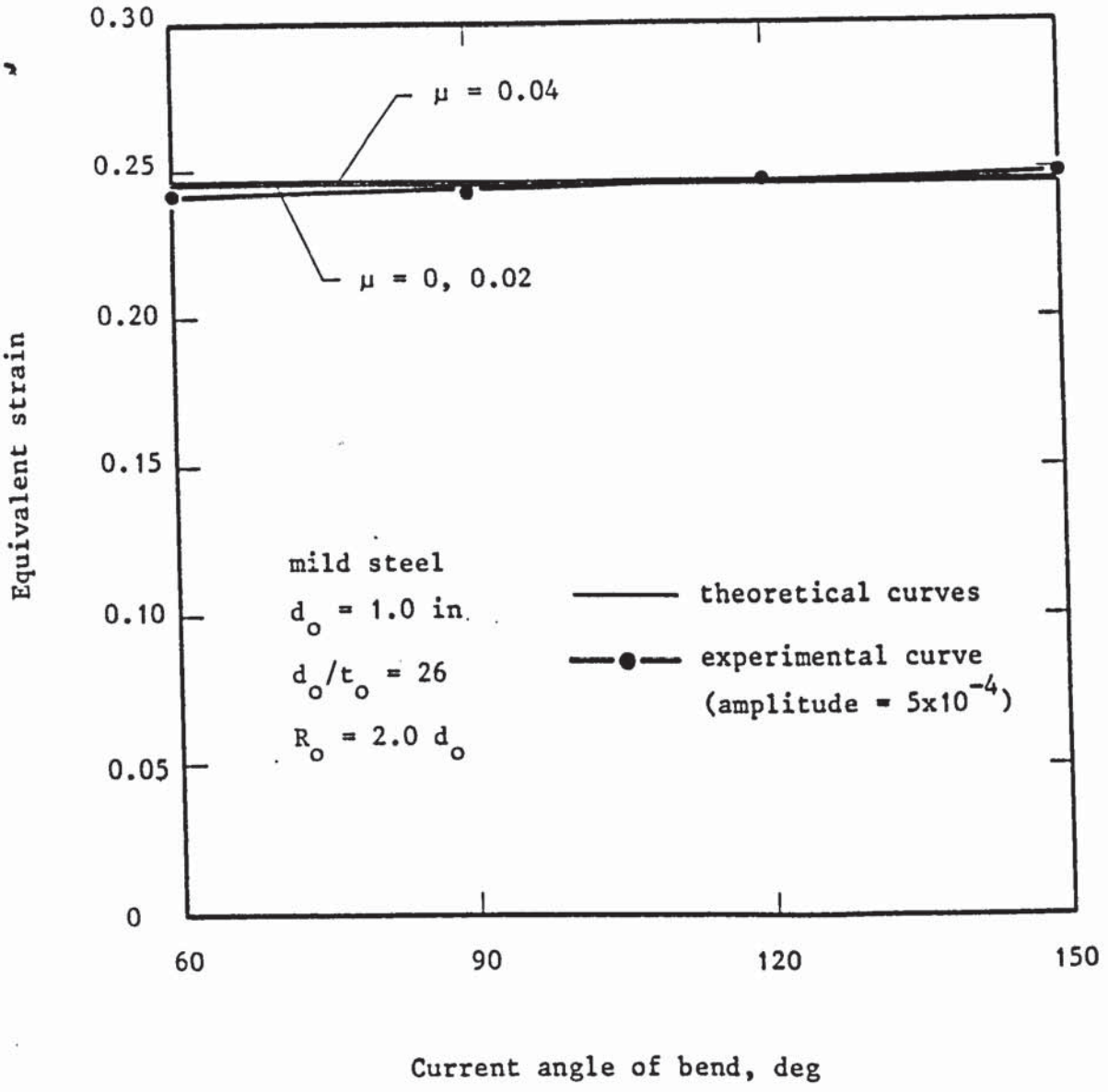

Figure 7.27: The equivalent strain on the outer periphery of bend vs. the current angle of bend under vibratory conditions

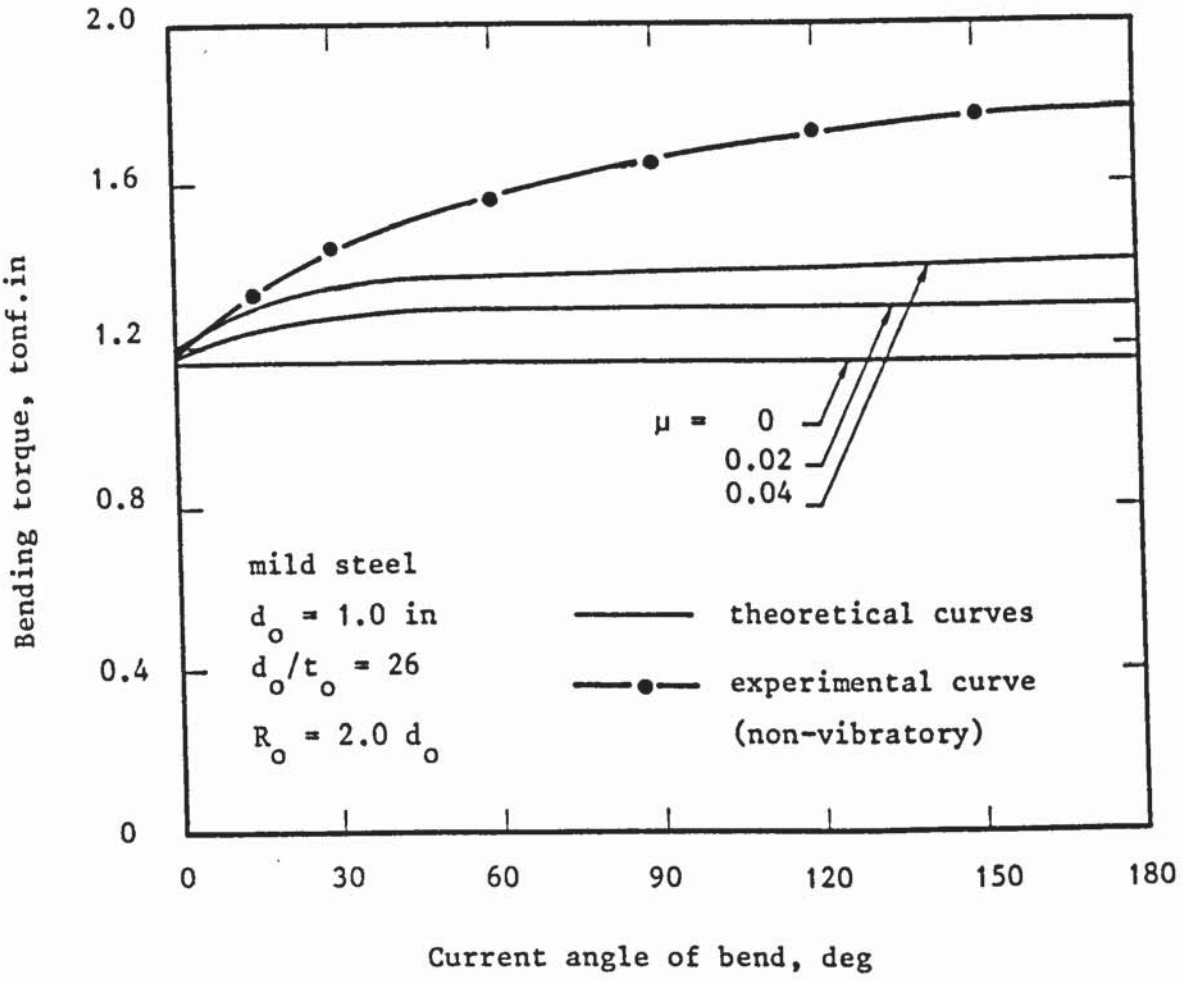

Figure 7.28: The progress of the bending torque with the current angle of bend under conventional conditions

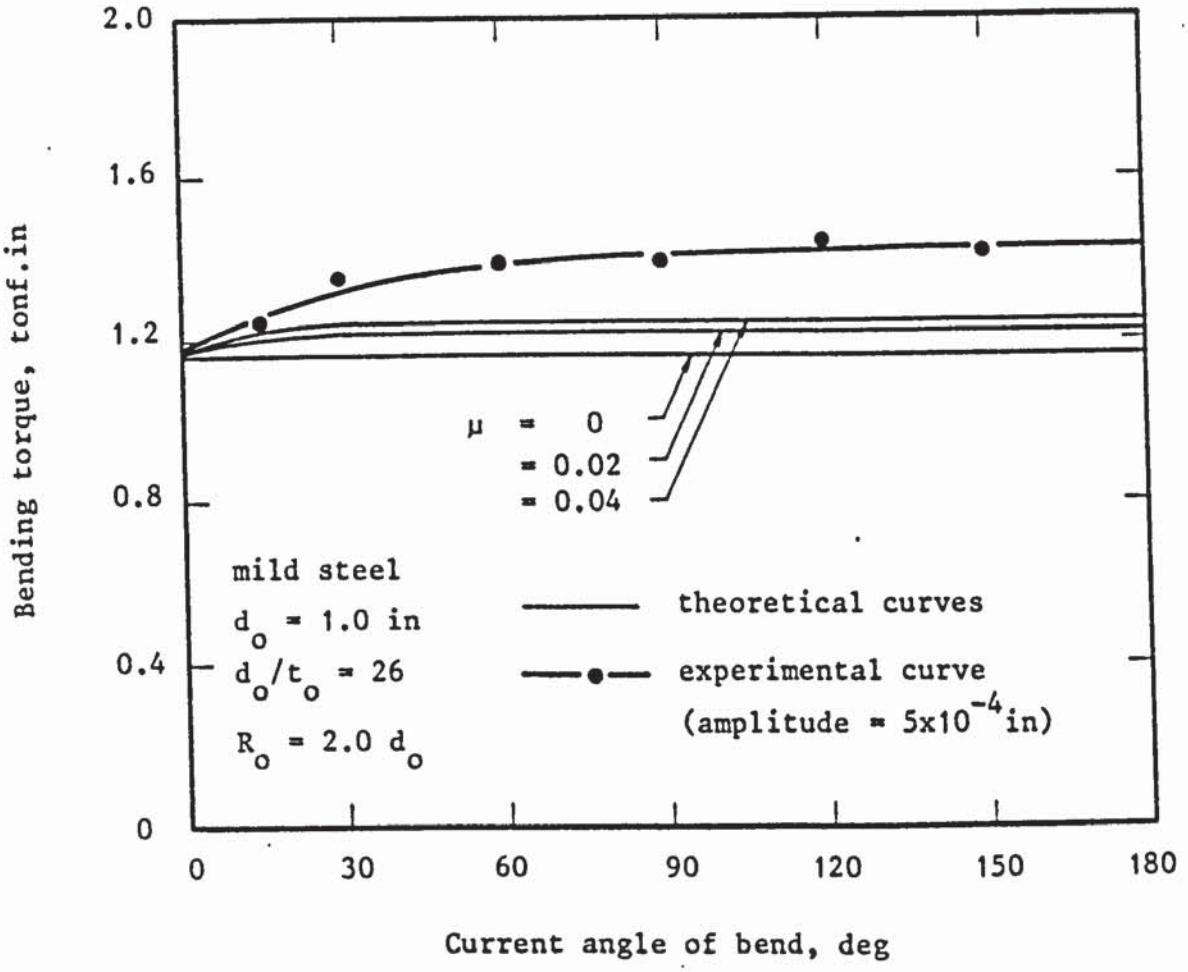

Figure 7.29: The progress of the bending torque with the current angle of bend with mandrel vibration

CHAPTER EIGHT

CONCLUSIONS

Referring to the discussion of the theoretical and experimental results for the mechanics of draw-bending of mild steel tubes with and without axial ultrasonic vibration of the supporting mandrel, the following main conclusions can be drawn:

1. During the process of tube draw-bending, the neutral plane moves inward from the central plane of the tube-section toward the centre of the bend. It was shown that as the mean bend radius becomes smaller, the displacement of the neutral plane increases.

2. The stresses and the strains developed during bending have maximum values at the outer and inner peripheries of the bend. Also, they are markedly higher for smaller bend radii and thus the producion of sharper bends is more difficult than bending to large radii.

3. The tube diameter to thickness ratio does not have a significant effect on the maximum stresses or strains at a constant mean bend radius for thin-walled tubes.

4. For a constant tube outside diameter, it was shown that the diameter to thickness ratio has a considerable influence on

the bending torque, while the mean bend radius has a less significant effect.

5. In the bending zone, the movement of the neutral plane closer to the centre of the bend increases with the increase in the initial friction force. This force results from the friction between the straight part of the tube and the supporting tools, and is largely affected by the slider force.

6. Friction causes an increase in the equivalent stresses and the equivalent strains at the outer periphery of the bend with the latter being the more significantly affected. On the bend inner periphery, the stresses and the strains decrease due to friction.

7. The additional straining of the tube material at the bend outer periphery due to friction causes an increase in the maximum longitudinal, hoop and thickness strains. The greatest effect of friction was observed on the thickness strain.

8. The bending forces were found to increase progressively with the angle of bend. These forces were significantly higher for thicker-walled tubes and/or tighter bend radii.

9. The continuous increase in the bending torque with the current angle of bend is largely dependent on the slider force and on the frictional conditions; the rate of increase was greater

for thicker-walled tubes. However, the percentage increase in the bending torque to overcome friction could be higher when bending thinner-walled tubes.

10. The application of ultrasonic vibrations to the process of tube draw-bending has proved to be advantageous. The benefits gained can be attributed to a substantial reduction in friction at the tube-mandrel interface.

11. The process forces were considerably reduced when the mandrel was axially vibrated at an ultrasonic frequency. The force reduction showed an increase with increasing the vibration amplitude.

12. The bending torque showed a reduction of up to 30 per cent under the vibratory conditions. The percentage amount of torque reduction was higher for larger tube diameter to thickness ratios and for smaller bend radii.

13. The longitudinal, hoop, thickness and equivalent strains at the outer periphery of the bend were reduced when the mandrel was axially vibrated. The most significant effect observed was on the maximum thinning of the tube-wall; a reduction of up to 15 per cent was achieved. It was also shown that the mandrel vibration caused the strains at the bend inner periphery to increase.

14. A substantial reduction in the mandrel force was observed

during the oscillatory bending tests. In some cases, the mandrel vibration caused the mean mandrel force to reverse from tension to compression.

15. The friction vector reversal combined with a reduction in the coefficient of friction can account for the changes in the forces and the strains developed during the oscillatory bending operation.

16. Draw-bending tubes over a vibrating mandrel can lead to several practical advantages which can help in increasing its industrial applications. Tubes may be bent, using conventional bending tools, to sharper radii with greater accuracy than those possible by conventional methods.

17. The developed theory was in good agreement with the measured values of the strains at the outer periphery of the bend under both vibratory and non-vibratory conditions. The predicted trend of the bending torque showed a reasonable correlation with the values recorded experimentally.

CHAPTER NINE

SUGGESTIONS FOR FURTHER WORK

The theoretical and experimental work reported in this thesis represents an extensive study into the mechanics and practice of the draw-bending of tubes. It also describes in detail a fundamental improvement of the process in which the supporting mandrel is axially vibrated at an ultrasonic frequency[76]. As a result of the experience gained and the conclusions drawn, further research is suggested in order to widen the scope of the investigation and provide for more generalisations.

(1) Bending different tube materials

Mild steel may be considered one of the most commonly used materials in many industrial applications of bent tubes. This made it a logical choice in deciding on the tube material used in the current project. However, other ferrous and non-ferrous materials are also in great demand. In addition to investigating the mechanics of bending such materials, it may be of great interest to relate the bending forces, torque and strains to the stress-strain properties of the tube material.

Draw-bending materials such as stainless steel and titanium alloys which are difficult-to-bend would benefit significantly from the use of ultrasonic vibrations. Obviously, these materials do have a high rate of strain-hardening which can result in greater bending forces and

torque than those recorded during bending mild steel tubes. In addition, there could be a large frictional component within the total work of deformation, which can cause an excessive thinning of the outer tube-wall periphery and also friction may limit the achievable minimum bend radii. For those two reasons, bending such materials is an ideal application for the ultrasonic vibrations.

The theoretical solution developed in this thesis can be used to assess the effect of the work-hardening characteristics of different tube materials on the mechanics of plastic deformation during bending. Theoretical data may be obtained using the available computer programme "UTB-INI" with only minor changes.

(2) Experiments with different tube sizes and bending speeds

Throughout the experiments of this research, the tube outside diameter was limited to 1 in and only one bending speed of 10 rev min^{-1} was used. However, further work is needed on bending tubes having different sizes and covering a wide range of bending speeds. This will allow the effect of such parameters to be evaluated on the bending torque and the developed strains during both oscillatory and non-oscillatory bending operations.

It is also proposed that tubes of constant diameter to thickness ratio but having different outside diameters should be bent to various mean bend radii conventionally and with the mandrel axially vibrating. It was shown that the tube diameter to thickness ratio has an insignificant effect on the strains developed in bending tubes of constant outside diameter. Changing the tube diameter, however, can have a considerable effect on the strain levels.

The experimental and theoretical results indicated that for the tube size and bending speed investigated, a power level in the range of 250 to 500 watt is sufficient to achieve a satisfactory reduction in the bending forces and strains. It was demonstrated that the reduction in friction at the tube-mandrel interface is largely due to the friction vector reversal which is influenced by the velocity ratio. Thus, bending large tubes or using higher bending speeds than those considered in the current research would require higher amplitudes of mandrel vibration to gain the same benefits during the oscillatory bending operation. Indeed high rates of production with the existence of automatic and sophisticated bending machines necessitate the use of relatively higher speeds than 10 rev min^{-1}.

(3) The use of other types of mandrel

In addition to the form-mandrel which was used throughout the current project, there are two other basic types of mandrel, namely: the plain mandrel (possibly with a hemispherical end) and the articulated or multi-ball mandrel. Further research may be carried out on bending thin-walled tubes using those and other types of mandrel.

Since the plain mandrel can be more economical and is usable for various bend radii, it may be of interest to examine the possibility of vibrating such a mandrel to produce good quality bends which are not achievable by conventional methods. The application of ultrasonic vibrations to the articulated mandrels may also deserve consideration in other investigations. The vibrations if successfully applied to the mandrel balls can achieve a substantial reduction in the existing high

friction forces when using this type of mandrel. However, it appears quite difficult to set-up a standing wave of vibration in the mandrel-balls.

It may also be of benefit to modify the reported theoretical analysis to consider the use of the plain and articulated mandrels. Theoretical results for the bending torque and the strains may then be obtained and compared with the experimental data.

(4) Investigating the effect of the mandrel advance

It was discussed that the advance of the mandrel beyond the tangent line has an influence on the bending torque and the developed strains during the bending operation. This is because it forces the tube material to stretch more on the ouside of the bend and also results in a higher pressure on the outside tube-wall with its consequential effect of high friction. It is suggested therefore that bending tests can be conducted with the mandrel set-up at different positions with respect to the tangent line, for various bend radii. Accordingly, the bending torque, the mandrel force, the distortion of tube-section and the strains can be established.

Taking into account the mandrel advance in the theoretical analysis will result in a more accurate prediction of the process parameters and the geometrical accuracy of the tube-section after bending.

(5) Prediction of the mandrel force

The developed theoretical analysis can be readily extended to derive expressions for the mandrel force, and the available computer

programme can be used for carrying out the calculations. Thus theoretical data will be obtained and these should be used to explain the experimental curves relating the variation of the mandrel force to the angle of bend under both vibratory and non-vibratory conditions. The effect of changing the process parameters, eg. the mean bend radius, the diameter to thickness ratio and the amplitude of mandrel vibration on the mandrel force and the torque should then be investigated.

(6) Bending thick-walled tubes and section tubing

The present research was concerned with bending thin-walled tubes to small bend radii. It may be of interest to investigate theoretically and experimentally the mechanics of bending thick-walled tubes. Such bends are greatly needed in several heavy technological applications such as in the chemical engineering and shipbuilding industries. Also, bending section tubing is difficult and complex, however the use of ultrasonic vibrations is likely to yield great benefits, and hence deserves extensive study. Section tubes are used in electronics, heavy and light engineering components and in architectural features.

(7) Determination of frictional conditions

The proposed theory underestimates the rate of increase in the bending torque with the current angle of bend. This was attributed to the underestimation of the initial friction force which is greatly influenced by the slider force. A more accurate estimating method of the initial friction force should be used, which should take into

consideration the friction between the tube and the wiper die and between the tube and the mandrel in the vicinity of the tangent line. One of the possible solutions is to measure experimentally the initial friction force at various values of the slider force with and without mandrel vibration. This may result in a more realistic relationship between the slider force and the initial friction force between the straight-part of the tube and the supporting tools. It would be desirable to monitor the frictional forces at the tube-slider and tube-wiper die interfaces. This would clarify the effect of ultrasonic vibrations on such forces.

It was observed that some of the oscillatory energy was transmitted through the tube-wall when a relatively high electrical power was used. It may be of interest, therefore, to measure practically the amplitude of tube vibration during the oscillatory bending tests and to examine its effect on the frictional conditions.

Bending tests may be performed using different grades of lubricants. The objectives should be the examination of the effectiveness of lubrication with the use of ultrasonic vibrations and the possibility of employing low quality and cheaper lubricants. Further, as the theoretical results indicated that the friction vector reversal due to the mandrel vibration is a dominant factor in reducing the mandrel friction, it may be possible to conduct 'dry' bending† tests which can confirm experimentally the frictional reversal effect. If proved satisfactory, 'dry' bending can be useful for some applications in which a dry clean surface of the tube bore is essential.

† 'dry' bending is used to convey the sense of bending tubes with dry lubricants.

(8) Establishing the minimum achievable bend radii

The research already undertaken has shown that tubes can be bent, with the axial vibration of the mandrel, to tighter radii than is possible by conventional methods. However, further theoretical and experimental work is needed in order to establish the minimum achievable bend radii round a former under conventional conditions for a variety of tube materials. The improvement expressed as the decrease in the minimum radius of bend with the application of ultrasonic vibrations to the tools can then be assessed. For example, mild steel tubes having different diameter to thickness ratios can be bent round formers of successively decreasing radii until the minimum radius is established before failure occurs.

(9) Development of other theoretical solutions

For the purpose of this investigation, the equilibrium of forces approach was adopted to arrive at a theoretical solution for the problem of draw-bending of tubes. It is suggested that other theoretical methods can be used to develop solutions to the same problem, which could then be utilised with the present solution to achieve a more accurate prediction of the process forces and strains. This may include the development of a theoretical model based on an energy method combined with the finite element technique.

(10) Practical implications of the ultrasonic tube bending process

The application of ultrasonic vibrations to the tube draw-bending

process has proved successful[77]. The careful consideration given to solving the theoretical and practical problems has contributed significantly to that success. Consequently, the new technology of ultrasonic tube-bending is very likely to be transferred soon to industry. For this industrial application to be successful, great care should be taken in accurately designing and tuning the oscillatory system, also in solving the practical problems which may arise. Indeed the laboratory conditions are quite different from those existing on the factory-floor. Therefore, a pilot research programme should be designed and experiments carried out using an experimental bending machine in industry. First, to develop and refine the new equipment and technique to suit the industrial environment. Special emphasis should be placed on the need of such equipment to be robust and simple to operate. Secondly, to assess the practical implications of this new development bearing in mind the particular needs and requirements of the bending technology and market. Thirdly, to achieve an optimum design of the integral system combining efficiently both the conventional and oscillatory equipment.

It is proposed to perform bending trials on a production basis such that: simple bending tools are employed, difficult or otherwise impossible bends are produced and savings in material and production costs are achieved.

REFERENCES

1. Colloff, N.J. — 'Preliminary results from tube bending trials with and without applied axial vibration of the supporting plug' unpublished report at the University of Aston in Birmingham, March (1979)

2. A non — 'Bending of rod, bar, tube and special shapes' Tools and Manuf. Engineers Handbook, SME, McGraw-Hill, 3rd edition, (1977), pp.16134-16144

3. Dewitt, E.J. and Alexander, F.D. — 'Cold bending of shapes' ASME Handbook, Metals Eng.-Processes, McGraw-Hill, New York, (1975), pp.153-166

4. Channing, J.K. — 'Tube bending' Booklet published by Power Dynamic Ltd, Hampshire, England, private communication

5. Stange, R.R. — 'Tooling specifications and bending techniques' Paper No. T-1070, Fab.Man.Ass., Inc., private communication

6. -Chamayou, -Garnier, -Duval and -Houdy — 'Le travail à froid des tubes en aciers inoxydables' Formage Traitements Métaux, May (1970) 15, pp.43-52

7. Corpet, P. — 'Le cintrage des tubes d'acier', Fils Tubes Bandes Profiles, Dec.(1977) 5, pp.28-32

8. Oehler, G. — 'Verfahren und Kräfte beim Rohbiegen' Mitt. Forsch. Ges. Blechver. (1968) 19, Nr.9, pp.121-127

9. Robinson, J.H. et al — 'Bending and forming of tubing' Metals Handbook, ASM, 8th edition, Vol.4, Forming, pp.308-317

10. Du Mez, F.M. 'Basic tube bending guide' Booklet published by H & H Tool Division, Teledyne Pines, private communication.

11. Krieg, A.H. 'Bending thin-walled pipe III' Welding Engineer, May (1972) 5, 57, pp.34,36,38-39

12. Du Mez, F.M. 'Precision and commercial tube bending tooling' Catalogue 651, H & H Tool Division, Teledyne Pines, private communication

13. Anon 'Tooling' Manufacturing Engineering and Management, Oct.(1972), Vol.69, No.4, pp.15-16

14. Stange, R.R. 'Bending ultrathinwall tubing' Machinery N.Y., March (1965), 71, pp.95-98

15. Stange, R.R. 'Draw bending tools' Catalogue No.1071, Tools for Bending, Inc., private communication

16. Weil, N.A., Brock, J.E. and Cooper, W.E. 'Stresses in a pipe bent to a circular arc' Trans. ASME, J.Eng. for Industry, Nov.(1961), pp.449-459

17. Inoue, K. and Mellor, P.B. 'Mechanics of radial draw bending of tube' Proc. 18th Int. Mach. Tool Des. Res. Conf., London, Sept. (1977), pp.127-131

18. Inoue, K. and Mellor, P.B. 'Radial-draw bending of stainless steel tube' J. of Mech.Working Tech., (1979), 3, pp.151-166

19. Inoue, K. 'Radial draw-bending of tube' MSc thesis, University of Bradford, (1978)

20. Kasim, A.H. 'Plastic-bending of thin-walled tubes'
PhD thesis, University of Bradford, (1982)

21. Möller, H. 'Wanddicken - Änderung und Unrundheiten an Rohrbögen'
Techn. Überwachung 2 (1961), Nr.4, pp.121-127

22. Oehler, G. 'Kaltbiegen von Rohren'
Klepzigs Fachberichte, 72(1964), Nr.11, pp.425-431

23. Sato, K. and Takahashi, S. 'Effects of anisotropy on the change in wall thickness during tube bending process'
J. of Japan Soc. for Tech. of Plasticity, Vol.23, No.252 (1982-1), pp.17-22

24. Franz, W.D. 'Über das Druckbiegen von Rohren auf Kaltem Wege'
Werkstatt und Betrieb, 98(1965), Nr.10, pp.748-752

25. Recker, B. und Buchmüller, H. 'Dornloses Kaltbiegen von Rohrschlangen mit kleinen Bieghalbmessern'
Energie, 16 (1964), Nr.9, pp.365-370

26. Stange, R. R. 'An incremental pressure die assist system in conjunction with conventional and empty bending tools'
Tools for Bending, Inc. (1982), private communication from R. Stange

27. Kasim, A.H. and Mellor, P.B. 'Development of strains in radial-draw bending of tube',
Proc. of Int. Tube Ass. Conf., Dec. (1980)

28. Sato, K., Uchida, F., Takahashi, S.,Ochiai, I. and Oizumi, K. 'Influence of the tube fabrication schedule on the anisotropy of copper tubes'
Metall, 35(1981), Nr.11, pp.1119-1123

29. Blaha, F. and Langenecker, B. 'Dehnung von Zink - Kristallen unter Ultraschalleinwirkung' Naturwissenschaften, 42(1955), 20, p.556.

30. Blaha, F. and Langenecker, B. 'Plastizitatsuntersuchungen von Metallkristallen in Ultraschallfeld' Acta Metall, 7(1959), pp. 93-100

31. Nevill, G.F., Jr. and Brotzen, F.R. 'The effect of vibrations on the static yield strength of low-carbon steel' Proc. Am. Soc. Test. Mat., 57(1957), pp.751-758

32. Pohlman, R. and Lehfeldt, E. 'Influence of ultrasonic vibration on metallic friction' Ultrasonics, Oct. (1966), pp.178-185

33. Winsper, C.E. and Sansome, D.H. 'The influence of oscillatory energy on the stresses during plastic deformation' J.I.M., 96(1968), pp.353-357

34. Langenecker, B. 'Workhardening of zinc crystals by high-amplitude ultasonic waves' Proc. Am. Soc. Test. Mat., 62(1962), p.602

35. Langenecker, B. 'Effect of sonic and ultrasonic radiation on safety factors of rockets and missiles', Am.Inst. Aeronaut Astronaut J., 1(1963), p.80

36. Langenecker, B., Frandsen, W.H., Fountain, C.W., Colberg, S.R. and Langenecker, J.A.M. 'Effects of ultrasound on deformation characteristics of structural metals' US Naval Ordnance Test Station, China Lake, California, NAVWEPS Rept.8482, NOTS TP 3447, March (1964)

37. Langenecker, B. 'Work hardening of zinc crystals by high amplitude ultrasonic wave' Proc. ASTM, 62(1962), p.602

38. Fridman, H.D. and Levesque, P.
'Reduction of static friction by sonic vibrations'
J.Appl.Phys., Oct.(1959), 30, pp.1572-1575

39. Severdenko, V.P., Stepaneko, A.V. and Zayash, I.V.
Dokl. Akad. Nauk BSSR, Vol.13, No.10, (1969)

40. Lenkiewicz, W.
'The sliding friction process - effect of external vibrations'
Wear, 13(1969), pp.99-108

41. Sansome, D.H.
'Fundamental principles of oscillatory metal working and their application'
published report at the Univ. of Aston in Birmingham

42. Eaves, A.E., Smith, A.W., Waterhouse, W.J. and Sansome, D.H.
'Review of the application of ultrasonic vibrations to deforming metals'
Ultrasonics, July (1975), pp.162-170

43. Green, R.E.
'Non-linear effects of high-power ultrasonics in crystalline solids'
Ultrasonics, May (1975), pp.117-127

44. Biddell, D.C. and Sansome, D.H.
'The development of oscillatory metal-drawing equipment - an engineer's view'
Ultrasonics, Sept.(1974), pp.195-205

45. Sansome, D.H.
'Recent developments in oscillatory metal working'
Engineering, April (1973)

46. Winsper, C.E., Dawson, G.R. and Sansome, D.H.
'An introduction to the mechanics of oscillatory metal working'
Metal and Materials, April (1970), pp. 158-162

47. Severdenko, V.P., Klubovich, V.V. and Stepaneko, A.V.
'Ultrasonic rolling and drawing of metals'
Consultants Bureau, New York and London, (1972)

48. Schmid, E.
'Plasticity of isonated metals'
Trans. Japan Inst. Metals, 9(1968), Suppl. 798

49. Langenecker, B., Jones, V.O. and Illievich, J. 'Metal plasticity in macrosonic fields' Proc. 1st Int. Symp. High-Power Ultrasonics, Sept. (1970), pp.83-87

50. Rothman, D. and Sansome, D.H. 'An investigation of rod-drawing with die rotation' Int. Jnl. Mach. Tool Des. & Res., 10 (1970), p.179

51. Severdenko, V.P. and Reznikov, Yu.N. 'The influence of ultrasonic oscillations in various directions in drawing metals' The Ductility and Working of Metals by Pressure, Nauka i Tekhnika, Minsk (1970)

52. Reznikov, Yu.N. Author's abstract of candidate's dissertation, BPI, Minsk (1966)

53. Severdenko, V.P., Stapaneko, A.V. and Vinerskii, S.N. 'A study of various ultrasonic drawing methods' Vesh Avad Navuk BSSR Ser Fiz Teuh-Navuk, 1 (1970)

54. Severdenko, V.P. et al 'Ultrasonic metal drawing parameters' Russian Ultrasonics, 1(1971), p.92

55. Nosal', V.V. and Rymsha, O.M. 'Reducing the drawing forces by ultrasonic oscillations of the drawplate and determining the technological parameters of tube drawing' Stal', 2(1966)

56. Zaporozhchenko, V.S. and Stepanenko, A.V. 'Calculation of tube-drawing stresses on a floating-mandrel with ultrasonics' Izv. VUZ Chern. Met., 12(1978), pp.74-77

57. Verderevskii, V.A., Nosal', V.V., et al Ultrasonic Technology TsINTIAM, 5(1964)

58. Winsper, C.E. and Sansome, D.H. 'Application of ultrasonic vibration to the plug drawing of tube' Metal Forming, 3 (1971), pp.71-75

59. Kolpashnikov, A.I., Savushkin, V.I. and Molodchinin, E.V. — 'Drawing of tubes of aluminium alloys with the use of ultrasound' Tsvetn Metall, 14 (1972), pp.60-62

60. Dragan, O. and Segal, E. — 'Cold drawing of carbon steel tubes under the influence of ultrasonics' Metalurgia (1970), pp.629-632

61. Dragan, O. — 'Cold drawing of tubes on an ultrasonically activated plug' Ultrasonics Int. (1973), Conf. Proc. pp.254-256

62. Segal, E. and Dragan, O. — 'Studies on the contact friction in the deformation area of cold drawn pipes on an ultrasonic activated piercer plug' Metalurgia, 24 (1972), 7, pp.469-471

63. Sugahara, T. et al. — 'Application of ultrasonic vibration to metal tube drawing process' Nippon Kokan Tech. Report - Overseas, Dec. (1970), pp.51-59

64. Dawson, G.R. — 'Ultrasonic radial die oscillations in floating-plug tube drawing' Ultrasonics Int. (1975), Conf.Proc., pp.206-209

65. Kariyawasam, V.P., Young, M.J.R. and Sansome, D.H. — 'An experimental and design study of fixed-plug tube-drawing with radial ultrasonic vibration of the die' Wire Industry, Feb. (1979), pp.104-108

66. McKaig, H.L. — 'The application of ultrasonic energy in the deformation of metals' Defence Metals Information Centre, Battell Memorial Inst., Columbus, Ohio, (1961)

67. Smith, A.W. — 'An investigation of the deep drawing process with the application of ultrasonic oscillations' PhD thesis, the University of Aston in Birmingham (1977)

68. Langenecker, B., Fountain, C.V. and Jones, V.O. — 'Ultrasonics: an aid to metal forming?' Metal Progress, April (1964), pp.97-101

69. Kristoffy, I. 'Metal forming with vibrating tools' Trans. ASME Jnl. Eng. Ind., Nov. (1969), pp. 1168-1174

70. Young, M.J.R. and Sansome, D.H. 'An oscillatory deep-drawing analogue'. 15th MTDR Conf., Sept. (1975), pp. 551-559

71. Smith, A.W. and Sansome, D.H. 'An experimental investigation of the effect of blank holder vibrations on an analogue of the deep-drawing process' Ultrasonics Int. Conf., March (1975), pp.210-213

72. Biddell, D.C. and Sansome, D.H. 'The deep-drawing of cans with ultrasonic radial oscillations applied to the die' Ultrasonics Int. Conf., March (1973), Conf. Proc., pp. 65-72

73. Johnson, W. and Mellor, P.B. 'Engineering plasticity' Van Nostrand Reinhold Ltd., London

74. Basily, B.B. 'The mechanics of section drawing' PhD thesis, The University of Aston in Birmingham (1976)

75. Stange, R.R. 'Rotary draw bending guide' Tools for Bending, Inc., Private communication.

76. Ibrahim, I.N. and Sansome, D.H. 'An experimental study of the mechanics of ultrasonic tube-bending' Ultrasonics International 83, Canada, July (1983)

77. Ibrahim, I.N. and Sansome, D.H. 'Ultrasonic tube bending: draw-bending apparatus and method' UK Patent No. 8318577, NRDC. 8 July (1983)

ACKNOWLEDGEMENTS

I am grateful to both the University of Aston in Birmingham and the Egyptian Government for financially supporting me.

I wish to express my deep gratitude to Professor D H Sansome for his continuing interest and invaluable discussions at all times.

My thanks to Mr G M Jones and Mr T Rudge for their assistance with the design and manufacture of the ultrasonic equipment and instrumentation.

My sincere thanks also to Dr N N Gindy for his help in many ways and for reading through the manuscript.

Finally, I am indebted to Mrs J Neale for typing this thesis with admirable patience.

****

APPENDICES

APPENDIX A

The computer programme and a sample of the output results

1. List of symbols in the computer programme "UTB-INI"

The input data:

DO	=	tube outside diameter
TO	=	initial wall-thickness of tube
Y	=	yield stress of tube material
H	=	strain-hardening coefficient
N	=	strain-hardening exponent
RO	=	mean radius of bend
ZT	=	current angle of bend
MU	=	coefficient of friction
MS	=	coefficient of friction at tube-slider interface
MM	=	coefficient of friction at tube-mandrel interface
MF	=	coefficient of friction at tube-former interface
NM	=	bending speed, rev min^{-1}
FRQ	=	frequency of mandrel vibration, Hz
AM	=	amplitude of mandrel vibration
CZT	=	angle of contact between the tube bore and the mandrel-tip, rad
FS	=	slider force
RM	=	mean radius of tube
AO	=	initial cross-sectional area of tube

The output results:

JIN	=	angular position of neutral plane
FI	=	the angle between any element of tube section and the neutral plane
VF0	=	vibratory initial friction force
F0	=	non-vibratory initial friction force
PF, BP	=	former pressure
PP, MP	=	mandrel pressure
DP, VP	=	pressure difference

in zone IIb:

LS, S1	=	longitudinal stress
HS, S2	=	hoop stress
RS, S3	=	radial stress
ES, GS	=	equivalent stress
FE, GE	=	equivalent strain
TC, AC	=	longitudinal natural strain
TH, AH	=	hoop natural strain
TT, AT	=	thickness natural strain
T1, T4	=	tube wall-thickness
A1	=	cross-sectional area of tube
R1	=	resultant of the internal forces in the longitudinal direction
Q1	=	bending torque
M1	=	bending moment

at the exit plane:

ELS, OS1	=	longitudinal stress
OS3	=	radial stress
EES, OGS	=	equivalent stress
EFE, OEE	=	equivalent strain

EC, OC	=	longitudinal natural strain
EH, OH	=	hoop natural strain
ET, OT	=	thickness natural strain
T3, T5	=	tube wall-thickness
A3	=	cross-sectional area of tube
R3	=	resultant of the internal forces in the longitudinal direction
Q3	=	bending torque
M3	=	bending moment

2. Listing of the computer programme "UTB-INI"

```
70 REM *** THE COMPUTER PROGRAMME "UTB-INI" FOR
75 REM THE MECHANICS OF TUBE BENDING WITH AND
80 REM WITHOUT MANDREL ULTRASONIC VIBRATION ***
90 GOTO 1690
92 REM *** SUBROUTINE 1 ***
95 REM *** REGION-C, ZONE-IIB ***
100 S1=(K4*VP+S2)/K5
110 GS=SQR (S1^2+S2^2+S3^2-S1*S2-S2*S3-S3*S1)
120 IF GS>25.796 THEN 170
130 IF GS>23.909 THEN 160
140 IF GS>Y THEN 150
150 GE=((GS-Y)/H1)^(1/N1)
160 GE=((GS-Y)/H2)^(1/N2)
170 GE=((GS-Y)/H3)^(1/N3)
180 ME=GE-YE
190 CL=RM*(SIN (F-DFI)-SIN (F))/(RO-RM*SIN (F-DFI))
200 CH=CL*(S1+S3-2*S2)/(S2+S3-2*S1)
210 CT=CL*(S1+S2-2*S3)/(S2+S3-2*S1)
220 CE=SQR (2*((CL-CH)^2+(CH-CT)^2+(CT-CL)^2)/9)
230 RETURN
232 REM *** SUBROUTINE 2 ***
235 REM *** REGION-C, ZONE-IIF ***
240 SO3=BP/2
250 OS1=S1+SS*(RO-RM*SIN (F))*CZT/T4
260 OGS=SQR (OS1^2+S2^2+SO3^2-OS1*S2-S2*SO3-SO3*OS1)
270 IF OGS>25.796 THEN 320
280 IF OGS>23.909 THEN 310
290 IF OGS>Y THEN 300
300 OEE=((OGS-Y)/H1)^(1/N1)
310 OEE=((OGS-Y)/H2)^(1/N2)
320 OEE=((OGS-Y)/H3)^(1/N3)
330 DGE=OEE-GE
340 DD=DGE/(2*OGS)
350 DC=DD*(S2+SO3-2*OS1)
360 DH=DD*(SO3+OS1-2*S2)
370 DT=DD*(OS1+S2-2*SO3)
400 OC=AC+DC
410 OH=AH+DH
420 OT=AT+DT
430 T5=T4*(1+DT)
440 EAD=RM*DFI*T5
450 ERD=-(OS1*EAD)
470 WF=DGE*(OGS+GS)/2
510 RETURN
512 REM *** SUBROUTINE 3 ***
520 REM ***PRINT-OUT OF RESULTS "COMPRESSION"***
530 PRINT "FI=";FI
540 PRINT "BP=";BP,"MP=";MP,"VP=";VP
550 PRINT "S1=";S1,"S2=";S2,"S3=";S3
560 PRINT "GS=";GS,"GE=";GE
570 PRINT "AC=";AC,"AH=";AH,"AT=";AT
580 PRINT "T4=";T4,"A1=";A1
590 PRINT "R1=";R1,"Q1=";Q1,"M1=";M1
600 PRINT "OS1=";OS1,"SO3=";SO3,"OGS=";OGS
610 PRINT "OEE=";OEE,"OC=";OC,"OH=";OH
620 PRINT "OT=";OT,"T5=";T5,"A3=";A3
630 PRINT "R3=";R3,"Q3=";Q3,"M3=";M3
645 PRINT
650 RETURN
```

```
652 REM *** SUBROUTINE 4 ***
660 REM ***REGIONS-A&B ,ZONE-IIB***
670 LS=(K1*DP+C4*HS)/K2
680 ES=SQR (LS^2+HS^2+RS^2+LS*HS-HS*RS+RS*LS)
690 IF ES>25.796 THEN 740
700 IF ES>23.909 THEN 730
710 IF ES>Y THEN 720
720 FE=((ES-Y)/H1)^(1/N1)
730 FE=((ES-Y)/H2)^(1/N2)
740 FE=((ES-Y)/H3)^(1/N3)
750 ME=FE-XE
760 BL=RM*(SIN (F)-SIN (F-C4*DFI))/(RM*SIN (F-C4*DFI)+C4*R0)
770 BH=BL*(RS-LS-2*HS)/(2*LS+HS+RS)
780 BT=BL*(HS-LS-2*RS)/(2*LS+HS+RS)
790 BE=SQR (2*((BL-BH)^2+(BH-BT)^2+(BT-BL)^2)/9)
800 RETURN
808 REM *** SUBROUTINE 5 ***
810 REM ***REGIONS-A&B ,ZONE-IIF***
830 IF AM<.0000000001 THEN 900
840 VRT=.10472*NM*(R0+RM*SIN (F))
850 A2A=.9*AM
860 XV=VRT*CZT
870 ZV=OMG*A2A*SIN (CZT)
880 VG=.63662*ATN (XV/SQR (ZV^2-XV^2))
890 ELS=LS+SS*(R0+C4*RM*SIN (F))*CZT*VG/T1
895 GOTO 910
900 ELS=LS+SS*(R0+C4*RM*SIN (F))*CZT/T1
910 EES=SQR (ELS^2+HS^2+RS^2+ELS*HS-HS*RS+RS*ELS)
920 IF EES>25.796 THEN 970
930 IF EES>23.909 THEN 960
940 IF EES>Y THEN 950
950 EFE=((EES-Y)/H1)^(1/N1)
960 EFE=((EES-Y)/H2)^(1/N2)
970 EFE=((EES-Y)/H3)^(1/N3)
980 DGE=EFE-FE
990 DD=DGE/(2*EES)
1000 DC=DD*(2*ELS+HS+RS)
1010 DH=DD*(RS-ELS-2*HS)
1020 DT=DD*(HS-ELS-2*RS)
1050 EC=TC+DC
1060 EH=TH+DH
1070 ET=TT+DT
1080 T3=T1*(1+DT)
1090 EAD=RM*DFI*T3
1100 ERD=ELS*EAD
1110 WF=DGE*(EES+ES)/2
1130 A2=A2+EAD
1140 A3=2*A2
1150 R2=R2+ERD
1160 R3=2*R2
1230 EMD=C5*ERD*RM*SIN (FI)
1240 M2=M2+EMD
1250 M3=2*M2
1270 TF=WF*(R0+C4*RM*SIN (F))*EAD
1280 QF=QF+2*TF
1285 Q3=Q1+QF
1290 RETURN
```

```
1302 REM *** SUBROUTINE 6 ***
1310 REM ***CAL OF BASIC PROCESS PARAMETERS***
1320 TC=TC+BL
1330 TH=TH+BH
1340 TT=TT+BT
1350 T1=T1*(1+BT)
1360 DA=RM*DFI*T1
1370 DR=LS*DA
1430 A=A+DA
1440 A1=2*A
1450 R=R+DR
1460 R1=2*R
1470 DQ=DR*(RO+C4*RM*SIN (F))
1480 Q=Q+DQ
1490 Q1=2*Q
1500 DM=C5*DR*RM*SIN (FI)
1510 M=M+DM
1520 M1=2*M
1530 RETURN
1532 REM *** SUBROUTINE 7 ***
1540 REM ***PRINT-OUT OF RESULTS "TENSION" ***
1550 PRINT "FI=";FI
1560 PRINT "PF=";PF,"PP=";PP,"DP=";DP
1570 PRINT "LS=";LS,"HS=";HS,"RS=";RS
1580 PRINT "ES=";ES,"FE=";FE
1590 PRINT "TC=";TC,"TH=";TH,"TT=";TT
1600 PRINT "T1=";T1,"A1=";A1
1610 PRINT "R1=";R1,"Q1=";Q1,"M1=";M1
1620 PRINT "ELS=";ELS,"EES=";EES,"EFE=";EFE
1630 PRINT "EC=";EC,"EH=";EH,"ET=";ET
1640 PRINT "T3=";T3,"A3=";A3
1650 PRINT "R3=";R3,"Q3=";Q3,"M3=";M3
1670 PRINT
1680 RETURN
1690 REM ***THE FOLLOWING ARE THE DATA***
1700 DO=1
1710 TO=.048
1720 Y=20.27
1730 H1=351
1740 H2=63
1750 H3=35.4
1760 N1=1.56
1770 N2=.928
1780 N3=.667
1790 RO=2
1800 ZT=150
1810 MU=.04
1820 MS=MU
1830 MM=MU
1840 MF=MU
1850 NM=10
1860 FRQ=0
1870 AM=0
1880 CZT=.506
1890 FS=.3
1910 RM=(DO-TO)/2
1920 AO=6.2832*RM*TO
```

```
1940 PRINT "DATA ARE:"
1950 PRINT "DO=";DO,"TO=";TO,"AO=";AO
1960 PRINT "Y=";Y,"H1=";H1,"H2=";H2
1970 PRINT "H3=";H3,"N1=";N1,"N2=";N2
1980 PRINT "N3=";N3,"RO=";RO,"MU=";MU
1990 PRINT "NM=";NM,"FRQ=";FRQ,"AM=";AM
2000 PRINT "CZT=";CZT,"ZT=";ZT,"FS=";FS
2010 PRINT
2020 REM ***ZONE-I***
2030 REM ***CAL OF THE INITIAL FRICTION FORCE***
2040 IF AM<.0000000001 THEN 2120
2050 VTM=.10472*NM*RO
2060 OMG=6.2832*FRQ
2070 AIA=.5487*AM
2080 GV=ATN (VTM/SQR ((OMG*AIA)^2-VTM^2))
2090 VFO=(1.5708*MS+GV*MM)*FS
2100 PRINT "GV=";GV,"VFO=";VFO
2110 GOTO 2140
2120 FO=1.5708*(MS+MM)*FS
2130 PRINT "FO=";FO
2135 REM *** ZONE-IIB ***
2140 REM ***TENSION***
2150 PRINT "TENSION"
2160 REM ***AT THE NEUTRAL PLANE***
2165 PRINT " AT THE NEUTRAL PLANE "
2170 JIN=.14
2190 FI=0
2200 B1=RM/TO
2210 F=JIN-FI
2220 Z=RM/(RO-RM*SIN (F))
2230 B2=Z*SIN (F)
2240 PF=.144
2250 RS=PF/2
2260 B3=B1*PF
2270 C1=1-B2+B2^2
2280 C2=RS+B3-2*B2*B3+B2*RS
2290 C3=B3^2+RS^2-B3*RS-Y^2
2300 LS=(SQR (C2^2-4*C1*C3)-C2)/(2*C1)
2310 HS=B3-B2*LS
2320 ES=SQR (LS^2+HS^2+RS^2+LS*HS+RS*LS-HS*RS)
2330 PRINT "JIN=";JIN,"PF=";PF,"RS=";RS
2340 PRINT "LS=";LS,"HS=";HS,"ES=";ES
2390 T1=TO
2400 FE=0
2410 NP=1
2420 NR=0
2430 NF=(JIN-.01-.005)/.01
2440 REM ***REGION-A***
2450 PRINT "REGION-A"
2460 FOR I=.01 TO JIN-.01+.004 STEP .01
2470 NR=NR+1
2480 C4=-1
2490 C5=1
2500 FI=I
2510 F=JIN-FI
2520 DFI=.01
2530 Z1=RM/(RO-RM*SIN (F))
```

```
2540 D=Z1*COS (F)*DFI
2550 E=D*LS
2560 HS=HS-E
2570 K1=RM/T1
2580 K2=Z1*SIN (F)
2590 XE=FE
2600 PF=PF+.0005
2610 PP=0
2620 RS=(PF+PP)/2
2630 DP=PF-PP
2640 LS=(K1*DP-HS)/K2
2650 IF LS<= 0 THEN 2600
2660 ES=SQR (LS^2+HS^2+RS^2+LS*HS-HS*RS+RS*LS)
2670 IF ES<= Y THEN 2600
2680 IF ES>25.796 THEN 2730
2690 IF ES>23.909 THEN 2720
2700 IF ES>Y THEN 2710
2710 FE=((ES-Y)/H1)^(1/N1)
2720 FE=((ES-Y)/H2)^(1/N2)
2730 FE=((ES-Y)/H3)^(1/N3)
2740 ME=FE-XE
2750 IF ME<= 0 THEN 2600
2760 GOSUB 760
2770 G=ME-BE
2780 IF G<= 0 THEN 2600
2790 PF=PF-.0002
2800 DP=PF
2810 RS=PF/2
2820 GOSUB 660
2830 GX=ME-BE
2840 IF GX>= 0 THEN 2790
2850 PF=PF+.00002
2860 DP=PF
2870 RS=PF/2
2880 GOSUB 660
2890 GY=ME-BE
2900 IF GY<= 0 THEN 2850
2910 PF=PF-.000002
2920 DP=PF
2930 RS=PF/2
2940 GOSUB 660
2950 GZ=ME-BE
2960 IF GZ>= 0 THEN 2910
2970 GOSUB 1320
2980 SS=MF*PF
2990 GOSUB 810
3000 NA=NR/10
3002 IF NR>NF THEN 3010
3004 IF NA=NP THEN 3010
3006 IF NA<NP THEN 3030
3010 GOSUB 1550
3020 NP=NP+1
3030 NEXT I
```

```
3032 REM *** AT THE CENTRAL PLANE ***
3035 PRINT " AT THE CENTRAL PLANE "
3040 FI=JIN
3050 DFI=.01
3060 C4=-1
3070 C5=1
3080 Z1=RM/RO
3090 D=Z1*DFI
3100 E=D*LS
3110 HS=HS-E
3120 K1=RM/T1
3130 DP=HS/K1
3140 PP=0
3150 PF=DP+PP
3160 RS=(PF+PP)/2
3170 EX=ES
3180 LS=LS+.01
3190 ES=SQR (LS^2+HS^2+RS^2+LS*HS-HS*RS+RS*LS)
3200 IF ES<= EX THEN 3180
3210 GOSUB 690
3220 IF ME<= BE THEN 3180
3230 GOSUB 1320
3240 SS=MF*PF
3250 GOSUB 810
3260 GOSUB 1550
3270 NP=NP-1
3280 NR=NR+1
3290 REM ***REGION-B***
3300 PRINT "REGION-B"
3310 FOR I=JIN+.01 TO 1.5708+JIN STEP .01
3320 NR=NR+1
3330 C4=1
3340 C5=1
3350 FI=I
3360 F=FI-JIN
3370 DFI=.01
3380 Z1=RM/(RO+RM*SIN (F))
3390 D=Z1*COS (F)*DFI
3400 E=D*LS
3410 HS=HS-E
3420 K1=RM/T1
3430 K2=Z1*SIN (F)
3440 XE=FE
3450 PF=0
3460 PP=PP+.01
3470 DP=PP
3480 RS=PP/2
3490 LS=(K1*DP+HS)/K2
3500 ES=SQR (LS^2+HS^2+RS^2+LS*HS-HS*RS+RS*LS)
3510 IF ES<= Y THEN 3460
3520 IF ES>25.796 THEN 3570
3530 IF ES>23.909 THEN 3560
3540 IF ES>Y THEN 3550
3550 FE=((ES-Y)/H1)^(1/N1)
3560 FE=((ES-Y)/H2)^(1/N2)
3570 FE=((ES-Y)/H3)^(1/N3)
3580 ME=FE-XE
```

```
3590 IF ME<= 0 THEN 3460
3600 GOSUB 760
3610 G=ME-BE
3620 IF G<= 0 THEN 3460
3630 PP=PP-.0005
3640 DP=PP
3650 RS=PP/2
3660 GOSUB 660
3670 GX=ME-BE
3680 IF GX>= 0 THEN 3630
3690 PP=PP+.00005
3700 DP=PP
3710 RS=PP/2
3720 GOSUB 660
3730 GY=ME-BE
3740 IF GY<= 0 THEN 3690
3750 PP=PP-.000005
3760 DP=PP
3770 RS=PP/2
3780 GOSUB 660
3790 GZ=ME-BE
3800 IF GZ>= 0 THEN 3750
3810 GOSUB 1320
3820 SS=MM*PP
3830 GOSUB 810
3840 NA=NR/10
3842 IF NA=NP THEN 3850
3844 IF I>1.563+JIN THEN 3850
3846 IF NA<NP THEN 3870
3850 GOSUB 1550
3860 NP=NP+1
3870 NEXT I
3880 REM ***COMPRESSION***
3890 PRINT "COMPRESSION"
3900 REM ***AT THE NEUTRAL PLANE***
3910 PRINT " AT THE NEUTRAL PLANE "
3920 FI=0
3930 F=FI+JIN
3960 Z=RM/(RO-RM*SIN (F))
3970 B1=RM/TO
3980 B2=Z*SIN (F)
3990 BP=.51
4000 MP=0
4010 VP=MP-BP
4020 S3=(MP+BP)/2
4030 B3=B1*VP
4040 C1=1-B2+B2^2
4050 C2=B3-2*B2*B3-B2*S3-S3
4060 C3=B3^2+S3^2+B3*S3-Y^2
4070 S1=(SQR (C2^2-4*C1*C3)-C2)/(2*C1)
4080 S2=B2*S1-B3
4090 GS=SQR (S1^2+S2^2+S3^2-S1*S2-S2*S3-S3*S1)
4100 PRINT "BP=";BP,"MP=";MP,"S3=";S3
4110 PRINT "S1=";S1,"S2=";S2,"GS=";GS
4120 PRINT
4160 T4=TO
4170 GE=0
4172 NP=1
4174 NR=0
```

```
4180 REM ***REGION-C***
4190 PRINT "REGION-C"
4200 FOR J=.01 TO 1.5708-JIN STEP .01
4210 NR=NR+1
4220 FI=J
4230 F=FI+JIN
4240 DFI=.01
4250 Z2=RM/(RO-RM*SIN (F))
4260 D=Z2*COS (F)*DFI
4270 E=D*S1
4280 S2=S2-E
4290 K4=RM/T4
4300 K5=Z2*SIN (F)
4310 YE=GE
4320 VP=VP+.02
4330 MP=BP+VP
4340 S3=(BP+MP)/2
4350 GOSUB 100
4360 G=ME-CE
4370 IF G<0 THEN 4320
4380 VP=VP-.001
4390 MP=BP+VP
4400 S3=(BP+MP)/2
4410 GOSUB 100
4420 GX=ME-CE
4430 IF GX>0 THEN 4380
4440 VP=VP+.0001
4450 MP=BP+VP
4460 S3=(BP+MP)/2
4470 GOSUB 100
4480 GY=ME-CE
4490 IF GY<0 THEN 4440
4500 VP=VP-.00001
4510 MP=BP+VP
4520 S3=(BP+MP)/2
4530 GOSUB 100
4540 GZ=ME-CE
4550 IF GZ>0 THEN 4500
4560 AC=AC+CL
4570 AH=AH+CH
4580 AT=AT+CT
4590 T4=T4*(1+CT)
4600 DA=RM*DFI*T4
4610 C4=-1
4620 C5=-1
4630 DR=-(S1*DA)
4650 GOSUB 1430
4660 SS=MF*BP
4670 GOSUB 240
4680 GOSUB 1130
4682 NA=NR/10
4684 IF NA=NP THEN 4690
4686 IF J>1.563-JIN THEN 4690
4688 IF NA<NP THEN 4700
4690 GOSUB 520
4692 NP=NP+1
4700 NEXT J
10000 END
```

3. A sample of the output results

```
DATA ARE:
DO= 1                    TO= .048                 AO= .1435E85536
Y= 20.27                 H1= 351                  H2= 63
H3= 35.4                 N1= 1.56                 N2= .928
N3= .667                 RO= 2                    MU= .04
NM= 10                   FRQ= 0                   AM= 0
CZT= .506                ZT= 150                  FS= .3

FO= .0376992
TENSION
 AT THE NEUTRAL PLANE
JIN= .14                 PF= .144                 RS= .072
LS= 19.8525828516        HS= .746021311306        ES= 20.27
REGION-A
FI= .1
PF= .044444              PP= 0                    DP= .044444
LS= 23.1037399616        HS= .223427567521        RS= .022222
ES= 23.2272183576        FE= 2.41895830749E-2
TC= .024241572061        TH=-1.24683463679E-2     TT=-1.17732256929E-2
T1= 4.74378697249E-2     A1= 4.54020956478E-3
R1= 9.955247910038E-2     Q1= .195129022935        M1= 2.6494493626E-3
ELS= 23.1413042606       EES= 23.2647816012       EFE= 2.46517025014E-2
EC= 2.47036785255E-2     EH=-1.27023970816E-2     ET=-1.20012814437E-2
T3= 4.74270512459E-2     A3= 4.5386737297E-3
R3= 9.98636853218E-2     Q3= .195266321441        M3= 2.65614222362E-3

FI= .13
PF= .011214              PP= 0                    DP= .011214
LS= 23.7467574187        HS= 5.61403284381E-2     RS= .005607
ES= 23.7776713563        FE= 3.12446787275E-2
TC= 3.14304166703E-2     TH=-1.60859180034E-2     TT=-1.53444986667E-2
T1= 4.72686577368E-2     A1= 5.89181326098E-3
R1= .131366424176        Q1= .2584548584          M1= 4.46302162284E-3
ELS= 23.756338024        EES= 23.7872519454       EFE= .031372710989
EC= 3.15584487151E-2     EH=-1.61501380184E-2     ET=-1.54083106966E-2
T3= 4.72656414278E-2     A3= 5.89011270094E-3
R3= .131699461373        Q3= .258607705307        M3= 4.47092395194E-3

 AT THE CENTRAL PLANE
FI= .14
PF=-3.7433025067E-5      PP= 0                    DP=-3.7433025067E-5
LS= 23.7867574187        HS=-3.769542184E-4       RS=-1.87165125335E-5
ES= 23.7865595853        FE= 3.13634526426E-2
TC= 3.38215199024E-2     TH=-.017281442611        TT=-1.65400772912E-2
T1= .04721214434         A1= 6.3412728751E-3
R1= .142057610986        Q1= .27978634282         M1= 5.17315722006E-3
ELS= 23.7867253998       EES= 23.7865275664       EFE= .03136302450 3
EC= 3.38210917628E-2     EH=-.017281228546        ET=-1.65398632166E-2
T3= 4.72121544467E-2     A3= 6.33957241128E-3
R3= .142390636081        Q3= .279939180594        M3= 5.18105874528E-3
```

REGION-B

FI= .2

PF= 0	PP= .068445	DP= .068445
LS= 24.9115297898	HS=-.343698946447	RS= .0342225
ES= 24.7589548878	FE= 4.52256977271E-2	
TC= 4.80088224369E-2	TH=-2.42798615316E-2	TT=-2.37389609051E-2
T1= 4.68737567415E-2	A1= 9.0267543866E-3	
R1= .20771387741	Q1= .412198199816	M1= 1.06194453838E-2
ELS= 24.9714822023	EES= 24.8189020746	EFE= 4.61341982029E-2
EC= 4.89172439151E-2	EH=-2.47236968577E-2	ET=-2.41935470573E-2
T3= 4.68519798432E-2	A3= 9.02436020026E-3	
R3= .208122705096	Q3= .412418650722	M3= .010633922406

FI= .3

PF= 0	PP= .185615	DP= .185615
LS= 26.5789391103	HS=-.934446005422	RS= .0928075
ES= 26.1732434331	FE= .068188994868	
TC= 7.10813724278E-2	TH=-3.53223746559E-2	TT=-3.57589977715E-2
T1= 4.63129065917E-2	A1= 1.34597180986E-2	
R1= .322293663808	Q1= .647636676148	M1= .024393833147
ELS= 26.747328401	EES= 26.3415360459	EFE= 7.11241296656E-2
EC= 7.40148328367E-2	EH=-3.67032577166E-2	ET=-3.73115751197E-2
T3= .046241002222	A3= 1.34527502275E-2	
R3= .323109196478	Q3= .648320330624	M3= 2.44584240284E-2

FI= .4

PF= 0	PP= .303595	DP= .303595
LS= 28.0439263331	HS=-1.5371884202	RS= .1517975
ES= 27.3903146267	FE= 9.03162714997E-2	
TC= 9.32758127788E-2	TH=-4.55594096566E-2	TT=-.047716403122
T1= 4.57620947181E-2	A1= 1.78397610991E-2	
R1= .442294939476	Q1= .89983968031	M1= 4.42583994594E-2
ELS= 28.3289102791	EES= 27.6748961082	EFE= 9.57817836076E-2
EC= 9.87336857233E-2	EH=-4.80381778998E-2	ET=-5.06955078233E-2
T3= 4.56257646466E-2	A3= 1.78226757105E-2	
R3= .443845581616	Q3= .901588951305	M3= 4.44457185496E-2

FI= 1.71

PF= 0	PP= 1.18411	DP= 1.18411
LS= 36.5240720613	HS=-6.49678028808	RS= .592055
ES= 34.1284099027	FE= .245115359359	
TC= .247504031223	TH=-.106725539911	TT=-.140778491318
T1= 4.16938035691E-2	A1= 7.15907432732E-2	
R1= 2.2545791993	Q1= 5.17170591568	M1= .751576113444
ELS= 37.9473235766	EES= 35.5293678521	EFE= .283187372385
EC= .285003392709	EH=-.119778111916	ET=-.1652252808
T3= 4.06745239305E-2	A3= 7.07402320416E-2	
R3= 2.27925493118	Q3= 5.27848965571	M3= .7610267103

```
COMPRESSION
 AT THE NEUTRAL PLANE
BP= .51                 MP= 0                   S3= .255
S1= 22.731513004        S2= 5.83837609791       G3= 20.27

REGION-C
FI= .1
BP= .51                 MP= .13094              VP=-.37906
S1= 25.6688531705       S2= 5.24230328356       S3= .32047
GS= 23.2809891598       GE= 2.48519925243E-2
AC=-2.44313556966E-2    AH= 7.80202674563E-3    AT= .016629328951
T4= 4.88042072853E-2    A1= .076202740057
R1= 2.14085718758       Q1= 4.95479769032       M1= .754602746732
OS1= 26.0679346876      SO3= .255               OGS= 23.7158988290
OEE= 3.04233677565E-2                           OC=-2.99095573421E-2 OH=
 9.66240888091E-3
OT= 2.02471484612E-2    T5= 4.89807720986E-2    A3= 7.53655524162E-2
R3= 2.16332238548       Q3= 5.06244950214       M3= .764111983278

FI= .2
BP= .51                 MP= .27651              VP=-.23349
S1= 27.2673634814       S2= 4.59609104766       S3= .393255
GS= 25.0386514341       GE= 4.95154926622E-2
AC=-4.88619194638E-2    AH= 1.65477707021E-2    AT= 3.23141487616E-2
T4= 4.95751178992E-2    A1= 8.08895198376E-2
R1= 2.01624185098       Q1= 4.72284061458       M1= .763792379954
OS1= 27.6507458013      SO3= .255               OGS= 25.5038140805
OEE= 5.69304833923E-2                           OC=-5.61959058876E-2 OH=
 1.92681657961E-2
OT= 3.69277400914E-2    T5= 4.98038372333E-2    A3= 8.00719951974E-2
R3= 2.03634653214       Q3= 4.83191616235       M3= .773475460248


FI= 1.43
BP= .51                 MP= 1.86547             VP= 1.35547
S1= 33.7853964296       S2=-1.22484795354       S3= 1.187735
GS= 33.8684609848       GE= .238254562345
AC=-.237794824943       AH= .105511338346       AT= .132283486593
T4= 5.47844027752E-2    A1= .142939980673
R1= 3.73604849056E-2    Q1= 1.50531555782       M1= 1.42903798117
OS1= 34.0725463913      SO3= .255               OGS= 34.5812264201
OEE= .257220295941      OC=-.256747529766       OH= .115596396802
OT= .14115113296        T5= 5.52702114856E-2    A3= .142594105915
R3= 2.23852917952E-2    Q3= 1.66240262213       M3= 1.45044777531
```

APPENDIX B

APPENDIX B.1

Tube-Bending machine specifications and sequence of operation

The 'Mark 13' bending machine is completely self-contained with built-in electrical equipment. The drive, gearing and the clutches are enclosed within the body of the machine. Lubrication is automatic from a pump in an oil sump at the machine base. The drive is from a totally enclosed fan cooled change pole motor, giving two bending speeds. Reverse gearing is arranged to give quick return to the bending arm. Starting and change speed equipment consists of a push button panel built into the machine. The panel is complete with overloads and 'no volt' release.

Machine specifications

Maximum capacity of mild steel tube	:	$1\frac{1}{4}$ in o.d. x 16 s.w.g.
Maximum capacity of British Standard pipe grade C	:	$\frac{3}{4}$ in bore, $1\frac{1}{16}$ in o.d.
Maximum capacity of solid steel bar	:	$\frac{3}{4}$ in diameter
Maximum bending radius to tube centreline	:	7 in
Minimum bending radius to tube centreline	:	$1\frac{1}{4}$ in on $\frac{1}{2}$ in o.d. tube
Bending speeds	:	10 and 15 rev min^{-1}
Return arm speed	:	15 and 22 rev min^{-1}

Sequence of operation

1. The tube is inserted between the gripper and the former and pushed over the mandrel to the length stop. When the pedal is depressed, the grips and the slider automatically close and the bending cycle commences.

2. The bending arm and the former move round to an angle previously determined by the cam setting, thus bending and drawing the tube over the mandrel. Also, the slider follows the tube forward.

3. On completion of the bending operation, the pressures on the gripper and the slider are automatically released and the slider returns to its original position. The reverse clutch returns the bending arm back to rest and the bent tube can then be removed.

APPENDIX B.2

Details of the various arrangements for the bending machine

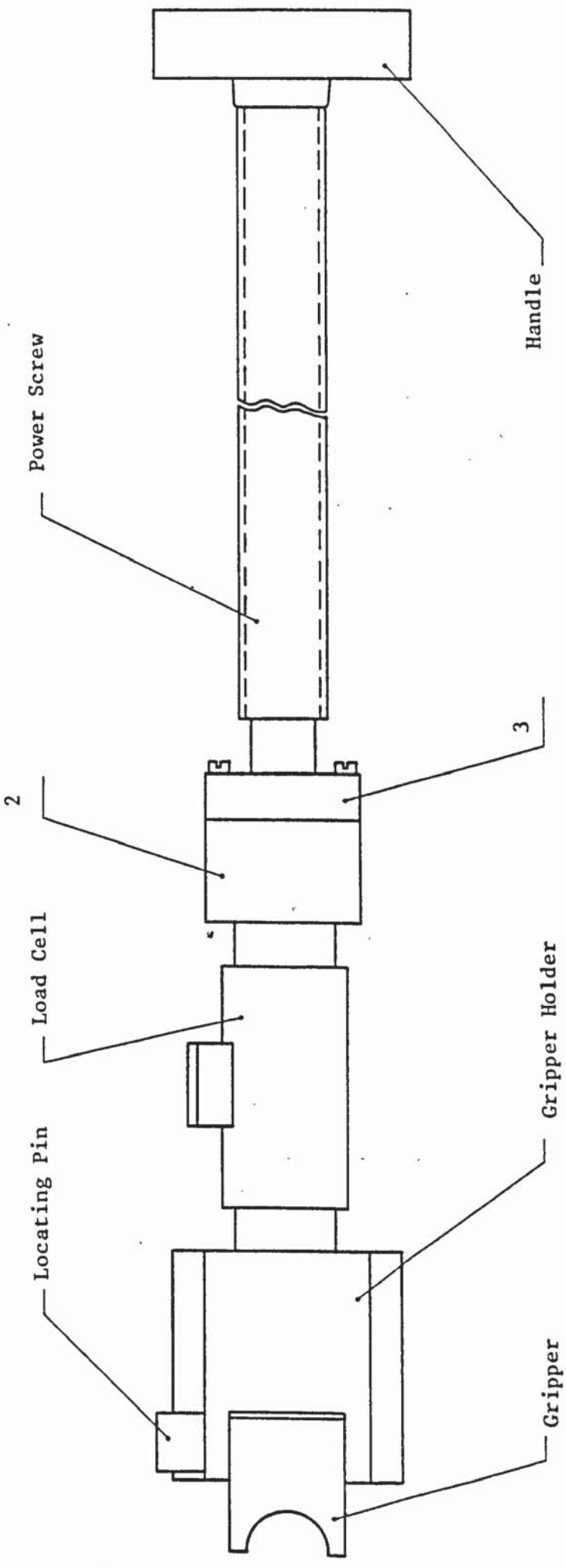

Figure B1: A diagram showing the gripper assembly and the gripper load-cell

ALL DIMENSIONS IN INCHES

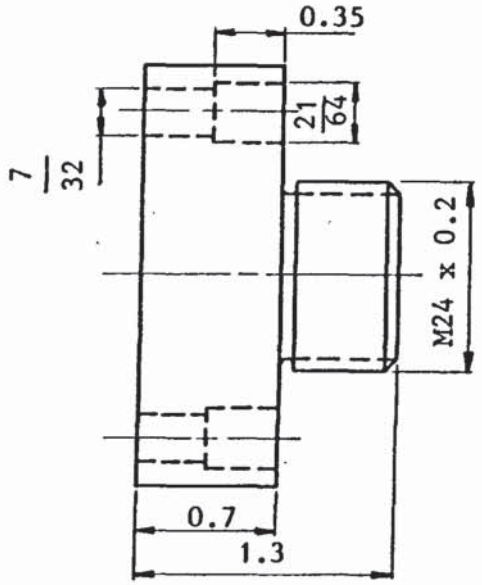

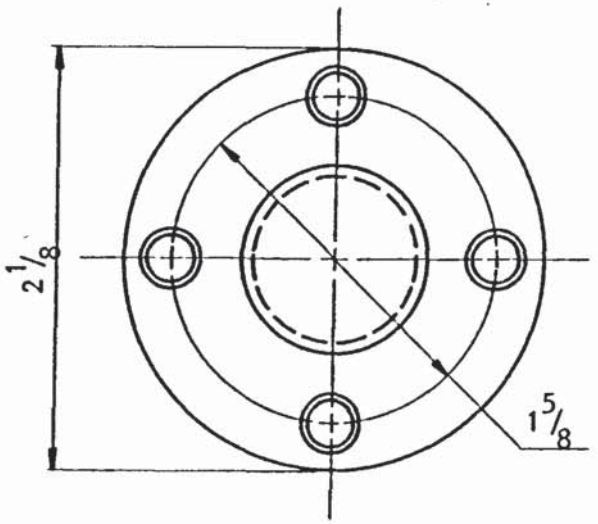

SCALE: Full	MAT^{L}:	DRN	I N IBRAHIM	Gripper Assembly	DRG NO:
TOLERANCES: LIMITS UNLESS OTHERWISE SPD. FRAC. ± 1/64" DEC. ±0.010" ANG. ± 15'	Mild Steel	DATE	11.12.1980		B2
	PART No: 1	APP		UNIV. OF ASTON IN BIRMINGHAM PROD. TECH. DEPT. G. ALEX. LABS.	
	No. REQ: 1	DATE			

ALL DIMENSIONS IN INCHES

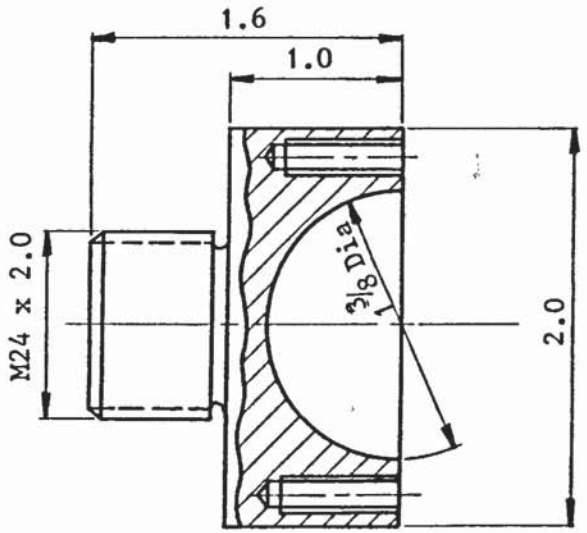

SECTION A-A

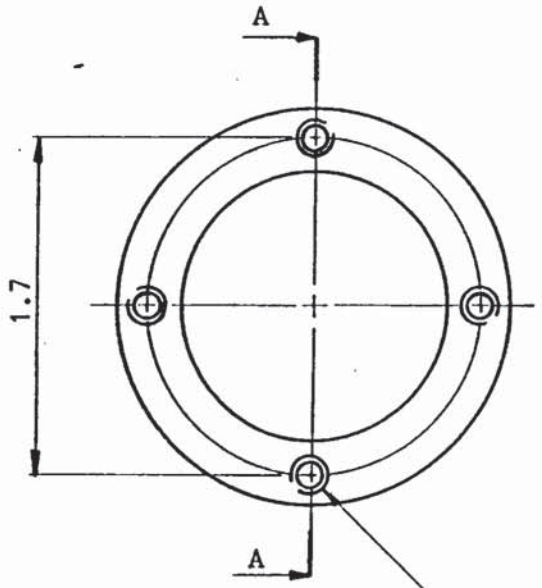

SCALE: Full	MATERIAL:	DRN	I N IBRAHIM	Gripper Assembly	DRG NO: B3
TOLERANCES: LIMITS UNLESS OTHERWISE SPD. FRAC. ± 1/64" DEC. ± 0.010" ANG. ± 15'	Mild Steel	DATE	11.12.1980		
	PART No: 2	APP		UNIV. OF ASTON IN BIRMINGHAM PROD.TECH.DEPT. G.ALEX.LABS.	
	No. REQ: 1	DATE			

ALL DIMENSIONS IN INCHES

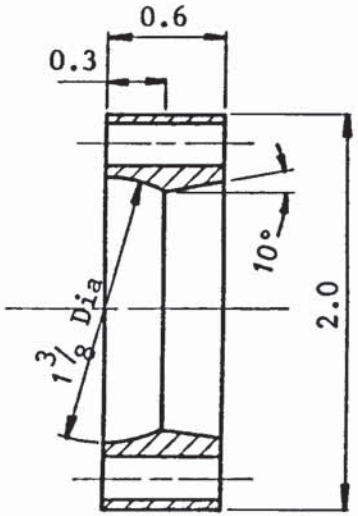

SECTION A-A

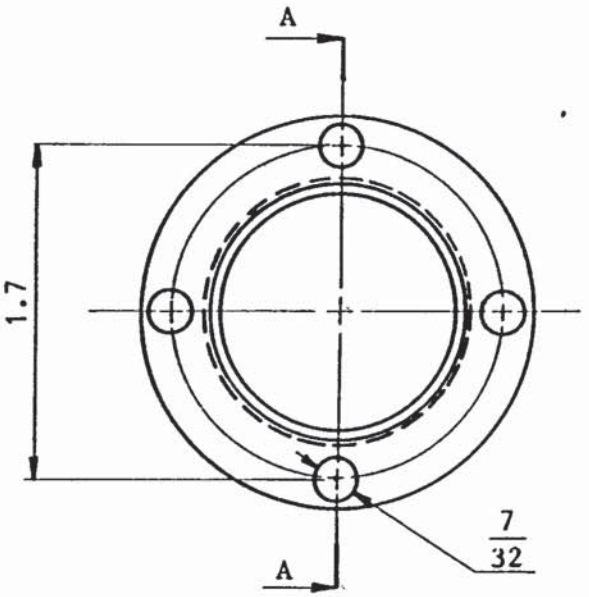

4 Holes drill

$\frac{7}{32}$ in.dia. thro'

SCALE: Full	MATERIAL: Mild Steel	DRN	I N IBRAHIM	Gripper Assembly	DRG No: B4
TOLERANCES: LIMITS UNLESS OTHERWISE SPD. FRAC. ± 1/64" DEC. ± 0.010" ANG. ± 15'		DATE	11.12.1980		
	PART No: 3	APP		UNIV. OF ASTON IN BIRMINGHAM PROD.TECH.DEPT. G.ALEX.LABS	
	No. REQ: 1	DATE			

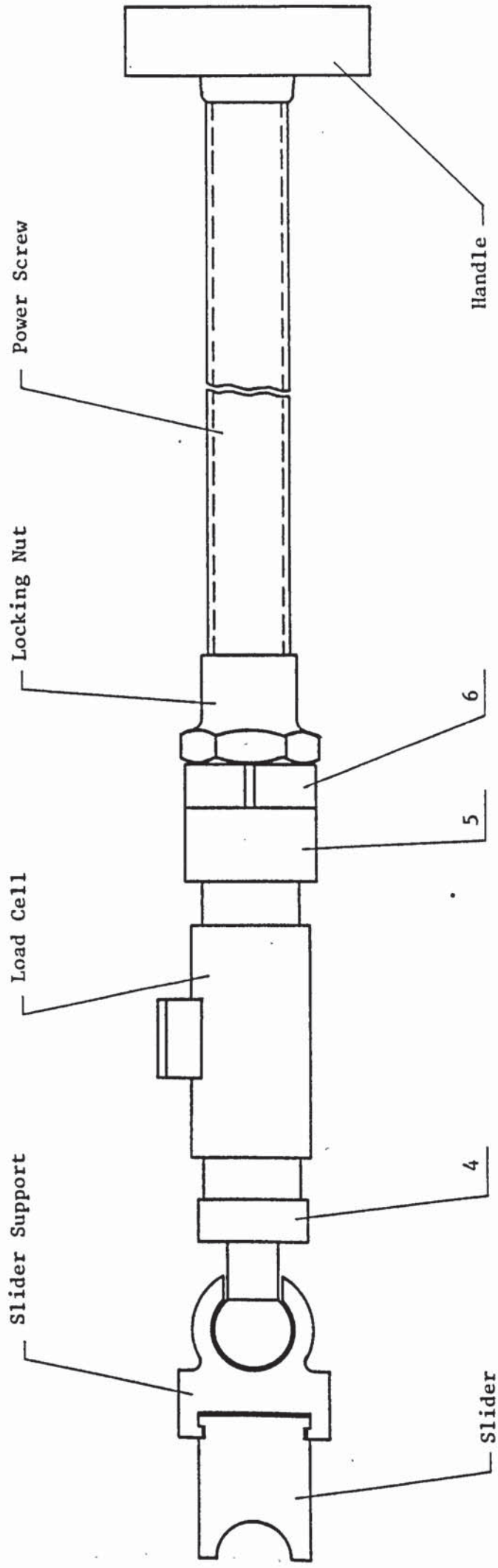

Figure B5: A diagram showing the slider assembly and the slider load-cell

ALL DIMENSIONS IN INCHES

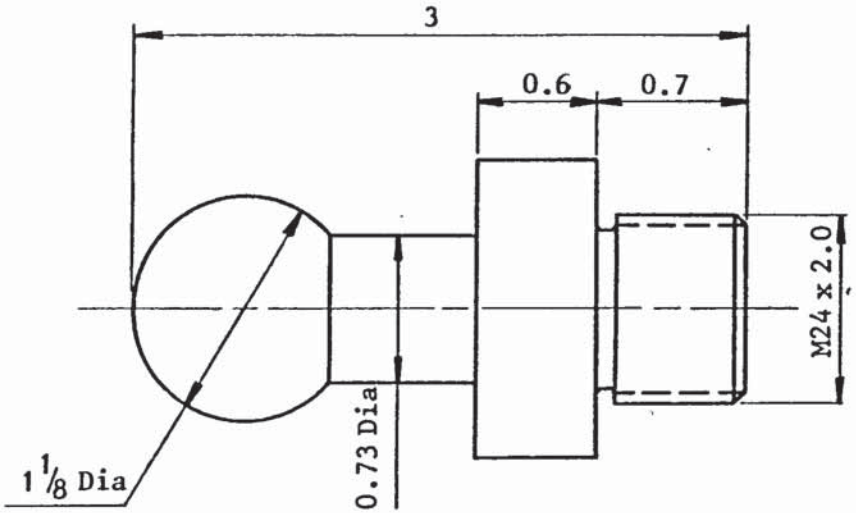

SCALE: Full	MATERIAL: Mild Steel	DRN	I N IBRAHIM	Slider Assembly	DRG No: B6
TOLERANCES: LIMITS UNLESS OTHERWISE SPD. FRAC. ± 1/64" DEC. ± 0.010" ANG. ± 15'		DATE	11.12.1980		
	PART No: 4	APP		UNIV. OF ASTON IN BIRMINGHAM PROD.TECH.DEPT. G.ALEX.LABS	
	No. REQ: 1	DATE			

ALL DIMENSIONS IN INCHES

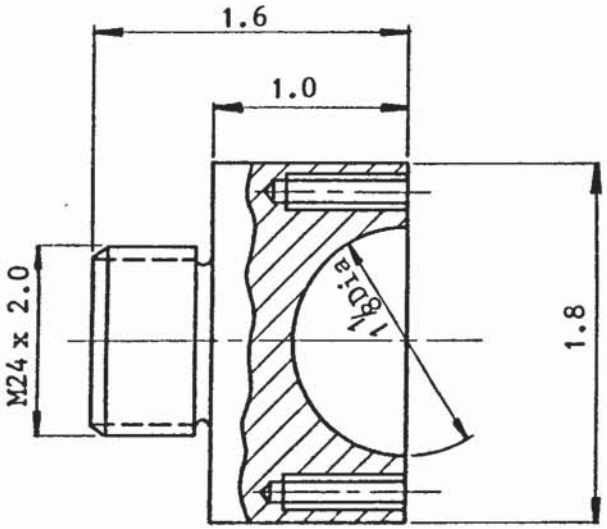

SECTION A-A

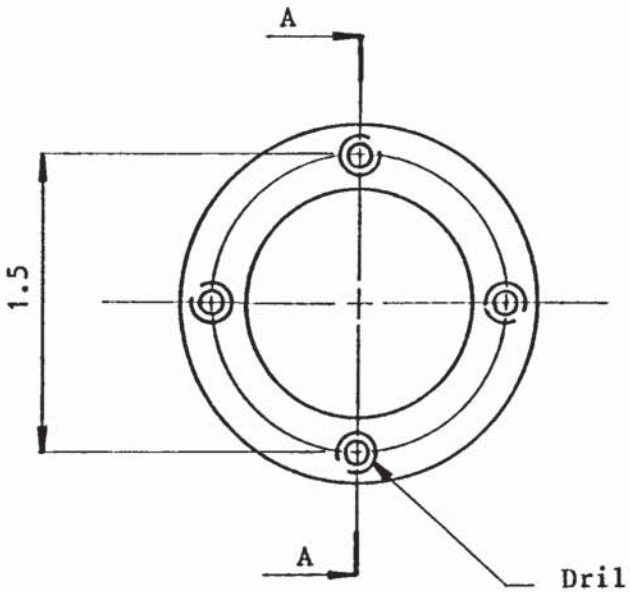

SCALE: Full	MATERIAL: Mild Steel	DRN	I N IBRAHIM	Slider Assembly	DRG No: B7
TOLERANCES: LIMITS UNLESS OTHERWISE SPD. FRAC. ± 1/64" DEC. ± 0.010" ANG. ± 15'		DATE	11.12.1980		
	PART No: 5	APP		UNIV. OF ASTON IN BIRMINGHAM PROD.TECH.DEPT. G.ALEX.LABS.	
	No. REQ: 1	DATE			

ALL DIMENSIONS IN INCHES

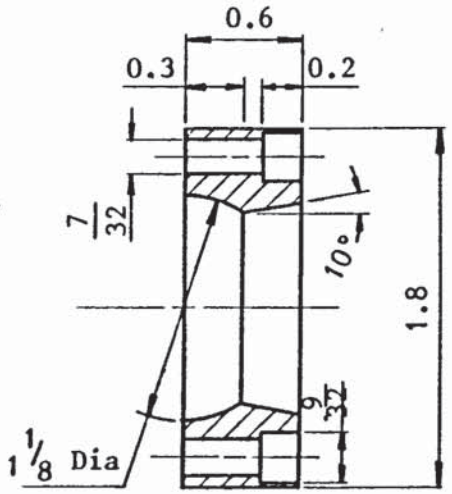

SECTION A-A

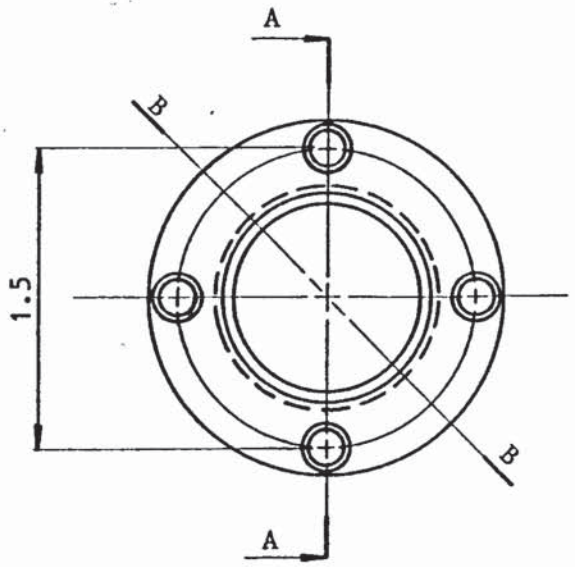

The finished part is to be split into two halves as shown in B-B

SCALE: Full	MATERIAL: Mild Steel	DRN	I N IBRAHIM	Slider Assembly	DRG No: B8
TOLERANCES: LIMITS UNLESS OTHERWISE SPD. FRAC. ± 1/64" DEC. ± 0.010" ANG. ± 15'		DATE	11.12.1980		
	PART No: 6	APP		UNIV. OF ASTON IN BIRMINGHAM	
	No. REQ: 1	DATE		PROD.TECH.DEPT. G.ALEX.LABS.	

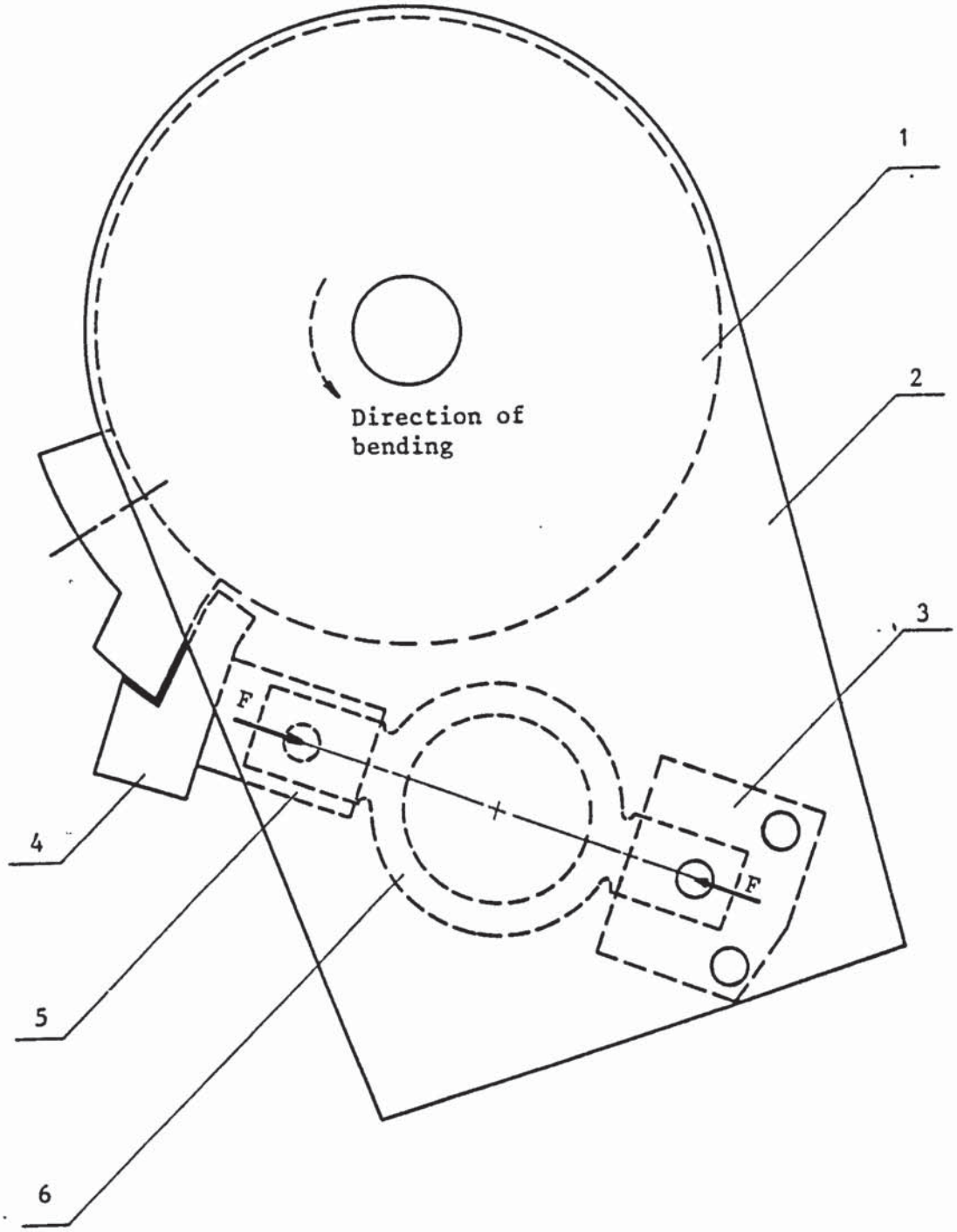

Figure B9: A diagrammatic sketch of the torque-meter assembly

1. Driving Shaft
2. Driven Bending Arm
3. Fixed Head
4. Support
5. Free Head
6. Torque Load-cell

APPENDIX B.3

Specifications and designs of the bending tools

(a) The grippers (clamp dies)

As shown in DRG No. B10 (dimensions in inches):

No	gripper code G(d)*	dimension 'D'	dimension 'H'
24	G($^3/_4$)	0.753 0.750	0.360 0.350
24A	G(1)	0.103 0.100	0.485 0.475
25	G($1^1/_4$)	1.253 1.250	0.610 0.600

(b) The sliders (pressure dies)

As shown in DRG No. B11 (dimensions in inches):

No	slider code S(d)	dimension 'D'	dimension 'H'
26	S($^3/_4$)	0.760 0.755	0.360 0.350
26A	S(1)	1.010 1.005	0.485 0.475
27	S($1^1/_4$)	1.260 1.255	0.610 0.600

* d is the nominal tube outside diameter

ALL DIMENSIONS IN INCHES

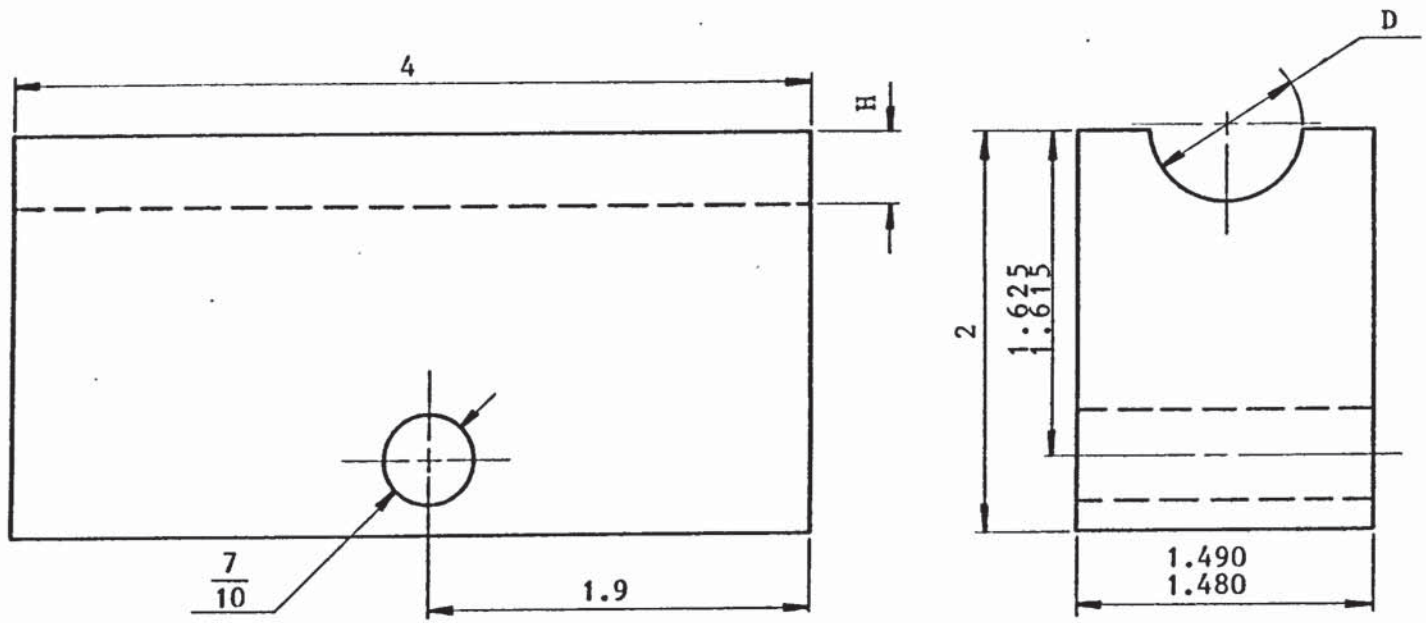

SCALE: Full	MATERIAL: Mild Steel	DRN	I N IBRAHIM	Gripper G(d)	DRG No: B10
TOLERANCES: LIMITS UNLESS OTHERWISE SPD FRAC. ± 1/64" DEC. ± 0.010' ANG. ± 15'		DATE	22.12.1980		
	PART No:	APP		UNIV. OF ASTON IN BIRMINGHAM PROD.TECH.DEPT. G.ALEX.LABS.	
	No. REQ: 1	DATE			

ALL DIMENSIONS IN INCHES

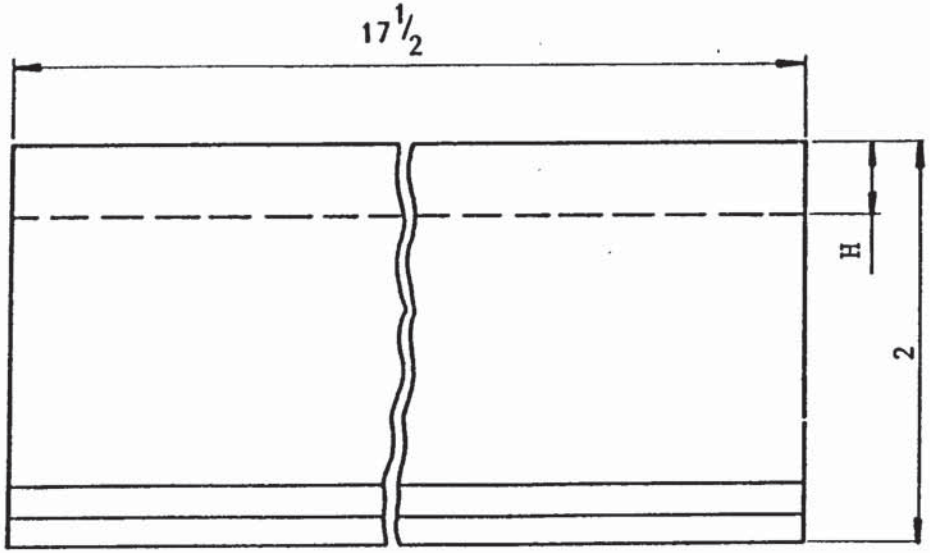

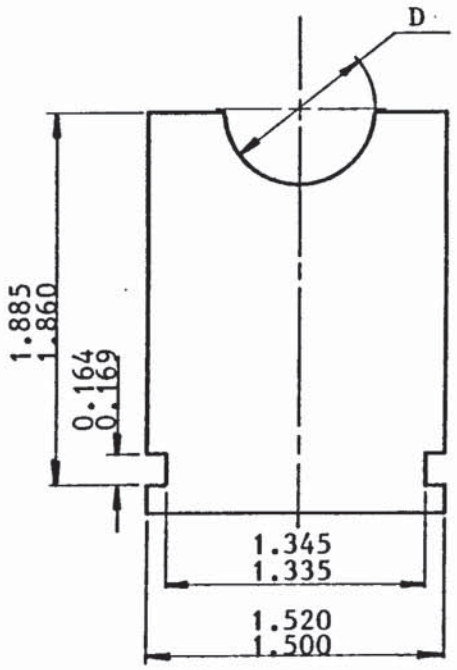

SCALE: Full	MATERIAL:	DRN	I N IBRAHIM	Slider S(d)	DRG No: B11
TOLERANCES: LIMITS UNLESS OTHERWISE SPD FRAC. ± 1/64" DEC. ± 0.010" ANG. ± 15'	Mild Steel	DATE	22.12.1980		
	PART No:	APP		UNIV. OF ASTON IN BIRMINGHAM PROD.TECH.DEPT. G.ALEX.LABS.	
	No. REQ: 1	DATE			

(c) The formers (bend dies)

As shown in DRGs No. B12 and B13 (dimensions in inches):

No	former code F(d - R)*	dimension 'D'	dimension 'R'	dimension 'H'	dimension 'H1'
40	F($^3/_4$ - $1^1/_2$)	0.756 0.752	1.503 1.497	$1^1/_8$	$^1/_4$
33	F($^3/_4$ - $1^1/_8$)	0.756 0.752	1.128 1.122	$1^1/_8$	$^1/_4$
7	F(1 - 2)	1.006 1.002	2.003 2.997	2	$^{11}/_{16}$
2	F(1 - $1^1/_2$)	1.006 1.002	1.503 1.497	$1^1/_2$	$^7/_{16}$
34	F(1 - 1)	1.006 1.002	1.002 0.998	1	$^3/_{16}$
38	F($1^1/_4$ - $2^1/_2$)	1.256 1.252	2.503 2.497	2	$^{11}/_{16}$
32	F($1^1/_4$ - $1^7/_8$)	1.256 1.252	1.878 1.872	$1^1/_2$	$^7/_{16}$
39	F($1^1/_4$ - $1^1/_4$)	1.256 1.252	1.253 1.247	1	$^3/_{16}$

* R is the mean bend radius

ALL DIMENSIONS IN INCHES

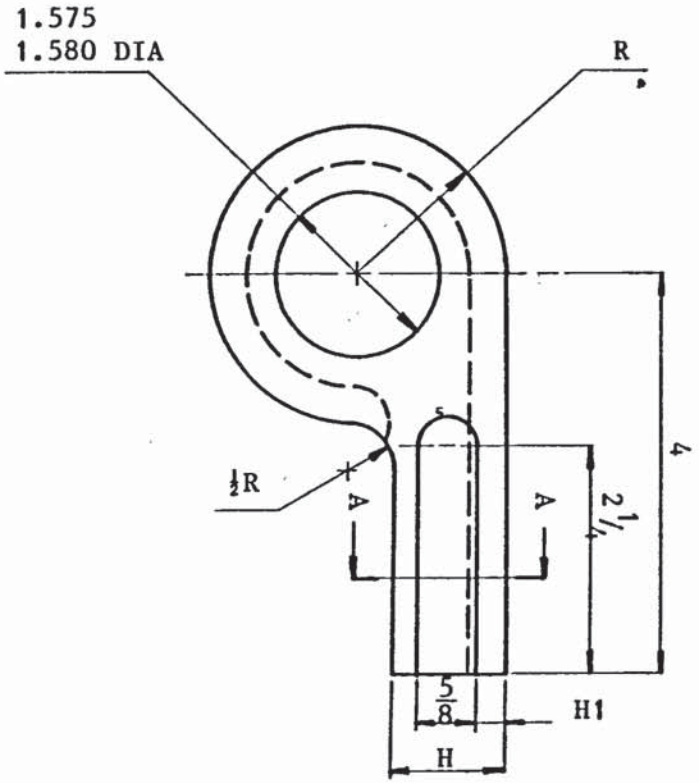

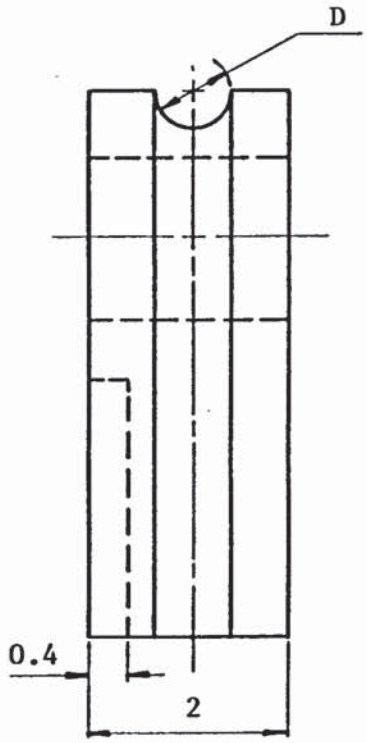

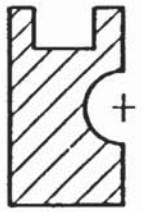

SECTION A-A

SCALE: 1:2	MATERIAL	DRN	I N IBRAHIM	Former F(d-R)	DRG No: B12
TOLERANCES: LIMITS UNLESS OTHERWISE SPD FRAC. ± 1/64" DEC. ± .010" ANG. ± 15'	Mild Steel	DATE	23.9.1981		
	PART NO:	APP		UNIV. OF ASTON IN BIRMINGHAM PROD. TECH. DEPT. G. ALEX. LABS	
	No. REQ: 1	DATE			

ALL DIMENSIONS IN INCHES

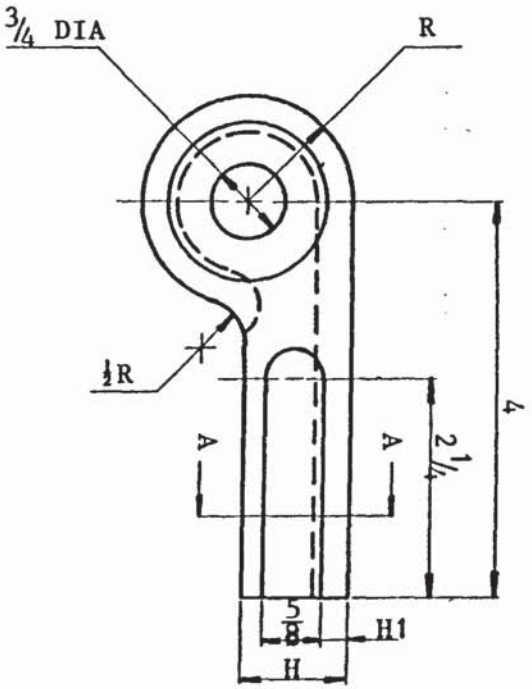

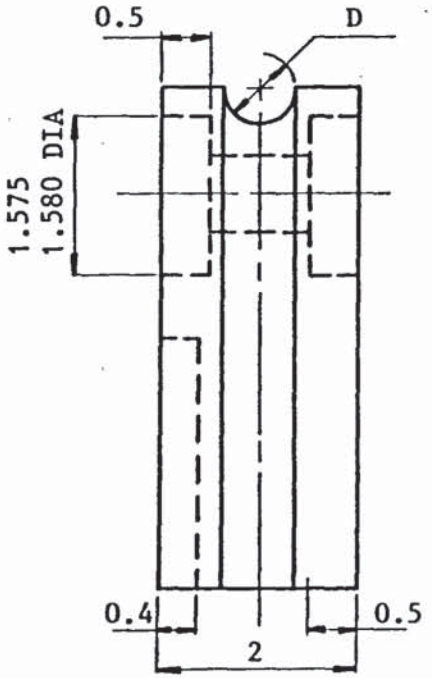

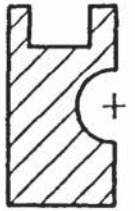

SECTION A-A

SCALE: 1:2	MATERIAL: Mild Steel	DRN	I N IBRAHIM	Former F(d-R)	DRG NO: B13
TOLERANCES: LIMITS UNLESS OTHERWISE SPD FRAC. ± 1/64" DEC. ± 0.010" ANG. ± 15'		DATE	31.3.1981		
	PART NO:	APP		UNIV. OF ASTON IN BIRMINGHAM PROD. TECH. DEPT. G. ALEX. LABS	
	No. REQ:	DATE			

(d) The wiper dies

As shown in DRG No. B14 (dimensions in inches):

No	wiper die code W(d - R)	dimension 'D'	dimension 'A'	dimension 'H'	dimension 'L'
42	W($\frac{3}{4}$ - 1$\frac{1}{2}$)	0.756 0.752	0.746 0.742	0.900	1.409 1.401
37	W($\frac{3}{4}$ - 1$\frac{1}{8}$)	0.756 0.752	0.746 0.742	0.900	1.034 1.026
50	W(1 - 2)	1.006 1.002	0.996 0.992	0.900	1.909 1.901
51	W(1 - 1$\frac{1}{2}$)	1.006 1.002	0.996 0.992	0.900	1.409 1.401
35	W(1 - 1)	1.006 1.002	0.996 0.992	0.900	0.909 0.901
41	W(1$\frac{1}{4}$ - 2$\frac{1}{2}$)	1.256 1.252	1.246 1.242	1.150	2.409 2.401
36	W(1$\frac{1}{4}$ - 1$\frac{7}{8}$)	1.256 1.252	1.246 1.242	1.150	1.784 1.776
41	W(1$\frac{1}{4}$ - 1$\frac{1}{4}$)	1.256 1.252	1.246 1.242	1.150	1.159 1.151

ALL DIMENSIONS IN INCHES

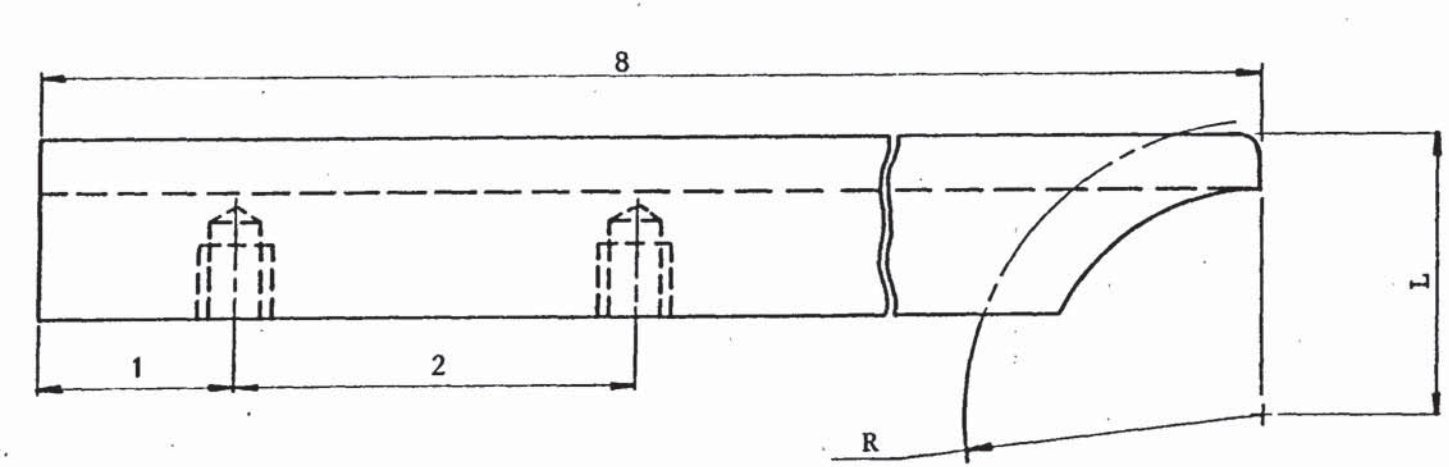

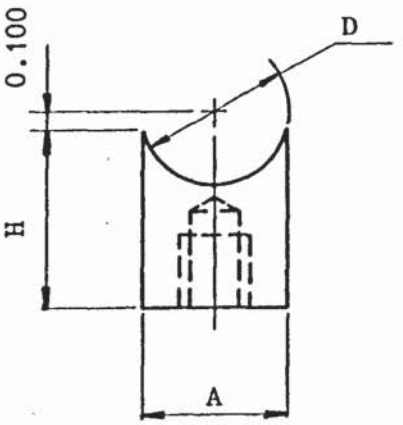

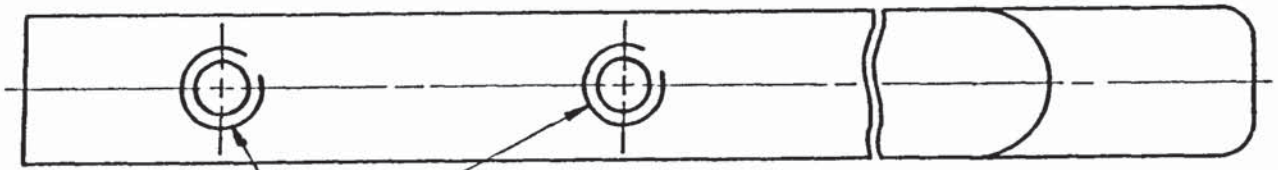

Drill and tap $\frac{3}{8}$ BSF x $\frac{3}{8}$ deep

SCALE: Full	MATERIAL: Mild Steel	DRN	I N IBRAHIM	Wiper Die W(d-R)	DRG NO: B14
TOLERANCES: LIMITS UNLESS OTHERWISE SPD FRAC. ± $\frac{1}{64}$" DEC. ± 0.010" ANG. ± 15'		DATE	24.9.1981		
	PART NO:	APP		UNIV. OF ASTON IN BIRMINGHAM PROD. TECH. DEPT.	
	No. REQ: 1	DATE			

(e) The mandrels

As shown in DRG No. B15 (dimensions in inches):

No	mandrel code M(d - s.w.g - R)*	dimension 'D'	dimension 'R'
48	M($^3/_4$ - 20g - 2)	0.671 0.667	2.005 1.995
30	M($^3/_4$ - 20g - 1.5)	0.671 0.667	1.505 1.495
43	M(1 - 16g - 2)	0.859 0.853	2.005 1.995
13A	M(1 - 18g - 2)	0.893 0.887	2.005 1.995
12A	M(1 - 20g - 2)	0.920 0.914	2.005 1.995
29	M(1 - 16g - $1^1/_2$)	0.859 0.853	1.505 1.495
8A	M(1 - 18g - $1^1/_2$)	0.893 0.887	1.505 1.495
9A	M(1 - 20g - $1^1/_2$)	0.920 0.914	1.505 1.495
44	M(1 - 16g - 1)	0.859 0.853	1.005 0.995
45	M(1 - 18g - 1)	0.893 0.887	1.005 0.995
28	M(1 - 20g - 1)	0.920 0.914	1.005 0.995
46	M($1^1/_4$ - 16g - $2^1/_2$)	1.109 1.103	2.505 2.495
31	M($1^1/_4$ - 16g - $1^7/_8$)	1.109 1.103	1.880 1.870
47	M($1^1/_4$ - 16g - $1^1/_4$)	1.109 1.103	1.255 1.245

* s.w.g. is the standard wall gauge of tube

ALL DIMENSIONS IN INCHES

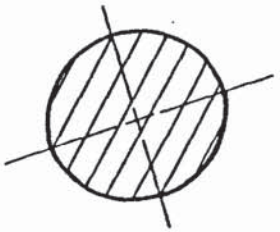

SECTION A-A

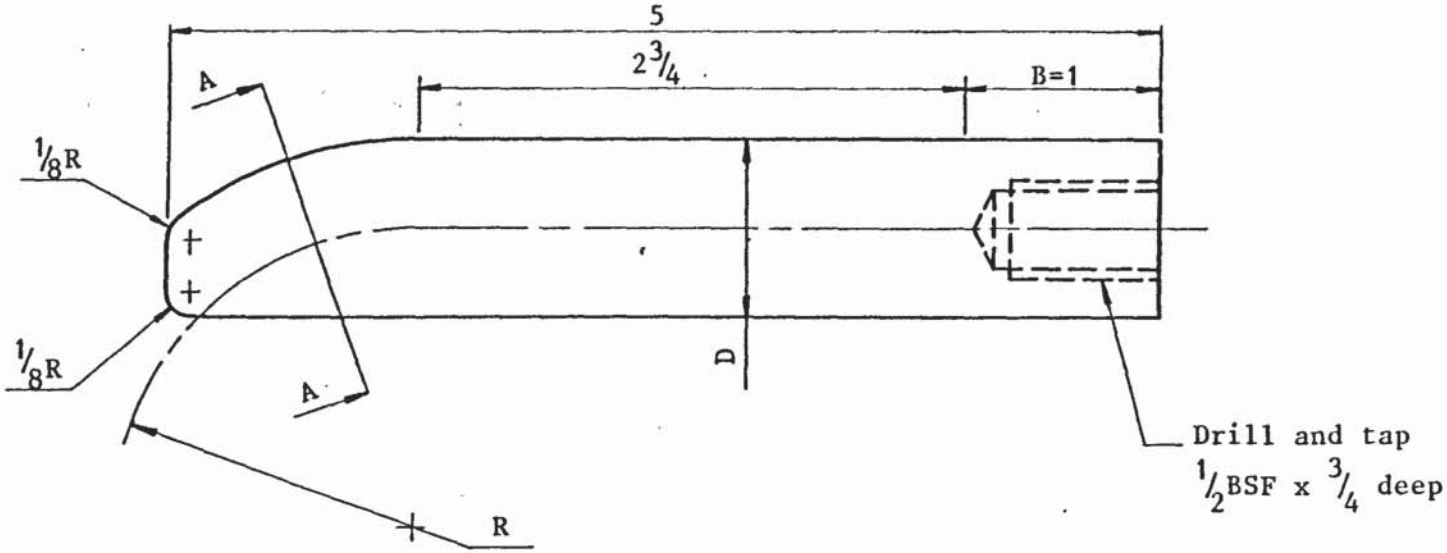

TAPER 0.007 IN PER INCH
OVER DIMENSION 'B'

SCALE: Full	MATERIAL: Tool Steel	DRN	I N IBRAHIM	Mandrel M(d-s.w.g.-R)	DRG NO: B15
TOLERANCES: LIMITS UNLESS OTHERWISE SPD FRAC. ± 1/64" DEC. ± 0.010" ANG. ± 15'		DATE	19.11.1980		
	PART NO:	APP		UNIV. OF ASTON IN BIRMINGHAM PROD. TECH. DEPT. G. ALEX. LABS.	
	No. REQ: 1	DATE			

APPENDIX B.4

Specifications of the electrical equipment

(a) EGR-3200 Power Generator

The Model EGR-3200 Power Generator is an all solid state source of up to 3000 watt of power for ultrasonic transducers, plasma etching, induction heating coils and a wide variety of gas discharge lamps.

Specifications

Frequency coverage	: 8 kHz to 111 kHz in two bands
Frequency stability	: better than 0.1 per cent after 15 minute warm-up
Frequency resolution	: better than 2 Hz using frequency vernier
Matched output load impedence	: 50 ohm; the unit will supply full rated power to any load impedence between 40 and 56 ohm resistive
Maximum generator power output	: more than 2800 watt - 8 to 14 kHz more than 3000 watt - 14 to 70 kHz more than 2800 watt - 70 to 100 kHz more than 2400 watt - 100 to 111 kHz
Power	: 230 volt 8 per cent, 50-60 Hz; fused line at 35 ampere capacity minimum
Operating temperature	: 0^{o} to 45^{o}C Ambient

Mismatch protection : the unit will tolerate 700 watt of power reflected from any load impedence, subject to operation of the thermal protection. Instantaneous overload protection is provided should the load impedence exceed allowable limits.

Thermal protection : Thermostatic protection provides automatic cut-out should the power transistors overheat due to load mismatch or cooling system failure. Automatic reset upon cooling.

Power meter : True average reading accurate to better than 2 per cent of full scale. Front panel switch permits measurement of the forward power (power leaving the generator) and the actual power absorbed by the load.

General tune-up procedure for ultrasonic transducers

To operate the EGR-3200 generator at its maximum efficiency the ultrasonic load impedence should be as close to 50 ohm resistive as possible. Tuning the load to 50 ohm can be achieved using the power meter. The following procedure is to be followed in tuning the piezoelectric ultrasonic transducers:

1. Connect the ultrasonic transducers to their matching network which is connected to the output of the generator.
2. Place the transducers into their actual operating environment.
3. Rotate the level control anticlockwise to zero.

4. Flip the circuit breaker to the ON position.
5. Slide the meter switch to the forward position. Then adjust the frequency dial so that it indicates the approximate operating frequency of the transducers.
   (Make sure that the low-high switch is in correct range position)
6. Push the On, Off remote switch upward to the ON position.
7. Adjust the level control clockwise for low forward power.
8. Slide the meter switch to the load position and vary the frequency dial until the load power is maximum. Fine frequency adjustment near the resonant frequency can be made using the vernier dial.
9. Adjust the matching network [see section (b)] until the forward power is as close as possible to the load power, which corresponds to the maximum generator efficiency.

(b) EVB-2 Piezoelectric Transducer Matchbox

The ENI Power Systems Model EVB-2 "Piezoelectric Transducer Matchbox" is a wideband switchable matching network suitable for matching most piezoelectric transducers in the frequency range from 9 kHz to 50 kHz to a 50 ohm power source impedence.

Specifications

Frequency coverage	:	9 kHz to 50 kHz
Type of load	:	piezoelectric transducers (single or arrays)
Matched input impedence	:	50 ohm
Maximum power input	:	4000 watt average; 5600 watt peak
Operating environment	:	0° to 45°C

Matching procedure

Connect the power generator to the type N connector labelled 'Generator' and the transducers to the type C connector labelled 'Transducer'. Set knobs N_2, N_1 and L to, say, 4.2, 1.2 and 0.1 respectively. Also, set the forward power output of the generator to a conveniently low level and test the load power. Rotate knob N_2 slowly until the load power increases such that it equals the forward power. If it does not, then reposition N_2 to 4.2 and change N_1 to 1.5. Rotate knob N_2 and again test the load power. Repeat this procedure for N_1 equal to 2.0 and 2.5. If match has not been achieved at any of these positions, rotate the L knob to the 0.3 millihenry and repeat the same procedure for N_2 and N_1. The last position of L equal to 0.7 mH is used in the same manner.

Having achieved matching at the low power level, the actual operating power can be inserted. Any trimming operation may be accomplished by controls N_1 and N_2. The optimum matching is obtained when the load power is equal to the forward power, at which the load impedence is 50 ohm resistive.

APPENDIX B.5

Details of the horn-mounting assembly

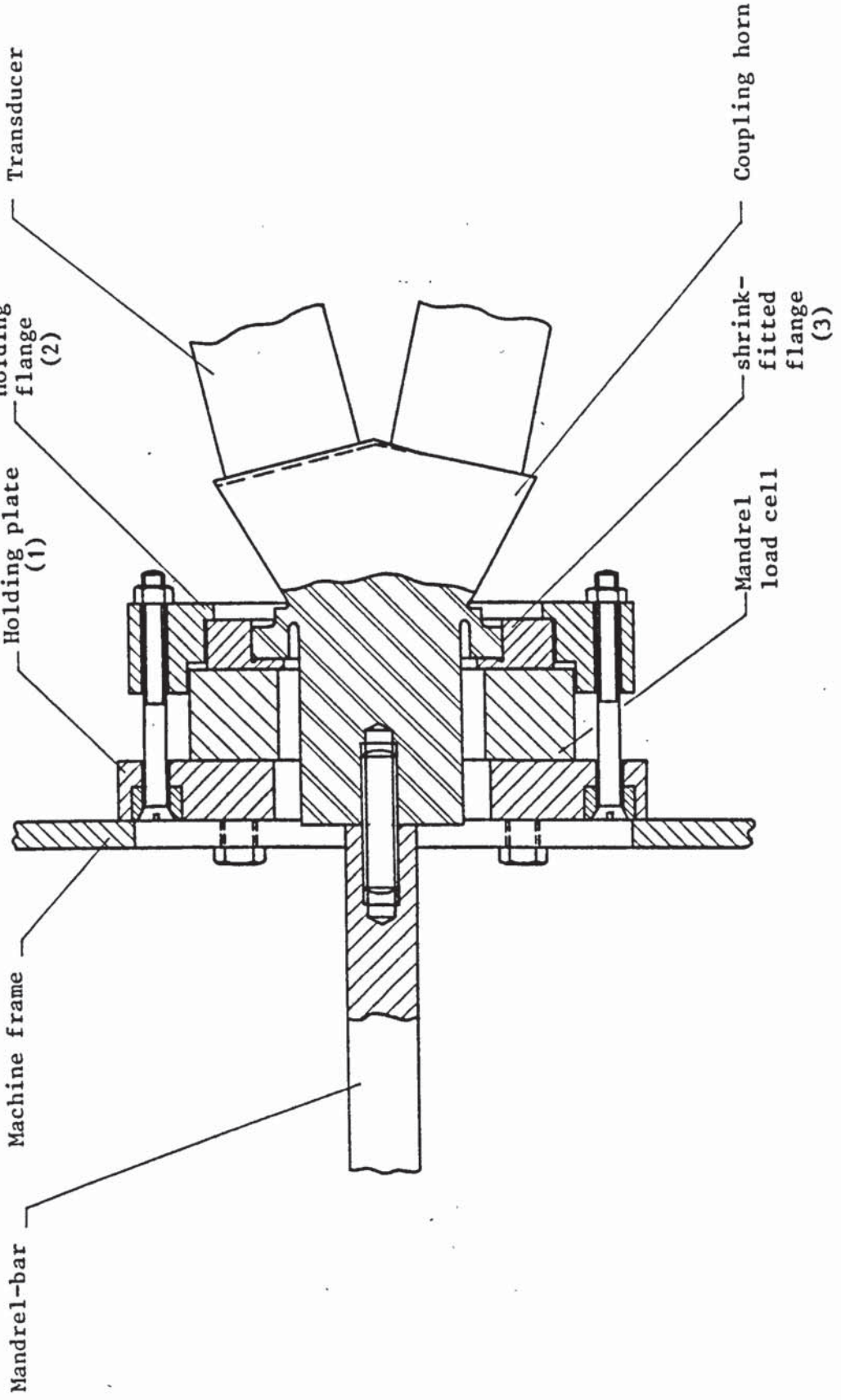

Figure B16: An assembly drawing of the coupling-horn mount

ALL DIMENSIONS IN INCHES

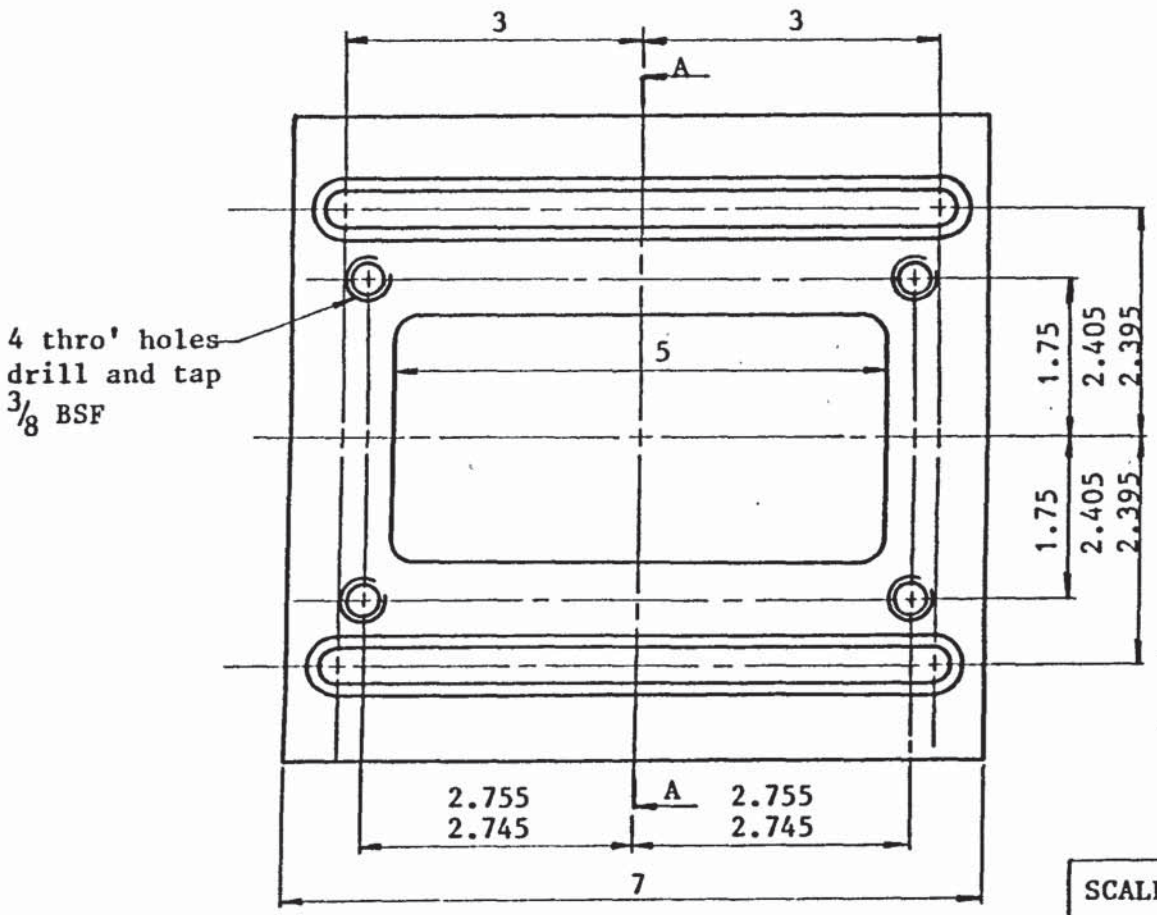

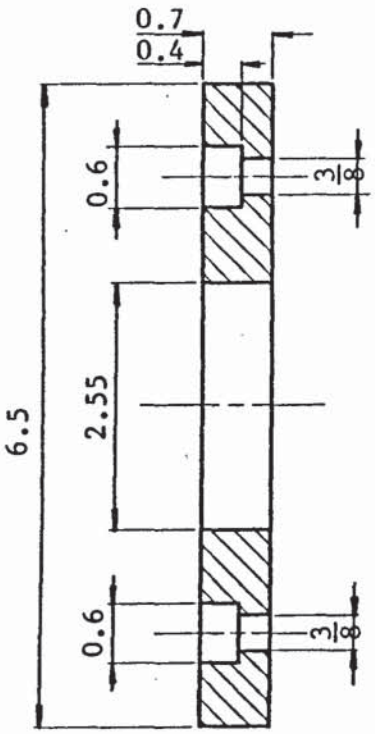

SECTION A-A

SCALE: 1:2	MATERIAL: Mild Steel	DRN	I N IBRAHIM	Holding Plate	DRG NO: B17
TOLERANCES: LIMITS UNLESS OTHERWISE SPD FRAC. ± 1/64" DEC. ± .010" ANG. ± 15'		DATE	25.2.1980		
	PART NO: 1	APP		UNIV. OF ASTON IN BIRMINGHAM PROD. TECH. DEPT. G. ALEX. LABS.	
	No. REQ: 1	DATE			

ALL DIMENSIONS IN INCHES

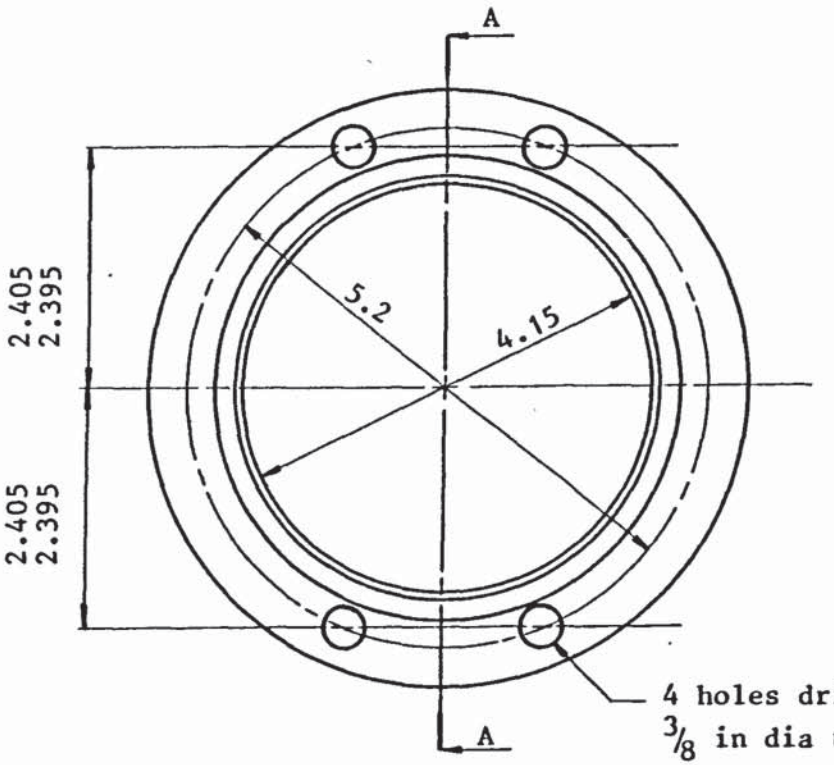

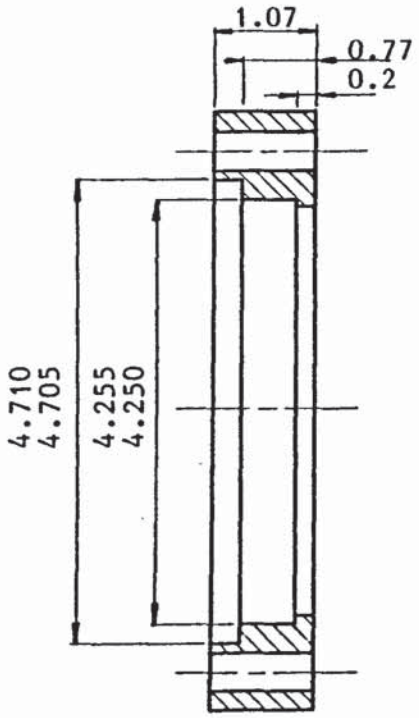

SECTION A-A

SCALE: 1:2	MATERIAL:	DRN	I N IBRAHIM	Holding Flange	DRG NO: B18
TOLERANCES: LIMITS UNLESS OTHERWISE SPD FRAC. ± 1/64" DEC. ± 0·010" ANG. ± 15'	Mild Steel	DATE	25.2.1980		
	PART NO: 2	APP		UNIV. OF ASTON IN BIRMINGHAM PROD. TECH. DEPT. G. ALEX. LABS.	
	No. REQ: 1	DATE			

ALL DIMENSIONS IN INCHES

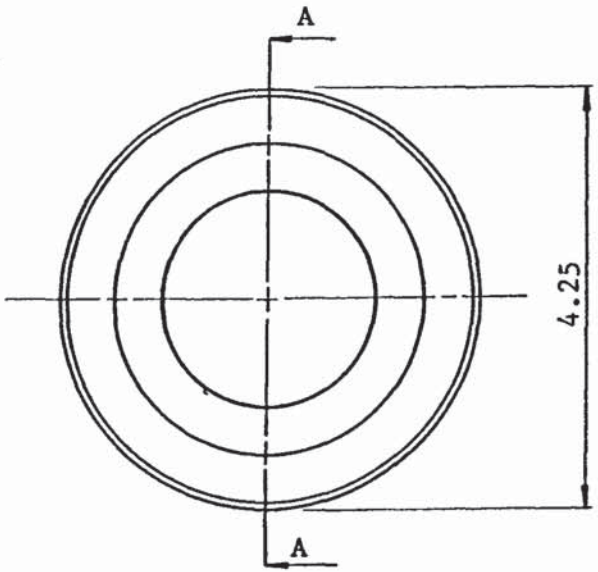

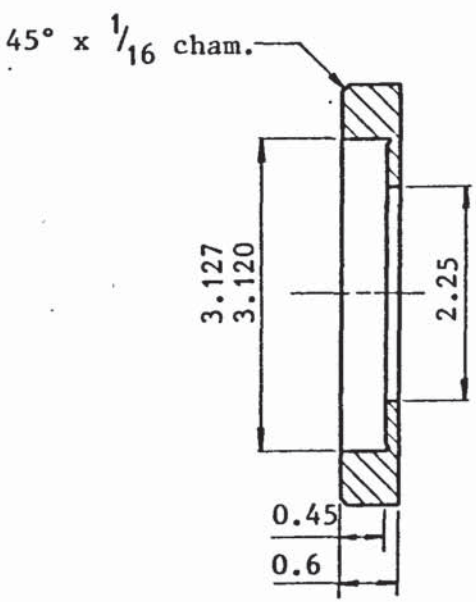

SECTION A-A

SCALE: 1:2	MATERIAL: Mild Steel	DRN	I N IBRAHIM	Shrink-fitted Flange	DRG NO: B19
TOLERANCES: LIMITS UNLESS OTHERWISE SPD FRAC. ± 1/64" DEC. ± 0.010" ANG. ± 15'		DATE	25.2.1980		
	PART NO: 3	APP		UNIV. OF ASTON IN BIRMINGHAM	
	No. REQ: 1	DATE		PROD. TECH. DEPT. G. ALEX. LABS.	

APPENDIX B.6

Calibration charts of the load cells and the 'Distec' displacement transducer

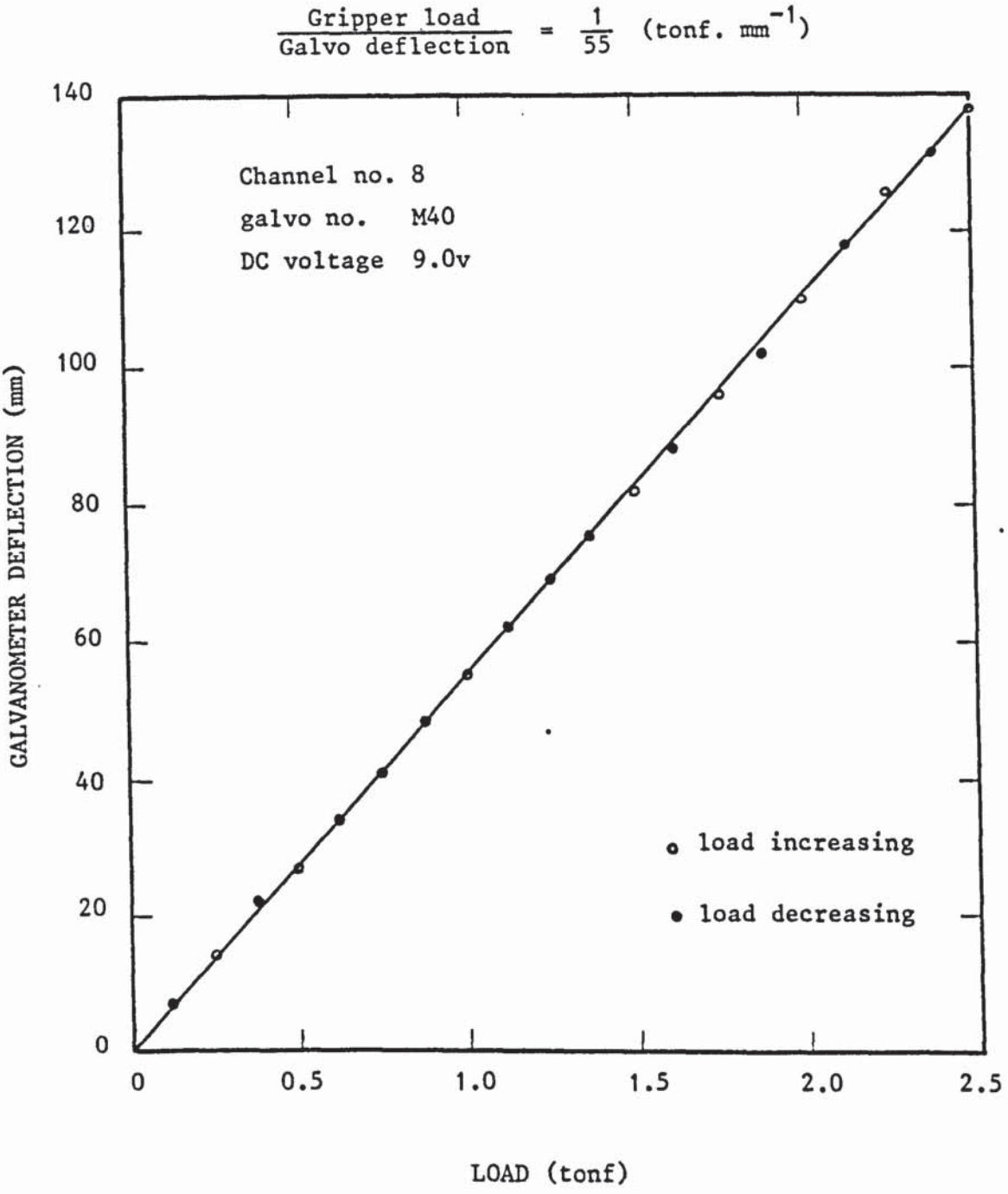

Figure B20: The calibration chart of the gripper load cell

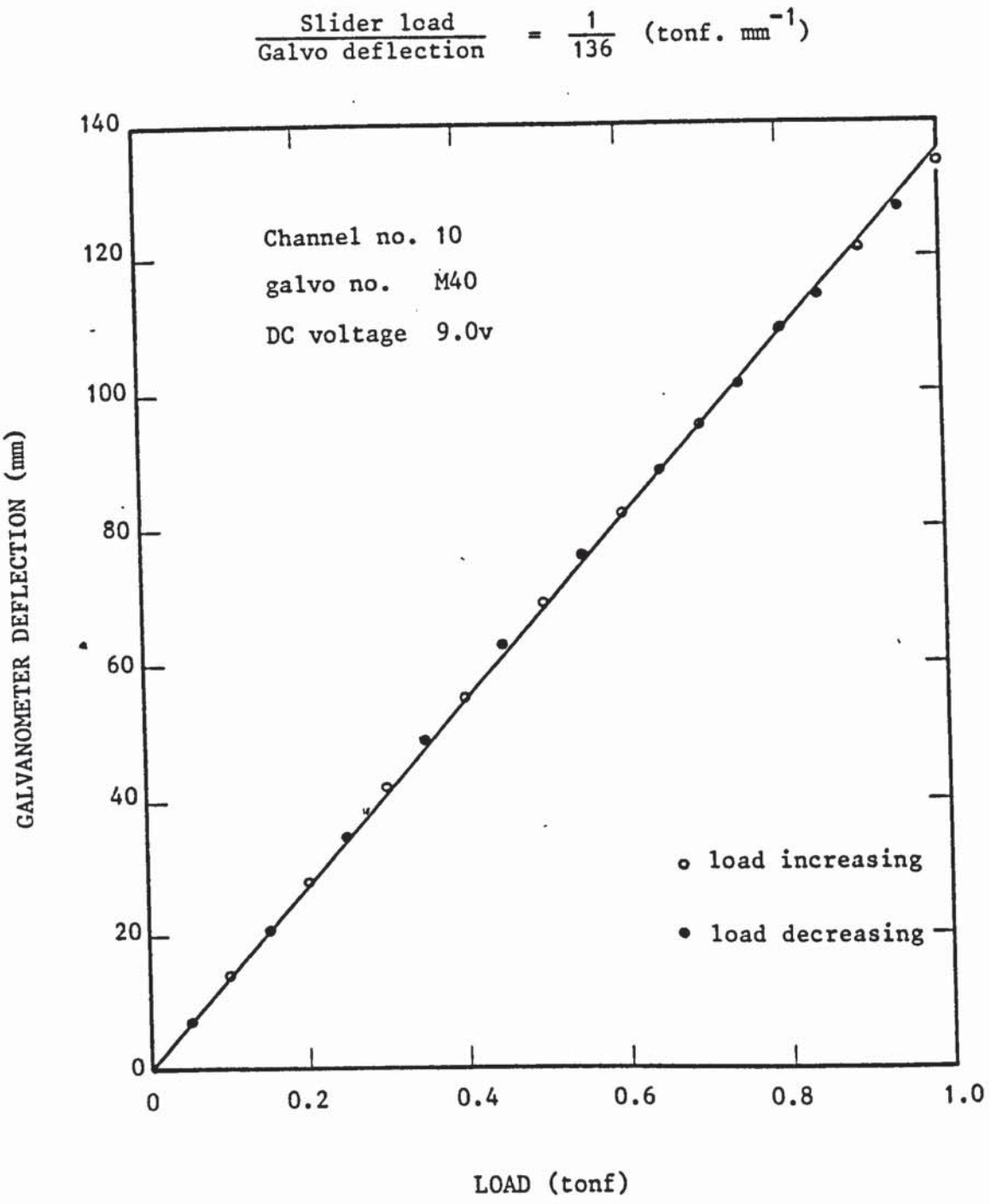

Figure B21: The calibration chart of the slider load cell

$$\frac{\text{Bending torque}}{\text{Galvo deflection}} = \frac{7.967}{138} \text{ (tonf. in. mm}^{-1}\text{)}$$

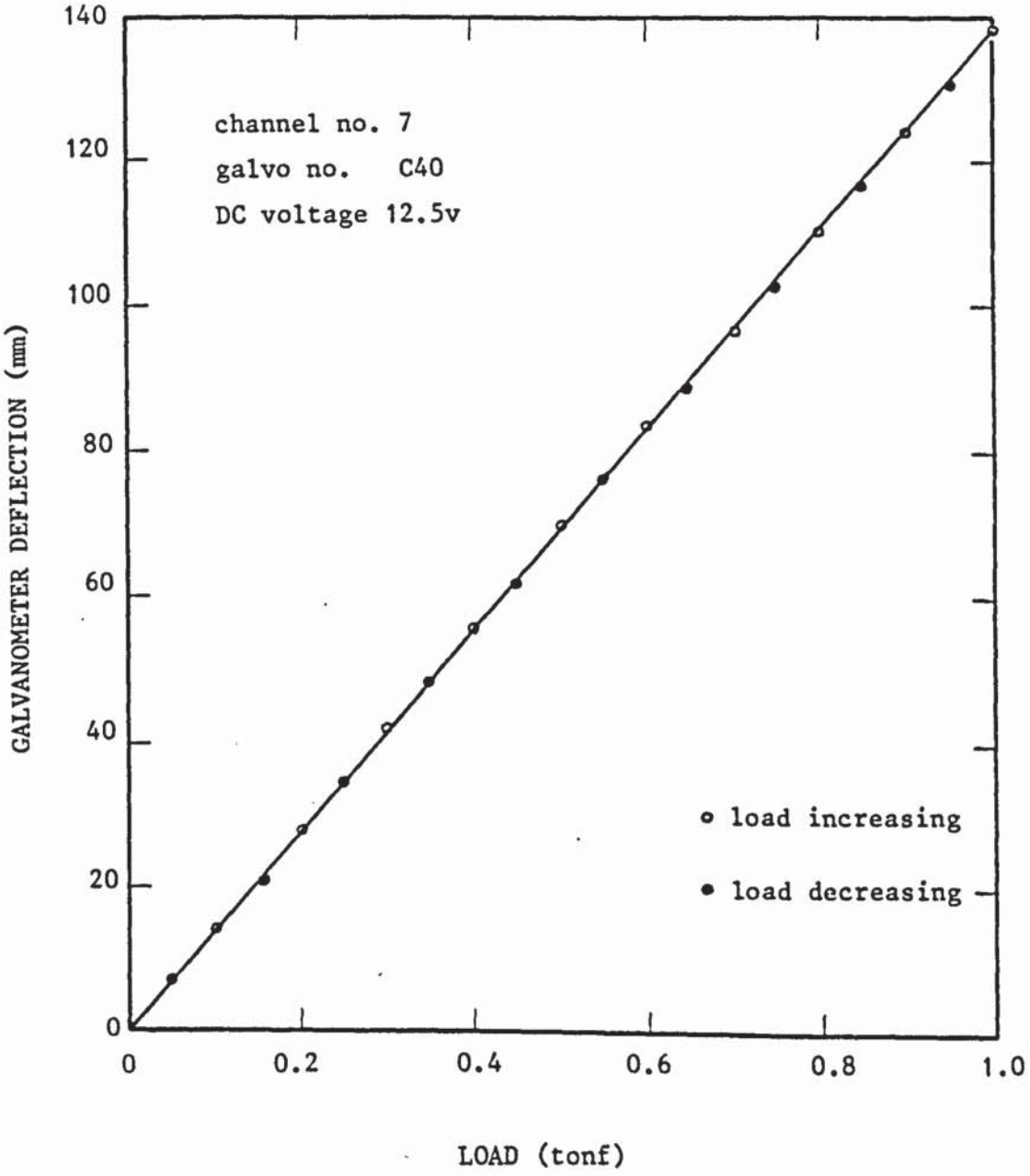

Figure B22: The calibration chart of the torque-meter load cell

$$\frac{\text{Mandrel load}}{\text{Galvo deflection}} = \frac{1}{144} \text{ (tonf. mm}^{-1}\text{)}$$

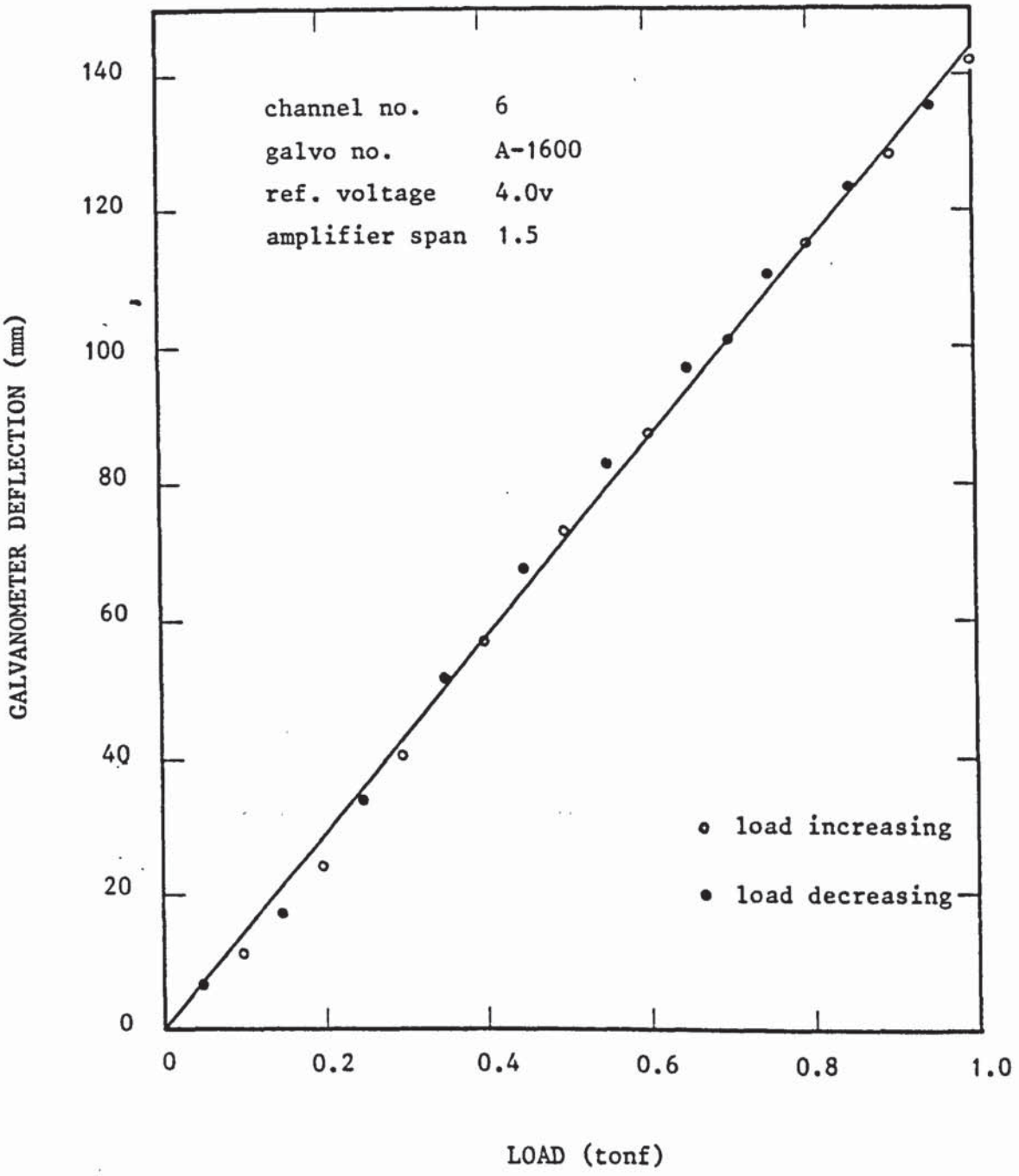

Figure B23: The calibration chart of the mandrel load cell

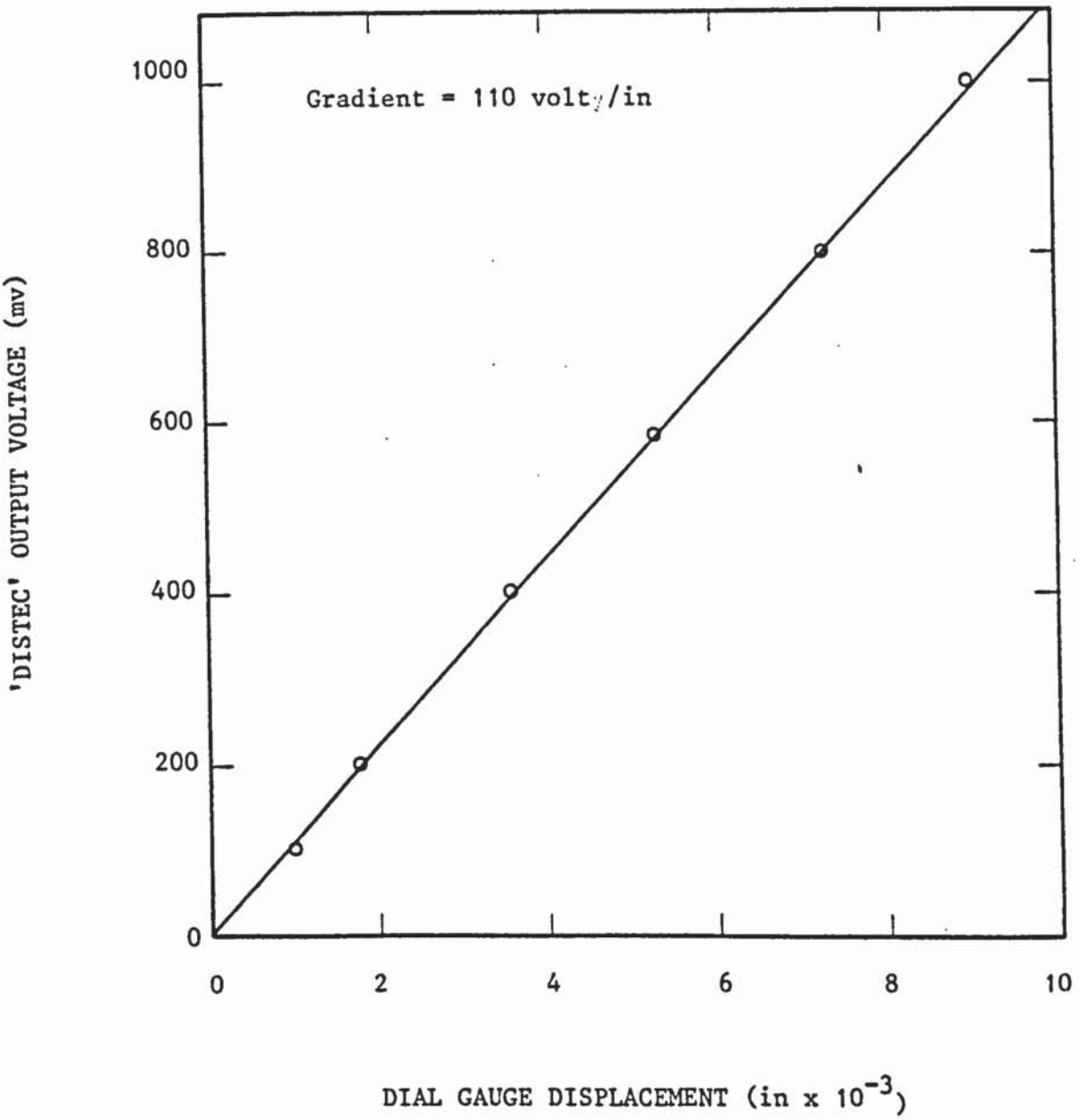

Figure B24: The calibration chart of the 'Distec' displacement transducer

APPENDIX C

Theoretical results

mild steel tubes; d_o = 1 in and $R_o = 2.0d_o$

tube diameter to thickness ratio (d_o/t_o)	initial friction force (F_o) lbf	position of neutral plane (ϕ_N) rad	bending torque in zone IIb (Q_o) tonf.in
15	0	0.1355	1.931
	72.35	0.14	1.990
	251.78	0.15	2.136
	428.96	0.16	2.280
	604.80	0.17	2.422
21	0	0.1337	1.445
	83.78	0.14	1.505
	205.18	0.15	1.604
	337.57	0.16	1.711
	469.50	0.17	1.817
26	0	0.13	1.160
	105.73	0.14	1.248
	194.66	0.15	1.321
	291.20	0.16	1.399
	389.31	0.17	1.479

TABLE C1: Effect of the initial friction force on the position of the neutral plane and on the bending torque in zone IIb for $R_o = 2.0d_o$

mild steel tubes; d_o = 1 in and R_o = 1.5 d_o

tube diameter to thickness ratio (d_o/t_o)	initial friction force (F_o) lbf	position of neutral plane (ϕ_N) rad	bending torque in zone IIb (Q_o) tonf.in
15	0	0.1833	2.088
21	0	0.1792	1.554
26	0	0.1748	1.247
	34.94	0.18	1.280
	142.91	0.19	1.342
	249.98	0.20	1.404
	364.90	0.21	1.470

TABLE C2: Effect of the initial friction force on the position of the neutral plane and on the bending torque in zone IIb for R_o = 1.5 d_o

mild steel tubes; d_o = 1 in and μ = 0

Mean bend radius (R_o)	1.5 d_o			2.0 d_o		
$\frac{d_o}{t_o}$	15	21	26	15	21	26
p_M tonf in^{-2}	2.200	1.567	1.240	1.660	1.182	0.930
σ_θ tonf in^{-2}	39.970	40.440	40.618	36.100	36.456	36.600
σ_ϕ tonf in^{-2}	8.919	9.145	9.245	6.315	6.507	6.550
σ_r tonf in^{-2}	-1.10	-0.78	-0.62	-0.83	-0.59	-0.47
$\bar{\sigma}$ tonf in^{-2}	37.092	37.265	37.298	33.900	34.067	34.107
ε_θ	.3293	.3345	.3359	.2417	.2460	.2470
ε_ϕ	-.1368	-.1394	-.1400	-.1038	-.1059	-.1060
ε_t	-.1925	-.1951	-.1958	-.1379	-.1400	-.1410
$\bar{\varepsilon}$	.3280	.3328	.3338	.2398	.2435	.2450
bending torque tonf.in	2.088	1.554	1.247	1.930	1.441	1.160

Table C3: The stresses and strains at the bend outer periphery and the bending torque under frictionless conditions

mild steel tubes; d_o = 1 in and μ = 0

mean bend radius (R_o)	1.5 d_o			2.0 d_o		
$\frac{d_o}{t_o}$	15	21	26	15	21	26
p_F tonf in^{-2}	0.97	0.67	0.53	0.77	0.54	0.42
σ_θ tonf in^{-2}	-36.801	-36.625	-36.589	-34.009	-33.969	-32.901
σ_ϕ tonf in^{-2}	1.939	2.272	2.444	0.930	1.029	1.201
σ_r tonf in^{-2}	-0.485	-0.335	-0.265	-0.384	-0.271	-0.210
$\bar{\sigma}$ tonf in^{-2}	-37.585	-37.661	-37.739	-34.301	-34.366	-34.418
ε_θ	-.3397	-.3419	-.3442	-.2490	-.2509	-.2524
ε_ϕ	0.1512	0.1498	0.1492	0.1121	0.1108	0.1112
ε_t	0.1884	0.1921	0.1950	0.1369	0.1401	0.1412
$\bar{\varepsilon}$	-.3423	-.3445	0.3468	-.2497	-.2545	-.2528
Φ_N rad	.1355	.1337	.1300	.1833	.1792	.1748

Table C4: The stresses and strains at the bend inner periphery and the position of the neutral plane under frictionless conditions

mild steel tubes; d_o = 1 in, R_o = 2.0 d_o and assumed μ = 0.04

bending operation	conventional (A_m = 0)			oscillatory ($A_m = 5 \times 10^{-4}$ in)		
$\frac{d_o}{t_o}$	15	21	26	15	21	26
p_M tonf in^{-2}	1.660	1.184	0.938	1.663	1.183	0.940
σ_θ tonf in^{-2}	37.603	37.942	38.117	36.192	36.522	36.714
σ_ϕ tonf in^{-2}	6.345	6.495	6.574	6.336	6.485	6.569
σ_r tonf in^{-2}	-.832	-.592	-.469	-.831	-.591	-.469
$\bar{\sigma}$ tonf in^{-2}	35.396	35.529	35.591	34.011	34.130	34.211
ε_θ	.2808	.2849	.2870	.2439	.2476	.2502
ε_ϕ	-.1176	-.1197	-.1210	-.1047	-.1066	-.1079
ε_t	-.1632	.1651	-.1660	-.1392	-.1410	-.1423
$\bar{\varepsilon}$	.2795	.2831	.2850	.2420	.2451	.2473
bending torque tonf.in	2.317	1.714	1.394	2.171	1.576	1.296

Table C5: The stresses and strains at the bend outer periphery and the bending torque with and without mandrel vibration

mild steel tubes; d_o = 1 in, R_o = 2.0 d_o and assumed μ = 0.04

bending operation	conventional (A_m = 0)			oscillatory ($A_m = 5 \times 10^{-4}$ in)		
$\frac{d_o}{t_o}$	15	21	26	15	21	26
p_p tonf in^{-2}	0.71	0.51	0.38	0.74	0.53	0.39
σ_θ tonf in^{-2}	-34.036	-34.073	-33.860	-34.192	-34.183	-33.929
σ_ϕ tonf in^{-2}	1.196	1.225	1.569	1.040	1.132	1.494
σ_r tonf in^{-2}	-0.353	-0.255	-0.189	-0.370	-.263	-.193
$\bar{\sigma}$ tonf in^{-2}	-34.484	-34.581	-34.584	-34.549	-34.637	-34.610
ε_θ	-.2540	-.2567	-.2571	-.2557	-.2581	-.2577
ε_ϕ	.1168	.1156	.1167	.1165	.1155	.1164
ε_t	.1371	.1412	.1404	.1392	.1427	.1413
$\bar{\varepsilon}$	-.2546	-.2572	-.2572	-.2563	-.2587	-.2580
ϕ_N rad	.1443	.1395	.1385	.1400	.1358	.1367

Table C6: The stresses and strains at the bend inner periphery and the position of the neutral plane with and without mandrel vibration

mild steel tubes; d_o = 1 in, d_o/t_o = 26, R_o = 1.5 d_o

and assumed μ = 0.04

amplitude of vibration, in	0	$.5\times10^{-4}$	1×10^{-4}	2×10^{-4}	5×10^{-4}	7×10^{-4}
p_M tonf in^{-2}	1.2455	1.2441	1.2438	1.2437	1.2436	1.2436
σ_θ tonf in^{-2}	42.934	41.309	41.019	40.879	40.796	40.780
σ_ϕ tonf in^{-2}	9.316	9.294	9.290	9.288	9.286	9.286
σ_r tonf in^{-2}	-.623	-.622	-.622	-.622	-.622	-.622
$\bar{\sigma}$ tonf in^{-2}	39.536	37.957	37.676	37.540	37.459	37.444
ε_θ	.4025	.3553	.3470	.3431	.3407	.3403
ε_ϕ	-.1618	-.1468	-.1442	-.1430	-.1422	-.1421
ε_t	-.2407	-.2085	-.2028	-.2001	-.1984	-.1981
$\bar{\varepsilon}$	.4017	.3534	.3450	.3410	.3386	.3381
bending torque tonf in^{-2}	1.546	1.428	1.407	1.397	1.391	1.390

TABLE C7: The influence of the amplitude of mandrel vibration on the stresses and the strains at the bend outer periphery and on the bending torque

mild steel; d_o = 1in, d_o/t_o = 26, $R_o = 2.0d_o$

μ = 0.02

current angle of bend, deg	60	90	120	150
slider force, tonf	0.254	0.287	0.301	0.316
initial friction force, lbf	35.8	40.3	42.3	44.6
bending torque tonf.in	1.2845	1.2890	1.2924	1.2940
longitudinal strain	0.2667	0.26685	0.26695	0.2670
hoop strain	-.1135	-.1136	-.1136	-.11365
thickness strain	-.1533	-.15333	-.1534	-.1534
equivalent strain	0.2642	0.2643	0.2644	0.2645

μ = 0.04

initial friction force, lbf	71.7	80.6	84.7	89.2
bending torque tonf.in	1.373	1.381	1.388	1.391
longitudinal strain	0.2844	0.2869	0.2871	0.2872
hoop strain	-.1206	-.1207	-.1208	-.12085
thickness strain	-.1660	-.1667	-.1662	-.16625
equivalent strain	0.2842	0.2845	0.2847	0.2848

Table C8: The progress of the bending torque and the developed strains at the bend outer periphery with the angle of bend under non-vibratory conditions

mild steel; d_o = 1in, d_o/t_o = 26, $R_o = 2.0d_o$ and $A_m = 5 \cdot x\ 10^{-4}$in

μ = 0.02

current angle of bend, deg	60	90	120	150
slider force, tonf	0.254	0.287	0.301	0.316
initial friction force, lbf	18.6	21.1	22.0	23.1
bending torque tonf.in	1.2174	1.2175	1.2176	1.2176
longitudinal strain	0.2480	0.2480	0.2480	0.2480
hoop strain	-.1069	-.1069	-.1069	-.1069
thickness strain	-.1411	-.1411	-.1411	-.1411
equivalent strain	0.2451	0.2451	0.2451	0.2451

μ = 0.04

initial friction force, lbf	37.2	42.1	43.9	46.1
bending torque tonf.in	1.2424	1.2426	1.2428	1.2429
longitudinal strain	0.2493	0.2494	0.2495	0.2496
hoop strain	-.1074	-.10745	-.1075	-.10753
thickness strain	-.1417	-.14175	-.1418	-.14183
equivalent strain	0.2464	0.2466	0.2467	0.2468

Table C9: The progress of the bending torque and the developed strains at the bend outer periphery with the angle of bend under vibratory conditions

APPENDIX D

Experimental results

1. Bending forces and torque

Bend No: B1* $d_o/t_o = 15$, $R_o/d_o = 2.0$ and 0 watt

current angle of bend, deg	0	15	30	60	90	120	150
slider force (tonf)	.07	.34	.42	.48	.52	.53	.53
mandrel force (lbf)	0	6.7	15.7	44.8	44.8	44.8	44.8
gripper force (tonf)	1.18	1.89	2.18	2.24	2.25	2.28	2.35
bending torque (tonf.in)	0	2.22	2.48	2.63	2.66	2.68	2.74

Bend No: B6 $d_o/t_o = 21$, $R_o/d_o = 2.0$ and 0 watt

slider force (tonf)	.09	.13	.14	.18	.21	.24	.24
mandrel force (lbf)	0	-54	-47	-47	-31	-38	-38
gripper force (tonf)	1.09	1.27	1.33	1.34	1.35	1.38	1.36
bending torque (tonf.in)	0	1.79	1.85	1.91	1.96	2.02	1.96

* All bends were made from mild steel tubes having a constant outside diameter (d_o) equal to 1.0 in

Bend No: B7 $d_o/t_o = 21$, $R_o/d_o = 2.0$ and 250 watt

current angle of bend deg	0	15	30	60	90	120	150
slider force tonf	.09	.14	.15	.18	.21	.24	.25
mandrel force lbf	0	-67	-67	-112	-112	-112	-112
gripper force tonf	1.09	1.31	1.33	1.31	1.33	1.34	1.34
bending torque tonf.in	0	1.53	1.56	1.62	1.62	1.65	1.67

Bend No: B8 $d_o/t_o = 21$, $R_o/d_o = 2.0$ and 500 watt

slider force tonf	.09	.13	.14	.17	.21	.23	.25
mandrel force lbf	0	-67	-67	-112	-112	-112	-112
gripper force tonf	1.09	1.27	1.29	1.27	1.27	1.29	1.29
bending torque tonf.in	0	1.50	1.56	1.59	1.59	1.62	1.62

Bend No: B10 $d_o/t_o = 21$, $R_o/d_o = 2.0$ and 1000 watt

slider force tonf	.09	.12	.13	.15	.19	.21	.22
mandrel force lbf	0	-67	-67	-112	-112	-112	-112
gripper force tonf	1.09	1.22	1.24	1.22	1.22	1.24	1.24
bending torque tonf.in	0	1.44	1.47	1.50	1.56	1.56	1.56

Bend No: B11 $d_o/t_o = 26$, $R_o/d_o = 2.0$ and 0 watt

current angle of bend deg	0	15	30	60	90	120	150
slider force tonf	.132	.176	.213	.254	.287	.301	.316
mandrel force lbf	0	-45	-38	-31	-16	-7	0
gripper force tonf	1.09	1.35	1.40	1.45	1.49	1.55	1.55
bending torque tonf.in	0	1.33	1.44	1.56	1.65	1.73	1.79

Bend No: B12 $d_o/t_o = 26$, $R_o/d_o = 2.0$ and 250 watt

slider force tonf	.132	.235	.294	.346	.375	.379	.390
mandrel force lbf	0	-22	-45	-45	-45	-45	-45
gripper force tonf	1.09	1.26	1.31	1.30	1.29	1.33	1.33
bending torque tonf.in	0	1.30	1.39	1.39	1.41	1.50	1.50

Bend No: B13 $d_o/t_o = 26$, $R_o/d_o = 2.0$ and 500 watt

slider force tonf	.132	.191	.254	.301	.335	.338	.338
mandrel force lbf	0	-22	-45	-45	-45	-45	-45
gripper force tonf	1.09	1.44	1.49	1.47	1.47	1.49	1.49
bending torque tonf.in	0	1.24	1.36	1.38	1.38	1.44	1.41

Bend No: B15 $d_o/t_o = 26$, $R_o/d_o = 2.0$ and 1000 watt

current angle of bend deg	0	15	30	60	90	120	150
slider force tonf	.132	.158	.176	.217	.239	.246	.261
mandrel force lbf	0	-22	-45	-45	-45	-45	-45
gripper force tonf	1.09	1.20	1.24	1.22	1.25	1.26	1.27
bending torque tonf.in	0	1.13	1.21	1.24	1.27	1.33	1.33

Bend No: B16 $d_o/t_o = 15$, $R_o/d_o = 1.5$ and 0 watt

slider force tonf	.19	.34	.43	.49	.55	.60	.66
mandrel force lbf	0	-94	-125	-134	-101	-63	-54
gripper force tonf	0.53	1.35	1.51	1.62	1.71	1.82	1.89
bending torque tonf.in	0	1.62	2.05	2.22	2.37	2.48	2.54

Bend No: B17 $d_o/t_o = 15$, $R_o/d_o = 1.5$ and 250 watt

slider force tonf	.25	.41	.46	.57	.62	.66	.72
mandrel force lbf	0	-63	-170	-201	-201	-217	-211
gripper force tonf	0.91	1.16	1.27	1.38	1.44	1.51	1.55
bending torque tonf.in	0	1.56	1.85	2.02	2.14	2.19	2.22

Bend No: B 18 d_o/t_o = 15, R_o/d_o = 1.5 and 500 watt

current angle of bend deg	0	15	30	60	90	120	150
slider force tonf	.24	.36	.51	.55	.60	.68	.71
mandrel force lbf	0	-78	-179	-217	-201	-217	-217
gripper force tonf	0.84	0.85	1.06	1.24	1.29	1.38	1.43
bending torque tonf.in	0	1.39	1.70	1.91	2.02	2.14	2.19

Bend No: B19 d_o/t_o = 15, R_o/d_o = 1.5 and 1000 watt

slider force tonf	.31	.46	.54	.63	.68	.73	.76
mandrel force lbf	0	-125	-217	-248	-233	-248	-248
gripper force tonf	0.89	1.16	1.29	1.40	1.45	1.55	1.58
bending torque tonf.in	0	1.62	1.91	1.99	2.08	2.14	2.14

Bend No: B20 d_o/t_o = 15, R_o/d_o = 1.5 and 1500 watt

slider force tonf	0.28	0.38	0.51	0.61	0.65	0.70	0.74
mandrel force lbf	0	-94	-154	-217	-201	-233	-233
gripper force tonf	1.11	1.34	1.42	1.48	1.55	1.62	1.64
bending torque tonf.in	0	1.56	1.85	1.93	2.02	2.08	2.08

Bend No: B21 $d_o/t_o = 21$, $R_o/d_o = 1.5$ and 0 watt

current angle of bend deg	0	15	30	60	90	120	150
slider force tonf	0.20	0.37	0.46	0.54	0.56	0.57	0.61
mandrel force lbf	0	47	63	69	94	101	123
gripper force tonf	0.78	1.09	1.27	1.40	1.45	1.56	1.60
bending torque tonf.in	0	1.44	1.73	1.90	2.02	2.11	2.14

Bend No: B23 $d_o/t_o = 21$, $R_o/d_o = 1.5$ and 500 watt

slider force tonf	0.26	0.41	0.49	0.56	0.59	0.61	0.65
mandrel force lbf	0	-31	-94	-155	-155	-155	-155
gripper force tonf	0.75	1.11	1.16	1.25	1.29	1.34	1.35
bending torque tonf.in	0	1.33	1.50	1.65	1.70	1.73	1.73

Bend No: B24 $d_o/t_o = 21$, $R_o/d_o = 1.5$ and 1000 watt

slider force tonf	0.22	0.38	0.45	0.50	0.51	0.53	0.56
mandrel force lbf	0	-38	-116	-148	-155	-164	-164
gripper force tonf	0.91	1.04	1.09	1.18	1.21	1.28	1.30
bending torque tonf.in	0	1.27	1.44	1.56	1.62	1.67	1.67

Bend No: B 26 $d_o/t_o = 26$, $R_o/d_o = 1.5$ and 0 watt

current angle of bend deg	0	15	30	60	90	120	150
slider force tonf	0.20	0.35	0.43	0.50	0.52	0.57	0.59
mandrel force lbf	0	31	32	38	69	110	117
gripper force tonf	0.76	0.93	1.04	1.15	1.19	1.29	1.31
bending torque tonf.in	0	1.10	1.33	1.50	1.59	1.70	1.73

Bend No: B 28 $d_o/t_o = 26$, $R_o/d_o = 1.5$ and 500 watt

slider force tonf	0.25	0.43	0.50	0.55	0.57	0.60	0.63
mandrel force lbf	0	-31	-94	-125	-139	-139	-139
gripper force tonf	0.85	1.02	1.05	1.09	1.15	1.18	1.18
bending torque tonf.in	0	1.04	1.15	1.24	1.33	1.39	1.39

Bend No: B 29 $d_o/t_o = 26$, $R_o/d_o = 1.5$ and 1000 watt

slider force tonf	0.22	0.34	0.39	0.45	0.46	0.48	0.51
mandrel force lbf	0	-34	-78	-110	-125	-132	-132
gripper force tonf	0.91	0.82	0.80	0.84	0.85	0.88	0.90
bending torque tonf.in	0	0.87	0.98	1.10	1.15	1.21	1.21

2. Distribution of the natural strains

at the outer periphery of the bend

Bend No: B6 $d_o/t_o = 21$, $R_o/d_o = 2.0$ and 0 watt

current angle of bend, deg	0	30	60	90	120	150	180
longitudinal strain	0.135	0.229	0.243	0.248	0.255	0.258	0.151
hoop strain	-.053	-.100	-.120	-.119	-.115	-.115	-.083
thickness strain	-.078	-.137	-.138	-.142	-.149	-.156	-.094
equivalent strain	0.134	0.233	-.248	0.252	0.259	0.263	0.160

Bend No: B7 $d_o/t_o = 21$, $R_o/d_o = 2.0$ and 250 watt

longitudinal strain	0.120	0.232	0.240	0.250	0.248	0.248	0.167
hoop strain	-.039	-.092	-.109	-.105	-.108	-.100	-.066
thickness strain	-.083	-.126	-.128	-.134	-.140	-.144	-.072
equivalent strain	0.123	0.228	0.239	0.247	0.249	0.248	0.157

Bend No: B8 $d_o/t_o = 21$, $R_o/d_o = 2.0$ and 500 watt

current angle of bend,deg	0	30	60	90	120	150	180
longitudinal strain	0.130	0.226	0.240	0.244	0.248	0.239	0.168
hoop strain	-.057	-.114	-.122	-.126	-.123	-.122	-.083
thickness strain	-.064	-.122	-.133	-.140	-.143	-.142	-.073
equivalent strain	0.134	0.229	0.245	0.251	0.254	0.248	0.164

Bend No: B10 $d_o/t_o = 21$, $R_o/d_o = 2.0$ and 1000 watt

longitudinal strain	0.137	0.222	0.239	0.243	0.246	0.247	0.161
hoop strain	-.052	-.101	-.113	-.106	-.114	-.113	-.068
thickness strain	-.065	-.129	-.128	-.137	-.147	-.140	-.075
equivalent strain	0.130	0.225	0.240	0.244	0.252	0.250	0.155

Bend No: B11 $d_o/t_o = 26$, $R_o/d_o = 2.0$ and 0 watt

longitudinal strain	0.120	0.216	0.249	0.254	0.259	0.257	0.176
hoop strain	-.032	-.081	-.099	-.102	-.102	-.103	-.071
thickness strain	-.097	-.144	-.154	-.154	-.153	-.159	-.108
equivalent strain	0.129	0.222	0.252	0.256	0.259	0.261	0.178

Bend No: B12 $d_o/t_o = 26$, $R_o/d_o = 2.0$ and 250 watt

current angle of bend,deg	0	30	60	90	120	150	180
longitudinal strain	0.118	0.213	0.242	0.231	0.243	0.232	0.165
hoop strain	-.027	-.075	-.090	-.098	-.091	-.087	-.065
thickness strain	-.083	-.113	-.122	-.128	-.133	-.128	-.085
equivalent strain	0.120	0.205	0.233	0.230	0.238	0.228	0.160

Bend No: B13 $d_o/t_o = 26$, $R_o/d_o = 2.0$ and 500 watt

longitudinal strain	0.121	0.212	0.239	0.243	0.237	0.240	0.168
hoop strain	-.022	-.072	-.088	-.089	-.083	-.087	-.060
thickness strain	-.074	-.115	-.130	-.120	-.128	-.132	-.080
equivalent strain	0.117	0.205	0.233	0.232	0.230	0.234	0.159

Bend No: B15 $d_o/t_o = 26$, $R_o/d_o = 2.0$ and 1000 watt

longitudinal strain	0.120	0.213	0.240	0.244	0.240	0.238	0.160
hoop strain	-.026	-.070	-.093	-.097	-.092	-.090	-.068
thickness strain	-.082	-.118	-.127	-.122	-.128	-.127	-.090
equivalent strain	0.120	0.206	0.234	0.236	0.234	0.232	0.160

Bend No: B16 $d_o/t_o = 15$, $R_o/d_o = 1.5$ and 0 watt

current angle of bend, deg	0	30	60	90	120	150	180
longitudinal strain	0.065	0.262	0.311	0.308	0.317	0.305	0.147
hoop strain	-.022	-.090	-.115	-.108	-.119	-.111	-.069
thickness strain	-.042	-.160	-.174	-.178	-.175	-.185	-.080
equivalent strain	0.066	0.261	0.306	0.303	0.311	0.305	0.148

Bend No: B18 $d_o/t_o = 15$, $R_o/d_o = 1.5$ and 500 watt

longitudinal strain	0.068	0.265	0.293	0.302	0.287	0.290	0.126
hoop strain	-.025	-.085	-.104	-.100	-.096	-.101	-.062
thickness strain	-.033	-.149	-.162	-.156	-.157	-.161	-.073
equivalent strain	0.065	0.257	0.286	0.288	0.278	0.283	0.129

3. Distribution of the natural strains

at the inner periphery of the bend

Bend No: B 16 $d_o/t_o = 15$, $R_o/d_o = 1.5$ and 0 watt

current angle of bend, deg	0	30	60	90	120	150	180
longitudinal strain	-.173	-.269	-.312	-.312	-.311	-.305	-.170
hoop strain	0.030	0.082	0.113	0.116	0.112	0.108	0.058
thickness strain	0.102	0.163	0.182	0.188	0.170	0.181	0.087
equivalent strain	-.165	-.265	-.309	-.312	-.303	-.303	-.163

Bend No: B 18 $d_o/t_o = 15$, $R_o/d_o = 15$ and 500 watt

longitudinal strain	-.161	-.263	-.320	-.326	-.332	-.327	-.158
hoop strain	0.023	0.095	0.125	0.127	0.124	0.130	0.056
thickness strain	0.095	0.176	0.200	0.202	0.207	0.194	0.095
equivalent strain	-.152	-.270	-.325	-.330	-.335	-.328	-.157

APPENDIX E

"An experimental study of the mechanics of ultrasonic tube-bending"

- A paper presented at the Ultrasonics International 83 Conference in Canada